

The role of forest trees and their mycorrhizal fungi in carbonate weathering and phosphorus biogeochemical cycling

Rachel Marianne Sarah Thorley

Department of Animal and Plant Sciences



The
University
Of
Sheffield.

A thesis submitted for the degree of Doctor of Philosophy

June 2016

Acknowledgements

After a rocky start to my PhD at the E-Futures Doctoral Training Centre, I realised that engineering research on renewable energy technologies was perhaps not my cup of tea, and was struggling to find a project I was enthusiastic about. So I would like to begin with a huge thank you to my supervisor, Professor David Beerling for his vision, and welcoming me into his group to study the importance of forests on terrestrial weathering and carbon cycling. I am very grateful for the guidance of all my supervisors, Professor David Beerling, Professor Jonathan Leake and Professor Steve Banwart. Their support, encouragement and ideas have all been invaluable over the last four years.

I would like to especially thank the following people for their academic and technical assistance: Dr. Lyla Taylor for sharing some of her enthusiasm and vast knowledge on which greatly helped me get to grips with the theory of Earth processes, weathering and plant evolution. Dr. Joe Quirk for his help with field experimental design; showing me how to operate the VSI, and his assistance and company, alongside Dr. Dave Johnson, whilst setting up my weathering trial at Bedgebury. Dr. Loredana Saccone for many pleasant walks in the park, advice and moral support.

The main experimental work of this thesis was carried out under the trees of Bedgebury Pinetum, and I gratefully acknowledge the co-operation of the, curator Daniel Luscombe. There are too many people to thank both in Sheffield, and further afield, so I shall just name a few here: Steve Muddimer, Despina Berdeni, Owen Hayman, Anna van Doorn, and all the members of CMezz and C204 who made the endless hours of phosphorus assays and soil extractions bearable!

Over the course of my PhD I was very fortunate to have many opportunities to travel, present my research and meet inspiring scientists, a few of whom I shall mention here. Dr. Mark Smits and Dr. Zsuzsanna Balogh-Brunstad for their company and encouragement at Goldschmidt in Prague. Dr. Caroline Thaler who I first met in California for her shared enthusiasm of carbonates and the opportunity to present my research at IPGP in Paris. Professor Julie Gray and Professor Andrew Fleming for involving me in Robert Hill Institute at Sheffield and inviting me to present my work at its Christmas Symposium.

I gratefully acknowledge the Engineering and Physical Sciences Research Council (EPSRC) and Industrial Cooperative Awards in Science & Technology (CASE) for funding my PhD studentship.

The last few years have had their ups and downs, but from starting life in a new city I have met many amazing people and now call Sheffield my home. A few people deserve a special mention: firstly, my family for their unconditional support, even if at times it has been frustrating when Dad tries to re-design all my experiments! Manu for adventures shared, dreams of travel, and copious amounts of coffee and wine - thanks for brightening the first few years of my PhD. Chris, for appropriately antisocial company on many bike rides and climbing sessions to stave off thesis-writing insanity, I look forward to more adventures in a bright post-thesis future! And finally, Callum, for your patience in putting up with my frustrations and bad tempers, your baking skills, excellent Eppendorf labelling and help fighting Monkey Puzzle trees. Without your unfailing friendship I'd have left Sheffield long ago and never have completed this PhD.

Summary

Over millions of years, atmospheric CO₂ concentrations, and Earth's climate, are regulated by continental silicate weathering and associated marine carbonate deposition. On this geological timescale, carbonate weathering has no net effect on CO₂ drawdown. However, over the coming decades-to-centuries, accelerated weathering of carbonate rocks may provide a sink for anthropogenic CO₂ emissions and increase alkalinity flux to the oceans to counteract ocean acidification. Recent experimental evidence strongly supports trees and their associated mycorrhizal fungi as key drivers of silicate mineral weathering; however, their role in the context of carbonate weathering is largely unknown. Carbonate lithology is abundant globally and underlies many boreal and temperate forest ecosystems in the northern hemisphere. If biological enhancement of carbonate weathering by forests occurs, this might present a new opportunity for CO₂ sequestration.

This thesis presents results from a 14-month field experiment at the UK's national pinetum investigating carbonate rock weathering under a common climate. Overall, I find original evidence for biotic enhancement of calcite- and dolomite weathering by an evolutionary diverse range of trees that host either arbuscular (AM) or ectomycorrhizal (EM) root-associating fungal symbionts.

Recent soil analyses are integrated with a re-interpretation of historic data to provide an 85-year record of in-situ soil development under different forestry species. This study challenges the classic dogma that divergence of properties is driven by the major tree functional groups, angiosperms and gymnosperms. Instead, we find that over decades, mycorrhizal functional type plays a dominant role in determining soil physico-chemical characteristics, and conditions generated by EM fungi are likely to enhance mineral weathering.

Field trials next investigated the impact of tree-mycorrhizal functional group on weathering of the four main carbonate rock types (chalk, limestone, marble and dolomite) and a quartz silicate. Under EM trees carbonate rock grain dissolution was 12 times faster than silicate weathering. In the initial 3 months, calcite weathering intensity increased from gymnosperm to angiosperm species and from AM to later, but independently-evolved EM fungal partnerships. More extensive weathering after 6 months, especially within EM forest soils, confirms the importance of these fungi for carbonate mineral dissolution and nutrient mobilisation. This effect is linked to rhizosphere acidification by EM fungi and is confirmed by a parallel study of tree species' influence on soil chemistry.

Both AM and EM fungi facilitate the mobilisation of nutrient elements, which are provided to their host plants in exchange for carbon from photosynthesis. I applied a suite of nanoscale surface analysis techniques (VSI, SEM) to quantify mineral alteration and provide direct evidence for mycorrhizal involvement in carbonate weathering in the field. Fungal hyphae preferentially colonised chalk and quartz silicate grains, which contained the highest concentrations of phosphorus (P), a growth limiting elemental nutrient. P was selectively depleted from silicate grains, especially in EM forest soils, but accumulated on carbonates. Although the origin of this accumulated P remains uncertain, extensive analyses of different potential P-pools indicated it is likely to be inorganic, but accumulated via active microbial import. These findings lead to new insights linking carbonate weathering with phosphorus biogeochemical cycling in soils. Results show that P from the surrounding environment is concentrated on carbonate grains and this potentially provides a renewable P resource accessible to host trees.

Overall, this thesis builds new support for the role of mycorrhizal partnerships in shaping soil properties important for accelerating carbonate rock weathering (Chapter 2); presenting the first field-based evidence for the enhancement of carbonate dissolution by tree roots and their associated mycorrhizal partners (Chapters 3-5) and generating new insights into biogeochemical P cycling in soils (Chapter 4). More broadly, these findings suggest targeted reforestation/afforestation with EM-tree taxa on carbonate-rich terrain as a possible regional-scale land management strategy for promoting short-term anthropogenic CO₂ sequestration and perhaps helping ameliorate ocean acidification.

Table of Contents

Acknowledgements	i
Summary	v
Table of Contents	ix
Chapter 1	1
<i>The role of forest trees and their mycorrhizas in carbonate weathering and its significance in global carbon cycling</i>	
1.1 Introduction	1
1.2 Carbonate weathering in the global carbon cycle	3
1.3 Anthropogenic disruption of weathering processes	5
1.3.1 Carbonate weathering and changing agricultural land use patterns	5
1.3.2 Impact of agricultural liming on carbonate weathering.....	6
1.3.3 Carbonation of industrial waste sequesters CO ₂ in urban soils	7
1.4 Carbonate mineral weathering in soils.....	8
1.4.1 Abiotic controls on carbonate weathering	8
1.4.1.1 Surface reaction versus mass transport weathering limitations.....	8
1.4.1.2 Carbonate weathering rate dependency on soil pH environment	9
1.4.1.3 Acidic forest soils in Europe	10
1.4.1.4 Weathering rate dependence on temperature.....	10
1.4.2 Biotic controls on carbonate weathering	11
1.4.2.1 The tree-mycorrhizal symbiosis.....	12
1.4.2.2 Arbuscular mycorrhizal fungi (AM)	12
1.4.2.3 Ectomycorrhizal fungi (EM)	12
1.4.3 Function of mineral plant-mycorrhizal weathering.....	13
1.4.3.1 Calcium and Magnesium	14
1.4.3.2 Phosphorus.....	14
1.5 Mechanisms of carbonate weathering by tree-mycorrhizal partnerships	16

1.5.1 Physical surface weathering by mycorrhizal hyphae.....	16
1.5.1.1 Contribution of hyphal tunnelling to total mineral weathering	17
1.5.2 Rhizosphere acidification by respiratory CO ₂ production	19
1.5.2.1 Role of carbonic anhydrase (CA) in enhancing carbonate weathering	19
1.5.3 Carbonate weathering by LMWOAs	20
1.5.3.1 Oxalate production by EM fungi.....	22
1.5.3.2 Secondary mineral formation: calcium oxalate	22
1.5.4 Siderophores	23
1.6 Effects of elevated CO ₂ on terrestrial carbonate weathering	23
1.6.1 Increased Net Primary Productivity (NPP)	24
1.6.2 Altered soil hydrology affects mineral weathering processes.....	24
1.6.3 Evidence of tree-mycorrhizal weathering enhancement in elevated CO ₂	25
1.7 Overarching aims.....	26
1.8 Thesis outline.....	27

Chapter 2

29

Tree species influence on soil characteristics at Bedgebury Pinetum

2.1 Introduction.....	29
2.1.1 Overarching aims.....	29
2.1.2 Trees alter soil biogeochemical properties	30
2.1.3 Tree species effects on SOM and soil nutrient availability.....	31
2.1.4 Inputs of SOM.....	32
2.1.4.1 Root DOM inputs and nutrient recycling	32
2.1.4.2 Litterfall	33
2.1.4.3 Canopy and litter composition.....	33
2.1.4.4 Nutrient recycling in leaf litter	34
2.1.5 Decomposition of Dead Organic Matter.....	35
2.1.5.1 Root decomposition	35
2.1.5.2 Litter decomposition.....	35
2.1.6 Forest soil pH	36
2.1.6.1 Seasonal variation	36
2.1.6.2 Species effects on pH	38
2.1.7 Summary of historical work at Bedgebury	40
2.2 Methods.....	42
2.2.1 Site description	42

2.2.2 Soil type and bedrock.....	43
2.2.3 Climate.....	44
2.2.4 Tree species influence on observed change in Bedgebury 1951-1971.....	44
2.2.4.1 Statistical treatment of historical data.....	45
2.2.4.2 Soil and litter sampling.....	46
2.2.4.3 Soil pH.....	46
2.2.4.4 2.5% acetic acid extraction.....	46
2.2.4.5 AAS Analysis.....	47
2.3 Results.....	48
2.3.1 Climate.....	48
2.3.1.1 Climate change at Bedgebury.....	48
2.3.2 Soil pH at Bedgebury pinetum.....	50
2.3.2.1 Seasonal pH variation.....	50
2.3.2.2 Species-specific differences in pH.....	50
2.3.2.3 Evolution of pH over time.....	51
2.3.3 Extractable phosphorus.....	52
2.3.4 Extractable calcium.....	54
2.4 Discussion.....	55
2.4.1 Climate.....	55
2.4.2 Discussion of results in relation to research hypothesis 1.....	55
2.4.2.1 Seasonal variation in pH.....	55
2.4.2.2 Species-specific impacts on forest soil characteristics.....	56
2.4.3 Discussion of results in relation to research hypothesis 2.....	57
2.4.3.1 Soil phosphorus content increases over time.....	57
2.4.3.2 Proximity to neighbouring species.....	58
2.4.4 Discussion of results in relation to research hypothesis 3.....	59
2.4.4.1 Species-specific pH divergence at 1971 sampling.....	59
2.4.4.2 Increased between-species variation for soil extractable P-content.....	60
2.4.4.3 Soil extractable calcium.....	60
2.4.4.4 Impact of soil Ca on weathering rates.....	60
2.4.4.5 Effect of brickearth and marling.....	62
2.4.4.6 Limitations of using different analysis methodologies.....	62
2.4.4.7 Limited temporal resolution of data.....	63
2.5 Conclusions.....	64

*Determination of carbonate weathering rates
and phosphorus geochemical cycling*

3.1 Introduction.....	67
3.1.1 Overarching aims.....	67
3.1.2 Weathering enhancement by plants and mycorrhizal fungi.....	67
3.1.3 Mycorrhizal weathering for acquisition of limiting nutrients.....	70
3.1.4 Interaction of mineral weathering and available soil P resources.....	71
3.2 Methods.....	72
3.2.1 Experimental design and sampling.....	72
3.2.2 Weathering estimation by mass loss.....	74
3.2.2.1 Calculating molar weathering rates normalised to particle surface area.....	74
3.2.3 XRF analysis of rock samples.....	75
3.2.4 Phosphorus determination of rock grain and soil samples.....	76
3.2.4.1 Aqua regia digests of rock grains.....	76
3.2.4.2 Chloroform fumigation for microbial P (Carter 1993).....	77
3.2.4.3 Olsen's extraction of orthophosphate from air dried soil.....	77
3.2.4.4 Chloroform and NaCl extraction for lipid P fractions.....	78
3.2.4.5 Murphy-Riley colourimetric phosphorus determination.....	79
3.2.5 Hyphal length.....	82
3.3 Results.....	83
3.3.1 SA normalisation of molar weathering rates.....	83
3.3.2 Rapid weathering of carbonate samples.....	83
3.3.3 Effect of tree-mycorrhizal functional group on calcite weathering rates.....	86
3.3.3.1 Tree-mycorrhizal functional group affects SA-normalised weathering rates.....	88
3.3.4 Phosphorus changes over weathering.....	90
3.3.4.1 Selective depletion of phosphorus in silicate samples.....	92
3.3.4.2 Accumulation of phosphorus in carbonate samples.....	92
3.3.4.3 Hyphal colonisation determined by initial P concentrations in rock samples.....	94
3.3.5 Investigating origins of P accumulated by carbonates.....	94
3.3.5.1 Influence of soil P content on P accumulation in carbonates.....	94
3.3.5.2 Phosphorus in lipids extracted from weathered carbonates.....	98
3.4 Discussion.....	101
3.4.1 Discussion of evidence related to research hypothesis 1.....	101
3.4.1.1 Calcite mass loss exceeds that of silicates.....	101
3.4.1.2 Intensification of calcite and silicate weathering over initial 7 months.....	101
3.4.1.3 Weathering rate decrease from 7-14 months.....	102

3.4.1.4 Dolomite weathering increases throughout the 14 month burial period	102
3.4.1.5 Mass gain of samples and net weathering rates	103
3.4.1.6 Comparison of SA normalisation with Thorley et al. (2015).....	104
3.4.1.7 Effect of tree-mycorrhizal functional group on carbonate weathering rates	104
3.4.1.8 Carbonate weathering intensification by EM fungi.....	105
3.4.2 Discussion of evidence related to research hypothesis 2	107
3.4.2.1 Hyphal colonisation proportional to rock grain P-content.....	107
3.4.2.2 Phosphorus depletion in silicates	108
3.4.2.3 Phosphorus accumulation by carbonates	108
3.4.2.4 Limitations of total rock grain phosphorus measurements.....	108
3.4.3 Discussion of evidence related to research hypothesis 2	110
3.4.3.1 Possible origins of accumulated phosphorus in weathered carbonates.....	110
3.4.3.2 Passive accumulation of P from soil.....	110
3.4.3.3 Active import of organic P.....	112
3.5 Conclusions	114
3.5.1 Research hypothesis 1	114
3.5.2 Research hypothesis 2.....	115
3.5.3 Research hypothesis 3.....	115

Chapter 4

117

Carbonate weathering rate dependence on soil acidity and grain surface area

4.1 Introduction	117
4.1.1 Soil pH is a major control on carbonate weathering rate.....	117
4.1.2 Physical properties of minerals affect weathering rates.....	119
4.1.2.1 Rock structure affects carbonate weathering mechanisms.....	119
4.1.2.2 Biological activity targeted to smaller grain sizes.....	120
4.1.3 Surface area evolution through weathering.....	121
4.1.4 Overall aims of chapter 5	122
4.2 Methods	124
4.2.1 Soil sampling and pH measurement	124
4.2.2 Calculation of theoretical weathering rates for calcite and dolomite	124
4.2.3 Brunauer-Emmett-Teller surface area determination.....	125
4.2.3.1 BET theory.....	125
4.2.3.2 Sample selection for BET	128
4.2.3.3 BET analysis methodology.....	128
4.2.3.4 Standard reference material.....	128

4.2.3.5 Replicate measurements of a single weathered sample.....	129
4.2.3.6 Limitations of BET analysis.....	129
4.2.4 Laser Diffraction Particle Size Analysis (PSA)	130
4.2.4.1 PSA Theory.....	130
4.2.4.2 PSA analysis methodology.....	131
4.2.4.3 Limitations of PSA analysis.....	132
4.2.4.4 Comparison of wet and dry dispersion techniques and limitations of PSA ...	133
4.2.5 Software and statistics.....	133
4.3 Results.....	134
4.3.1 Soil acidity as a driver of carbonate weathering.....	134
4.3.1.1 Soil acidification and enhanced carbonate dissolution under EM trees.....	134
4.3.2 Comparison between field and theoretical rates for calcite and dolomite	135
4.3.3 BET and PSA Results	139
4.3.3.1 Surface area of unweathered rock grains measured by BET analysis	139
4.3.3.2 Unweathered chalk particle size distribution	140
4.3.4 Evolution of surface area and particle size distribution during weathering.....	141
4.3.4.1 Change in particle size distribution with weathering	141
4.3.4.2 Change in BET surface area with weathering.....	145
4.3.5 Chalk grain porosity measured by gas adsorption.....	150
4.3.6 Comparison of measured BET and calculated PSD surface areas.....	151
4.4 Discussion.....	153
4.4.1 Carbonate weathering rate dependence on environmental pH.....	153
4.4.2 Why is calcite weathering rates different in field and laboratory studies?.....	154
4.4.2.1 Inappropriate thermodynamic constants.....	154
4.4.2.2 Incomplete understanding of weathering agent dynamics in the field	156
4.4.2.3 Transport limitation.....	156
4.4.2.4 Incomplete understanding of reactive surface area	156
4.4.2.5 Reduced reactive surface area in the field.....	158
4.4.3 Evolution of surface area and particle size distribution during weathering.....	159
4.4.3.1 Unweathered carbonate particle size distribution.....	159
4.4.3.2 Surface area of unweathered carbonate grains.....	159
4.4.3.3 Modelling log-Gaussian distribution of particles in chalk samples	159
4.4.3.4 Silicate rock grain weathering behaviour	160
4.4.3.5 Chalk and dolomite particle weathering behaviour.....	161
4.4.3.6 Effect of organic matter adsorption on carbonate weathering.....	164
4.4.3.7 Chalk grain porosity measured by gas adsorption.....	165
4.4.3.8 Comparison of measured BET and calculated PSD surface areas for chalk .	165
4.5 Conclusions	168

*Physical surface alteration of carbonate
rocks during weathering*

5.1 Introduction	171
5.1.1 The role of biofilms in mineral weathering.....	172
5.1.2 Mycorrhizal hyphae can etch channels on mineral surfaces	172
5.2 Methods	174
5.2.1 Field experiment design.....	174
5.2.2 Mesh bag pH	174
5.2.3 Rock thin sections	174
5.2.4 SEM imagery.....	174
5.2.4.1 Hyphal width measurements from SEM images.....	175
5.2.5 Vertical scanning interferometry (VSI)	175
5.2.5.1 VSI Theory	175
5.2.5.2 Mineral chip preparation for VSI analysis.....	176
5.2.5.3 VSI scanning methodology.....	177
5.2.5.4 Roughness measurement.....	178
5.2.5.5 Quantifying biological surface weathering features	180
5.2.6 Software and statistics.....	181
5.3 Results	182
5.3.1 Unweathered Thin Sections.....	182
5.3.2 SEM Imagery of weathered carbonates	185
5.3.3 VSI topography analysis of weathering carbonate and silicate surfaces.....	188
5.3.3.1 Difficulties in identifying pre-scanned areas on VSI chips	188
5.3.4 Biological surface weathering features	188
5.3.4.1 Dimensions of channels and hyphae in muscovite.....	188
5.3.4.2 Comparison of hyphal channels formed under AM and EM tree stands	189
5.3.5 Mineral surface roughness	192
5.3.5.1 R_a scales with scan area.....	192
5.3.5.2 Increase in average roughness over 7 months weathering.....	193
5.3.5.3 Influence of tree-mycorrhizal functional type on R_a evolution.....	196
5.3.5.4 Influence of pH and field weathering rates on surface roughness changes ..	196
5.4 Discussion	199
5.4.1 Micro-organisms observed on weathering surfaces.....	199
5.4.2 Comparison of hyphal width measurements using SEM and VSI techniques.....	199
5.4.3 Hyphal channels observed on muscovite surfaces and carbonate rock grains.....	201
5.4.4 Correspondence between hyphal and channel widths.....	201

5.4.5 Correspondence between width and depth of hyphal channels	202
5.4.5.1 Weathering duration and hyphal colonisation rate	202
5.4.6 Comparison of hyphal channel morphology under AM and EM tree stands	203
5.4.6.1 Climatic factors might cause different hyphal channelling behaviour	204
5.4.6.2 Plant growth conditions and fungal colonisation affect channelling.....	205
5.4.7 Evidence of organic exudates or biofilm formation	207
5.4.8 Etch pit formation and changes in mineral surface texture observed with SEM ..	207
5.4.8.1 Increase in average roughness over 7 months weathering	207
5.4.8.2 Influence of tree functional group on surface roughness changes	209
5.4.8.3 Influence of pH and field weathering rates on surface roughness changes ..	209
5.4.8.4 Limitations of VSI roughness measurements.....	210
5.5 Conclusions.....	211

Chapter 6 213

General discussion

6.1 Introduction.....	213
6.2 Principle conclusions.....	214
6.3 Mycorrhizas as drivers of soil physico-chemical differences	215
6.3.1 Limitations of common garden experiments	216
6.4 Reconciling field and laboratory carbonate weathering rates	217
6.5 Evolving plant-mycorrhiza associations affect carbonate weathering ...	218
6.6 Closing Remarks.....	220

7 Appendix 221

8 References 229

Chapter 1

The role of forest trees and their mycorrhizas in carbonate weathering and its significance in global carbon cycling

1.1 Introduction

Over the coming century we will be faced with the challenge of controlling anthropogenic CO₂ emissions, which are causing rapid climate change and ocean acidification (NOAA/ESRL 2016; Schmidt *et al.* 2016). Global CO₂ concentration has increased by ca. 40% since 1800, driven by deforestation and burning fossil fuels (IPCC 2014). This year sets a record for the first time atmospheric CO₂, measured at Mauna Loa, is predicted to remain above 400ppm throughout the year (Betts *et al.* 2016). This level was initially reached earlier in my PhD, in May 2013 (Tans and Keeling 2013) and is probably the highest atmospheric CO₂ concentration of the last 10-20 million years (Beerling and Royer 2011). Global surface temperatures are rising in response to accumulated greenhouse gases, making each of the last 3 decades warmer than any other since 1950 (IPCC 2013).

On million-year timescales, atmospheric CO₂ concentration regulation is dominated by the balance between its release by volcanic degassing and its uptake during terrestrial weathering of silicate minerals (Berner 2003). Until recently, carbonate weathering has been dismissed as inconsequential for atmospheric carbon sequestration due to eventual re-precipitation of marine carbonates (Berner 1992; Liu *et al.* 2011; Zeebe 2012). This means that over geological timescales carbonate weathering provides no significant net storage of CO₂. However, recent observational evidence (Gislason *et al.* 2009) and modelling studies (Beaulieu *et al.* 2010, 2012; Goll *et al.* 2014) suggest that the timescale, over which climate change impacts weathering feedbacks, could be as short as decades. Contemporary climate change is likely to particularly affect terrestrial carbonate weathering rates (Beaulieu *et al.* 2012), providing a source of ocean alkalinity and a net sink for CO₂ over decades-to-centuries.

Chapter 1

Carbonate lithology (>80% CaCO₃) occupies 10.4% of the earth's terrestrial surface (Dürr *et al.* 2005), and considerable amounts of carbonate are contained within many silicate and sedimentary lithologies (Hartmann *et al.* 2009). In the northern hemisphere, carbonates are abundant between 15-65°N (Amiotte-Suchet *et al.* 2003; Dürr *et al.* 2005), underlying many temperate and boreal forest ecosystems (Figure 1.1). In contrast to the old, highly weathered soils under forests in the humid tropics, these boreal and temperate forests are especially important for weathering as the soils are often young, developing over fresh regolith deposited after the last glaciation. The contribution to land-ocean flux of alkalinity and base cations from areas with young soils will be far more sensitive to changes in weathering rates compared to areas with older, weathered and base-depleted soils. However, despite their importance for weathering, the interaction between the roots and associated soil micro-organisms of N. Hemisphere forests and carbonate rocks is relatively unstudied.

Silicate weathering processes are enhanced up to tenfold by vegetation cover (Berner 1997; reviewed in Ruddiman *et al.* 2001), and there is an increasing body of evidence to link root-associated mycorrhizal fungal activity with silicate rock weathering. Mycorrhizas use energy from plant photosynthates to grow, reproduce and dissolve minerals by localised mycorrhizosphere acidification (Casarin *et al.* 2003; Rosling *et al.* 2004b; van Scholl *et al.* 2006b). Both dominant functional groups of these fungi, arbuscular mycorrhizas (AM) and ectomycorrhizas (EM) have been observed to weather minerals (Koele *et al.* 2014), and actively target their efforts (Quirk *et al.* 2012) to source growth-limiting nutrients such as phosphorus or potassium (Blum *et al.* 2002; Hoffland *et al.* 2003). However, little is known about the activity of mycorrhizal fungi in relation to carbonate rock weathering.

This chapter first gives an overview of the importance of carbonate weathering in the global carbon cycle and the impact of recent land-use changes and agricultural practices on land-ocean alkalinity flux. The second part reviews the role of trees and their root-associated, mycorrhizal fungi in accelerating carbonate weathering.

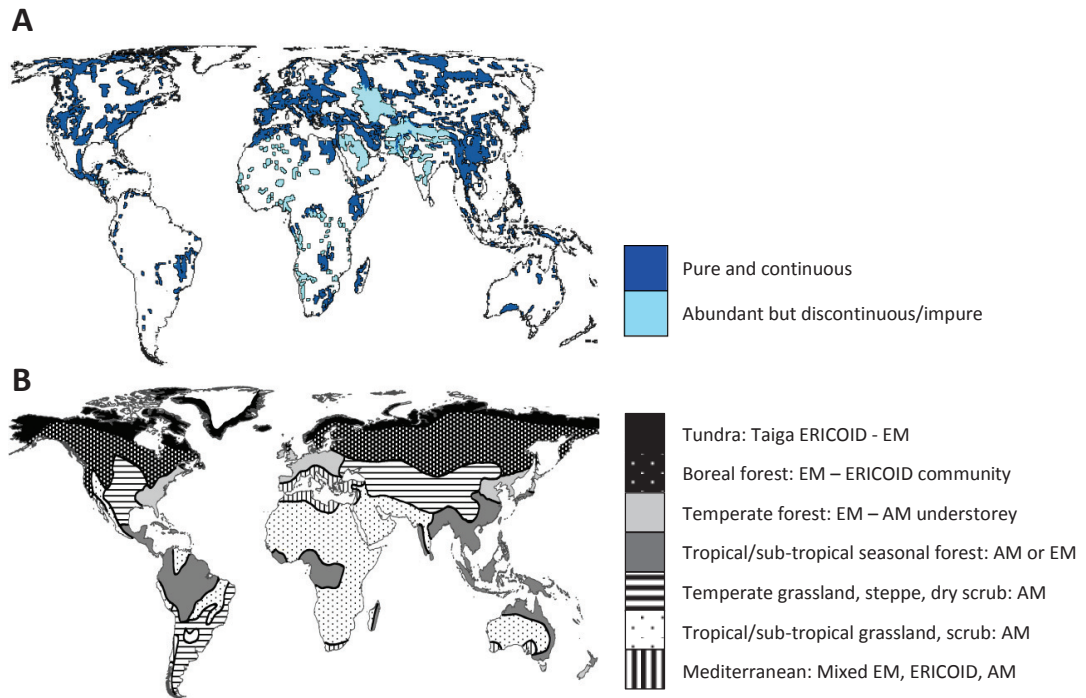
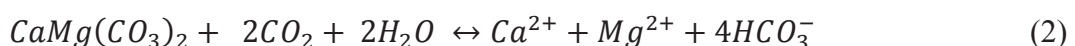


Figure 1.1. Global distribution of **A)** carbonate lithologies (Williams and Fong 2010) and **B)** major tree-mycorrhizal functional groups (Read 1991; Read *et al.* 2004).

1.2 Carbonate weathering in the global carbon cycle

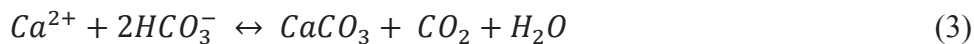
Continental weathering of carbonate and silicate minerals plays an important role in the long- and short-term global carbon cycles. They both supply a vital flux of alkalinity to the oceans and are a key process in soil formation, providing essential plant nutrients. The long-term sink of Mg^{2+} and Ca^{2+} ions released from continental silicate weathering, in marine carbonates, regulates global atmospheric CO_2 concentration, and therefore climate, over millions of years. Contrastingly, due to the stoichiometry of dissolution reactions, carbonate weathering by forested ecosystems is inconsequential for global climate regulation over the same multi-million year timescales. Over $>10,000$ years, CO_2 consumed during weathering is balanced by that released as carbonates precipitate in the oceans (Bernier 1992; Liu *et al.* 2011; Zeebe *et al.* 2012). Generalised weathering reactions for calcite (Eqn 1) and dolomite (Eqn 2), the two most abundant carbonate minerals in continental lithologies are:



Chapter 1

Over shorter timescales, of decades to millennia, carbonate dissolution may provide both a transient sink for anthropogenic CO₂ and, through land-ocean transport of Ca²⁺, Mg²⁺, HCO₃⁻ and CO₃²⁻. These ions provide a source of alkalinity to raise surface ocean pH, increase carbonate mineral saturation state and thus combat ocean acidification (Zeebe *et al.* 2012). Carbonate dissolution acts as a CO₂ sink, potentially sequestering up to 0.15 Gt C per year for the duration that Ca²⁺, Mg²⁺ and HCO₃⁻ remain in solution (Hartmann *et al.* 2013). This equates to approximately half the annual 0.288 Gt C sink, from total carbonate and silicate weathering (Gaillardet *et al.* 1999), and occurs when the rates of forward and reverse reactions in Eqns 1 and 2 are unbalanced (Berner *et al.* 1983). This imbalance occurs when carbonate weathering on the continents is faster than its deposition in marine environments, as may be the case during the accelerated carbonate weathering predicted in response to rising CO₂ and global warming (Beaulieu *et al.* 2012).

The duration of carbon sequestration depends primarily on the residence time of ions in the oceans, and may be as short as 10,000 years (Zeebe *et al.* 2012). These are roughly 10,000 years for HCO₃⁻; 750,000-1,200,000 years for Ca²⁺ and may be >4 million years for Mg²⁺ (calculated after Berner *et al.* 1983; Li 1982; Ronov 1968). Over geological timescales, longer than these considered in the current study, calcite precipitation in the oceans, from carbonate derived Ca²⁺ and Mg²⁺ cations, re-releases CO₂, thus balancing continental carbonate weathering flux (Eqn 3).



Carbonate mineral dissolution is an order of magnitude faster than that of silicates, and the estimated land-ocean flux of total dissolved solids from carbonate weathering, at 588×10^6 - 640×10^6 t year⁻¹, is almost double that originating from silicate weathering, 300×10^6 t year⁻¹ (Gaillardet *et al.* 1999). Globally, carbonate dissolution accounts for 34-68% of the net CO₂ consumption by terrestrial weathering (Berner *et al.* 1983; Gaillardet *et al.* 1999; Amoiette-Suchet *et al.* 2003; Hartmann *et al.* 2009), however, there are still large uncertainties in this value; relating to the strong dependence of carbonate weathering rates on runoff and discharge patterns, and the behaviour of highly active, tropical, weathering hotspots (Hartmann *et al.* 2014).

1.3 Anthropogenic disruption of weathering processes

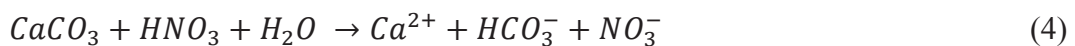
1.3.1 Carbonate weathering and changing agricultural land use patterns

In a warmer climate, sensible planning and management of forestry and agricultural land use patterns may make it possible to enhance weathering rates of carbonate minerals. The impacts of this are twofold, firstly increasing atmospheric CO₂ sequestration, and secondly, countering high-CO₂ related ocean acidification.

Studies analysing historical datasets highlight land use as a critical factor in determining rates of carbonate weathering and alkalinity fluxes to the oceans. Ecosystem disturbance caused by the conversion of natural vegetation to agricultural land leads to increased surface runoff and river discharge (Raymond and Cole 2003; Raymond *et al.* 2008).

In the United States, in both the upper Mississippi and Ohio river catchments, discharge and chemical weathering fluxes of elements such as Ca are higher from agricultural watersheds than from areas with natural vegetation cover, as a result of increased leaching (Raymond and Cole 2003; Raymond *et al.* 2008). Here, conversion of forests to agricultural land is linked to a dramatic, 60%, increase in riverine export of carbonate alkalinity (HCO₃⁻ + CO₃²⁻) from the Mississippi basin in the last 50 years (1954 to 2001), due to both increased runoff and agricultural lime application and dissolution (Raymond and Cole 2003). Agricultural runoff of alkalinity and associated nutrients, including phosphate and nitrate, stimulate algal growth and have contributed to extreme eutrophication in the Gulf of Mexico, severely disrupting its ecology through the formation of anoxic ‘dead zones’ covering an average area of 15,000km², and reaching a record extent of 22,000 km² in 2002 (Diaz and Rosenberg 2008; NOAA 2015). In these hypoxic areas, subsurface ocean acidity is increased, inhibiting biogenic carbonate formation (Cai *et al.* 2011).

In some cases, carbonate weathering may be a net source of CO₂ if weathered by an agent not derived from atmospheric CO₂, such as nitric or sulphuric acids derived from nitrogen-fertilisers or anthropogenic atmospheric pollution (Hartmann *et al.* 2013; Perrin *et al.* 2008). Where manure or nitrogenous fertilisers are applied, microbial nitrification in the soil produces nitrates, which in turn react to form nitric acid, HNO₃, which can substitute for CO₂-derived carbonic acid in carbonate weathering reactions (Eqn 4, 5).



Chapter 1

Fertiliser-derived acids have produced a deficit in the contribution of atmospheric and soil CO₂ to river alkalinity by 7-17% over 30 years in 25 agricultural catchments with carbonate lithology in the Gascogne region of France (Perrin *et al.* 2008). This decrease represents only an estimated 1.6-3.8% of carbonate weathering flux globally, however, is equivalent to 6-15% of global silicate weathering, and may counterbalance this natural weathering CO₂ sink. The effects of anthropogenic acids on carbonate weathering as a CO₂ source are even more dramatic in agricultural areas that are concurrently limed and fertilised, and estimated to release up to 3.35 Tg yr⁻¹ CO₂ in the US (West and McBride 2005).

1.3.2 Impact of agricultural liming on carbonate weathering

In some parts of Europe and North America, forests have been limed to rejuvenate areas damaged by acid rain by ameliorate surface and ground water acidity, replenish leached calcium and reduce associated aluminium toxicity (Blum *et al.* 2002). Amending forest soils with either calcite or dolomite substantially increases carbonate weathering rates (Eqns 1,2) and associated riverine fluxes of carbonate alkalinity (CO₃²⁻, HCO₃⁻), Ca²⁺ and Mg²⁺. In the Hubbard Brook forest watershed weathering of native calcium phosphate apatite grains in the soil has been an important source of alkalinity and calcium ions (Blum *et al.* 2002).

If forest liming is primarily to neutralise acidic pollution by nitric or sulphuric acids, the weathering of additional carbonates will improve stream water quality. However, it will not sequester CO₂ because the acidic weathering agents are not produced from atmospheric CO₂ (Eqns 4, 5), thus paralleling the situation with nitrate fertiliser application.

Liming may indirectly alter soil mineral weathering activity through inducing a shift in the soil microbiome. In Höglwald experimental Forest, Germany, limed plots of Norway spruce had a distinctive mycorrhizal community, including calcium tolerant species, and those with a preference for higher pH (Nowotny *et al.* 1998a,b). It is uncertain how these fungi achieve tolerance, but one mechanism could include increasing mycorrhizosphere acidification and consequent carbonate weathering. Because forests and their associated mycorrhizas are key drivers of mineral weathering, any changes in tree growth or fungal community structure will undoubtedly affect mineral weathering rates; however, this is poorly documented and should be an area for future forestry research.

The role of trees and their mycorrhizas in carbonate weathering

1.3.3 Carbonation of industrial waste sequesters CO₂ in urban soils

Human activity disrupts weathering process not only in forests and agricultural land, but also in urban soils. Enhanced carbonate weathering may provide a new means of CO₂ sequestration, via the carbonation of industrial waste materials.

Every year, an estimated 7-17 billion tonnes of artificial silicate waste materials are produced globally. These have the potential to sequester 190-332 million tonnes urban C through carbonation and precipitation of pedogenic carbonates (Renforth *et al.* 2011). If these carbonates later weather, temporary CO₂ consumption could be even greater over the duration weathering products remain in solution. Inevitably, carbonation of artificial silicates in soils, and pedogenic carbonate weathering, only sequesters a fraction of the CO₂ released during manufacture. It is unlikely to totally compensate for material manufacturing emissions and should not, therefore be looked on as a net carbon store.

Carbonation partially reverses the CO₂ emissions produced as limestone is burned in cement manufacture, consuming CO₂ and precipitating carbonates, at a rate far higher than typically seen in agricultural soils (Renforth *et al.* 2011; Manning and Renforth 2013). Carbonation may occur via reaction with soil CO₂ derived H₂CO₃ (Renforth *et al.* 2011), or potentially from photosynthetically-derived organic exudates (Landi *et al.* 2003; Manning and Renforth 2013).

Following construction or demolition activities, material derived from artificial sources such as cements, mine waste, iron slag and ash dusts become incorporated into urban soils. Those materials which are Ca-silicate based have carbonation potential (Renforth *et al.* 2011), and this process has been studied over the last decade at two brownfield sites in the north of England, both in Newcastle and at former steelworks in Consett. At these sites, carbonation of industrial waste materials is primarily an abiotic process and sequesters an estimated $25 \pm 12.8 \text{ t C ha}^{-1} \text{ yr}^{-1}$ (Renforth *et al.* 2009). The size of this potential CO₂ sink could be enhanced by vegetation planting in order to increase soil CO₂ concentration, a possible limitation on carbonation rate.

1.4 Carbonate mineral weathering in soils

The controls on weathering in soils can be split into two main categories; firstly, relating to the weathering rock itself and secondly, to its surrounding environment. Environmental variables mainly relate to either climate, or properties of the surrounding soil, including water residence times, pH, and the effects of vegetation and microbiota. The environmental and biological factors mediating mineral dissolution are summarised in Figure 1.2, and effects of the abiotic controls; hydrology, temperature and pH are reviewed in the following section.

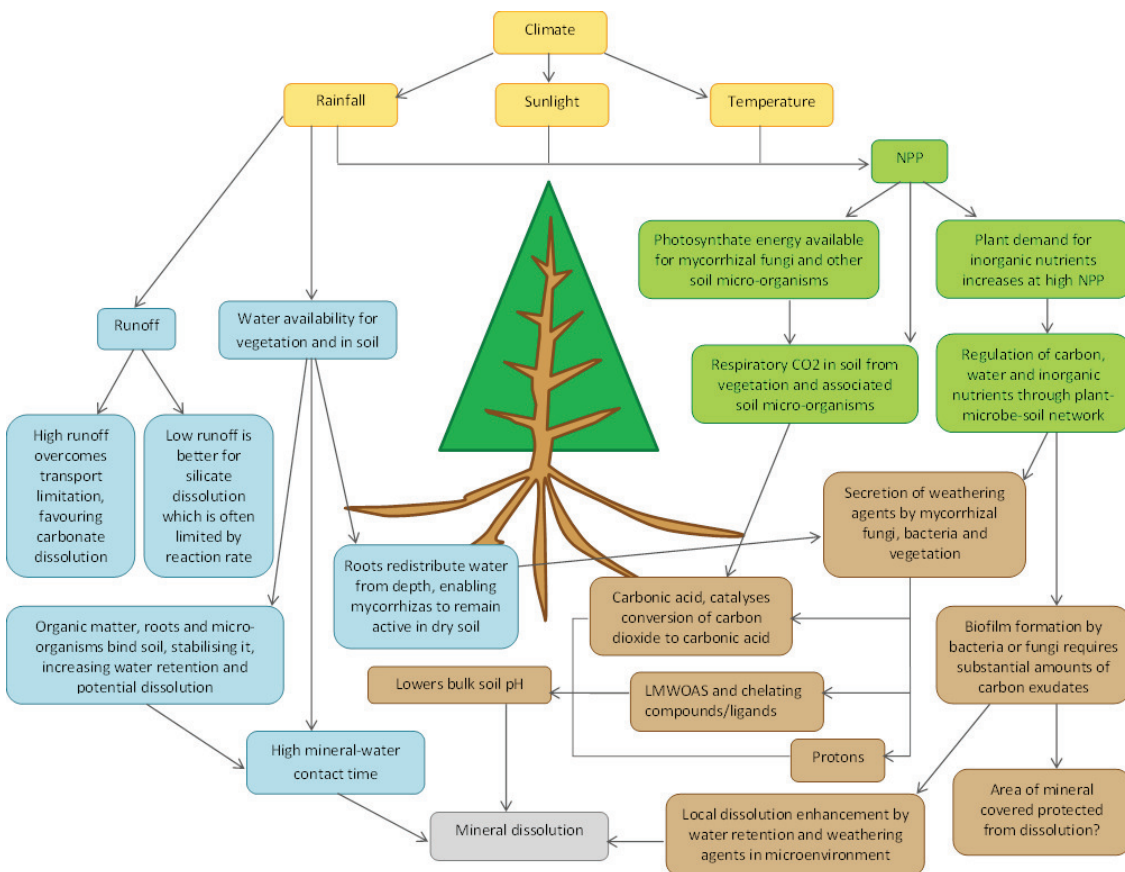


Figure 1.2. Flow diagram summarising major environmental and biological controls on mineral dissolution in forest soils. Of the environmental controls, factors linked to climate are highlighted in yellow and those linked to water and its interactions with soil hydrology in blue. Biological factors regulating weathering are coloured in green if they are primarily controlled by vegetation and brown where they mainly involve soil-micro-organisms.

1.4.1 Abiotic controls on carbonate weathering

1.4.1.1 Surface reaction versus mass transport weathering limitations

Rocks only weather when exposed to water. This makes soil hydrology very important as it determines water-mineral contact times, and consequently, the potential for dissolution reactions. Carbonate dissolution rates may be either transport-limited or surface reaction-limited. Transport limitation occurs when equilibrium (Eqns 1 & 2) is reached, but further dissolution is inhibited by inadequate removal of weathering

products, which can also lead to secondary mineral precipitation. Reaction-limited systems lie far from equilibrium and although weathering products can be removed rapidly, slow dissolution kinetics prevents any increase in reaction rate.

Carbonate dissolution kinetics are rapid, and as a result, weathering is usually most effective in environments with high runoff. Laboratory experiments showed both dolomite and limestone dissolution could be increased by a factor of 3 and 4, respectively, if transport limitation was reduced by increasing water flow over weathering surfaces (Liu 2001; Liu *et al.* 2005a).

1.4.1.2 Carbonate weathering rate dependency on soil pH environment

Carbonates are highly susceptible to dissolution in acid environments (Cubillas *et al.* 2005). Their dissolution occurs via three main mechanisms (Eqns 6-8) and the dominant weathering reaction is determined by the specific pH and pCO₂ environment (Chou *et al.* 1989; Palandri and Kharaka 2004; Brantley *et al.* 2008). Between pH 3.5-5.5, calcite dissolution is strongly dependant on pH (Arvidson *et al.* 2003; Cubillas *et al.* 2005); in lower pH environments (pH < 3.5) calcite dissolution is generally transport controlled and not dependent on pCO₂ (Brantley *et al.* 2008). When pH > 5.5, re-precipitation reactions are sufficiently thermodynamically favourable and can impact dissolution rate. However, all these relationships are based on experiments performed at 25°C in laboratory batch or flow experiments. In the field situation; it is likely that transport will still be rate-limiting even at pH > 3.5, due to longer water residence times in soils and dissolution reactions occurring close to equilibrium.

Acidic pH (< pH 7) with low pCO₂:



Neutral pH (ca. pH 7) with high pCO₂:



High pH (> pH 7) with low or no pCO₂:



Chapter 1

1.4.1.3 Acidic forest soils in Europe

In general, most soils in northern Europe, where this study is based, are acidic (Figure 1.3). The lowest pH values occur where soils have formed from acidic parent materials such as granite, quartz and sandstones and the highest values are found where soils overlie calcareous sediments and basic rocks, and lowest pH. Forests, on average exhibit the lowest topsoil pH, due to both organic acids from organic matter decomposition and the abundant supply of photosynthates supporting microbial communities and enabling high soil respiration.

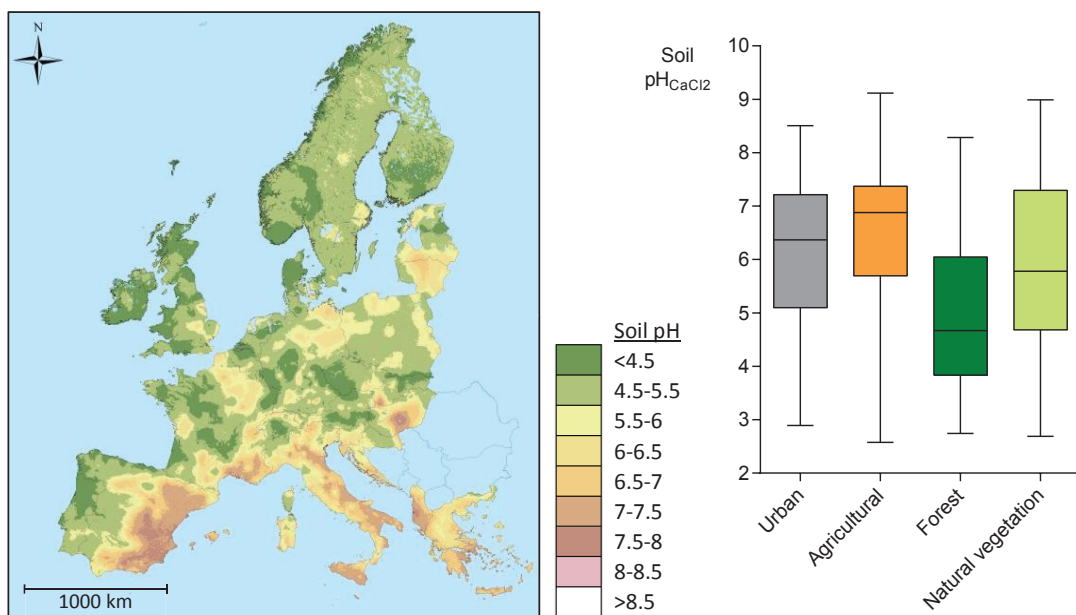


Figure 1.3. **A)** Estimated pH of European topsoil modelled using data compiled from 11 datasets containing pH measurements from the European Soil Data Centre (Montanarella 2010). **B)** Estimated soil $\text{pH}_{\text{CaCl}_2}$ by land use within Europe. Box plot shows median, 25th and 75th percentile values and whiskers denote maximum and minimum pH measurements, adapted from Montanarella (2010).

1.4.1.4 Weathering rate dependence on temperature

Temperature is the climatic variable with the most easily predicted impact on mineral dissolution rates. The rates of most chemical reactions increase exponentially with temperature, for which there is a well-established thermodynamic basis.

In order for a chemical reaction to occur, molecules must collide in the correct orientation with sufficient energy. The rate of most chemical reactions can be increased by either decreasing the activation energy, E_a , or increasing reaction temperature. This relationship is described by the Arrhenius equation (9), with k , the temperature dependant rate constant at temperature T ; R , the molar gas constant; and A , the pre-exponential factor. The pre-exponential factor, A , has the same units as the rate constant, and represents the number of collisions between reagent molecules that have

The role of trees and their mycorrhizas in carbonate weathering

the correct orientation for a reaction. The second term, $e^{-E_a/RT}$ describes the probability that any single collision will result in a reaction.

A higher proportion of successful collisions can be realised through increasing the temperature; effectively increasing the frequency of collisions as particles move faster; or through lowering the activation energy barrier, E_a . Activation energies, E_a , are largely approximated to remain constant over the range of temperatures used within weathering experiments. E_a for dissolution of common Ca- and Mg-silicate minerals generally lies between 50-120 kJ mol⁻¹ (reviewed in White 2003).

$$k = Ae^{-E_a/RT} \quad (9)$$

As carbonates are more soluble than silicates, these tend to have lower activation energies. Values of E_a for carbonate dissolution in acidic conditions, from a compilation of weathering rate constants (Palandri and Kharaka 2004), are 36.1 kJ mol⁻¹ and 14.4 kJ mol⁻¹ for sedimentary dolomite and calcite respectively.

Kirstein *et al.* (2016) recently performed a study investigating the effect of low-temperatures between 5 and 26°C on the dissolution of dissolution naturally occurring carbonates. This looked at the behaviour of three Triassic carbonates; fine-grained micrite and coarser-grained spartic limestone, in comparison with dolomite in batch and flow-through dissolution experiments. Results were used to calculate apparent dissolution rates and activation energies in a system far from equilibrium. These were 22.3 kJ mol⁻¹ for dolomite, 19.8-22.2 kJ mol⁻¹ for spartic limestone and 51.0 kJ mol⁻¹ for micrite. The values of E_a obtained for limestones fell within the range of E_a s determined in higher temperature studies of calcite, 6-50 kJ mol⁻¹ (reviewed in Kirstein *et al.* 2016) as do those compiled by Palandri and Kharaka (2004). However, this study does highlight the natural variation in thermodynamic constants, and its dependence not only on mineralogy, but also rock structure.

1.4.2 Biotic controls on carbonate weathering

Forests are the main biotic drivers of continental mineral weathering through symbioses with root-associated soil fungi, known as mycorrhizal fungi. Mycorrhizal fungi act as a pathway for carbon and nutrient fluxes through soil and are central in the supply of mineral nutrients to most plants on Earth, utilising energy from plant photosynthates to grow, proliferate and actively dissolve soil minerals (reviewed in Brantley *et al.* 2011).

Chapter 1

This section first describes the tree-mycorrhizal partnership and evolutionary basis for biotic weathering, before reviewing the key mechanisms by which trees and their symbiotic AM and EM fungi accelerate carbonate mineral weathering.

1.4.2.1 The tree-mycorrhizal symbiosis

Mycorrhizal fungi have co-evolved with plants since their origin ~400 million years ago (Reviewed in Taylor *et al.* 2009). They are ubiquitously associated with plants dominating terrestrial ecosystems (Smith and Read 2008). There are two major groups of mycorrhizal fungi within forest rhizosphere microbial communities, arbuscular mycorrhizas (AM) and ectomycorrhizas (EM). The mycelia of both AM and EM fungi may constitute 20%–30% of total soil microbial biomass, often extending to tens of metres per gram of soil. Mycorrhizas provide extensive pathways for carbon and nutrient fluxes, receiving in excess of 10% of net host C-fixation (Leake *et al.* 2004); the main features of AM and EM fungal types are summarised below.

1.4.2.2 Arbuscular mycorrhizal fungi (AM)

AM associations are formed by 70% of plant species globally, both angiosperm and gymnosperm, and have been identified in the fossil record of early gymnosperm roots dating from at least the Carboniferous (Wang and Qiu 2006; Smith and Read 2008). AM fungi are obligate biotrophs, and colonise host plant roots using intracellular structures called arbuscules (Figure 1.4). These highly branched, filamentous structures are linked by intraradical hypha and form the main site for carbon and nutrient exchange between symbionts. AM fungi forage for nutrient elements in soils via a network of extraradical mycelia which grows out of the host root and is anchored by its arbuscules (Smith and Read 2008). In particular, AM fungi have a high affinity for the uptake of phosphorus (Smith and Smith 2012), which is relatively immobile in soils (Section 1.4.3.2) and commonly limits host plant growth.

1.4.2.3 Ectomycorrhizal fungi (EM)

EM fungi evolved in the Cretaceous, independently of, and more recently than AM fungi, and belong to the two higher fungal phyla Basidiomycota and Ascomycota. Only 2% of plant species associate with EM fungi, however, this 2% includes gymnosperm Pinaceae, and angiosperm Betulaceae and Fagaceae, that dominate most boreal and temperate forests, in addition to some abundant tropical forest species such as angiosperm Dipterocarpaceae, Fabaceae and Myrtaceae (Smith and Read 2008; Taylor *et al.* 2009).

The role of trees and their mycorrhizas in carbonate weathering

The symbiosis between host plants and EM fungi is very different from that with AM fungi. EM fungi form a mycelial sheath, or fungal mantle which interfaces with host plant cells via the Hartig net. This intercellular structure is the site of carbon and nutrient exchange and forms as hyphae penetrate between root cortical cells (Figure 1.4). The extraradical mycelium allows EM fungi to interact with the surrounding substrate. The fungal mantle may completely surround over 95% of host plant root tips (Taylor *et al.* 2000), making EM mycelium the primary organ interacting with surrounding substrate and transferring water and nutrient elements (Leake *et al.* 2004).

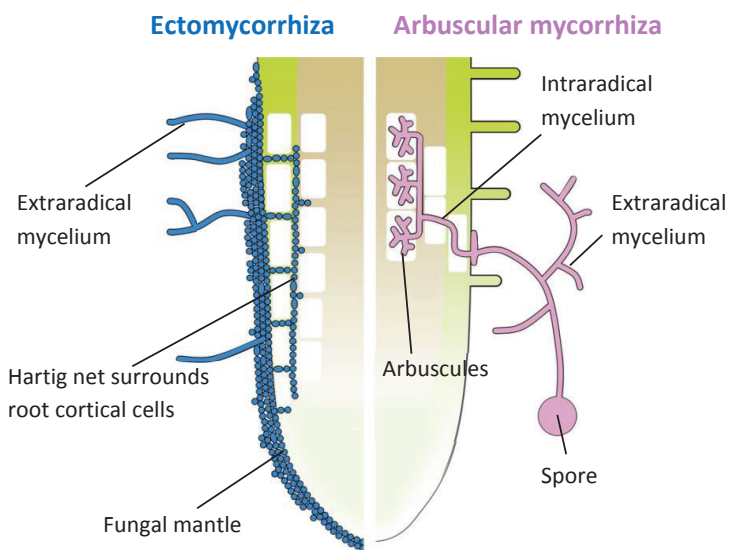


Figure 1.4. Illustration of EM (blue) and AM (pink) root colonisation highlighting main structural differences. From Bonfante and Genre (2010)

1.4.3 Function of mineral plant-mycorrhizal weathering

If mycorrhizal mineral weathering is an active process by plants or micro-organisms, it must have an evolutionary basis or confer some physiological advantage, such as access to growth-limiting nutrients.

Roots promote mineral weathering, but their distribution throughout the soil is limited, restricting their ability as a weathering agent. Mycorrhizal fungal, on the other hand, have an extensive mycelium, accelerating weathering by both physical and chemical methods giving them a far greater ability to rapidly colonise and exploit pockets of essential nutrients, for example phosphorus from apatite inclusions within feldspars (Reviewed in Landeweert *et al.* 2001). Rock dissolution is energetically costly, but enables mycorrhizas to access newly exposed mineral surfaces in a competition-free niche (Cockell and Herrera, 2008).

Chapter 1

1.4.3.1 Calcium and Magnesium acquisition

In carbonate rocks, the main inorganic nutrients are calcium, and also magnesium in dolomitic rocks. These elements are usually not of limiting availability in forest soils, so it is unlikely that active weathering would occur solely for the acquisition of these elements. However, carbonate weathering may be a mechanism to access growth-limiting trace elements within the rock, possibly P, with the release of Ca and Mg as by-products.

This is probably the case in one base-poor forest surveyed in New Hampshire, USA. Here, Strontium isotope tracer experiments indicate that up to 95% of Ca in EM spruce and fir tissues originates from weathered apatite, despite this accounting for only 12% of total soil Ca (Blum *et al.* 2002). Apatite refers to a group of minerals, rich in phosphorus, and used in fertiliser manufacture. The most common minerals in this group are hydroxylapatite, fluorapatite and chlorapatite, which contain high concentrations of OH⁻, F⁻ and Cl⁻ respectively, and have the general formula $\text{Ca}_{10}(\text{PO}_4)_6(\text{OH},\text{F},\text{Cl})_2$.

There are examples where soil Ca-limitation, caused by acid rain, has disrupted physiological function of trees, such as in the Hubbard Brook Experimental Forest, New Hampshire (Schaberg and Hawley 2010; Halman *et al.* 2008). Ca solubility and leaching was increased by soil acidification through a ~50 year period of pollution by acid rain decreased atmospheric Ca deposition and extensive leaching; which concurrently increased availability of available Al in soil. A number of physiological disruptions specific to Ca-limitation were observed in Red spruce (*Picea rubens*) and Sugar maple (*Acer saccharum*) seedlings. These included reduced cold tolerance and sugar storage in the leaves, both of which were alleviated by addition of wollastonite (CaSiO₃) to provide a gradual release of Ca into soils to raise concentrations to pre-industrial levels.

1.4.3.2 Phosphorus acquisition

Phosphorus exists in a variety of forms in the soil; however, little of this is available for uptake by plants. Plants can only use P in the form of orthophosphate which is typically present only in low concentrations (0.5 – 10 μM), and other inorganic and organic forms must first be made available through weathering or mineralisation, respectively (Smith and Read 2008). As plants and micro-organisms remove P from the soil water pool, it is continually replenished by P from other sources within soil (Figure 1.5). These are primarily inorganic P adsorbed to soil aggregates; that in metal-phosphate compounds, such as those formed with aluminium and calcium, iron and

The role of trees and their mycorrhizas in carbonate weathering

magnesium (Walker and Syers 1976; reviewed in Liu *et al.* 2016); and organic P that can be easily mineralised by soil micro-organisms.

Mycorrhizal weathering for P acquisition effectively bypasses the gradual processes replenishing orthophosphate in the soil solution, and permits direct uptake of P from minerals such as apatite. Microcosm experiments indicate that when phosphorus supply is limited, host plants provide their mycorrhizal fungi with a greater quantity of photosynthetic carbon in order to facilitate growth, soil exploration and P-uptake (Hagerberg *et al.* 2003; Leake *et al.* 2008; Smits *et al.* 2012).

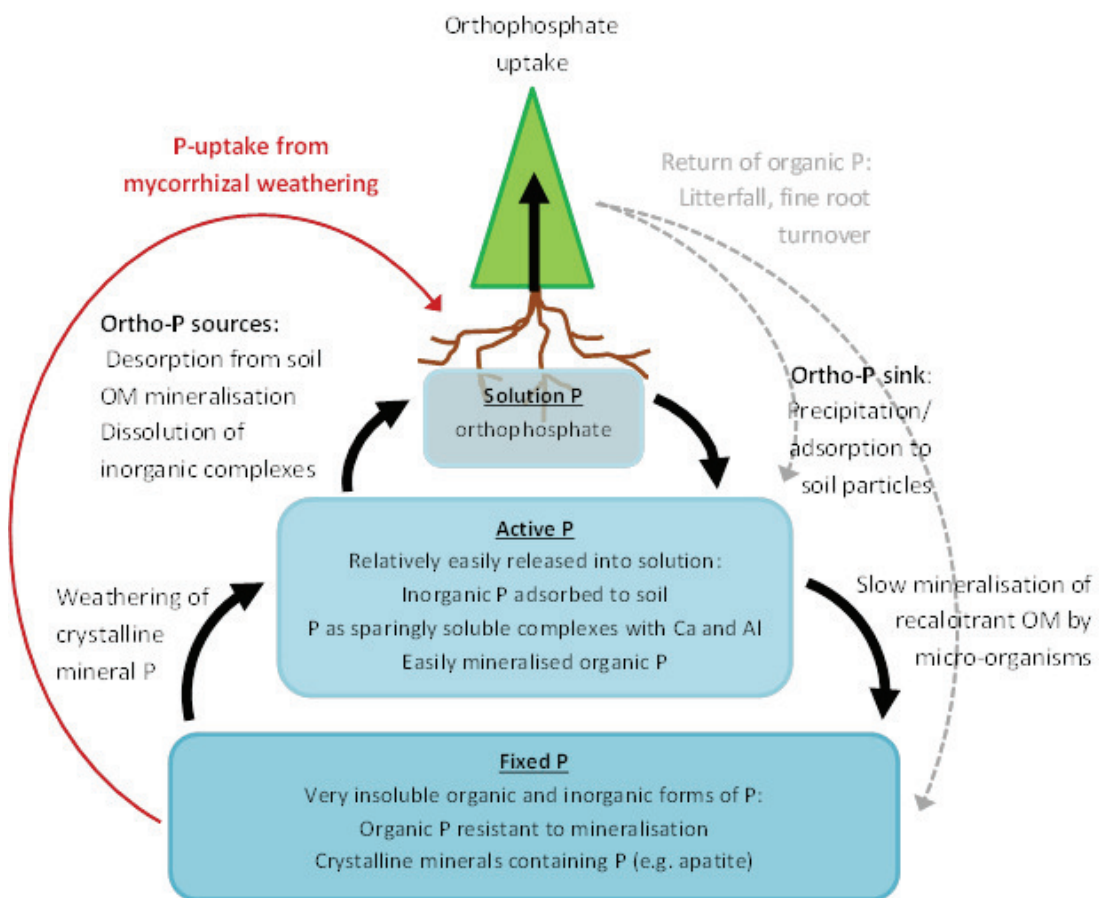


Figure 1.5. Summary of phosphorus cycling in soils. Only orthophosphate, from solution is available for plant uptake, and this is continually replenished by mineralisation of organic matter (OM), and weathering of mineral P from fixed and active soil pools. Mycorrhizal weathering (red) enables host plants to directly uptake P from mineral sources.

1.5 Mechanisms of carbonate weathering by tree-mycorrhizal partnerships

Mineral weathering mechanisms of both AM and EM fungi have been recently reviewed in relation to silicate weathering (Rosling *et al.* 2004a,b; Wallander & Thelin 2008; Taylor *et al.* 2009; Brantley *et al.* 2011). In this section, we highlight three key weathering strategies of mycorrhizal fungi with emphasis on how they relate to carbonates:

1. Physical weathering by hyphae penetrating or trenching minerals.
2. Action of respiratory CO₂-derived carbonic acid, and mycorrhizal secretion of carbonic anhydrase enzyme to catalyse its formation.
3. Chemical weathering by secreted organic acids and chelating cations that acidify the rhizosphere and complex metal cations.

The order of importance of these methods is debatable (Li *et al.* 2009) and weathering is likely to be due to a combination of these in addition to other mechanisms, such as secondary mineral formation and secretion of iron-chelating siderophores. These latter methods probably have a lesser effect on carbonate rock weathering and are discussed briefly at the end of this section.

1.5.1 Physical surface weathering by mycorrhizal hyphae

Narrow mycorrhizal hyphae (typically 3-10 µm diameter) can follow contours of rock surfaces, growing along scratches or grooves and entering rock pores or cracks (Figure 1.6), promoting weathering by widening existing fissures or delaminating mineral cleavage planes as they grow between them (reviewed in Landeweert *et al.* 2001; Hoffland *et al.* 2002, 2003). Hyphae are able to strongly attach to rock surfaces, exerting physical force via turgor pressure. The force produced by growing tips of EM hyphae can distort mineral structure, as has been seen for biotite (Bonneville *et al.* 2009, 2011). It is commonly quoted that appressoria of fungal pathogens can exert pressures up to 8 MPa as they enter plant cells (Howard *et al.* 1991), however, the forces produced by growing over mineral surfaces are far less than this, and usually in the range 0.4 – 1 MPa (reviewed in Gazzè *et al.* 2013).

Little research has focused on the importance of hyphal contact for carbonate weathering, compared to that for silicates. One liquid culture experiment using *Penicillium* spp. found that limestone dissolution was reduced by 22% when a fine mesh separated weathering rock grains from the fungal culture. In this experiment a saprotrophic *Penicillium* spp. was incubated with limestone grains for 25 hours and weathering rates calculated from measurements of solution pH and Ca²⁺ concentration.

The role of trees and their mycorrhizas in carbonate weathering

However, results from such experimental setups may bear little resemblance to fungal-mineral interactions in more complex substrates, such as soil. Carbonate surface trenching has been observed on polished marble in one peat microcosm experiment containing *Pinus sylvestris* with *Heboloma crustaliniforme* as a mycorrhizal partner (Rosling 2003; Figure 1.6C), although the morphology of this putative channel cannot be elucidated from this SEM image.

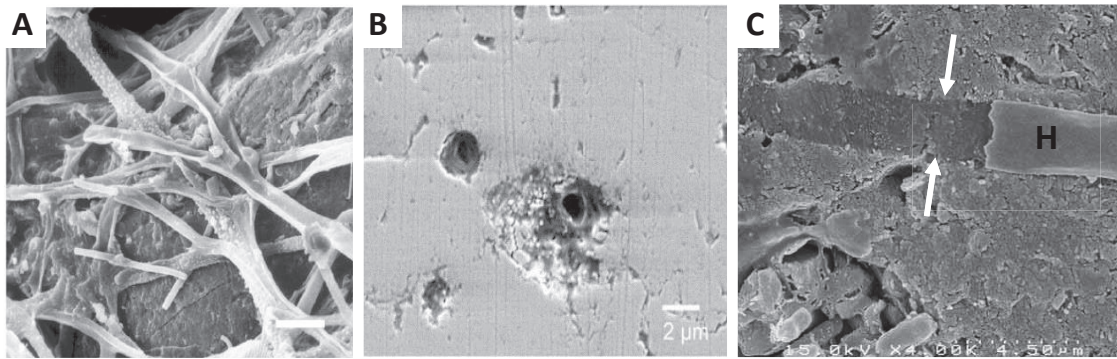


Figure 1.6. Scanning Electron Microscopy (SEM) images of **A**) EM fungal mycelium surrounding a rock grain (From Landeweert *et al.* 2001); **B**) ericoid fungal hyphae penetrating Dachstein limestone, colonised by an endolithic lichen, 30-100 years after rock exposure by glacial retreat (Hoppert *et al.*, 2004); **C**) hyphal track on a marble surface, following 4 months of *H.crustuliniforme* colonisation in a peat microcosm (Rosling 2003). A fungal hypha (H) has been partially removed to expose the marble surface between the white arrows.

1.5.1.1 Contribution of hyphal tunnelling to total mineral weathering

One facet of mycorrhizal mineral weathering that is often discussed and investigated is the ability of hyphae to etch channels across mineral surfaces, and even to tunnel into the interior of homogenous rock grains (Figure 1.6B, Figure 1.7), possibly as a mechanism to access limiting inorganic nutrients.

Tunnels are likely to be formed through a combination of physical force and exudation of localised chemical weathering agents such, as by Low Molecular Weight Organic Acids (LMWOAs), from hyphal tips (Jongmans *et al.* 1997; Hoffland *et al.* 2002; Smits 2006). Tunnels are more frequently observed at sites where plants have limited nutrient availability, indicating that their formation may be driven by mineral nutrient demand (Hoffland *et al.* 2003). Although it is energetically costly to tunnel into minerals, it could provide mycorrhizal fungi with exclusive access to fresh mineral surfaces and competition-free nutrient sources such as P-rich apatite inclusions in feldspar grains (Blum *et al.* 2002; Cockell and Herrera 2008).

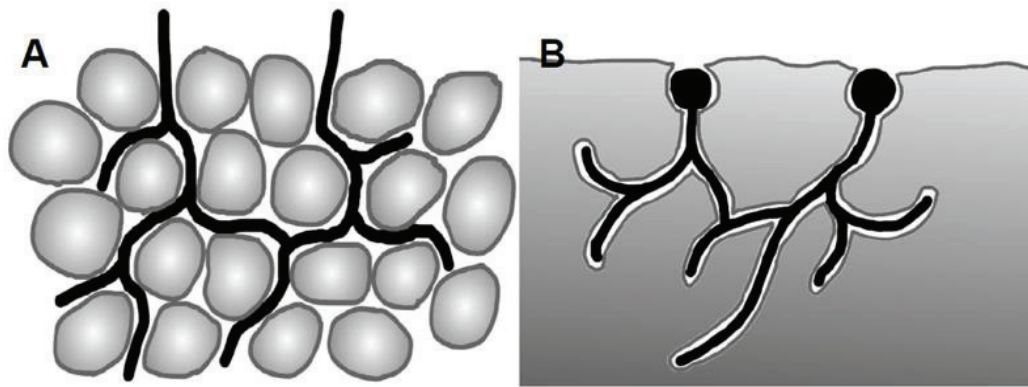


Figure 1.7. Rock penetration by fungal hyphae. **A)** Exploitation of weaknesses such as grain boundaries or mineral cleavage planes; **B)** Pitting and tunnelling into homogenous rock likely to be achieved through exudation of weathering agents such as LMWOAs from hyphal tips and removal of weathering products. Hyphal tunnelling may be promoted on rock surfaces where etch pits have already formed.

Hyphal tunnelling has been observed both in silicate rocks, in ecosystems dominated by EM-associated plants (Hoffland *et al.* 2002, 2003; Smits *et al.* 2005; Koele *et al.* 2014); and in limestone colonised by an endolithic lichen, where both fungal and algal partners live beneath the rock surface (Hoppert *et al.* 2004). Fungal tunnels are identified based on their morphology, having smooth sides, rounded ends and constant diameters (Koele *et al.* 2014; Hoffland 2003). Tunnel diameters measure 4.8-5.6 μm in Ca- and K-feldspars in Michigan (Smits *et al.* 2005); and generally between 3-10 μm , as for tunnels measured in K- feldspar grains in N.Swedish podsols (Hoffland 2002, 2003); and in both feldspar and hornblende in podsol E-horizons below *P.sylvestris*, *Picea abies* and ericaceous shrubs in Sweden, Denmark, Finland, Switzerland and the Netherlands (Jongmans 1997).

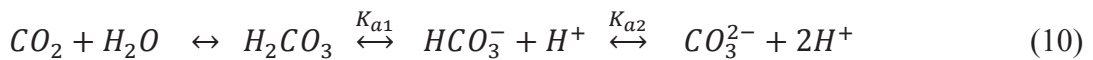
Tunnelling is likely to account for only a small proportion of total mineral weathering. When tubular tunnel volume is quantified relative to total volume of weathered mineral, it contributes only 0.5% of total feldspar weathering in a temperate coniferous ecosystem at Lake Michigan, USA (Smits *et al.* 2005) and potentially up to a maximum of 2% (reviewed in Smits *et al.* 2005 and Sverdrup 2009). Fungal tunnelling is slow, and such weathering features are more common in older soils and only seen where soils have been forming for over 1000 years (Hoffland *et al.* 2002, Smits *et al.* 2005, 2006), however, tunnel formation may be hastened by targeted dissolution of existing etch pits. While the direct contribution of tunnel formation to total weathering is not large, there may be a greater indirect effect on weathering through increasing surface area and providing access routes to previously unavailable mineral surfaces.

The role of trees and their mycorrhizas in carbonate weathering

It is also important to note that tunnels can be formed by purely abiotic factors and their interaction with the heterogeneous crystal structure of different minerals in rocks (Sverdrup 2009). Dissolution tunnels observed in Hawaiian basalts, surveyed by Cochran and Berner (1996), were likely to be of abiotic origin. Here, voids in weathered rock sections often trace back to cooling cracks or other defects in relatively unweathered rock sections. In these basalts, the width of fine dissolution channels changed abruptly across mineral grain boundaries, with narrow, 2-3 μm , tunnels widening five-fold to 10-15 μm .

1.5.2 Rhizosphere acidification by respiratory CO_2 production

Carbonic acid forms when carbon dioxide from the atmosphere or soil reacts with water (Eqn 10). It is the primary abiotic weathering agent of soil minerals (reviewed in Landeweert *et al.* 2001), and in many regions with limestone bedrock, where it causes the formation of karstic features as rock weathers. Carbonic acid is diprotic and has two protons that are able to dissociate, with dissociation constants of $K_{a1} = 4.4 \times 10^{-7}$ and $K_{a2} = 4.7 \times 10^{-11}$ respectively (Masterton and Hurley 2005). At atmospheric pCO_2 and 298K, the first proton partially dissociates to form a weakly acidic solution of approximately pH 5.65.



The rate of carbonic acid formation depends on the availability of CO_2 substrate, or pCO_2 , and possibly also on the type of carbonate mineral weathering (Liu 2001; Liu *et al.* 2005a). Carbon dioxide partial pressures in the atmosphere (~ 40 Pa; Tans and Keeling 2013) are far lower than within soil where it accumulates from the respiration of plant roots and soil micro-organisms. Soil pCO_2 is highly variable and, in part, depends on the environment, with tropical forests (Trinidad; $\text{pCO}_2 = 25500$ Pa) exhibiting greater soil pCO_2 than either temperate forests (Germany; $\text{pCO}_2 = 15300$ Pa) or Arctic regions (Alaska; $\text{pCO}_2 = 7600$ Pa; Brook *et al.* 1983). As soil pCO_2 is higher than that in the atmosphere, carbonic acid can dissociate to form solutions of greater acidity than possible than under atmospheric conditions.

1.5.2.1 Role of carbonic anhydrase (CA) in enhancing carbonate weathering

Because carbonic acid formation is slow at ambient pCO_2 , this can limit rates of limestone dissolution (Eqns 1 & 2; Liu *et al.* 2005a). Soil microbial communities can enhance carbonate weathering processes by producing carbonic anhydrase (CA), an enzyme that catalyses the conversion of soil CO_2 into carbonic acid (Eqn 11; Li *et al.* 2005a,b). CA activity therefore reduces the impact of the rate limiting carbonic acid

Chapter 1

formation step as long as soil drainage permits the end-products of dissolution to be removed (Lian *et al.* 2011).



Abiotic kinetic experiments tracking solution conductivity, as a proxy for dissolved Ca^{2+} and Mg^{2+} , have shown an addition of 0.2 μ M bovine CA can accelerate initial calcite dissolution rates up to 10-fold, but only when solution pCO_2 exceeds than 100 Pa. The magnitude of rate enhancement by CA depends on both grain size and rock type (Liu *et al.* 2001, 2005a), and its addition has much less effect on dolomite dissolution, only increasing initial dissolution rates 2-4-fold. Dolomite dissolution kinetics are far slower than those of calcite, and this may impose greater restriction on its weathering rate than the availability of carbonic acid.

CA secreting bacteria have been isolated from Karstic environments (Li *et al.* 2005b), and genes coding for CA synthesis are expressed in EM fungi (reviewed in Landeweert *et al.* 2001; Elleuche and Pöggeler 2009) and have been identified in AM fungi (Tisserant *et al.* 2012). In the field, densely vegetated areas overlying limestone areas in China, areas with were found to have high CA activity, which was linked to CA secretion by fungi (Li *et al.* 2005a). Soil CA activity was highest at the surface, in proximity to plant roots, and declined sharply with depth. No mycorrhizal fungi were explicitly identified; however, their involvement was implicated as several plots were sited within evergreen broad-leaf and needle-leaf woodlands, where trees universally form mycorrhizal associations. There is still no consensus on the extent CA increases carbonate weathering rates in forest ecosystems, nor on the contribution of mycorrhizal fungi to this process; presenting an interesting angle for future studies.

1.5.3 Carbonate weathering by LMWOAs

Due to the susceptibility of carbonates to acid dissolution (Cubillas *et al.* 2005), LMWOAs are potentially their most important biological weathering agent (Landeweert *et al.* 2001). LMWO anions are powerful chelators by virtue of their ability to delocalise several negative charges across carboxyl groups. They are able to form several ionic bonds when they surround small, charge-dense cations (Figure 1.8). This allows them to chelate a variety of metal cations, facilitating weathering when the bonding between the LMWO anion and cation is stronger than that between the cation and mineral surface. The most effective dissolution by LMWOAs occurs near the pH of the organic acid pK_a . At this point the organic acid is half dissociated, so there are both protons and organic anions available to promote mineral weathering via both acid dissolution and chelation on metal cations (reviewed in Konhauser 2009).

The role of trees and their mycorrhizas in carbonate weathering

These compounds are secreted by plants, fungi and other soil micro-organisms, and have previously been implicated in laboratory weathering studies through acting to enlarge existing scratches and pits on mineral surfaces (Gazzè *et al.* 2012). Where present in adequate concentrations, these LMWOAs may be more important than carbonic acid in accelerating mineral dissolution, as they combine soil solution acidification with the ion chelating ability of their organic anions. Their relative importance was suggested by the results of a liquid culture experiment investigating the influence of *Penicillium* spp. inoculation on carbonate dissolution (Li *et al.* 2009). This study showed that carbonate dissolution was inhibited more when organic acids in solution were neutralised than when CA production was inhibited by addition of acetazolamide.

Both tree species and mycorrhizal partner influence the range of LMWOAs produced, which can include butyric, citric, formic, lactic, malonic, oxalic, phthalic, succinic and tartaric acids (Arvieu *et al.* 2003; Casarin *et al.* 2003; Sandnes *et al.* 2005). Several mono- di- and tri-carboxylic acids are secreted by EM fungi, depending on the fungal species; these include malic and citric acids and the most acidic EM exudate, oxalic acid (Gadd 1999; Arvieu *et al.* 2003; van Scholl *et al.* 2006a). AM fungi are generally thought to be unable to secrete LMWOAs, however, one study of clover plants associated with AM fungi identified two mono-carboxylates, formate and acetate, in culture medium surrounding AM mycelium (Toljander *et al.* 2007). Although these mono-carboxylates do form acidic solutions, compared to the di- and tri-carboxylic acids produced by EM fungi, they have limited capacity for complexing cations as they can only carry a single negative charge.

The overall contribution of LMWOAs to mineral weathering is still uncertain as in bulk soil their concentrations may be too low for any significant impact on weathering rates. Typical concentrations in the field are in the range <0.1-17 μM , and in laboratory pot experiments from <0.1-2.3 μM (van Hees *et al.* 2002, 2003). LMWOAs form only a minor component of the total organic acid complement of soils; are easily adsorbed to soil particles; rapidly precipitated in complexes; and have a rapid turnover rate, partly due to their low molecular mass making them an easily biodegradable substrate (van Hees *et al.* 2002). The main dissolution mechanism of LMWOAs is likely to be more targeted than that of other weathering agents, through formation of a layer of organic exudates, or a biofilm, and causing local rhizosphere acidification directly in contact with mineral surfaces (Saccone *et al.* 2012).

Chapter 1

1.5.3.1 Oxalate production by EM fungi

Oxalic acid is likely to be the most important LMWOA involved in carbonate weathering (Gadd 1999), partly because it is typically secreted faster than other minor LMWOAs. Oxalate secretion causes simultaneous mycorrhizosphere acidification as its release is coupled to that of protons. This coupling is suggested by the strong correlation between oxalate concentration and pH in liquid culture experiments (Arvieu *et al.* 2003; Casarin *et al.* 2003), and will intensify its effect on carbonate dissolution.

Oxalate production is well characterised in many EM species as well as other soil micro-organisms (Arvieu *et al.* 2003; van Scholl *et al.* 2006a). Depending on the soil redox environment, oxalate can form complexes with a range of metal cations including K, Mn, Zn, Cu, Al and Fe from silicate minerals, and Mg and Ca cations from carbonates (Figure 1.8; Gadd 1999; Landeweert *et al.* 2001).

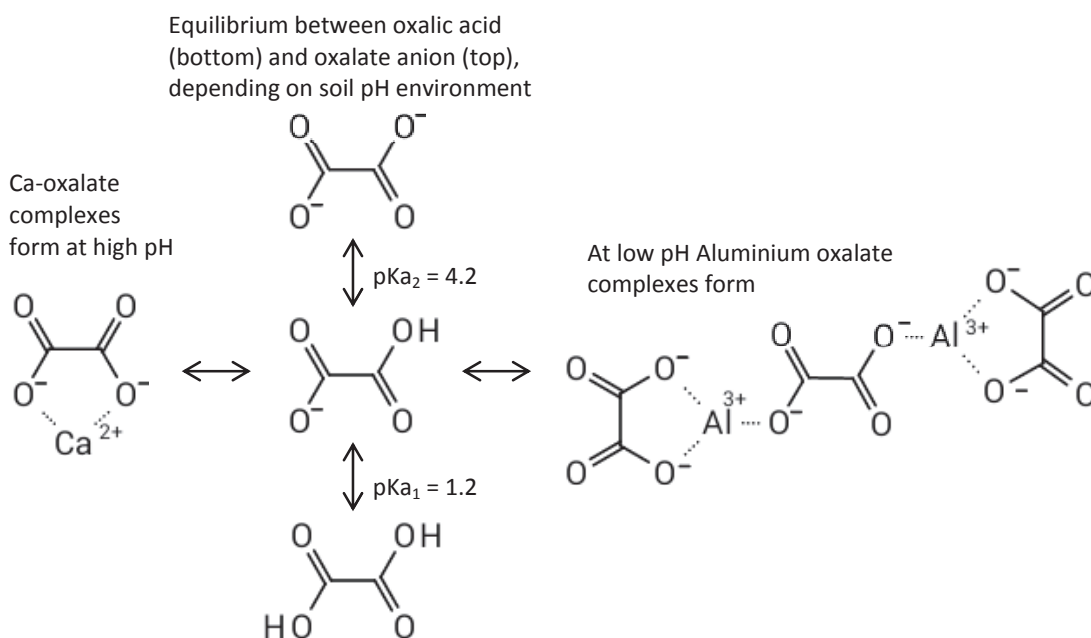


Figure 1.8. Oxalic acid dissociation (centre) and formation of LMWOA-metal complexes with Ca^{2+} or Mg^{2+} (left) and with Al^{3+} or Fe^{3+} (right). Formation of metal complexes may alleviate toxic effects of elements such as Al by reducing their bioavailability and up-take by roots, or through preventing their complexation with other nutrients, particularly P, resulting in higher nutrient availability (Jones and Darrah 1994; Eldhuset *et al.* 2007).

1.5.3.2 Secondary mineral formation: calcium oxalate

Ca-oxalate crystals are commonly identified surrounding fungal hyphae on agar; in leaf-litter microcosms (Gadd 1999); on rotting wood (Verrecchia *et al.* 2006) and on chips of limestone and dolomite (Kolo *et al.* 2007). These crystals are likely to form as a by-product as a result of excess calcium in the mycorrhizosphere, and indicate that oxalate secreting organisms are not directly using Ca mobilised (Section 1.4.3.1), and dissolution may primarily be to solubilise other trace elements, such as phosphorus.

The role of trees and their mycorrhizas in carbonate weathering

1.5.4 Siderophores

Most bacteria and fungi, including EM species, produce iron-chelating ligands called siderophores (Szaniszlo *et al.* 1981). Siderophores may also be produced by the AM fungal clade *Glomus*, but this is unproven (Haselwandter 2008). These low molecular weight ligands aid iron uptake, and react with otherwise insoluble Fe (III) to form thermodynamically stable complexes (Renshaw *et al.*, 2002).

In laboratory studies, fungal cultures deprived of iron have been demonstrated to secrete a range of different hydroxamate siderophores (Szaniszlo *et al.* 1981; Renshaw *et al.* 2002), and their production may be stimulated by the presence of CaCO₃. The reason for this are unclear, but it is most likely to be due to trace levels of iron within the calcium carbonate additive and not in response to Ca²⁺ as there was no equivalent stimulatory effect with CaCl₂ (Szaniszlo *et al.*, 1981). This effect may be particularly important in calcareous soils where Fe(III) is virtually insoluble, often limiting plant and fungal growth or resulting in lime-induced chlorosis (Marschner 1995).

1.6 Effects of elevated CO₂ on terrestrial carbonate weathering

Detailed modelling studies coupling vegetation-soil interactions to weathering in arctic ecosystems have addressed the potential responses of carbonate rock weathering rates to climate change and escalating atmospheric CO₂ concentrations (Figure 1.9). In the arctic Mackenzie River Basin, a 205 ppm rise in atmospheric CO₂ from 355 ppm to 560ppm, and associated climate change, are expected to increase riverine bicarbonate flux from carbonate weathering by 18% and by 40% from silicates (Beaulieu *et al.* 2012). Although the increase in weathering rate is greater for silicates, bicarbonate flux originating from carbonate dissolution remains an order of magnitude greater than that from silicates. Modelled weathering rate enhancements at elevated CO₂ are not only related to changes in precipitation and temperature, but also to increased Net Primary Production (NPP) from CO₂-fertilization of vegetation (DeLucia *et al.* 1999) and greater autotrophic and heterotrophic respiration (Allen *et al.* 2000; Andrews and Schlesinger 2001).

Chapter 1

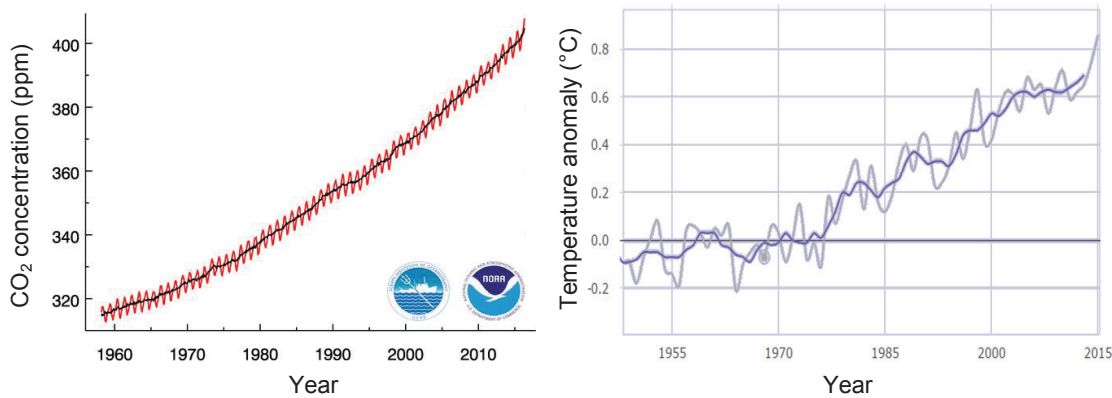


Figure 1.9. A) Monthly mean (red) and seasonally corrected (black) atmospheric CO₂ concentrations (ppm) measured at Mauna Loa, Hawaii 1960-2016 (NOAA/ESRL 2016) and **B)** associated global annual (grey), and 5-year (purple), land-ocean surface temperature anomaly (Schmidt *et al.* 2016).

1.6.1 Increased Net Primary Productivity (NPP)

The general response of plants to increased atmospheric CO₂ is increased NPP (Woodward and Lomas, 2004), and biomass production (Ainsworth and Long, 2004; Oren *et al.*, 2001; Rouhier and Read, 1998). Ainsworth and Long (2004) present a meta-analysis of the results of 120 Free-Air CO₂ Enrichment (FACE) experiments and conclude that trees tend to show a greater response than other plant functional types to elevated CO₂.

Greater atmospheric CO₂ and rising average temperatures, combined with changes in precipitation patterns are likely to affect some regions more than in others, with the most dramatic NPP increases at higher latitudes in North and South America and across Russia, in Siberia. This will have important consequences for weathering, as forest ecosystems in some of these regions overlies extensive areas of carbonate rock (Figure 1.1).

1.6.2 Altered soil hydrology affects mineral weathering processes

While CO₂-fertilisation of NPP may accelerate carbonate weathering over the coming century, the overall effects of increased CO₂ and associated climate change on weathering are complex and many, and some modelling studies indicate that carbonate dissolution may in fact decrease. Elevated CO₂ can indirectly alter soil hydrology through its effect on plants, closing stomata and improving water use efficiency by reducing transpiration (reviewed in Ainsworth and Rogers 2007). This will consequently increase soil drainage, speeding removal of weathering products and thereby maintaining rapid carbonate weathering rates as the system remains far from equilibrium (Eqns 1, 2).

The role of trees and their mycorrhizas in carbonate weathering

Modelling studies of the Mississippi valley watershed provide further evidence for this, demonstrating changes in soil drainage to be the most important factor affecting dolomite dissolution over the period 1950-2100, assuming a CO₂ increase from 315-700ppm (Godderis *et al.* 2013). Because the equilibrium of carbonate alkalinity is maintained (Eqn 1) dolomite dissolution responds linearly to drainage. Over the entire modelled period to 2100, CO₂ consumption from carbonate weathering is predicted to decrease. This is primarily the result of a decrease in dolomite solubility caused by a 4°C temperature increase (Godderis *et al.* 2013) and contrasts with experimental results of Kirstein *et al.* (2016) who noted no significant impact of temperature on dolomite dissolution between 5-26°C in the laboratory.

1.6.3 Evidence of tree-mycorrhizal weathering enhancement in elevated CO₂

Rising atmospheric CO₂ concentrations and associated climate change are predicted to have a large impact on the function of ecosystems. They will influence plant growth both above and belowground, altering the allocation of carbon to plant roots and their mycorrhizas, which will, in turn, affect weathering processes.

Mineral weathering responses to elevated CO₂ concentrations were investigated experimentally at the Duke FACE experiment. Over 2 years, loblolly pine trees (*Pinus taeda* L.) were exposed to either atmospheric or +200 ppm CO₂ concentrations. Over this period soil CO₂ concentrations increased, driven by both autotrophic and heterotrophic respiration, increasing soil acidity and providing a more favourable environment for weathering carbonates and other minerals (Andrews and Schlesinger 2001). Overall, there was a 271% increase in soil cation concentration and a 33% higher flux of inorganic carbon dissolved within groundwater, most likely to be from weathering-derived HCO₃⁻ and CO₃²⁻.

Soil at the Duke FACE experiment is clay-rich with an igneous silicate rock parent material. However, if this experiment was repeated on carbonate-containing soils, we may expect to see a similar but potentially more dramatic, increase in weathering, due to the overall faster weathering kinetics of carbonates and strong dependence on carbonic acid (Section 1.5.2).

In the Duke forest, CO₂ fertilisation had no effect on carbon allocation to AM fungi of either understorey vegetation or saplings, including *Acer rubrum* (Garcia *et al.* 2008). EM fungi, on the other hand, proliferated when host trees were exposed to higher CO₂, as was observed earlier in microcosm studies of *P. sylvestris* with *P. involutus* or *Suillus bovinus* mycorrhizal partners (Rouhier and Read, 1998).

Chapter 1

1.7 Overarching aims

Based on current knowledge, this chapter has outlined the key mechanisms by which trees and their associated mycorrhizas accelerate mineral weathering in forest soils, and its place in the short and long-term global carbon cycles. However, while there is an extensive literature relating to weathering of silicates, this review has highlighted the limited extent of current knowledge about that of carbonates, particularly in the field situation. Key knowledge gaps are identified in the following section, and those addressed within this study are detailed in the thesis outline, below.

Previous field studies have shown that trees hosting EM fungal partners can promote more rapid silicate weathering than those hosting AM fungi (Quirk *et al.* 2012); however it is unknown to what extent this relationship can be generalised to carbonates with their drastically different dissolution kinetics. This study aims to provide a unique comparison of how major tree-mycorrhizal functional groups regulate carbonate and silicate weathering in forest soils.

To date, carbonate dissolution has mainly been investigated in abiotic laboratory experiments, far from equilibrium. With exception of one study by Kirstein *et al.* (2016), dissolution temperatures investigated in the laboratory exceed those typical of temperate or boreal forest ecosystem soils. The ready availability of water and rapid dispersion of dissolution products makes these experiments unrepresentative of the field situation. In forest soils, weathering minerals are interacting with a complex substrate, at fluctuating temperatures, and water-mineral contact time is limited by cycles of wetting and drying. It has been observed that, for weathering silicates, these factors contribute to a large discrepancy between field, laboratory and theoretical rates (White and Brantley 2003), which this study attempts to reconcile in relation to carbonate weathering.

Interactions between weathering minerals and biota can accelerate silicate weathering for trace nutrient acquisition, in particular for phosphorus, which commonly limits plant growth. Mycorrhizal fungi utilise a variety of mechanisms to modify their immediate surroundings, the mycorrhizosphere, forming channels on, and tunnelling into, silicate mineral surfaces. Carbonate rocks can also contain biologically relevant trace elements, but aside from one indication of hyphal channelling on polished marble in a peat microcosm (Rosling 2003), plant-fungal-carbonate interactions are unstudied in the context of P acquisition. This study provides an overview of carbonate weathering in the field investigating both grain-scale geochemical changes and probing hyphal-mineral surface alterations.

Finally, there are great uncertainties in how carbonate weathering will respond to future climate change. At the Duke FACE experiment, there are indications that atmospheric CO₂ enrichment increases alkalinity flux, probably by accelerating silicate weathering in forest soils (Andrews and Schlesinger 2001). However, a later 5-year analysis at the same site does not find atmospheric CO₂ to produce such a marked effect on soil water chemistry, compared with local variations due to soil heterogeneity (OH *et al.* 2007). In relation to carbonates, results of laboratory (Kirstein *et al.* 2016) and modelling studies (Godderis *et al.* 2013) conflict when investigating the impact of rising temperatures on dissolution rates. However, no field studies investigate the impacts of CO₂ enrichment or global warming on carbonate weathering within vegetated ecosystems. While not directly addressed here, results within this thesis may be used to guide future studies on this important question, key to understanding changing feedbacks within the short-term carbon cycle.

1.8 Thesis outline

Chapter 2 describes Bedgebury Pinetum, my study site, including information about climate, soil characteristics and seasonality. The second part of the chapter presents results from a study into species-specific influences on soil biogeochemical characteristics or relevance to mineral weathering. This investigates classic questions on the role of angiosperm and gymnosperm tree functional groups on soil pH and elemental nutrient availability and re-interprets data in light of potential confounding implications of mycorrhizal association, not hitherto considered in long-term common garden experiments. This study combines two historical soil chemistry datasets with a 2014 re-analysis of remaining sampling sites to provide an 85 year record of in-situ soil development under different forestry tree species.

Chapter 3 introduces my main weathering field experiment, conducted within established stands of tree species under a common climate. This investigates the role of tree-mycorrhizal evolution in enhancing biologically-mediated carbonate weathering and aims to quantify weathering rates of both calcite- and dolomite-containing rock grains, relative to that of a quartz silicate. Acquisition of the growth-limiting nutrient, phosphorus, is thought to be the primary driver of active, mycorrhizal colonisation and weathering of silicate minerals. It is unknown whether this is also the case for carbonate minerals, and this is addressed by studying phosphorus cycling dynamics within chalk and quartz rock grains with similar initial P content.

Chapter 4 compares field weathering rates of carbonates with those obtained from theoretical calculations using laboratory-derived kinetic constants, in particular

Chapter 1

studying their dependency on soil pH. Many studies of silicate minerals find a large discrepancy between calculated, laboratory and field-derived weathering rates, often attributed partly to an inadequate understanding of the behaviour of weathering mineral surfaces. The second part of this chapter discusses this discrepancy in relation to carbonate rocks and tracks carbonate grain surface area evolution throughout weathering.

Chapter 5 examines the dynamics of weathering of carbonate and silicate mineral surfaces in the field by analysing specially-prepared mineral chips incubated within the same plots at Bedgebury. Chemical weathering by mycorrhizal fungi is considered to be most intense in the mycorrhizosphere, where minerals are in direct contact with hyphae, possibly via formation of a biofilm, or within range of localised secretions. In particular this section seeks to establish the relative roles of bulk mineral surface alterations and formation of local-scale putative hyphal channel features, as influenced by different tree-mycorrhizal functional groups.

Chapter 6 pulls together findings of Chapters 2-5 to present an overall picture of how trees and their symbiotic mycorrhizal partners regulate the weathering of carbonate minerals in forest soils and the relevance of this in the short-term global carbon cycle.

Chapter 2

Tree species influence on soil characteristics at Bedgebury Pinetum

2.1 Introduction

2.1.1 Overarching aims

The influence of tree species on soil biogeochemical properties has long been of interest to foresters in an attempt to enrich rather than impoverish soil for future plantations. Understanding this topic is increasingly important as global demand for forestry plantations grows; to fulfil our needs for fuel, building materials and food. In the UK, plans to rejuvenate the forestry industry (Read *et al.* 2009) make this research topic especially relevant. Currently, only 20% of timber required in this country can be supplied from home-grown plantations and over the coming years, timber harvests from public land will steadily decrease as plantations established 40-50 years ago are felled.

An independent review panel commissioned by the UK government in 2011 recommended that the forested area of England should be increased to 15% by 2060 from the current 10% to assist with timber demands and public access to woodlands for mental and physical wellbeing, education and other ecosystem services (Independent Panel on Forestry 2012). In addition to this, species distributions shift, migrating toward higher and cooler latitudes and altitudes, as vegetation responds to both contemporary (Chen *et al.* 2011) and historic climate change (Davis and Shaw 2001). These range shifts may potentially lead to colonisation of areas by angiosperm trees that were previously occupied by gymnosperm species, for instance in the southernmost part of the boreal zone.

Despite numerous studies, there is still no conclusive mechanistic understanding of the processes that underpin forest soil chemistry. This study aims to challenge the classic view that angiosperm and gymnosperm tree functional groups are the primary drivers of soil property divergence, and analyse the role of their root-associated

Chapter 2

mycorrhizal fungi, which has not hitherto been considered in any long-term common garden experiment. Evergreen gymnosperm (EG) and deciduous angiosperm (DA) forests are considered to have differences in soil development due to their different phenology and annual yield (Augusto *et al.* 2015); slow growing angiosperms with marked seasonal fluctuations in canopy cover, litter input and photosynthetic activity, and fast-growing gymnosperms with leaf cover year round. Experimental work in this chapter focuses on soil pH, base and phosphate content, all of which have been highlighted as exhibiting distinctive differences between evergreen gymnosperm and deciduous angiosperm tree groups (Anderson 1987), reviewed in the following sections.

This study examines the overarching hypothesis that mycorrhizal type is instrumental in determining soil characteristics and tests this using historical data and a common-garden experiment investigating the long-term effects of angiosperm and gymnosperm tree species on forest soils. The goal is to combine historical data (Ovington 1953; Howard and Howard 1984) with a recent resampling of Ovington's plots at Bedgebury Pinetum, to document soil evolution as influenced by different forestry tree species, over a continuous period of 85 years growth. Characterising the impacts of different tree species on soil characteristics will help understand the implications of shifting vegetation distributions on soil nutrient stocks and allow for selection of suitable species for conserving and improving soils.

2.1.2 Trees alter soil biogeochemical properties

Two main contrasting theories explain how trees alter soil properties. The first is that evolutionary selection for tree fitness either directly or indirectly improves soil environments for that species. This could occur through a certain tree species controlling soil chemistry in a way that allows it to gain a competitive advantage, either by producing more favourable soil environments for itself, or through disadvantaging competitors (Binkley and Giardina 1998). Alternatively, a more environmental view can be taken, with species-specific soil modification being simply a feature of ecosystems but not a selective process.

Different tree species make different relative contributions to changing soil chemistry (Binkley and Valentine 1991). Trees can alter soil properties through litter supply and chemistry; variation in canopy interception of precipitation and atmospheric deposition; and also due to species' characteristic nutrient demands and productivity (Miles 1985, 1986). Although there have been several comprehensive reviews of studies investigating the influence of tree species or functional group on ecosystem biogeochemistry, there remains much uncertainty (Binkley 1994). In addition, many

experimental results are confounded by interactions between site factors and tree species such as pre-existing preferences of certain trees for particular landscapes or soil types (Augusto *et al.* 2015, Binkley and Giardina 1998).

2.1.3 *Tree species effects on SOM and soil nutrient availability*

At a basic level, causes of tree species impacts on soil nutrient pools can be split into 2 groups: differences in net primary production (NPP) and C-inputs; and differences in soil organic matter (SOM) decomposition and C-losses (Hobbie *et al.* 2007). NPP can, in turn, influence organic C-inputs from litterfall and root exudates, and also determines tree nutrient requirements, which has knock-on effects on weathering and mineral nutrient supply. The focus of this thesis is on mineral weathering, and this chapter reviews the impact SOM cycling has on inorganic nutrients, including P, K Ca and Mg.

The precise influences of tree species on different soil components are still under debate. Effects on the organic horizon C-pool are largely produced by mismatch between inputs and outputs: where the rate of litterfall exceeds that of decomposition, DOM will accumulate, thickening forest floors, as was described by Binkley and Giardina (1998), Ovington (1953) and Augusto *et al.* (2015). Species influences on SOM within mineral soil are subject to many controls, the relative importance of which have not been fully examined. Most of these factors link to producing differences in the abundance or ability of rhizosphere micro-organisms to access and decompose SOM, summarised in Figure 2.1.

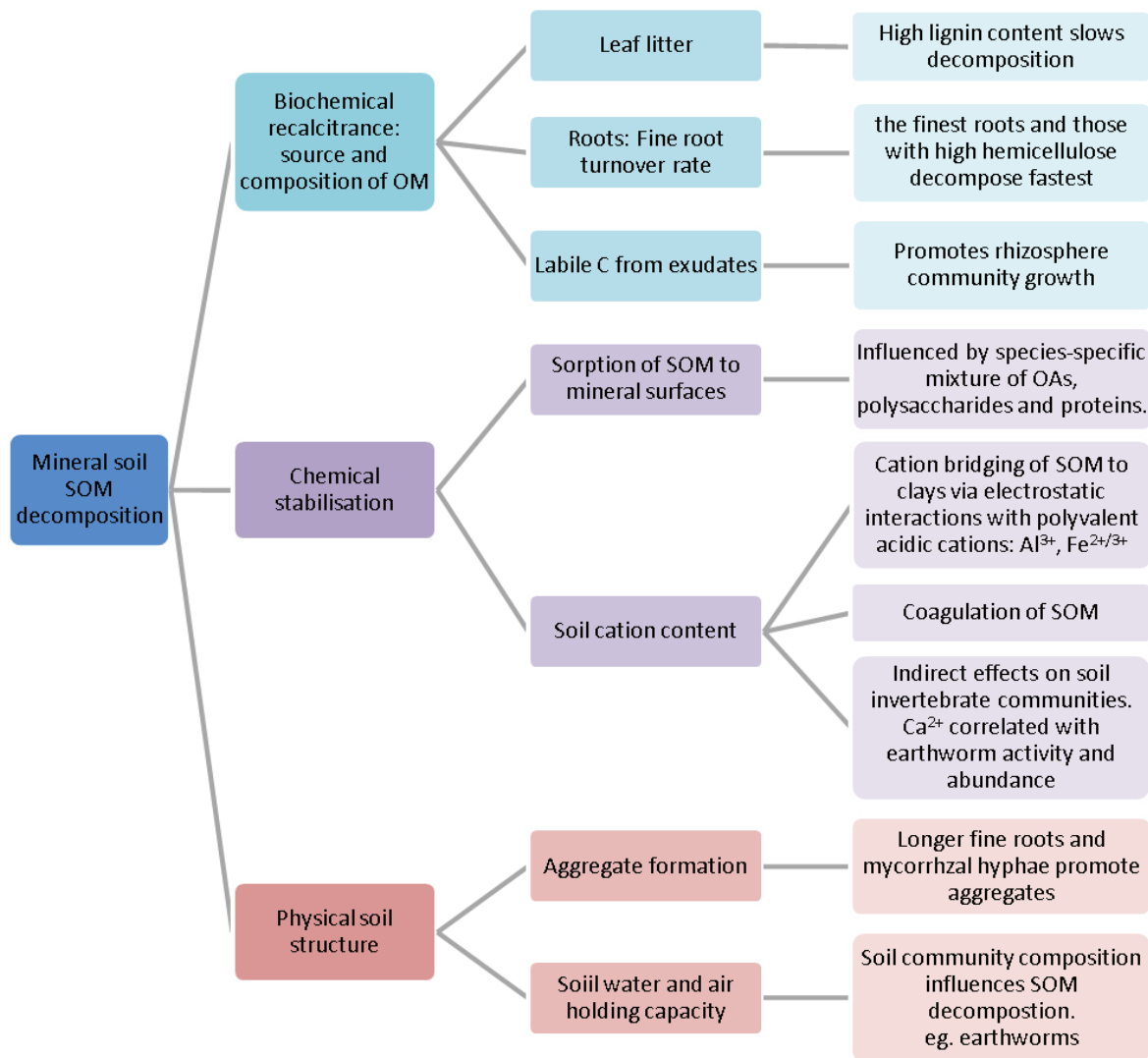


Figure 2.1. Summary of mechanisms through which tree species affect SOM in mineral soil, compiled from the work of Binkley and Giardina (1998), Hobbie *et al.* (2007), Talbot *et al.* (2008) and Augusto *et al.* (2015).

2.1.4 Inputs of SOM

2.1.4.1 Root DOM inputs and nutrient recycling

There is no conclusive picture as to how or if tree species affect belowground Dead Organic Matter (DOM) production, it cannot be predicted by using climatic variables, nor litterfall. To date, studies attempting to resolve this have given inconsistent results; however, in general, DOM production is thought to be of the same order of magnitude below and aboveground on a site-specific basis (Augusto *et al.* 2015).

In both leaves and roots, nutrient recycling occurs to some extent. A meta-analysis by Gordon and Jackson (2000) showed that dead fine roots had the same mean N concentration as live ones, but significantly lower P and K. This gives a mixed

picture of fine root resorption capacity, which may be reasonable for P and K, but minimal for N and other elements. Nutrient resorption may also depend on the type of roots as fine roots (<2 mm) had significantly higher N, P and Mg concentrations than roots with a wider diameter (2-5 mm).

2.1.4.2 Litterfall

Augusto's meta-analysis (2015) indicated that on average, deciduous angiosperm (DA) and evergreen gymnosperm (EG) species accumulate litter at the same rate. Litterfall does, of course, spread over a large range of values, but this appears to be driven by variation between individual species, rather than any trait that can be characterised as characteristically DA or EG. Seasonal patterns obviously play a much larger role in determining litterfall for DA species, which peaks in autumn as leaves senesce. Litterfall flux is mainly controlled by climate with site specific factors also participating to a lesser extent. In general, litterfall decreases as growth conditions worsen, for instance if moving to higher latitudes or less fertile soils (reviewed in Augusto *et al.* 2015)

2.1.4.3 Canopy and litter composition

Fresh leaf chemical makeup is largely determined by tree species, with little effect of site-specific factors, which, in turn influences SOM elemental composition (Ovington 1956). Overall, Ovington found large variation between gymnosperms and angiosperms tree types, and no consistent patterns in Ca-, Fe- or Si- content between hardwoods and conifers; however, no statistical interpretation of results was presented. Figure 2.2 presents a re-analysis of 1951 data, and suggests that there are distinct differences in elemental composition of angiosperm and gymnosperm canopies. This pattern also holds for evergreen and deciduous grouping of species, but due to experimental design, there is a lot of overlap between these categories, as all angiosperms surveyed were deciduous and all gymnosperms except for *Larix* spp were evergreen. Fresh leaves of angiosperm species are characterised by elevated N, Mg, P and K, and those of gymnosperms by slightly higher Na, but lower concentrations of all other elements quantified.

For almost all variables measured in the fresh leaves, the two main factors that explained the distribution of data were site location and tree type, angiosperm or gymnosperm. The impact of site conditions may be seen most obviously in elements such as manganese. Availability of manganese increases with soil acidity, and Mn accumulation in leaves is directly linked to its availability in soils. Manganese can accumulate indefinitely, as trees cannot completely control its uptake (Marschner 1995).

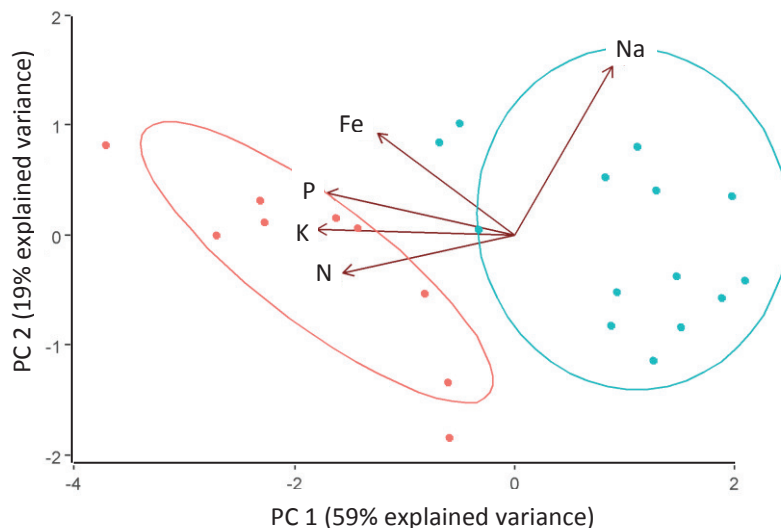


Figure 2.2. Principle component analysis (PCA) of angiosperm (red) and gymnosperm (blue) fresh leaf elemental composition data from Ovington (1955), with 95% confidence limits.

2.1.4.4 Nutrient recycling in leaf litter

Before leaves senesce, trees have the ability to resorb nutrient elements: There is generally a high ability to resorb N, P and K, medium for Mg and low for Ca. Ca- and Mg-content of litter closely correlates with that of fresh leaves (Ovington 1956, 1958b), however, the overall quantity of these elements was consistently lower in the litter than the fresh leaves, indicating some degree of resorption and or decomposition (Figure 2.3). Ca-content of leaves and organic soil seems to depend on species, and at Bedgebury *Thuja plicata*, *Chamaecyparis lawsoniana* and *Pseudotsuga taxifolia* had the greatest Ca contents (Ovington 1958b). At Bedgebury, the surface litter is poorer in Ca than the underlying organic soil layers, potentially as a result of leaching and accumulation of basic cations in these lower layers.

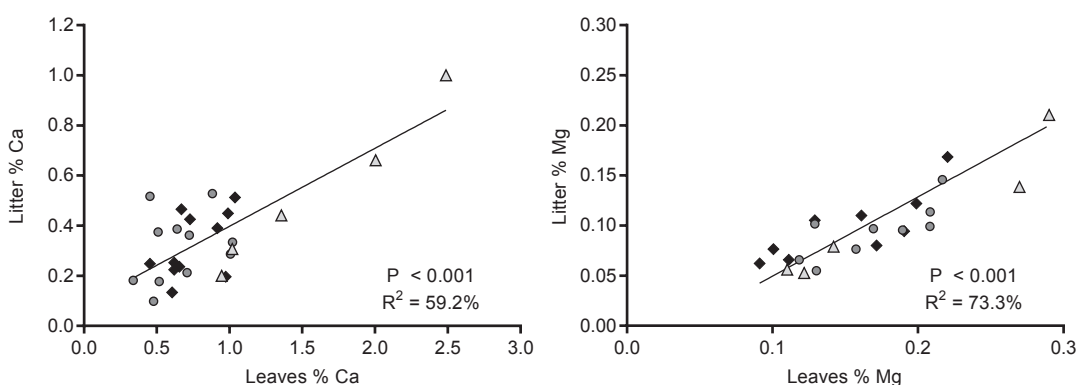


Figure 2.3. Ca and Mg contents of fresh leaves and leaf litter at sites sampled by Ovington (1956), Data are compiled from 3 forestry sites in the UK at Abbotswood (black diamonds), West Tofts (light grey triangles) and Bedgebury (dark grey circles). Data digitised from Ovington 1958b, and analysed individually with linear regression presented for each Ca and Mg.

2.1.5 Decomposition of Dead Organic Matter

2.1.5.1 Root decomposition

Decomposition of DOM is primarily regulated by microbial activity and its rate is influenced by different factors above and belowground. Belowground, the thinnest roots and those with high hemicellulose content decompose fastest, but this is seemingly unlinked to tree type. Hobbie *et al.* (2010) observed no significant differences in fine root decomposition between angiosperm and gymnosperms in the 11 temperate tree species they surveyed in a Polish experimental forest. Variation in decomposition rates may result from different microbial community compositions above and belowground, or through divergent decomposer nutrient requirements.

Fine root density may affect belowground SOM decomposition, and microbial biomass was greater in soils containing more fine roots (Hobbie *et al.* 2007). The soil fumigation techniques used to produce this result probably excluded mycorrhizas (Hobbie *et al.* 2007), however, their response is likely to mirror that of bacteria and saprotrophic fungi, as they are also hosted by fine roots.

2.1.5.2 Litter decomposition

In contrast to findings for fine roots, DA and EG tree groups may differentially affect leaf litter breakdown. EG species tend to produce thicker forest floors than DA species (Ovington 1953, Augusto *et al.* 2015), which may be due partly to the high recalcitrance of coniferous litter (Figure 2.4, Hobbie *et al.* 2010). EG litter tends to have a high C:N ratio, which correlate with slow decomposition in forest floors (Figure 2.4; Reich *et al.* 2005; Hobbie *et al.* 2007; Augusto *et al.* 2015), although often, it is not clear whether experimentally observed high C:N ratios determine or result from slow decomposition.

Aboveground, low cellular lignin and high Ca-concentrations (Dijkstra 2003, Reich *et al.* 2005, Challinor 1968, Hobbie *et al.* 2010, Mueller *et al.* 2015) are the most important factors contributing to rapid DOM breakdown. An earlier study by Hobbie *et al.* (2007) does not support litter lignin as a predictor for SOM decomposition, however, does suggest that decomposition is most rapid when litter Ca is high. Species with this characteristic tended to have thinner forest floors, indicating more rapid decomposition.

Decomposition rates of SOM are influenced by the rate at which products of decomposition are removed, potentially reflecting patterns of biological demand. Leaching of DOC (dissolved organic carbon) from the O-horizon was lowest where litter contained high Ca-concentrations, and highest where there was a lot of available P from SOM (Hobbie *et al.* 2007). This effect was linked to soil microbial communities,

Chapter 2

as DOC production was highest where soil respiration was greatest, potentially a reflection of microbial demand for P. Leaf litter P could stimulate demand for N and species with higher litter P also had greater rates of N mineralisation.

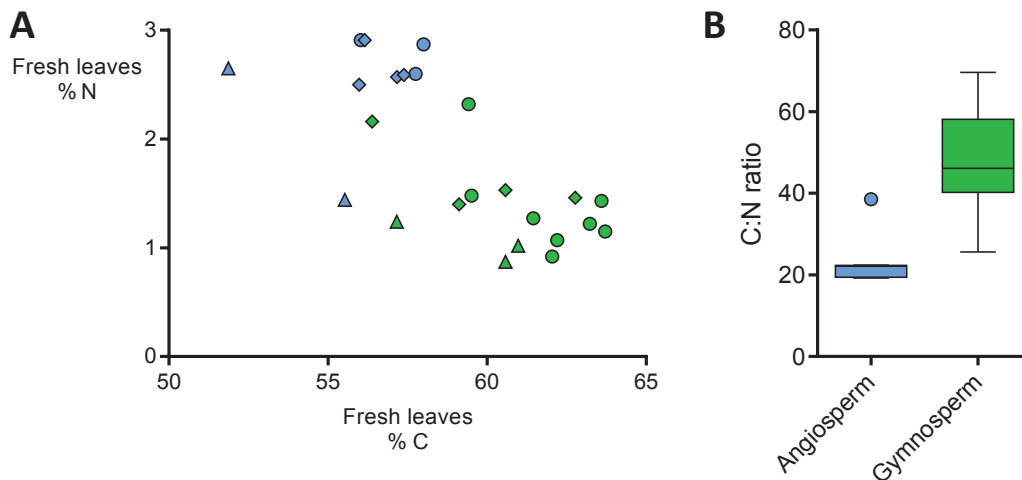


Figure 2.4. C:N ratio of fresh leaves of angiosperm (blue) and gymnosperm (green) trees using data collected by Ovington (1955-fresh leaves). A) Data are separated by site: Bedgebury (circles), Abbotswood (diamonds), and West Tofts (triangles). There is no significant effect of site (Kruskal-Wallis, $\chi^2 = 2.95$, d.f. = 2, $P = 0.23$), but there is of tree type (Kruskal-Wallis, $\chi^2 = 15.3$, d.f. = 1, $P < 0.001$), with B) angiosperm leaves having lower C:N ratios than gymnosperms.

2.1.6 Forest soil pH

Understanding pH is key to successfully establishing commercial plantations, and because of this, soil pH has been studied for many decades, attempting to anticipate changes that will occur as tree crops establish, and also to aid species selection for improving soil fertility at a given site. There is considerable inter-annual and seasonal variation in soil pH both within and between tree species. Soil hydrology; organic acid and basic cation concentrations and microbial activity all affect pH and are influenced by the interaction between tree characteristics and specific site factors. Resulting forest soil pH will be subject to fine spatial variation, which stresses the importance of careful sampling and calculation of robust average values.

2.1.6.1 Seasonal variation

Soil pH varies dramatically year to year, potentially in response to annual climatic conditions, in particular precipitation; or to changing patterns of soil acidification balancing base cation uptake. Monthly soil analysis during a 5-year study in Bagley wood, Oxfordshire (1932-1937), indicated that the magnitude of interannual pH fluctuation was partly determined by soil type (Baker and Clapham 1939). Soil was found to acidify in the late summer and autumn, followed by a pH increase over the winter-summer period for both clay ($N = 2$) and gravel ($N = 3$) soils.

Loamy soils (N = 2) exhibited a similar pattern, however, fluctuations were small enough to be of no statistical significance. The authors proposed that soil acidification in the late summer-autumn period may be due to higher activity of soil micro-organisms during this period. In the deciduous forest studied, the majority of areas surveyed were dominated by *Quercus* and *Betula* (EM), with a few sites partly colonised by *Acer* and *Fraxinus* (AM). It is very likely that micro-organisms, in particular, mycorrhizal fungi would be contributing to this, as the supply of carbon, from host plant photosynthesis, into the soil will be greatest during this period, as will be tree demand for soil nutrients and water, for which mycorrhizas are largely responsible (Leake *et al.* 2008). Mycorrhizal fungi are also known to acidify soil through proton pumping, and also through the release of LMWOAs from ectomycorrhizas.

Secondly, a decline in soil acidity throughout the winter until the following spring/summer may be attributed to decreased microbial activity. This could be mediated through a variety of mechanisms such as a reduction in available photosynthetic carbon and deciduous host plant nutrient demand and colder winter temperatures and soil waterlogging inhibiting microbial growth. Another possible influence in the spring/summer is capillary action in drying soils. Here, water rises to replenish the upper profile, simultaneously drawing up base cations from the mineral soil which contributes to increasing soil pH.

Chapter 2

2.1.6.2 Species effects on pH

Tree species may alter soil pH via four main mechanisms (Binkley 1994):

1. Changing soil anion content and associated H^+ availability. This can occur through differential anion uptake, leaching or exudation.
2. Modifying soil acid concentration, including both LMWOA exudates and humic acids from decomposition of SOM
3. Differences in organic acid strength. Stronger acids protonate more easily, donating H^+ to the soil solution.
4. Changing redox status of soil acids: increasing proportion of H^+ or Al^{3+} and therefore protonation increases H^+ availability and therefore soil acidity.

The most recent meta-analysis of tree species influence on soil biogeochemistry by Augusto *et al.* (2015) generalises that EG species decrease soil pH relative to DA species. This does not imply that DA soils are close to neutral, and can be very acidic, as they are in the plots reanalysed in this study (Ovington 1953). The effect is very small, far less than one pH unit (Binkley and Giardina 1998), typically with a large overlap in soil pH between these tree groups. This result may only be seen when averaging results across many studies in a meta-analysis, and different experiments have seemingly conflicting outcomes, summarised with examples in Table 2.1.

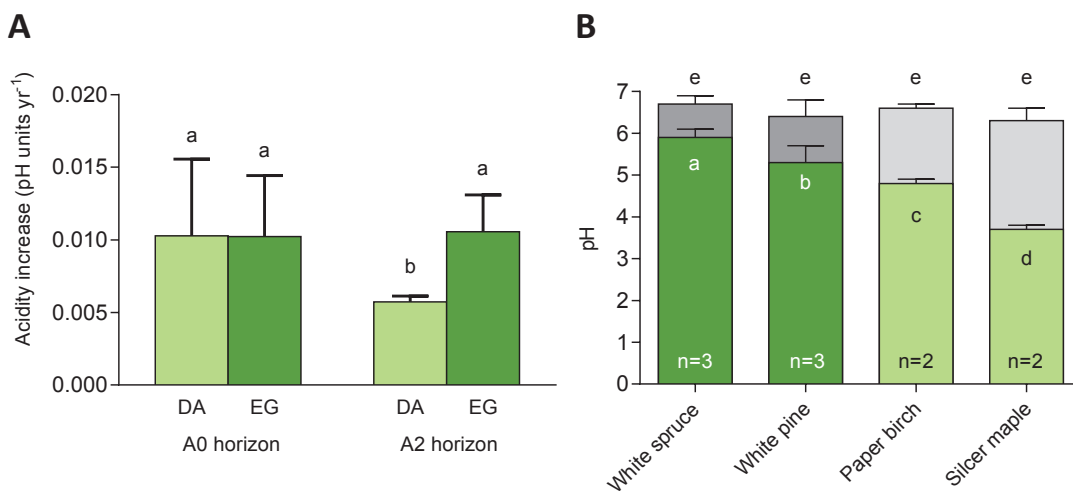


Figure 2.5. A) Acidification rates of EG (dark green) and DA (dark green) stands of different ages over 50 year study period (1927-1983) for both A0 and A2 soil horizons. Figure based on data of Hallbäck and Tamm (1986). **B)** Forest soil pH reported by France *et al.* (1989) after 27 years development in replicate stands of EG (dark green, organic; dark grey, mineral soil) and DA species (light green, organic; light grey, mineral soil). Bars sharing the same letter indicate there is no significant difference between plots (Tukey HSD, $P < 0.05$).

Table 2.1. Summary of experiment outcomes comparing pH effects of deciduous angiosperm (DA) and evergreen gymnosperm (EG) species.

Effect of tree functional group on pH	Examples	Experiment description
pH DA > pH EG	Nihlgard (1971)	The first generation of Norway spruce, growing on land formerly occupied by beech in Sweden, acidified A-horizon soil by up to pH 0.5, accompanied by a simultaneous reduction in exchangeable base cations, K and Ca. This is potentially due to more rapid infiltration through EG than DA litter and increased leaching (Challinor 1968).
	Challinor (1968)	Four plantation species, Norway spruce, red oak, white pine and red pine, were planted on former pasture and observed after 30 years. The upper soil under red oak was significantly less acidic than any of the EG species, however, total soil pH range was small.
pH DA = pH EG	Hallbäcken and Tamm (1986)	Soil pH changes in beech, oak and spruce stands of different ages were surveyed over 55 years in southwest Sweden. Over the study period, all tree species acidified the upper soil horizons. This effect decreased with depth and was less pronounced for DA than for EG in some, but not all soil horizons. Tree functional group had no effect on A0 horizon pH, a result that might be partly due to acid rain. There was, however, greater acidification under EG spruce stands than DA beech or oak in the underlying A2 horizon (Figure 2.5A).
pH DA < pH EG	France (1989)	France investigated pH differences after 27 years of white pine, white spruce, silver maple and paper birch stand development in Southern Ontario (Figure 9). Significant pH differences were found in the organic soil layer: silver maple produced a pH of 3.7, far lower than white spruce, pH 5.9; however, no pH differences were measured in the upper 0-15cm of mineral soil (Figure 2.5B). Overall, the mineral soil had relatively high pH due to calcareous parent lithology, which may buffer against dramatic pH changes lower in the profile.

Research hypothesis 1

All forest soil at Bedgebury is acidic, and its pH varies intra-annually, becoming more acidic in late summer and autumn compared to winter, spring and early summer. Evergreen gymnosperm (EG) species produce more acidic bulk soil conditions than deciduous angiosperms (DA).

Chapter 2

2.1.7 Summary of historical work at Bedgebury

The following hypotheses are based on the conclusions of the resampling of Ovington's plots in 1974, summarised in Table 2.2 (Anderson 1987; Howard and Howard 1984).

Table 2.2. Summary of historical work on soil development at Bedgebury, 1951-1971. Results are highlighted as significant where $P < 0.05$, reported by Anderson (1987), on whose work this table is based. Abbreviations used for evergreen gymnosperm (EG) and deciduous angiosperm (DA).

Soil property	Description of changes between plots 1951-1971
Total N	In both 1951 and 1974, <i>Quercus rubra</i> , one of the DA species, had the lowest soil N, and the highest was under <i>Pinus nigra</i> , an EG. However, this contrast between EG and DAs was not a general trend and the other DA species surveyed were spaced through the entire range of soil N contents.
Extractable P	In 1951 P in forest plots did not differ significantly from the shelterbelt at any depth. By 1971 a small but significant increase in soil P was found across species at Bedgebury. P-content fell into two groupings; two EG species <i>Picea abies</i> and <i>P. nigra</i> had significantly higher P, in both 1951 and 1974, than other plots; and the three DA species, <i>Nothofagus obliqua</i> , <i>Q. rubra</i> and <i>Quercus petraea</i> , had the lowest soil P contents in 1951. However, the P content of DA soils increased to converge with that of the conifers by 1971. It is not known whether these angiosperms had significantly lower P content than all conifers in 1951 as within-plot variance is not recorded.
Extractable K	There were no significant differences between K concentration of any plot and the shelterbelt in 1951, however, by 1971, K significantly increased across the entire site. The two species with highest overall K were both conifers, <i>Pseudotsuga menziesii</i> and <i>P. nigra</i> , however, this may be due to the location of these plots in an area containing patches of brickearth, which commonly contains K-feldspar.
Extractable Ca	Extractable Ca decreased significantly between 1951 and 1974. Although the highest soil Ca-concentrations recorded were below EG species and the lowest within both oak plots, soil Ca was not significantly affected by tree type (gymnosperm, angiosperm). Greatest soil Ca was measured below <i>P. nigra</i> and <i>P. menziesii</i> , and for these species there was a dramatic decline in soil Ca between 1974 and 1951.
Extractable Mg	Mg decreased throughout the soil profile over the study period. This effect is so striking and consistent between species it might be due to some change in experimental technique, despite attempts to apply correction factors to adjust for this in 1974.
Soil similarity between plots	In terms of most soil characteristics surveyed, plots containing different species became more similar over the period 1951 - 1974. This effect is most pronounced for Ca, however, is likely to be largely driven by the dramatic difference in <i>P. nigra</i> plots, which is excluded from analyses in this study. K shows minimal change in variation, and soil P concentrations show a slight narrowing of range, probably due to the faster rate of increase within plots containing DA species.

Research hypothesis 2

Trees alter soil geochemical properties in a species-specific manner. Soils forming below fast growing gymnosperm species have higher extractable base cation and phosphorus concentrations than those below angiosperms.

Research hypothesis 3

The greatest species-specific differences in soil characteristics are observable during the early-mid rotation of plantation forests, and declining as forest stands establish. Divergence in soil characteristics takes longer for angiosperms than for gymnosperms, due to slower litter decomposition rates and the longer time required for these slower-growing trees to complete a forestry rotation.

2.2 Methods

2.2.1 Site description

The forest plots used to investigate hypotheses of mineral weathering and soil property evolution proposed in this thesis are located at Bedgebury Pinetum (51.07°N, 0.44°E), Kent. These experimental plots were established in 1929, shortly after the first trees were transferred to Bedgebury from Kew gardens to avoid the poor soils and air pollution in London. The initial purpose of these plots was to monitor the growth of many different broadleaf and coniferous species under similar environmental conditions to assess their potential as forestry species, but they were opportunistically sampled by J.D. Ovington in 1951 to try and understand tree species effects on soils. Each plot measures 30 × 30 m and contains a single-species of mature trees (Forestry Commission 1951, 1961, 1972). The site for planting was selected to keep soil type and aspect as uniform as possible.

The original field trial was closed in 1987 as a result of damage caused by the intense storm in October that year (Figure 2.6). This site is now used for a conifer conservation project, and is being re-planted with rare conifer species from across the world. However, some of the original plots remain, yet these have not been surveyed since 1974. In these remaining original plots, the same trees have been growing for 85 years, since 1929. Prior to this, there is a detailed record of many soil characteristics, reported in 1951 and again in 1974. This study aims to replicate the measurements taken in 1951 (Ovington 1953, 1958a,b) and 1974 (Anderson 1987; Howard and Howard 1984a,b; Howard *et al.* 1998) to produce an ongoing record of soil development under the influence of different tree species.



Figure 2.6. **A)** Ariel photograph of forest plots at Bedgebury 14th May 1947 (Royal Air Force, in Ovington (1953)). **B)** Current state of forest plots at Bedgebury. Note the loss of trees in many plots, marked by asterisks, in the more recent photo (Google 2013). There are now large areas of cleared ground and younger, replanted plots where the canopy has not yet closed. **C)** Location of original forest plots analysed at Bedgebury, from: Ovington (1953). Detail of labelled plots described in **Table 2.4**.

2.2.2 Soil type and bedrock

In the current study, monospecies stands are planted on the same site, experience the same climate and have similar soil parent material. Soils are either brown earth (BE), brown gley (BG) or surface water gley (SWG), underlain by mudstone from the Tunbridge Wells Sand Formation, TWS (Table 2.4, Figure 2.7). The previous land use across the entire site was hazel coppice. Similar initial conditions allow direct comparisons to be made between plots since occupied by different species.

Caution is advised when interpreting the soil map (Figure 2.7A) because observations in the field did not show any clear-cut differences in soil type based on location alone. Generally soil had a thick, dark brown, O horizon overlying mineral soil. There was usually a very distinct interface between these two layers and little mixing of the organic and mineral soils. Underlying mineral soil was paler in colour, either grey or with orange tinting, and a higher content of sand or sandy clay, as might be expected with a parent material of mudstone, sandstone or siltstone. Tree species seemed to have a large impact on soil appearance within individual forest plots, with the upper soil profile sometimes varying drastically between adjacent plots. The methodology and resolution of sampling to produce Figure 2.7 are unknown, so this map has only been used to advise of underlying preference for different soil type by factors that do vary across the site, such as drainage.

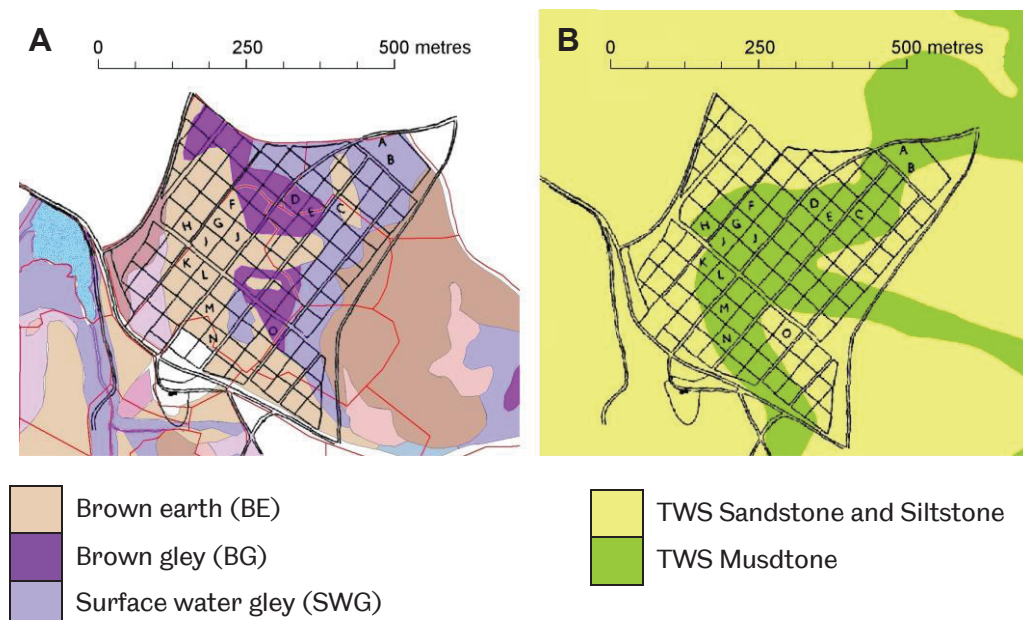


Figure 2.7. Maps of **A)** soil type (Forestry Commission) and **B)** bedrock geology underlying forest plots at Bedgebury Pinetum, overlain by plot identity. Both underlying lithologies are sedimentary and belong to the Tunbridge Wells Sand Formation (TWS) deposited in swampy, estuarine or delta environments during the Cretaceous (approximately 134 to 140 million years ago). All re-surveyed sites overlie TWS mudstone bedrock. Map based upon 1:50000 scale bedrock geology, Geology of Britain Viewer, with the permission of the British Geological Survey.

Chapter 2

2.2.3 Climate

Weather data collected by on-site data loggers were obtained (1950-2012). Unfortunately data are not available from Bedgebury prior to 1950 so in an attempt to extend the dataset to the date of tree planting (1920-30), data were analysed from the nearest weather stations. Earlier maximum and minimum temperature data are available from historic MET office records from Southampton (130 km away; 1855-).

At Bedgebury annual precipitation data are available for the entire period 1950-2012. Temperature data are available 1959-2012. Years with inadequate data (<364 days) were excluded from this figure, these are 2003, 2006-9.

2.2.4 Tree species influence on observed change in Bedgebury 1951-1971

A summary of historical soil characteristics for selected tree species was prepared from available literature (Table 2.3), and methods used for these and recent sampling in 2014 are described in this section. There is no record of soil properties prior to felling of the hazel coppice and tree planting, so 1951 and 1974 samplings are compared to sites within the shelterbelt zone as a proxy for pre-plantation soil. This shelterbelt contained remains of the original vegetation, consisting of chestnut or hazel coppice with oak standards, a few scots pine, Norway spruce and larch (Howard and Howard 1984). It was not possible to make this comparison for the 2014 resampling as this area has been felled and partly replanted (Figure 2.6).

Table 2.3. Literature references used to compile summary of historical soil characteristics at Bedgebury, organised by sampling date.

Soil characteristic	Sampling date	
	1951	1971
pH	Ovington (1953)	Anderson (1987)
P, K	Ovington (1958a)	Howard and Howard (1984a)
Ca, Mg	Ovington (1956, 1958b)	
<i>P. nigra</i> resampling		Howard and Howard (1984b)

Table 2.4. Species investigated in 1953, plots resampled in 2014 are highlighted in blue.

Plot ID (Fig. 3)	Species	Family	Identified in 2014?	Soil type (Fig 3)
A	Shelterbelt		Felled and replanted, original shelterbelt remnant inaccessible	SWG
B	<i>Picea omorika</i> (EM)	Pinaceae	Yes	SWG
C	<i>Pseudotsuga taxifolia</i> (EM)	Pinaceae	Yes (Sampled Aug 2014, but felled by Dec 2014)	BE/SWG
D	<i>Nothofagus obliqua</i> (EM)	Fagaceae	Yes, but very overgrown	BG
E	<i>Pinus nigra</i> (EM)	Pinaceae	Felled	BG
F	<i>Larix eurolepis</i> (EM)	Pinaceae	Yes	BE
G	<i>Thuja plicata</i> (AM)	Cupressaceae	Yes	BE
H	<i>Chamaecyparis lawsoniana</i> (AM)	Cupressaceae	Yes	BE
I	<i>Tsuga heterophylla</i> (EM)	Pinaceae	Yes	BE
L	<i>Quercus rubra</i> (EM)	Fagaceae	Yes	BE
M	<i>Quercus petraea</i> (EM)	Fagaceae	Close duplicate plot selected	BE
N	<i>Picea abies</i> (EM)	Pinaceae	Yes	BE
J, K, O	Planting failure		Replanted or unidentifiable	BE/BG

2.2.4.1 Statistical treatment of historical data

For the first sampling by Ovington, there has been no statistical interpretation of data. Five points within each plot were sampled, but only mean values are presented and there is no indication of within-plot variance. Howard and Howard (1978) attempted to estimate the within-plot variation, for comparison with data from a later sampling in 1971, by pooling within-site variances for the second sampling and assuming that variance was the same in both samplings. In the 1971 sampling, some sites did not have 5 replicates for the organic litter layers, and Dunnett's modification for unequal sample sizes was used to adjust for this. Subsequent analyses were performed using ANOVA and PCA to investigate correlations of all the chemical variables for each site. All T-tests used in this analysis are 2-Tailed and use Welch's correction for unequal variances.

In 1984, the interpretation of resampling data for *P. nigra* is dealt with separately from the other plots surveyed by Howard and Howard (1984b). An explanation for this is given in the discussion; however, because this plot could not be located in 2014, this is not dealt with in much detail.

Two analyses were performed with soil Ca and P data from both historic and 2014 samplings. The first included all tree species (N = 9), and the second a subset of only those species growing on brown earth soil type (N = 7), as identified from Figure 2.7 (Table 2.4). This subset excluded both *Nothofagus* and *Pseudotsuga*. This second analysis was performed to investigate the influence of tree species soil development in the absence of any pre-existing differences in soil type.

Chapter 2

2.2.4.2 *Soil and litter sampling*

Soil samples (N = 5 per species) were collected from forest plots over a 2 day period in July 2014 (15/7/14 – 16/7/14). Soil samples were separated into upper O horizon and lower mineral soil, air dried and powdered in an agate ball mill (Fritsch Pulverisette) prior to analysis.

In this repeat sampling of the Ovington plots at Bedgebury, soil properties were only measured in both the decomposed O horizon and in the upper mineral soil (5-10 cm depth, depending on thickness of organic horizon). Previous sampling in 1971 by Howard and Howard (1984) to 70cm depth demonstrated that there was little change in soil properties below 10 cm. This is reinforced by an earlier study by Challinor (1968) who only observed differences in soil N, K and Ca for 4 plantation tree species in the top 5 cm of soil. Hallbäcken and Tamm (1986) found the influence of stand age and species composition on soil physical properties to reduce with depth in 50-year old stands of beech, oak and spruce in SW Sweden. In addition to this, Binkley and Valentine (1991) only reported differences between Norway spruce and Green ash soils in the top 15 cm.

2.2.4.3 *Soil pH*

Soil pH was measured both during a dry period in August 2013, for consistency with Ovington (1953) to minimise seasonal variation between sampling years; and in December to investigate seasonal variation (Baker and Clapham 1939). Air-dried, ball-milled soil was mixed with water in a 1:1 ratio v/v and pH measured using a pH meter (Jenway 3540 pH meter; calibrated at pH 4, pH 7 and pH 10).

2.2.4.4 *2.5% acetic acid extraction*

Elutable Ca concentration was determined after extraction with 2.5% acetic acid (0.5 ± 0.1 g air dried and powdered O-horizon soil; 12.5 ml of 2.5% acetic acid). Extractions were performed in 15 ml centrifuge tubes shaking tubes horizontally, using a reciprocal shaker (1 hour, 150 rpm), for maximum disruption. Following extraction, soil particles were sedimented by centrifugation and the supernatant filtered (Whatman 42) into a clean, labelled 15 ml tube before analysis by AAS (Atomic Absorption Spectroscopy) the same week. Extraction blanks were prepared in the same manner as samples.

2.2.4.5 AAS Analysis

Following sample filtration (0.2 μm), soil extractable Ca was determined by atomic absorption spectroscopy (AANALYST200; PerkinElmer, Waltham, Massachusetts, USA), calibrated using a certified multi-element standard (100 ± 3 mg Ca/l; ICP multi-element standard VIII, Merck KGaA, Darmstadt, Germany). When required, samples were diluted with dH_2O prior to analysis using an automatic micropipette (Microlab 500 series, Hamilton Laboratory Products, Ghironda, Romania). Lanthanum chloride (100 μl / 10ml diluted sample; 10% v/v) was added prior to analysis for Ca in order to reduce interference. Lanthanum forms more stable salts than Ca does with anions such as sulphate, thus leaving Ca free for atomisation.

2.3 Results

2.3.1 Climate

Kent, where Bedgebury Pinetum is located, has a relatively warm climate for the UK. Weather data collected by from on-site data loggers were obtained and are shown in figure 5, below. Since 1950, Bedgebury has had an average rainfall of 841 ± 19 mm, ranging between 518 mm in the driest year, 2011, and 1306 mm in 2000, which was the wettest year on record at this site (Figure 2.8).

Mean annual temperature (1950-2012) was $9.8 \pm 0.1^\circ\text{C}$, with a maximum of 34.7°C in 1990 and -14°C in 1972 (Figure 2.9). Unfortunately data are not available from Bedgebury prior to 1950. Earlier maximum and minimum temperature data are available from historic MET office records from Southampton, 130 km away (1855-; Figure 2.9D).

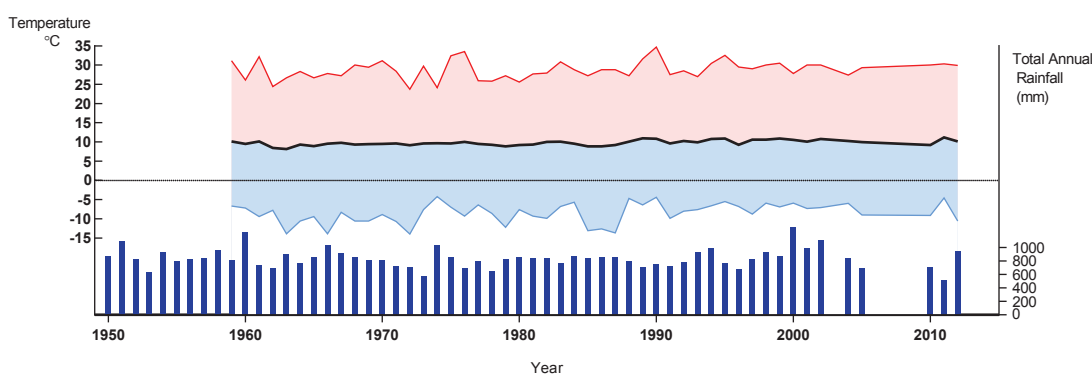


Figure 2.8. Bedgebury climate 1950-2012. Summary data for temperature on the left Y-axis (mean = black, max = red, min = blue) is plotted alongside annual precipitation on the right Y-axis (blue bars).

2.3.1.1 Climate change at Bedgebury

Over the 53 years with on-site temperature records, there has been a persistent warming by an average of $0.026 \pm 0.006^\circ\text{C}$ per year (linear regression; $F_{1,47} = 20.5$; $P < 0.0001$), amounting to an estimated $2.2 \pm 0.5^\circ\text{C}$ over the study period 1929-2014 (Figure 2.9B). The increase in mean temperature is accompanied by a significant rise of annual minimum temperature by $0.06 \pm 0.024^\circ\text{C}$ per year (Figure 2.9C), but not of maximum temperature (Figure 2.9A). This increase in minimum temperature is striking as it is occurring at a faster rate than change in mean temperature. In the 25 years since 1987, there have been no days in which the temperature fell below -12°C , and only one year where the temperature fell below -10°C , in 2012. In the same period, of 25 years, before 1987, temperatures sub -10°C were recorded in 11 years, 7 of which had minimum temperatures of below -12°C .

Warming was also seen in longer-running datasets from Southampton (0.002°C per year; Figure 2.9D) and Marston (data not shown), mainly manifesting in a steady increase in minimum temperature (Southampton: Linear regression; $F_{1,69} = 5.1$; $P = 0.03$).

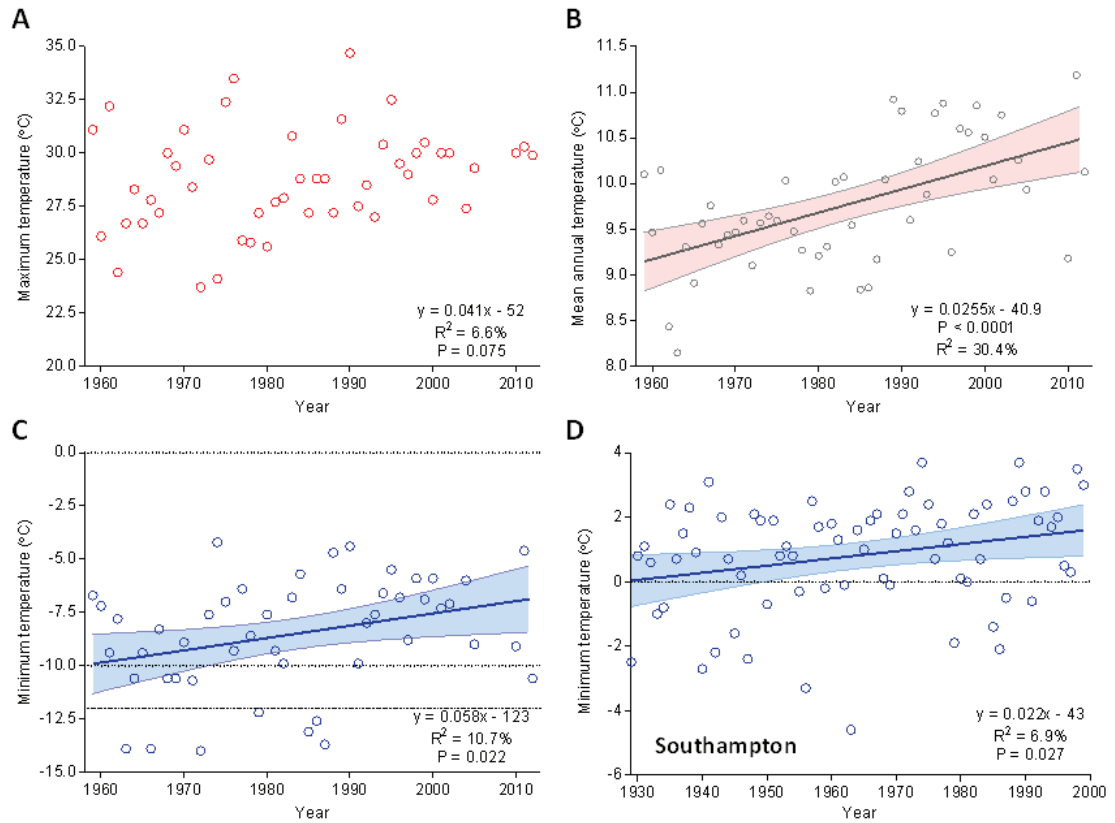


Figure 2.9. **A)** Maximum, **B)** man and **C)** minimum annual temperatures at Bedgebury pinetum, Kent. In **C)** Horizontal dotted lines are drawn at -10 and -12°C to highlight the number of years where temperatures fell below these levels. **D)** Minimum temperature for Southampton, a candidate dataset to extend the range of temperature data recorded at Bedgebury. Trendlines show results of linear regression with 95% confidence interval, where significant.

2.3.2 Soil pH at Bedgebury pinetum

2.3.2.1 Seasonal pH variation

At Bedgebury, during 2013, there was soil acidification in early December, relative to an earlier, summer sampling (31st July – 2nd August; Figure 2.10). This difference was slight and only statistically significant for 3 tree species, *Ilex aquifolium* (ILE; 2-tailed T-test; $t(8) = -4.26$; $P = 0.0014$), *Pinus sylvestris* (PIN; 2-tailed T-test; $t(8) = -3.03$; $P = 0.0081$) and *Sequoia sempervirens* (SEQ; 2-tailed T-test; $t(8) = -3.53$; $P = 0.0038$).

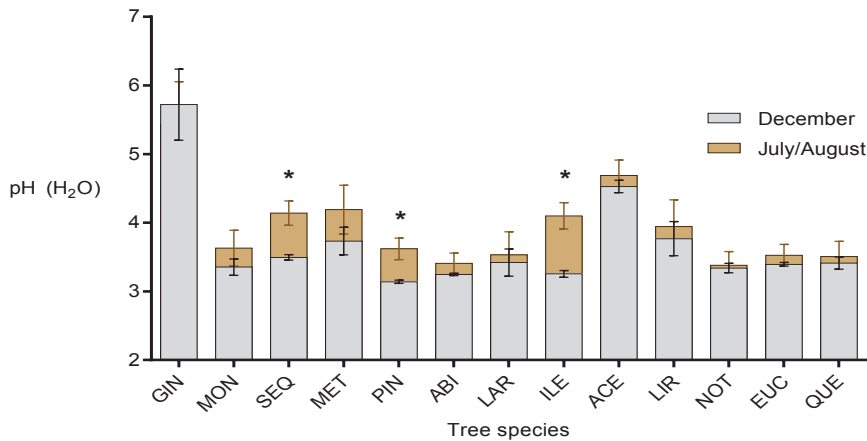


Figure 2.10. Seasonal variation in soil pH at Bedgebury pinetum, arranged by tree species (N = 5 for all species except *Ginkgo*, GIN, where N = 4). Measurements were performed in summer (31st July – 2nd August; brown) 2013 and again in December (grey) the same year. * denotes species where pH is significantly affected by season (2-tailed T-Test, $P < 0.05$).

2.3.2.2 Species-specific differences in pH

Only mycorrhizal type had a significant effect on soil pH in summer 2013 at Bedgebury, considering all tree species surveyed at Bedgebury, both for the weathering study and re-analysis of Ovington plots (Figure 2.11, N = 23 species). A 3-way ANOVA was used to test the effects of tree functional group (Angiosperm/Gymnosperm; $F_{1,15} = 1.96$, $P = 0.18$), associated mycorrhizal type (AM/EM; $F_{1,15} = 7.35$, $P = 0.016^*$) and leaf habit (E: evergreen/ D: deciduous; $F_{1,15} = 1.28$, $P = 0.28$), interaction terms were not significant and are not reported here.

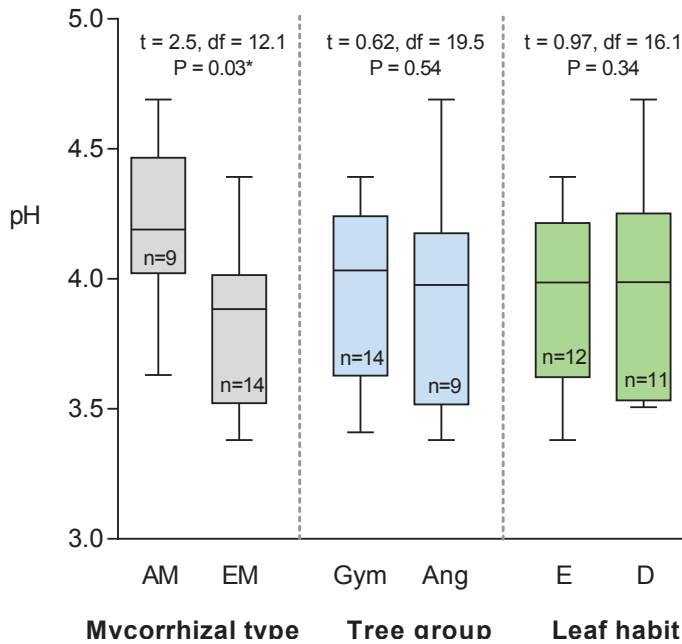


Figure 2.11. Soil pH (July/August 2013; measured in dH_2O) for all species surveyed at Bedgebury, both for weathering study and re-analysis of Ovington plots (N = 23 species total; pH is average of 5 measurements per species). Data grouped by mycorrhizal type (grey; AM/EM), tree type (blue; angiosperm/gymnosperm) and leaf habit (green; E: evergreen, D: deciduous). Results of unpaired T-Test with Welch’s correction shown for each grouping.

2.3.2.3 Evolution of pH over time

There is no significant difference between soil pH for angiosperm species between the 3 sampling years 1951, 1971 and 2014 (Figure 2.12; 1-way repeated measures ANOVA; $F_{1,3} = 1.3$, $P = 0.37$); however, there is for gymnosperms (1-way repeated measures ANOVA; $F_{1,6} = 14.0$, $P = 0.008^{**}$). This is largely due to a significant acidification between 1951 and 1971 ($t = 3.54$, $df = 9.28$, $P = 0.006^{**}$). At the first sampling, in 1951, there is no significant difference in soil pH between angiosperms and gymnosperms ($t = 1.20$, $df = 3.22$, $P = 0.31$). By 1971, the pH of gymnosperm soil acidifies, diverging from that of angiosperms ($t = 4.91$, $df = 6.61$, $P = 0.002^{**}$), before converging again by the 2014 sampling ($t = 0.72$, $df = 4.33$, $P = 0.51$).

Considering all species, regardless of functional group, there is a significant difference in soil pH between samplings (1-way repeated measures ANOVA; $F_{1,11} = 8.1$, $P = 0.012^{*}$; Figure 2.12), however, this is driven by the acidification under gymnosperm species in 1971, as there is no difference between pH in 1951 and that in 2014 ($t = 0.14$, $df = 15.0$, $P = 0.89$).

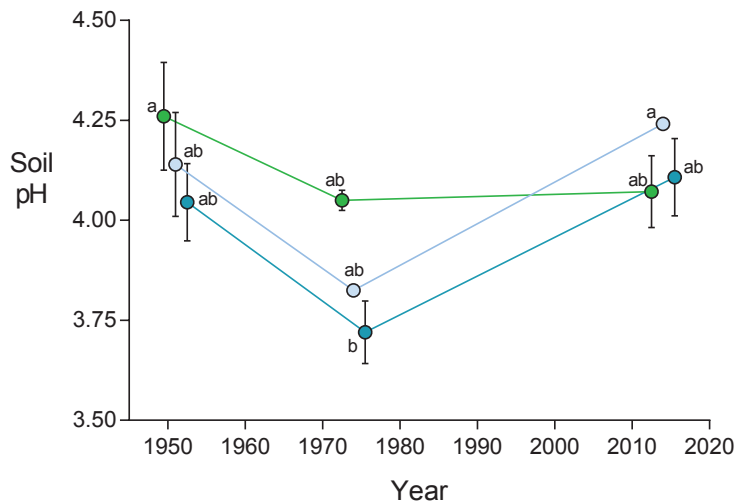


Figure 2.12. Soil pH at 1951, 1971 and 2014 samplings, grouped by tree-mycorrhizal functional group (EM angiosperm, green (N = 3); EM gymnosperm, dark blue (N = 4); AM gymnosperm, light blue (N = 2)). Letters denote results of Tukey HSD test, points sharing the same letter are not significantly different.

Chapter 2

2.3.3 Extractable phosphorus

Phosphorus content of organic and mineral soil is significantly higher in 2014 compared with either 1951 or 1971 (1-way repeated measures ANOVA; $F_{1,9} = 8.7$, $P = 0.015^*$; Figure 2.13A), however, does not increase continually throughout stand development (Linear regression: organic soil, $F_{1,1} = 70.4$, $P = 0.076$; mineral soil, $F_{1,1} = 25.3$, $P = 0.13$). Over the duration of the study, phosphorus content of organic soil is significantly greater than that of the upper mineral horizon (ANCOVA; $F_{1,3} = 44.8$, $P = 0.0068$). While there is a large variation in extractable phosphorus content between tree species (Figure 2.13B), this cannot be attributed to any individual functional group characteristic such as tree or mycorrhizal type either when all species are analysed nor when only those growing on BE soil are considered (3-way ANOVA, Table 2.5).

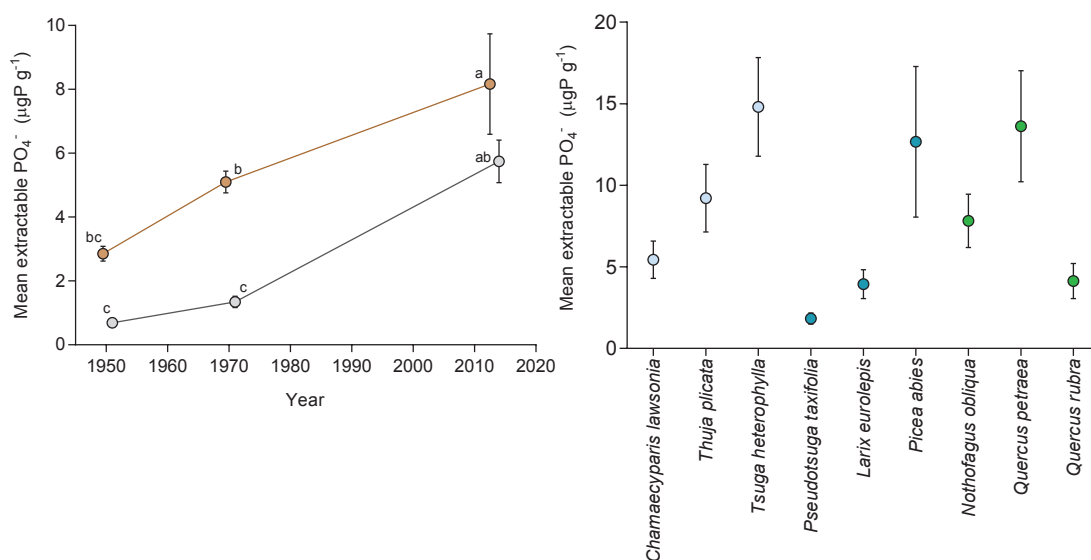


Figure 2.13. A) Phosphate content of organic (brown) and mineral (grey) horizons extracted from air dried and powdered soil ($N = 9$ tree species). Letters denote results of Tukey HSD test, points sharing the same letter are not significantly different. **B)** 2014 Extractable phosphate content of organic soil, summarised by tree species and coloured to identify tree-mycorrhizal functional group (EM angiosperm, green; EM gymnosperm, dark blue; AM gymnosperm, light blue). *Pseudotsuga* and *Nothofagus* have been excluded from the second analysis considering only species growing on BE soil type.

Table 2.5. Results of 3-way ANOVAs, showing the F statistic and significance, for phosphorus content ($\mu\text{g g}^{-1}$ air dried soil) of organic and mineral soil for each of 3 sampling years for all tree species (top of table) and of the subset containing only species growing on BE soil (bottom of table). ANOVAs were used to test the effects of tree functional group (angiosperm/gymnosperm), associated mycorrhizal type (AM/EM) and leaf habit (E: evergreen, D: deciduous). Non-significant interaction terms were not included in this table.

Year	Soil Horizon	Mycorrhizal type (AM/EM)	Tree type (Ang/Gym)	Leaf habit (E/D)
1951	Organic	$F_{1,5} = 0$ $P = 0.99$	$F_{1,5} = 0.16$ $P = 0.71$	$F_{1,5} = 0.19$ $P = 0.19$
	Mineral	$F_{1,5} = 0.20$ $P = 0.68$	$F_{1,5} = 0.30$ $P = 0.61$	$F_{1,5} = 1.06$ $P = 0.35$
1971	Organic	$F_{1,5} = 0.34$ $P = 0.59$	$F_{1,5} = 0.47$ $P = 0.47$	$F_{1,5} = 0.39$ $P = 0.40$
	Mineral	$F_{1,5} = 0.58$ $P = 0.058$	$F_{1,5} = 2.52$ $P = 0.17$	$F_{1,5} = 0.003$ $P = 0.96$
2014	Organic	$F_{1,5} = 0.06$ $P = 0.82$	$F_{1,5} = 0.003$ $P = 0.96$	$F_{1,5} = 0.85$ $P = 0.40$
	Mineral	$F_{1,5} = 0.33$ $P = 0.59$	$F_{1,5} = 0.17$ $P = 0.70$	$F_{1,5} = 0.09$ $P = 0.78$
1951	Organic	$F_{1,3} = 0.01$ $P = 0.94$	$F_{1,3} = 0.23$ $P = 0.66$	$F_{1,3} = 1.55$ $P = 0.30$
	Mineral	$F_{1,3} = 0.69$ $P = 0.47$	$F_{1,3} = 0.32$ $P = 0.61$	$F_{1,3} = 2.5$ $P = 0.21$
1971	Organic	$F_{1,3} = 0.61$ $P = 0.47$	$F_{1,3} = 0.10$ $P = 0.77$	$F_{1,3} = 0.51$ $P = 0.53$
	Mineral	$F_{1,3} = 0.27$ $P = 0.64$	$F_{1,3} = 1.27$ $P = 0.34$	$F_{1,3} = 0.02$ $P = 0.91$
2014	Organic	$F_{1,3} = 0.50$ $P = 0.53$	$F_{1,3} = 0.17$ $P = 0.71$	$F_{1,3} = 3.53$ $P = 0.16$
	Mineral	$F_{1,3} = 0.02$ $P = 0.90$	$F_{1,3} = 0.37$ $P = 0.58$	$F_{1,3} = 0.54$ $P = 0.52$

2.3.4 Extractable calcium

Calcium content of top soil (0-5cm depth) is significantly different between the 3 sampling years (1-way repeated measures ANOVA; $F_{1,9} = 7.2$, $P = 0.022^*$; Figure 2.14). Between 1951-1971, there is a significant decline (Paired T-test; $t = 2.90$, $df = 8.0$, $P = 0.020$) in extractable soil calcium, however, by 2014 there is a much wider range and an overall increase in mean calcium content compared to 1971 (Paired T-test; $t = 3.18$, $df = 8.0$, $P = 0.013$). Considering each sampling year individually, there is no effect of tree or mycorrhizal type or leaf habit on soil-Ca content either when all tree species are analysed nor when only those growing on BE soil are included in the analysis (Table 2.6).

Chapter 2

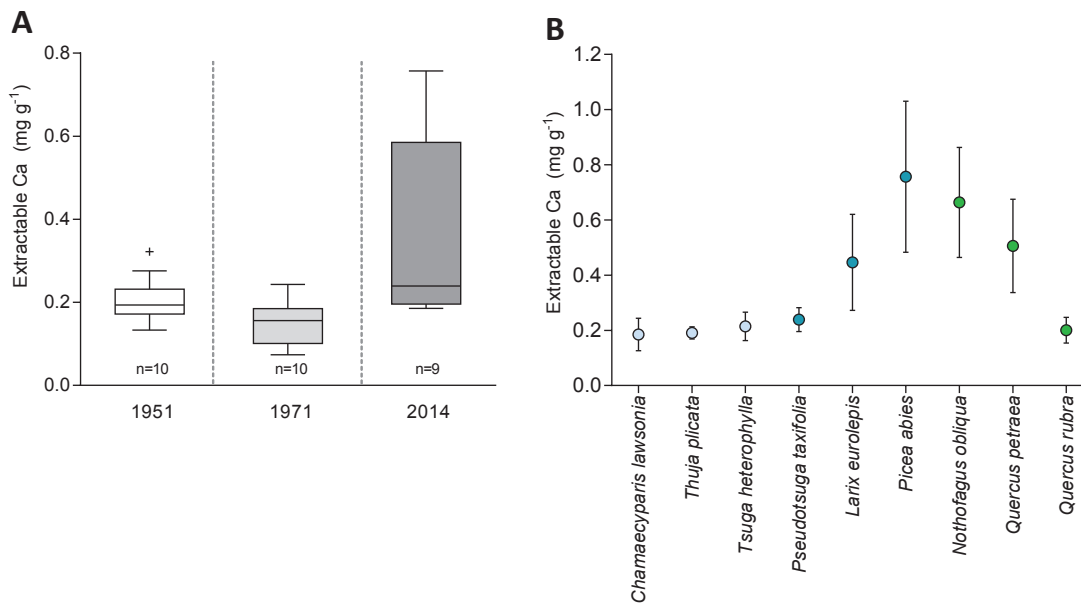


Figure 2.14. Calcium content of upper soil (0-5cm) determined after acetic acid (2.5%) extraction of air dried soil in A) 1951, 1971 and 2014, and B) in 2014, summarised by tree species and coloured to identify tree-mycorrhizal functional group (EM angiosperm, green; EM gymnosperm, dark blue; AM gymnosperm, light blue). *Pseudotsuga* and *Nothofagus* data excluded from reanalysis in **Error! Reference source not found.** as these species are not included in the subset on BE soil.

Table 2.6. Results of 3-way ANOVAs, used to test the effects of tree functional group (Angiosperm/Gymnosperm), associated mycorrhizal type (AM/EM) and leaf habit (E: evergreen, D: deciduous) on extractable soil calcium content (mg g⁻¹ air dried soil) for each of 3 sampling years for each of 3 sampling years for all trees sampled (top of table) and for the subset of only species growing on BE soil (bottom of table). Interaction terms were not statistically significant and are not included in this table.

Year	Mycorrhizal type (AM/EM)	Tree type (Ang/Gym)	Leaf habit (E/D)
1951	F _{1,5} = 1.02 P = 0.36	F _{1,5} = 0.08 P = 0.79	F _{1,5} = 0.25 P = 0.64
1971	F _{1,5} = 0.05 P = 0.83	F _{1,5} = 0.59 P = 0.47	F _{1,5} = 3.02 P = 0.14
2014	F _{1,5} = 2.07 P = 0.21	F _{1,5} = 0.86 P = 0.40	F _{1,5} = 2.93 P = 0.15
1951	F _{1,3} = 3.00 P = 0.18	F _{1,3} = 5.36 P = 0.10	F _{1,3} = 0.90 P = 0.41
1971	F _{1,3} = 0.01 P = 0.96	F _{1,3} = 0.43 P = 0.56	F _{1,3} = 3.22 P = 0.17
2014	F _{1,3} = 2.83 P = 0.19	F _{1,3} = 2.60 P = 0.21	F _{1,3} = 6.17 P = 0.09

2.4 Discussion

2.4.1 Climate

Over the study period where weather data were available, the climate at Bedgebury experienced average warming of 0.026 ± 0.006 °C per year (Figure 2.9B). At a local scale, this reflects ongoing observations that global mean temperature has been increasing steadily since 1960 (Hansen *et al.* 2013). Daily minimum temperature (Figure 2.9C) exhibits a much stronger positive trend than maximum temperature (Figure 2.9A), a trend that has been seen in Europe (Mogberg and Jones 2005), the US (Brown *et al.* 2010), Iran (Ghasemi *et al.* 2015) and globally since the 1950s, especially at high latitudes in Russia and Canada where minimum temperatures rose up to 4°C (Brown *et al.* 2008). Global warming is expected to affect terrestrial mineral weathering rates (Section 1.6); however the exact nature of these feedbacks between climate change and carbonate weathering are not yet fully understood.

In an attempt to extend the climate record at Bedgebury back to the date of tree planting (1929), data from the nearest weather stations Southampton and Marston were analysed. The climate at both these sampling locations is milder than that at Bedgebury, with a much narrower temperature range (Figure 2.9D). Both Bedgebury and Southampton exhibit the same trend of rising minimum temperature, but this occurs to a lesser extent at Southampton, likely due to its coastal location. The much milder climate with fewer extremes in temperature makes this data unsuitable for predicting changes at Bedgebury.

2.4.2 Discussion of results in relation to research hypothesis 1

All forest soil at Bedgebury is acidic, and its pH varies intra-annually, becoming more acidic in late summer and autumn compared to winter, spring and early summer. Evergreen gymnosperm (EG) species produce more acidic bulk soil conditions than deciduous angiosperms (DA).

2.4.2.1 Seasonal variation in pH

At Bedgebury, during 2013, the soil of some tree species were more acidic in early December, relative to the summer sampling (31st July – 2nd August; Figure 2.10). Superficially this contrasts with our first hypothesis that interannual variation in soil pH will result in greater acidity in late summer and autumn than in winter, spring or early summer (Baker and Clapham 1939). However, prior to the December sampling there had only been 6 days where air temperatures fell below freezing, so greater winter soil acidity could still be due to preceding high levels of microbial activity.

Chapter 2

2.4.2.2 *Species-specific impacts on forest soil characteristics*

All soils at Bedgebury were acidic, with pHs below 5 (Figure 2.11), however, there was no significant difference between angiosperm and gymnosperm soil pH, except in 1971. After 50 years of stand establishment, gymnosperm soils were more acidic than those of angiosperms, however, soil characteristics converged again by the second resampling in 2014 (Figure 2.12).

The 1971 difference in soil properties may be due to faster soil development under some EG species, before reaching the same eventual end-point (Binkley and Menyailo 2005). This serves as a reminder that tree-species influence on soil properties is dynamic, with their impact varying throughout stand establishment and maturation. Another explanation may be due to differing weather between the three samplings. While the lack of temperature data prior to 1959 precludes us from making a comparison based on this, differences in rainfall correlate with the divergence in pH. Both 1951 and 2014 were exceptionally wet, with 1096 and 1041 mm rain, respectively, contrasting with 1971 which was relatively dry with only 728 mm rain (1951 and 1971: Bedgebury weather station data, Figure 2.8; 1971: Met Office summary data for SE and S England (2016)). Most of the gymnosperms were evergreen, and the closed canopy may have shaded the soil, reducing evaporation, thus maintaining greater soil microbial activity and base cation leaching relative to that in deciduous angiosperm soils.

The results of this studies supports that of previous works that have found no impact of tree type on soil pH (Hallbäck and Tamm 1986), and contrary to our hypothesis that there would be greater acidification by EG than by DA species, based on the meta-analysis of Augusto *et al.* (2015). However, the current study is limited by the low resolution of temporal data and the smaller sample size for angiosperm (1971: N = 3; 2014: N = 9) than for gymnosperm (1971: N = 6; 2014: N = 14) species.

Considering a larger range of species than those selected by Ovington, soil under trees forming EM associations tends to be more acidic than that under species forming AM associations both in summer (Figure 2.11) and in winter (Thorley *et al.* 2015). This acidification is probably due to a combination of factors including LMWOA (Arvieu *et al.* 2003; Casarin *et al.* 2003; van Scholl *et al.* 2006) and carbonic anhydrase (Li *et al.* 2005) secretion by EM fungi, and greater carbon input into soil from host trees enabling increased microbial respiration and consequent acidification from CO₂ dissolution (Andrews and Schlesinger 2001).

EM soil acidification, and the nature of acids contributing (Binkley and Valentine 1991), has important implications for mineral weathering, with organic acid concentrations key to determining the supply of bioavailable base cations Ca, Mg and

Fe (Raulund-Rasmussen 1998). These acids increase the chelating capacity of soil, for instance, analysis of spruce forest soil solution indicated DOC content, and not purely pH, to be the main factor influencing inorganic nutrient release from mineral soil (Raulund-Rasmussen 1998).

2.4.3 Discussion of results in relation to research hypothesis 2

Trees alter soil geochemical properties in a species-specific manner. Fast growing gymnosperm species have higher nutrient stocks than slower growing and angiosperm species.

Soil phosphate (here referred to as P) and calcium are highly dependent on tree species, with large inter-species variation (Figure 2.13B and Figure 2.14B), however, these between-species differences could not be attributed to any overarching characteristic such as tree or mycorrhizal type, or leaf habit (Table 2.5; Table 2.6). With the particular plots investigated by Ovington, there may have been some variation in original soil type across the site (Figure 2.7), however, most species surveyed lay within areas denoted as having a brown earth soil type. When this possible bias was removed by repeating the analysis for only the subset of species growing on BE soil, there were still no evidence that tree-mycorrhizal functional group was the underlying driver of species-specific differences for either Ca or P (Table 2.5; Table 2.6).

2.4.3.1 Soil phosphorus content increases over time

Over time, there is an increase in concentration of extractable soil phosphate, with significantly higher soil P-content in 2014 compared to earlier samplings. Phosphate content was especially high in the upper, organic soil horizon (Figure 2.13), suggesting that it is sourced from mineralisation of OM. Gradual leaching of relatively immobile P will slowly increase extractable-P content of mineral soil (Stevens *et al.* 1995), but if the dominant P-source is OM mineralisation, which is occurring at and near to the soil surface, it is likely that P-content decreases descending the soil profile.

Increased availability of phosphate in topsoil has been observed over the course of grassland afforestation, and is largely due to increased mineralisation of OM under conifers compared to grasses (Condon *et al.* 1996; Chen *et al.* 2008). For the conifers, this P-increase was attributed to greater tree P-demand and uptake; increased P-solubilisation by root and microbial exudates, including LMWOAs; and increased phosphatase activity surrounding EM, compared with AM fungi associated with grasses (Chen *et al.* 2008). While this is not the exact situation at Bedgebury, there are parallels. At the beginning of the study, soil P is probably depleted due to clear felling

Chapter 2

and removal of biomass (Stevens *et al.* 1995), however, roots and discarded branches form a source of organic P that can be accessed as they decompose.

It may be that some angiosperm species may increase P-mineralisation to a greater extent than conifers, as shown by the dramatic increase in extractable phosphate content of topsoil within a Douglas fir, *P. menziesii*, plantation, following dispersed planting of red alder, *Alnus rubra* (Giardina *et al.* 1995). However, given the large inter-species variation in organic soil P-content (Figure 2.13B), it is more likely that this effect is specific to *A. rubra*, and not angiosperms in general.

2.4.3.2 Proximity to neighbouring species

One major limitation limiting the understanding of species-specific soil development using the experimental forest plots setup at Bedgebury is the proximity of neighbouring plots. The close proximity of plots will inevitably create overlap between root systems (Kallioikoski *et al.* 2008), so there will effectively be more than one species exerting influence on pH and other soil characteristics, particularly at the edge of plots where species are closest. In addition to rooting overlap, litterfall may also come from neighbouring species (Binkley and Valentine 1991). The chequerboard experimental design of their study had 11×11 m sized alternating single species blocks containing pairs of green ash, white pine and Norway spruce. Between 20 and 30% of litter collected from neighbouring plots and a combination of this and rooting overlap and of produced intermediate soil characteristics. For instance, pine plots bordered by ash had far higher pH than pine neighbouring spruce (Binkley and Valentine 1991).

Overlapping root systems will inevitably change forest processes relative to single species stands. This is likely to be though a combination of changed litter input and decomposition; organic acid production and different exudates in the rhizosphere or mycorrhizosphere. Roots of mature tree species in this experiment are likely to extend well into adjacent plots (Figure 2.15), as described by measurements and modelling studies of Kallioikoski *et al.* (2008) in mixed species boreal forests. There is some indication that angiosperm species may have more extensive root systems than gymnosperms (Figure 2.15). This is shown by the greater rooting extent of *B. pendula* compared to *P. sylvestris* and *P. abies* (Kallioikoski *et al.* 2008) and by Yeager *et al.* (1935) who estimated the tree height ratio of green ash (*Fraxinus lanceolata*) to be 1.2, compared to two spruce species, *Picea canadensis* and *Picea pungens* which had ratios of 0.7 and 0.4 respectively.

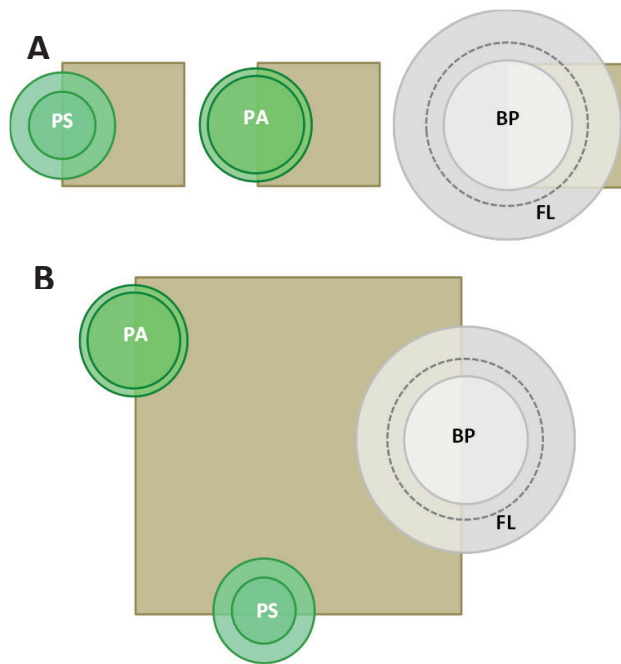


Figure 2.15. Illustration of rooting sizes to demonstrate how far rooting systems would extend into neighbouring **A)** 11×11 m and **B)** 30×30 m plots (brown squares) if planted on the border between plots. Mean (inner circle) and maximum (outer circle) rooting extension of mature *P. sylvestris* (PS), *P. abies* (PA), *B. pendula* (BP) and *F. lanceolata* (FL: dashed line on BP). Based on data from Kallioski *et al.* (2008) and Yeager (1935).

2.4.4 Discussion of results in relation to research hypothesis 3

The greatest species-specific differences in soil characteristics are observable during the early-mid rotation of plantation forests, and declining as forest stands establish. Divergence in soil characteristics takes longer for angiosperms than for gymnosperms, due to the longer time required for these slower-growing trees to complete a forestry rotation.

2.4.4.1 Species-specific pH divergence at 1971 sampling

Research hypothesis 3 is partly supported by the observation that the only significant difference in soil pH between angiosperm and gymnosperm species were measured in 1971, after 50 years of stand maturation. This result is not mirrored for any other soil characteristic measured in the 2014 re-analysis, namely Ca and P. It is probable that temporal evolution of soil characteristics is confounded by differences in analytical methodology and treatment of data between the three sampling years. For instance, in 1971, pH results were ‘corrected’ by adding 0.3 pH units (Howard and Howard 1984), however, in the absence of information as to how this correction was derived, for instance, by use of a standard reference material, no correction factors were applied to 2014 pH data.

Chapter 2

2.4.4.2 Increased between-species variation for soil extractable P-content

Over time, there is an increase in between-species variation for organic soil extractable phosphate content (Figure 2.13). This partly supports the third hypothesis that soil properties diverge over time as a result of species-specific alterations, however, conflicts with the expectation that they would again converge as the trees matured. Unfortunately, it is not known if this increase in variation is statistically significant, not only due to differences in analytical methods, but also as a result of incomplete data reporting from 1951 and 1971 samplings. There is no measure of within-species variance for either historical dataset as although 5 sites within each forest stand were sampled, as in the 2014 study, individual values not reported and it is not possible to perform a robust statistical analysis.

2.4.4.3 Soil extractable calcium

Soil extractable Ca at Bedgebury decreased over the period 1951-1971 (Figure 2.14), probably due to tree uptake. However, as the depletion of Ca was less than would be expected, from Ca-incorporation into woody biomass, it is suggested that Ca must have been replenished over the study period, probably by weathering (Howard and Howard 1984). This is plausible as the parent lithology underlying surveyed forest plots at Bedgebury is mudstone (Figure 2.7B), a sedimentary rock composed of mud and clays, which can contain variable quantities of Ca, mainly deriving from Ca-rich plagioclase or from calcite or dolomite (0.4-6.5% wt. Ca; Boggs 2009).

Between 1971 and 2014, on the other hand, soil extractable Ca increased significantly. There are three possible explanations for this. Firstly, it may be that this additional Ca comes from weathering, which has intensified as tree stands matured and the mycorrhizal community established. Secondly, there is potentially reduced leaching of Ca from the 1980s onwards after the introduction of UK government policies to combat acidic emissions and combat the impact of acid rain impact on vegetation and aquatic environments (Kernan *et al.* 2010). This is unlikely, as although there is an increase in gymnosperm soil pH, this is not true for angiosperms, and both tree groups would be equally impacted by an environmental factor such as acid rain (Figure 2.11). The third, and most likely explanation, is that differences in analytical methodology and improved detection resolution by AAS contribute to this apparent increase, and it may be that data are not comparable between sampling years.

2.4.4.4 Impact of soil Ca on weathering rates

Soil calcium content can indirectly affect mineral weathering rates via its control over soil pH (Ovington 1953; Challinor 1968; Dijkstra 2003) and macro-

invertebrate communities (Ponge *et al.* 1999; Reich *et al.* 2005). The greatest source of available Ca in upper forest soils is thought to be decaying organic matter from litter and roots (Dijkstra 2003); however, some will come from weathering of Ca-containing carbonate and silicate rocks, the relative importance of this input depending on the nature of the soil parent lithology.

Calcium cations adsorb to decaying organic matter in exchange for acidic H^+ which is then leached. This results in Ca immobilisation in the upper horizons, buffering the soil against acidification by organic acids. This has been observed in a Norway spruce forest, planted on a site formerly occupied by beech trees (Nihlgard 1971). Spruce planting reduced the concentration of base cations, K^+ and Ca^{2+} , coincidentally lowering soil pH. These effects on both soil cation content and pH are strongest directly below the decomposing litter (Augusto *et al.* 2000).

Studies in both Polish (Reich *et al.* 2005) and French forests (Ponge *et al.* 1999) have shown both abundance and diversity of earthworms to be greatest in Ca-rich soils with low carbon content. For example, in the old growth beech forests of Fontainebleu, Ponge *et al.* (1999) demonstrated an increase in earthworm abundance with increasing proximity to the underlying limestone bedrock. Earthworms mix organic and mineral soil horizons (Ovington 1953) and decompose and redistribute fresh litter. Sites with large earthworm populations generally have only a thin litter layer of relatively undecomposed leaves (Hobbie *et al.* 2007), and this rapid litter decomposition increases N-mineralisation, thus fertilising tree growth. This has knock-on effects for mineral weathering for acquisition of limiting nutrients, such as P, and together with increased soil mixing may accelerate dissolution reactions (Figure 2.16).

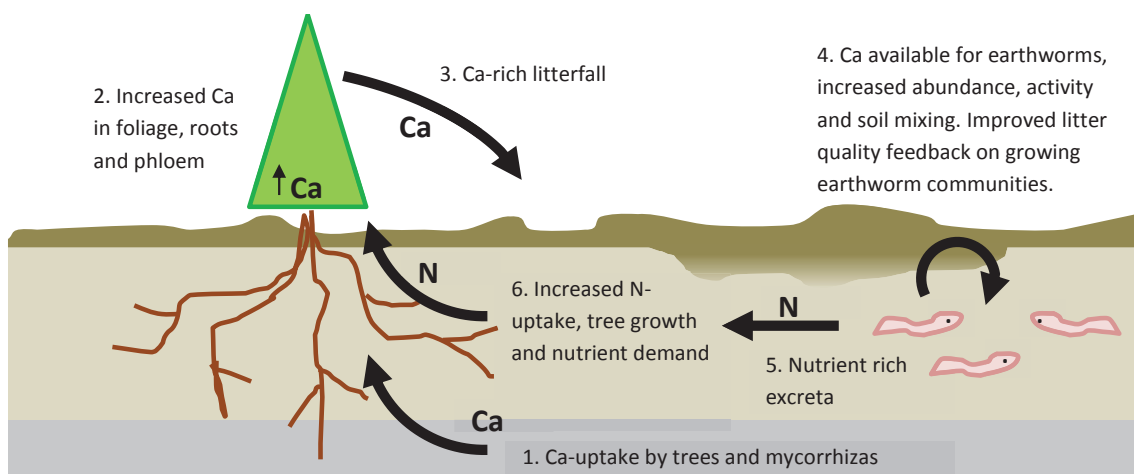


Figure 2.16. Impact of weathering Ca-availability on foliage composition, litterfall and decomposition by macroinvertebrate communities.

Chapter 2

2.4.4.5 *Effect of brickearth and marling*

One additional difficulty in understanding species-specific influence on soil Ca at Bedgebury stems from heterogeneous soil types, including brickearth, and historical land management practices such as marling (Howard and Howard 1984b). Marling was a common agricultural practice in the UK from the 16th to 18th centuries and involves the application of calcite-rich mud to improve soil properties, including increasing water holding capacity. Marl pits have been identified in Sussex, which borders our study site at Bedgebury (Jeffery 2008).

Brickearth is a superficial deposit of wind-blown silt that was deposited during the Late Devensian Stage of the last glacial period. It is generally found as thin and patchy deposits throughout the south of England, in particular in Kent, where our study site Bedgebury is located. Where present these deposits produce rich and fertile soils as a result of abundant silt particles, enabling greater water holding capacities, better aeration and reserves of both macro and micro nutrients from easily weatherable minerals. In Kent, loess brickearth has a characteristic mineral composition which has been determined using XRD across several sites by Derbyshire and Mellors (1988). All deposits contained a range of clay phyllosilicates (Kaolinite, Illite, Montmorillonite, Vermiculite), quartz and feldspars with some additionally containing both calcite and dolomite.

The extent or location of either brickearth patches or marling at Bedgebury has never been surveyed or reported, but is likely that these conditions may occur within the plot of *P. nigra* where soils exhibited high extractable Ca and K, potentially due to accidental sampling of brickearth patches, which may contain K-feldspars, or marled areas containing relatively high calcite (Table 2.2). Sampling differences may also explain an apparent ‘rapid change’ in *P. nigra* soil characteristics between the 1951 and 1971 (Howard and Howard 1984b), if on one occasion a brickearth patch was sampled, however, this plot was felled prior to the current study and has not been re-surveyed.

Even after removing obvious anomalous plots there may still have been some underlying site characteristics that could have driven differences in soil biogeochemical characteristics. One such factor was slight differences in soil type (Figure 2.7A). Most of the 9 plots reanalysed were denoted as having brown earth soil, however, 2 had brown gley soil. Despite repeating the analysis taking these potential differences in soil type into account this was found to have no significant impact on the results described in this chapter. In reality, field observations call into question the usefulness of the soil map in Figure 2.7A. As it is unknown what sampling resolution was used to produce

this map and the boundaries between soil type were not evident in the field, it may have limited relevance at the fine spatial scales used for a plot-plot study.

2.4.4.6 Limitations of using different analysis methodologies

Where possible, the 2014 resampling attempted to replicate laboratory procedures used in 1951 and 1971. However, due to either incomplete methodological reporting, or development of new techniques, some methods differed between these years. For example, colourimetric P measurement using molybdenum blue was performed at all 3 sampling points after acetic acid extraction; however, it is still not clear whether these data are directly comparable.

Results of P-extractions are known to be highly dependent on soil extraction technique (Giardina *et al.* 1995), and soil preparation methods varied between sampling years. In 1951 and 1971, soil was oven dried at 80 and 105°C respectively, but in 2014 it was air dried in 2014 and powdered to ensure sample homogeneity. Neither Howard and Howard (1984), nor any of Ovington's papers, detail further soil preparation techniques, so it is unclear whether soil samples were representative of each site. It may be that finely milling soil, as in 2014, increased the extractability of Ca and P, accounting for their higher concentrations at the most recent sampling (Figure 2.13A, Figure 2.14A).

2.4.4.7 Limited temporal resolution of data

Increased sampling frequency is required to more fully investigate both the second and third research hypotheses. There is a lack of appropriate baseline data for the forest plots at Bedgebury, and changes in soil characteristics within the early stages of stand establishment are not known at this site. When plots were sampled in 1951 they had only been developing for 20 years, and changes may also result from the preceding clear felling of coppice (Stevens *et al.* 1995).

2.5 Conclusions

The 2014 re-analysis of experimental plots at Bedgebury provides an 85 year record of soil development under different forestry tree species. Forest plots were established in the late 1920s to test the potential yields of native UK and imported forestry species, and soil geochemical properties surveyed in both 1951 and 1971. This study reports results of a recent re-analysis (2014) focusing on soil pH and extractable P and Ca. To the best of my knowledge, through literature searches on the web, this is the longest-running, in-situ, record of forest soil changes, not just in the UK, but globally.

This study supports the emerging view that mycorrhizal type plays a critical role in determining soil pH, with the most acidic soils developing under trees forming EM rather than AM associations. Acidification by EM fungi is likely to result from a combination of factors including LMWOA and carbonic anhydrase secretion, in addition to greater carbon input into soil from host trees. This contrasts with the classical viewpoint that coniferous trees form the most acidic soils (Ovington 1953; Augusto *et al.* 2015). Overall, the results of our re-analysis demonstrate no consistent impact of tree type on soil pH, with highly acidic soils forming below both angiosperm and gymnosperm species.

The impact of AM versus EM fungi on soil chemistry was first proposed by Binkley (1994) in a theoretical model of processes that might explain tree species-specific influences on nutrient flows and soil fertility (Binkley 1994). Mycorrhizal type has also been cited as a confounding factor within studies comparing evergreen gymnosperm (coniferous) trees to deciduous angiosperms (hardwoods), which comprise the bulk of classical studies (Augusto *et al.* 2015). However, the impacts of mycorrhizal partner have only been quantified in the context of N-mineralisation, and phosphatase activity which were both greater by AM than EM species (Philips and Fahey 2006). This lack of awareness of mycorrhizal influence in early studies presents an opportunity for re-interpreting results of many historical studies, and presents an avenue for future work.

Other soil chemical characteristics measured during this re-analysis, namely extractable Ca and P, varied drastically between species. Extractable P content increased steadily in both organic and mineral soil horizons, which is probably due to increasing microbial P-mineralisation of organic matter within established tree stands with abundant litter. Although concentrations of both elements changed significantly over time, this could not be attributed to any simple factor such as tree or mycorrhizal type or leaf habit, nor any interaction between these. This study has highlighted many challenges in integrating historical and contemporary soil chemistry datasets.

Differences in both sampling and analysis methods used during each sampling period make it very difficult to compare soil geochemical characteristics over a long a time scale as the current study, not to mention inconsistencies in data and methodological reporting.

While this study has provided some insights into mycorrhizal influence over soil pH and phosphorus dynamics over stand maturation, there is some conflict with literature findings (France 1989; Nihlgard 1971; Challinor 1968), emphasising the complex nature of species effects on soil development. A wealth of literature surrounds the topic of species impacts on soil properties: Augusto *et al.* (2015), Binkley and Giardina (1998), Binkley and Valentine (1994), Hobbie *et al.* (2007), Howard and Howard (1984) and Ovington (1953-1958), to name a few, however, it is still unknown to what extent results, even from replicated, common-garden experiment can be made into reliable generalisations applicable across different sites. As a necessity, such studies evaluate limited numbers of species, and due to the high inter-specific variation of many soil geochemical characteristics, the exact selection of species will have a great effect on average characteristics calculated for any particular functional group.

In reality, soil properties develop as a result of complex interactions between site-specific environmental factors, and the biota, including trees, other vegetation and microbial community (Augusto *et al.* 2015, Binkley and Giardina 1998). Soil chemistry depends strongly on underlying geology, land use history (Howard and Howard 1984b), forest management practices such as felling regimen (Stevens *et al.* 1995) and other environmental factors such as microclimate, drainage and invertebrate community (Reich *et al.* 2005). The forest plots at Bedgebury come close to fulfilling all the prerequisites for an appropriate site for a common-garden replicated experiment. All plots experience identical climate and have the same parent lithology, and recent cultivation history, yet there are still very clear differences in pedogenesis between plots that may not be wholly accounted for by biological factors.

Understanding species effects on soil remains a key challenge in ecology. This leaves much scope for both novel investigations, and re-analysis of historical studies in light of a more modern ecological framework. This long-standing challenge can be appropriately summarised in the words of Dan Binkley (1994):

“The effects of tree species on forest soils have been discussed for more than a century. The limits of knowledge have often been clouded by conclusions based on weak evidence. Replicated plantations within a single location have not supported many generalisations about the influence of trees on soil

Chapter 3

Determination of carbonate weathering rates and phosphorus biogeochemical cycling

3.1 Introduction

3.1.1 Overarching aims

Trees and their associated mycorrhizas are thought to be key drivers of rock weathering. The first part of this chapter aims to quantify the weathering rates of different calcite and dolomite containing rocks, when exposed to different tree and mycorrhizal functional groups. This is followed by an investigation of the behaviour of phosphorus, a plant growth limiting nutrient, during the weathering of carbonate and silicate rock grains.

Experimental work for this chapter is based at the UK's national pinetum in Bedgebury, Kent, UK, and aims to characterise the weathering of different carbonate rock types within the soil of single-species stands (30 m²) of mature trees. Five replicate trees of 13 species (Table 3.1) were selected to represent the four main functional groups that make up northern hemisphere forests. These are: AM gymnosperms, AM angiosperms, EM gymnosperms and EM angiosperms.

3.1.2 Weathering enhancement by plants and mycorrhizal fungi

The plant-microbe system regulates flows of carbon, water and nutrients throughout the soil and is important within mineral weathering processes. Carbonate weathering by micro-organisms or plants can be promoted by a variety of direct and indirect mechanisms. The interplay feedbacks between plants, mycorrhizal fungi and weathering soil minerals are summarised here.

There are several mechanisms by which carbonate weathering may occur in forest soils as consequence of biological activity; primarily soil acidification through production and decomposition of organic matter, acid exudates and dissolution of

Chapter 3

respiratory carbon dioxide (reviewed in Landeweert *et al.* 2001). These same mechanisms also apply to some extent if organisms in forest soils are evolutionarily adapted to weather carbonates, as they are to weather silicates. The most notable adaptation is the secretion of substances to aid nutrient acquisition, which are reviewed more fully in Section 1.5.3.

Microorganisms can access mineral nutrients through secretion of weathering agents such as LMWOAs and protons. The resulting provision of inorganic nutrients can increase plant growth and therefore feedback on photosynthetic carbon supply to their associated soil microbiota, including symbiotic mycorrhizal fungi, thereby further promoting soil mineral weathering.

Evidence of silicate weathering enhancement by EM angiosperm tree species has been provided by field and controlled-environment studies (Quirk *et al.* 2012, 2014). In the field, rates of Ca-release from basalt grains were twice as rapid under EM as under AM trees (Quirk *et al.* 2012), and also higher under angiosperm than gymnosperm species. Over 14 months weathering in forest soils, calcium is primarily mobilised from trace carbonates, despite most calcium in North Atlantic Tertiary flood basalts being contained within silicate minerals, such as plagioclase (Scarrow *et al.* 2000). These trace carbonates only constitute approximately half the total extractable Ca in basalt, and their dissolution may affect subsequent silicate weathering through increasing surface area. Both this and the depletion of trace carbonates make it likely that over longer weathering durations, Ca release from silicates may become the dominant Ca source (Figure 3.1).

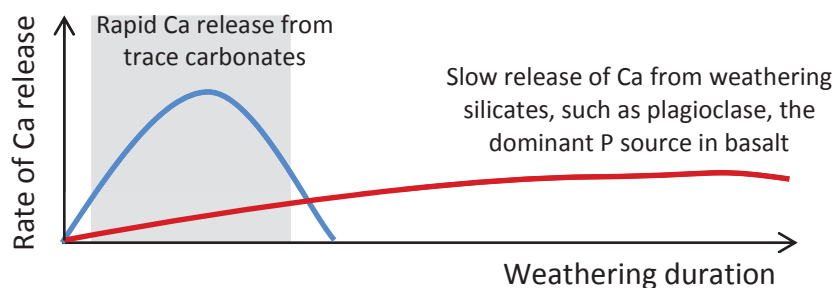


Figure 3.1 Illustration of Ca-release from trace carbonate (blue) and silicate (red) fractions of Tertiary Northern Irish basalt. Shaded area indicates range over which 14-month weathering study in Quirk *et al.* (2012) may have fallen, where Ca-release from carbonates exceeds that from silicates.

Carbonate weathering rates and phosphorus biogeochemical cycling

Weathering may be intensified by forests hosting EM compared to AM fungi as a result of the wider range of weathering mechanisms available to them, and the greater supply of carbon from host trees. Many micro-organisms, including EM fungi, secrete carbonic anhydrase enzyme, which catalyses the formation of carbonic acid from carbon dioxide and water (Li *et al.* 2005). Carbonic acid is possibly the main inorganic weathering agents of carbonates, and its action is responsible for much of the Karst scenery around the world. Release of this enzyme intentionally acidifies the local rhizosphere environment. As CA secretion has a measurable carbon cost, this acidification must have some beneficial function to the organism producing it, which may well be to aid mineral dissolution.

Similarly, oxalate production is well characterised by many EM species as well as other soil micro-organisms. LMWOAs such as oxalate aid mineral dissolution, both through acidification and via complexation of metal cations and thought to be responsible for formation of tunnels into interior of rock grains (van Breemen *et al.* 2000). Ca-oxalate crystals are commonly identified surrounding fungal hyphae (Verrecchia *et al.* 2006), and form as a by-product as a result of excess calcium in the mycorrhizosphere. These crystals are another indication that oxalate secreting organisms are not directly using Ca mobilised, and dissolution may primarily be to solubilise trace elements.

Many experimental studies have attempted to characterise and quantify biological silicate weathering due to its importance in the global carbon cycle and potential for long-term climate regulation through CO₂ sequestration. However, the weathering of some silicates, particularly basalt, is directly linked to that of associated carbonates, which have hitherto not been investigated in such detail. For instance, the majority of Ca-released from Tertiary, Northern Irish basalt, during its weathering in forest soils, is preferentially mobilised from trace carbonates (Figure 3.1). Given both the range of weathering strategies available to EM fungi, and observed silicate weathering enhancement by EM angiosperm species lead to the first hypothesis of this chapter:

Research hypothesis 1

In forest soils, carbonate weathering rates exceed those of silicate minerals and are most intense below EM Angiosperm tree species

Chapter 3

3.1.3 Mycorrhizal weathering for acquisition of limiting nutrients

Mycorrhizal fungal hyphae radiate from root tips forming a network throughout the soil and effectively increasing the surface area of roots for absorption of nutrients (reviewed in Wallander and Thelin 2008). Where rock grains contain inorganic nutrients unavailable elsewhere in the soil, weathering provides exclusive access to that source for the organisms in close contact, such as fungal hyphae. EM fungal weathering can mobilise a range of essential plant nutrients including P, K, Fe, Ca and Mg from mineral substrates including apatite and biotite (Wallander 2000; Leake *et al.* 2008; Bonneville *et al.* 2009). One nutrient commonly limiting and often suggested as a driver of weathering is phosphorus.

Mycorrhizal weathering for phosphorus acquisition has been observed in microcosms containing *P.involutus* in association with *P.sylvestris* (Leake *et al.* 2008). Here, ^{14}C radiolabelling showed EM hyphae were able to biosense, when presented with different mineral resources, based on the interaction between phosphorus content and grain size. In the vicinity of P-rich apatite, there was a proliferation of fungal biomass and increased microbial activity, reflected in increased ^{14}C in soil respiration.

Evidence of biosensing has also been seen in forest soils hosting both AM and EM fungi (Quirk *et al.* 2012). Preferential hyphal colonisation of basalt compared to granite and quartz, indicated that most carbon resources from host plant photosynthesis were allocated to the silicate rocks with greatest concentrations of phosphorus and other weatherable nutrients.

Given that soils at Bedgebury Pinetum contain little available P (Ovington 1958) and that mycorrhizal fungi are able to target mineral weathering to acquire growth limiting nutrients, it is likely that in our study site, P-acquisition will be a major factor influencing weathering. The observation of more rapid Ca-mobilisation from trace carbonates, than from the bulk of silicates in basalt may make P-bearing carbonates even more attractive to fungal weathering than silicates, which leads to the second hypothesis:

Research hypothesis 2

Mycorrhizal dissolution of carbonate rock grains in forest soils increases access to mineral phosphorus, which is selectively depleted over the course of weathering.

Carbonate weathering rates and phosphorus biogeochemical cycling

3.1.4 Interaction of mineral weathering and available soil P resources

Weathering for phosphorus acquisition does not occur in isolation, P availability in soil and the demand for it by plants and micro-organisms must also be considered. Because plants primarily uptake P as orthophosphate, H_2PO_4^- or HPO_4^{2-} , most phosphorus present in soils is unavailable to them. Orthophosphate is the main form of P in soil water, but is usually present only at very low concentrations because inorganic phosphorus compounds are only sparingly soluble in water.

The form of P present in soil depends on the redox potential of the surrounding environment. In acidic conditions ($\text{pH} < 5.5$), reactions between phosphate and aluminium are most favourable, and complexes form with Al, Fe and to some extent, Ca. Where the soil is alkaline, the reaction with Ca dominates. Although in alkaline conditions precipitation with Ca removes P from the soil water pool, calcium phosphate compounds are more soluble than those formed with Al or Fe, and can be later redissolved to replenish the soil water pool.

Carbonate minerals provide an abundant source of base cations and are likely to produce a highly alkaline micro-environment surrounding rock grains as they dissolve. This interaction between Ca and P might be relevant in the weathering of carbonate minerals and leads to the formation of the third hypothesis:

Research hypothesis 3

Additional phosphorus in weathering carbonate grains accumulates passively from inorganic phosphate in the immediate soil environment.

3.2 Methods

3.2.1 Experimental design and sampling

Hyphal in-growth bags containing 2.5g crushed and sieved carbonate rock samples (Particle size 0.5–1.18 mm diameter; Figure 3.2) were incubated below mature stands of angiosperm and gymnosperm trees hosting either AM or EM partners (Table 3.1). Four carbonate rock types were included in this study: (1) marble (Carrara, Italy); (2) oolitic limestone (Oxfordian, N. Yorkshire); (3) chalk (Cretaceous, N. Yorkshire); and (4) dolomite (Permian, Doncaster). These span the entire range of carbonate lithologies beneath N. Hemisphere forests. In-growth bags filled with silicate rock grains were also included in the study as a comparison with previous work based mainly on silicate weathering. The silicate rock used was metamorphosed sandstone and is predominantly composed of quartz (ca. Tertiary, Skye; XRF data, Table A. 3; thin section photos, Figure 5.7, Section 5.3.1). It contains no carbonate, but comparably high phosphorus to the chalk used in this study (Table A. 3, Table 3.11).

Table 3.1. Tree species used in mycorrhizal weathering field study at Bedgebury Pinetum. Tree group: gymnosperm or angiosperm; Mycorrhizal type: ectomycorrhizal (EM) or arbuscular mycorrhizal (AM); leaf habit: evergreen (E) or deciduous (D). Species abbreviations used in figure and table legends.

Mycorrhiza	Tree group	Leaf habit	Species (and abbreviation)	Family	
AM	Gymnosperm	E	Ginkgo biloba	GB	Cupressaceae
		E	Metasequoia glyptostroboides	MG	Cupressaceae
		E	Sequoia sempervirens	SS	Cupressaceae
	Angiosperm	E	Araucaria araucana	AA	Araucariaceae
		E	Ilex aquifolium	IA	Aquifoliaceae
		D	Acer pseudoplatanus	AP	Sapindaceae
		D	Liriodendron tulipifera	LT	Magnoliaceae
EM	Gymnosperm	E	Pinus sylvestris	PS	Pinaceae
		D	Larix decidua	LD	Pinaceae
		E	Abies alba	AA	Pinaceae
	Angiosperm	E	Nothofagus dombeyi	ND	Nothofagaceae
		D	Quercus petraea	QP	Fagaceae
		D	Eucalyptus coccifera	EC	Myrtaceae

Mesh bags were buried at 10 cm depth, approximately 1m from the base of each tree (N = 5 bags per rock type per species; Figure 3.3, Figure 3.4). The pore size of the mesh bags (35 µm pore size) allows hyphal access and exchange of substances with soil pore water colonization but excludes roots. One replicate set of samples was collected from under each of the 5 trees of each species after 3, 7 and 14 months (Table 3.2). After recovery mesh bags were kept cool until back in the laboratory where they were frozen and eventually freeze-dried.

Carbonate weathering rates and phosphorus biogeochemical cycling

Table 3.2. Burial and harvest dates for hyphal in-growth bags containing rock grains. As site selection and experiment preparation was time consuming, initial burial was performed in two sessions in April-May 2013.

	Dates	Days burial
Burial of mesh bags	16-18 th April and 13-14 th May 2013	
First harvest (3 months)	August 1 st 2013	78 or 106
Second harvest (7 months)	2-3 rd December 2013	203 or 229
Third harvest (12 months)	14-17 th July 2014	428 or 454
Fourth harvest (24 months)	21-23 rd May 2015	739 or 765

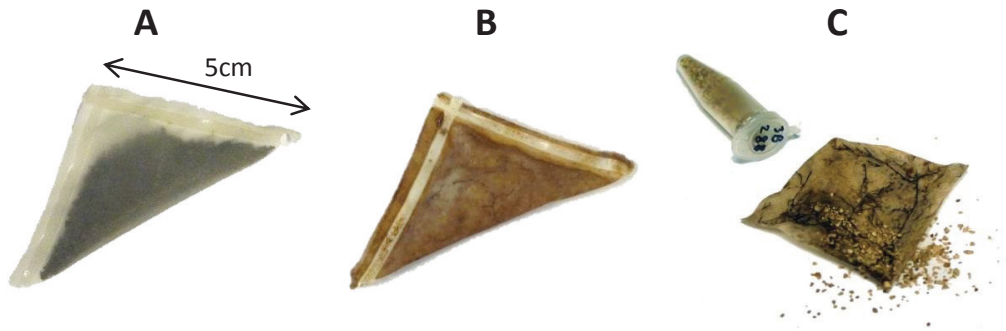


Figure 3.2. Hyphal in-growth bags **A)** before burial **B)** after 7 months burial at Bedgebury and **C)** ingrowth and colonisation of oolite grains by a rhizomorph forming species under *L. decidua*.



Figure 3.3. Fieldwork at Bedgebury with Dr. Joe Quirk and Dr. Dave Johnson. **A)** Burying in-growth bags, April 2013. **B)** 4 Replicate sets of In-growth bags planted, sufficient for 3, 7 and 14 month harvests plus spare in case of sample loss or breakage. Facing towards tree, each set of 5 bags is buried in the same order, clockwise from top left: chalk, dolomite, oolite, marble and silicate in the centre. **C)** Retrieving mesh bags after 7 months burial in December 2013. **D)** Soil sampling using soil corer in Eucalyptus stand.

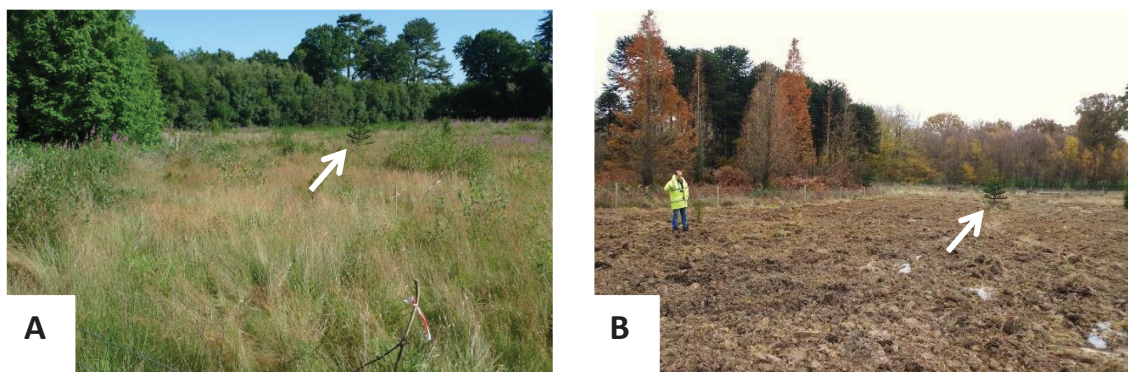


Figure 3.4. Spot the difference! Originally, this study included one tree-free site, however, unfortunately this was ploughed and all samples lost prior to the 7 month harvest in December 2013. These samples have not been included in any analysis in this chapter. As it's almost totally unrecognisable, I've pointed out one small monkey puzzle tree with an arrow to show this is the same field!

3.2.2 Weathering estimation by mass loss

Two measures of weathering rate were calculated, both based on measurements of mass loss of rock grains contained within mesh bags, and retrieved after 3, 7 and 14 months burial under stands of mature trees. Total weathering rates were calculated for 0-3, 0-7, 0-14 months, and also net weathering rates for 3-7 and 7-14 months. For each consecutive harvest, net weathering rates were calculated from the change between sample mass at that harvest and the average mass for a given tree species and rock type from the preceding harvest. Weathering rates are expressed in terms of mass loss with units of $\text{ng m}^{-2} \text{s}^{-1}$, and a negative weathering rate signifies mass gain over the burial period.

3.2.2.1 Calculating molar weathering rates normalised to particle surface area

For comparison between rock types, molar weathering rates were calculated and normalised to particle surface area. Surface area normalised weathering rates in Thorley *et al.* (2015) used estimated molar masses based on bulk sample mineralogy, and surface areas calculated from particle geometry and experimentally determined rock densities. These factors led to uncertainty in our reporting of carbonate weathering rates, and in particular, substantially underestimated the weathering rate of dolomite grains. Since then, we have obtained more accurate measurements of rock grain mineralogy, which have been used to reduce uncertainty in weathering rates. In addition to this, our understanding of the behaviour of carbonate rock grain surface area throughout weathering has improved, and this research forms the focus of Chapter 5.

In Thorley *et al.* (2015), rock grains were divided into 3 groups: calcite (marble, chalk and oolite), dolomite and silicate. Each of these groups was assigned a specific molar mass (Table 3.3), based on their chemical formula: calcite, CaCO_3 and dolomite

Carbonate weathering rates and phosphorus biogeochemical cycling

$\text{CaMg}(\text{CO}_3)_2$. The molar mass of silicate grains was estimated from literature XRF data for basalt from the Morvern peninsula, NW Scotland (Bain *et al.* 1980), the closest sampling site to Skye, where the silicate rock used in this study was sourced.

In the current study, total weathering rates at 0-3, 0-7, and 0-14 months were normalised to unweathered BET surface area for each rock type individually. Net weathering rates for the periods 3-7 and 7-14 months were normalised to take account of changes in particle size and geometry that have occurred over the time they were buried. This normalisation constant was calculated for each tree species and rock type individually and is based on the linear relationship between mass loss of weathered samples and their corresponding BET surface area, discussed in more detail in Chapter 5. Net weathering rates were only calculated for chalk and dolomite, as there is insufficient BET data for weathered samples of other rock types.

3.2.3 XRF analysis of rock samples

In Thorley *et al.* (2015) estimated molar masses (M_r) based on bulk mineralogy were used to calculate of weathering rates (Table 3.3), which led to an underestimation of weathering rates, particularly for dolomite. To overcome limitations, revised molar masses have been calculated from XRF data of each rock type.

Powdered samples were dried (100°C, 2 hours) prior to being made into glass beads for XRF analysis. Samples were analysed using a Philips Magix-Pro wavelength dispersive XRF spectrometer (PANalytical, Cambridge, UK) by the GAU-Radioanalytical Laboratories at the National Oceanography Centre, Southampton.

Calculations to determine effective M_r of rock samples based on XRF data were performed using %wt data and molar masses of constituent fractions (

Chapter 3

Table A. 3; trace elements were not included in this calculation). For all samples there was a mass deficit accounting for 2.5 – 48% of the total mass, depending on rock type. This is composed of CO₂ and H₂O which were not discriminated between during XRF analysis. To account for the extra mass, first CaO and MgO mass fractions were scaled to represent CaCO₃ and MgCO₃ and increase their wt% to include CO₂, which is the most likely component for carbonate rocks, as used in this study. Following this, the remaining mass deficit (0.11-0.35%) was assigned to H₂O, which is likely to be adsorbed to mineral surfaces in micropore sites or as present in hydrated forms of minerals. The ionic mass of each fraction was finally weighted by its mass % and results are shown in Table 3.3.

Table 3.3. Molar masses (Mr) and dominant mineralogy of each rock type used in study. Revised XRF Mr is a composite molar mass, calculated from the mass % and elemental composition of mineral constituents, and is used in weathering rate calculations (mol m⁻² s⁻¹).

	Thorley <i>et al.</i> (2015)		This study
	Mineral	Mr	XRF Mr
Chalk	Calcite	100	98.12
Dolomite	Dolomite	184	91.49
Marble	Calcite	100	98.65
Oolite	Calcite	100	97.73
Silicate	Quartz	75	69.59

3.2.4 Phosphorus determination of rock grain and soil samples

This section provides a description of the phosphorus extraction and quantification methods used within this chapter (summarised in Table 3.4). Total phosphorus was measured in all 3, 7 and 14 month weathered samples of chalk, dolomite, oolite, marble and silicate rock grains. In general, phosphorus accumulated over the course of carbonate weathering. To investigate the reason for this, the last part of this chapter provides a more thorough investigation of bioavailable P in soils and organic P fractions within weathered rock grain samples.

3.2.4.1 Aqua regia digests of rock grains

Total phosphorus of samples was measured by Murphy-Riley spectrophotometric P-determination following aqua regia digestion of samples. This method of digesting samples is reasonably aggressive and does not discriminate between different forms of P, so for the purposes of this study this is hereon referred to as ‘Total P’. This method was used to provide a measure of total sample phosphorus for two reasons. Firstly, for weathered samples, total digestion is likely to result in a more repeatable measurement than any method for elution of P from grain surfaces. Total digestion removes the influence any splitting of rock grains or exposure of new surfaces

Carbonate weathering rates and phosphorus biogeochemical cycling

may have, thus making the measurement of sample P independent of surface area.

Secondly, mycorrhizal hyphae are known to be able to tunnel into rocks and may have altered internal surfaces, and total digestion is the most straightforward technique that would permit measurement of any P-changes occurring within rock grains.

500 ± 10 µg Freeze dried weathered or unweathered rock grains were weighed into an acid washed digest tube (0.1% HNO₃ acid wash, trace metal grade, followed by 5 rinses with 18.2MΩ UHP H₂O). Samples were treated with HCl and HNO₃ in a 3:1 ratio (6ml HCl, 2ml HNO₃, trace metal grade). For carbonate rock grains, HCl was added first in 2ml aliquots, and vortexed between additions in order to minimise fizzing and avoid sample loss through overflowing. When HCl treated samples had stopped fizzing HNO₃ was added, each tube topped with an acid washed condenser and heated to reflux at 150 ± 1 °C for 30 minutes. Two digestion blanks without any rock grains were included in each run of 18 samples per dry heating block (Grant BT5D, Grant Instruments (Cambridge) Ltd, UK). Digested samples were left to cool to room temperature then diluted to 25 ml in a volumetric flask using 1% HNO₃ (UHP water and 1% HNO₃, trace metal grade). Samples were stored in 50ml centrifuge tubes (Fisher Scientific) at room temperature before analysis for total phosphorus and longer-term at -20°C before ICP-AES or ICP-MS analysis for trace metals.

3.2.4.2 Chloroform fumigation for microbial P (Carter 1993)

Phosphorus in microbial biomass is estimated by subtracting the quantity of P extracted from fresh damp soil (N = 3) from that in soil which has been fumigated with CHCl₃ (N = 3). Most P released upon fumigation is inorganic orthophosphate, so fumigation can be followed by Olsen's extraction as below. Fumigation was performed in a humid environment within a sealed desiccator, ensuring that desiccators containing soil samples were evacuated until CHCl₃ boiled vigorously to flood the internal atmosphere before leaving for 24 hours in the dark. Extractions of fumigated soil were paired with otherwise identically prepared samples spiked with 1ml of standard P solution (1.098 g KH₂PO₄/l H₂O m/v; 250 µg P ml⁻¹) to estimate P extraction efficiency (N = 3).

3.2.4.3 Olsen's extraction of orthophosphate from air dried soil

Olsen's phosphorus extraction method extracts orthophosphate from soil (~2.5g dry mass, air dried and powdered in an agate ball mill, fresh or fumigated) using sodium bicarbonate solution (50 ml 0.5M NaHCO₃, adjusted to pH 8.5 with NaOH). Samples were agitated for 30 mins at 150 rpm on a reciprocal shaker then filtered (Whatman 42) before Murphy-Riley P determination. The P-content of all samples is reported per

Chapter 3

gram of dry soil, so where extractions were performed on fresh or fumigated soil, soil samples were dried in tandem for calculation of total moisture content and equivalent dry soil mass.

This study investigates inorganic P-release by weathering, and therefore the extraction method must be able to provide a measure of all forms of P that are equally or more accessible than that in CaCO₃ rock grains. A 0.5M solution of NaHCO₃ can remove both dissolved P and that adsorbed to calcium carbonate and Fe-oxide surfaces. For this reason NaHCO₃ is used in this study in preference to a simple water extractant as although water is able to elute dissolved forms of P, it has very little effect on adsorbed and mineral forms. This method was used as it is suitable for P-extractions from both acid and calcareous soils and provides an estimate of bioavailable phosphorus in the form that can be used directly by plants. Some micro-organisms are able to use more recalcitrant forms of P, such as nucleic acids; however, these are not affected during Olsen's extractions (P extraction methods reviewed in Turner *et al.* 2005; Soinne, 2009).

3.2.4.4 Chloroform and NaCl extraction for lipid P fractions

As the aqua regia digest method used to measure total P does not discriminate between biological and inorganic P, a second extraction procedure was performed on both chalk and silicate rock grains to give some measure of organic P.

Total lipids were extracted from 14-month weathered chalk and silicate rock grains (250 ± 20 mg samples) using a modified Bligh and Dyer (1959) extraction method (3ml CHCl₃: 4 ml MeOH: 2.4 ml 1M NaCl made up with UHP dH₂O). Prior to extraction, rock grain samples were shaken in 5 ml UHP water whilst still in mesh bags to elute most soluble P then freeze dried. Lipid extractions were performed in acid washed glass centrifuge tubes and control samples of unweathered rock grains, and extractant blanks were included. Samples were agitated on a reciprocal shaker (250 rpm, 1 hour), keeping tubes horizontal for maximum disruption. After leaving to settle, the bottom phase was collected taking care not to disturb the interface between phases (Figure 3.5). A portion of this phase (5 ml) was transferred to an acid washed boiling tube, dried down (80°C with fume extraction) treated with sulphuric acid (1ml conc. H₂SO₄), vortexed and left overnight before digestion in a pre-heated dry block (350°C, 15 minutes; Grant BT5D, Grant Instruments (Cambridge) Ltd, UK). Samples were cooled, diluted (5 ml UHP dH₂O), vortexed and stored until P-determination.

The Bligh and Dyer method used in this study is one of the most common methods for extracting total lipids from biological samples, and is reasonably accurate

Carbonate weathering rates and phosphorus biogeochemical cycling

for samples with lipid contents below 2%. More specific extraction procedures have been used recently to estimate mycelial biomass of mycorrhizal fungi in soils through the quantification of phospholipid fatty acids (PLFAs). Specific PLFAs have been used as markers for EM (Linoleic acid, 18:2 ω 6,9) and AM (16:1 ω 5c) fungi, however, exact scaling factors between these biomarkers and fungal biomass can be different between fungal genera and species (Olsson 1999; Olsson *et al.* 2003). Quantifying the total amount of P within lipids extracted from rock grain samples is intended to provide an estimate of the total P contained by mycorrhizal and saprotrophic fungi, and probably other micro-organisms with PLFA membrane components. This method does not measure total biological phosphorus within samples, only that within the extractable lipid fraction, in an attempt to provide a rough comparison of the relative quantities of biological P between samples. Not only are there other biological components that contain P, such as nucleic acids, there is likely to have been some deterioration of organic components of samples, such as lipids, during storage.

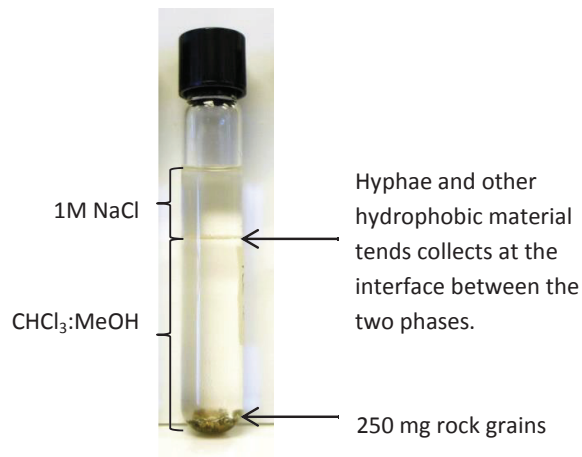


Figure 3.5. Modified Bligh and Dyer lipid extraction of silicate rock grain sample. After extraction, the lower phase is collected, dried and digested before spectrophotometric P determination.

3.2.4.5 Murphy-Riley colourimetric phosphorus determination

Samples for P determination (1 ml; Olsens's extracts, aqua regia digests, H₂SO₄ digests), UHP dH₂O (1.9 ml), and L-ascorbic acid (100 μ l; 0.03M) were pipetted into clean cuvettes (4.5 ml, Starstedt). The assay reaction was allowed to progress for 15 minutes after the addition of colour developer solution (0.5 ml; Method A. 1; Table A. 4), Murphy and Riley 1962) before spectrophotometric P determination (Absorbance, 882 nm; Figure 3.6A). Sample P was calculated against a calibration curve prepared using varied volumes of 10 ppm P stock solution of sodium hydrogen orthophosphate (45.84 mg anhydrous Na₂HPO₄ /100 ml UHP dH₂O m/v; Table A. 1). Sample calibration curves are shown in Figure 3.7. When analysing Olsen's soil extracts, samples were coloured by organic matter, even after filtering, and it was necessary to

Chapter 3

run paired samples with and without ascorbic acid to provide a baseline absorbance. This was particularly important for extracts of *Ilex*, *Larix* and *Sequoia* soils.

This method was adapted to overcome interference with colour development caused by using highly acidic samples from aqua regia digests. For these samples after 15 minutes had elapsed, the addition of NaOH solution (0.5 ml, 3.44M) was required to enable colour development (10 minutes) prior to spectrophotometric analysis (Figure 3.6B; Table A. 1). Aqua regia digest samples of chalk and silicate rock grains required an additional dilution stage before P determination as the P content of these samples exceeded the maximum value of the linear range of the calibration curve (Figure 3.7C). For H₂SO₄ digests of CHCl₃ extracts very little P was present in samples and a calibration curve with a narrower range was required (25, 50, 75, 100, 125, 150, 175 µl 10 ppm P standard solution; Figure 3.7B).

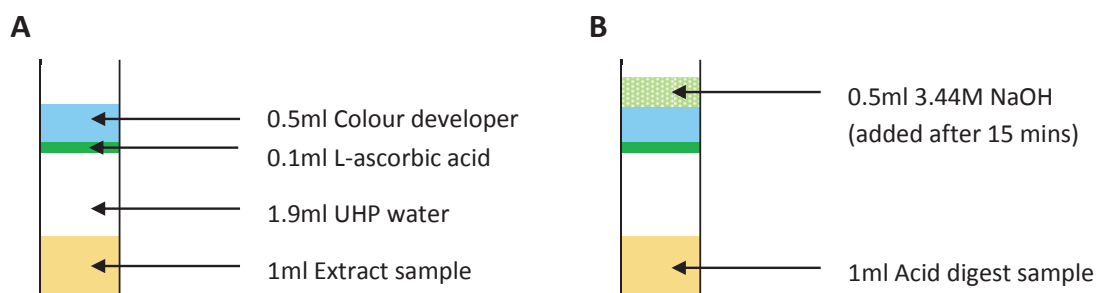


Figure 3.6. Schematic of cuvette contents for Murphy-Riley spectrophotometric P determination for **A)** Olsen's extract samples and **B)** for acidic samples such as those from aqua regia digests.

Table 3.4. Summary of phosphorus fractions accessed using different extraction methods. Murphy-Riley colorimetric P-determination method depends on sample pH, as described in **Figure 3.6.**

Method	Fraction of P accessed	Murphy-Riley
Aqua regia	Total phosphorus of carbonates, total extractable P of silicates as silicate matrix requires more aggressive extraction.	Figure 5B
Olsen's extraction	Measure of bioavailable P in soils. Extraction with 0.5M NaHCO ₃ , can remove P adsorbed to calcium carbonate and Fe-oxide surfaces.	Figure 5A
Chloroform fumigation	Microbial P in soil released by CHCl ₃ fumigation. This is used as a proxy for microbial activity. Followed by Olsen's extraction	Figure 5A
Chloroform/ NaCl extraction, followed by H ₂ SO ₄ digestion	P contained within lipids eluted from carbonate and silicate rock grains	Figure 5B

Carbonate weathering rates and phosphorus biogeochemical cycling

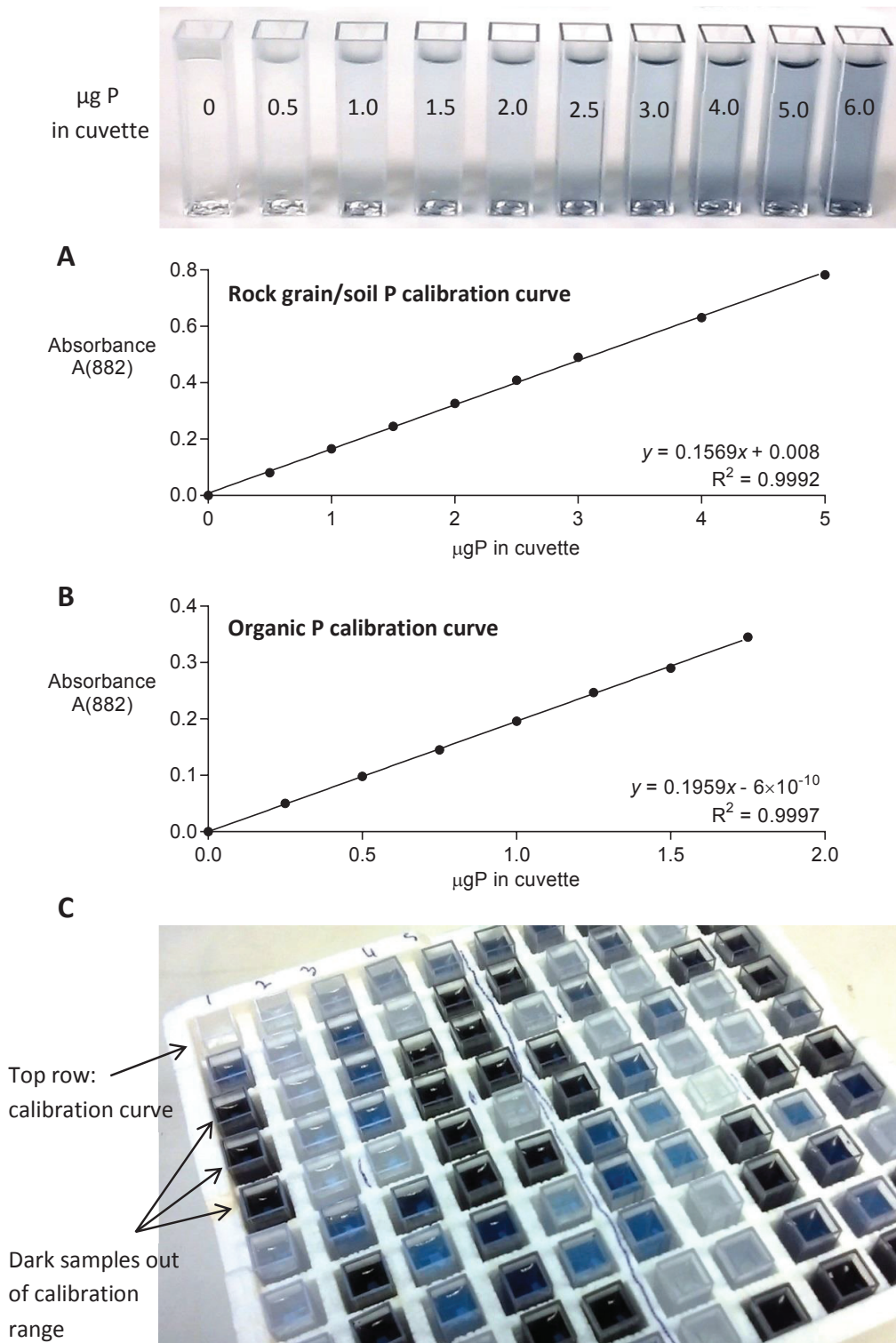


Figure 3.7. Murphy-Riley spectrophotometric P determination of aqua regia digest samples of carbonate rock grains. Sample calibration curves for P determination in **A**) Rock grain digest samples and soil extractions, and **B**) lipid extractions. **C**) Very dark-coloured samples are those for silicate and chalk rock grains and required further dilution to bring them within range of the calibration curve before spectrophotometric analysis.

Chapter 3

3.2.5 Hyphal length

Carbonate and silicate rock grains (~1 g) recovered from hyphal ingrowth bags after 3 months of weathering were sonicated (10 min; Branson B32 sonic bath; Danbury CT, USA) in a 100 ml conical flask with 20 ml HCl (10% v/v, made up with UHP dH₂O) and UHP dH₂O (10 ml) to suspend hyphae adhering to rock grains. HCl was used to solubilise carbonate grains and free any hyphae tunnelling into the interior.

Avoiding remaining rock grains, aliquots (4 ml) of the suspension were filtered under vacuum through gridded cellulose membrane filters (25 mm diameter, 0.45 µm pore size; Whatman, GE Healthcare Life Sciences, UK). Filter papers were treated with Trypan blue lacto-phenol (See Method A. 2 for preparation) to stain hyphal fragments caught on the filter. After 10 minutes staining, filters were rinsed through the vacuum filter apparatus with UHP H₂O, taking care not to dislodge any trapped hyphae. Hyphal lengths were measured using a modified line-intersect technique at 200× magnification (Wallander *et al.*, 2004; Quirk *et al.* 2012).

3.3 Results

3.3.1 SA normalisation of molar weathering rates

There was large variation in the unweathered surface area (SA) of between the five rock types used in this study (Figure 3.8), and for this reason, it is important to normalise weathering rates by SA. Thorley *et al.* (2015) normalised weathering rates to an estimated geometric SA, calculated using experimentally determined rock densities and assuming spherical particle geometry. Figure 3.8 shows that there are two orders of magnitude difference between measured BET SA (Brunauer, Emmett and Teller SA; Section 4.2.3) and geometric SA, however, surprisingly, these are roughly proportional and inclusion of a surface roughness scaling factor would be reasonable to adjust weathering rates. This section provides a re-analysis of molar weathering rates after 3 months, and after subsequent harvests, normalising by BET SA instead of estimated geometric SA as in Thorley *et al.* (2015).

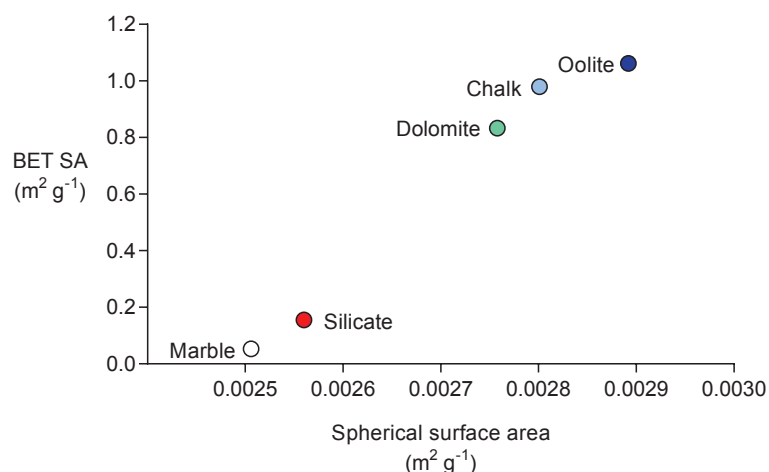


Figure 3.8. Comparison of geometric surface area (m² g⁻¹) of unweathered rocks, as calculated in Thorley *et al.* (2015), and corresponding BET SA measurements (This study).

3.3.2 Rapid weathering of carbonate samples

The first samples retrieved had been buried for 3 months at Bedgebury over the active growing season, May to August 2013. Samples from this harvest showed that in general carbonates weathered faster than silicates (Table 3.5, Table 3.6). Marble was the fastest weathering carbonate after 3 months both in terms of mass loss (Table 3.5) and when normalised by surface area (Table 3.6). Rates of mass loss from calcite-containing rock grains in the root-excluding mesh bags were nearly an order of magnitude faster than those from silicate grains (calcite average mass loss 8 times higher than for silicate, average of 13 tree species for chalk, oolite and marble at 3 months).

Chapter 3

Aside from marble, calcite-containing rock grains of both chalk and oolite showed increasing net weathering rates from 3 to 7 months and later plateauing or slightly decreasing after 7 months (Table 3.6; Figure 3.9). The same pattern was shown by silicate rock grains, however, these trends were not significant at $P < 0.05$. Dolomite weathering was also higher in the period 3-7 months than initially, however, unlike calcite and silicate rock grains; this increase in rate was sustained from 7-14 months (Table 3.7; Figure 3.9).

Table 3.5. Average weathering rates in terms of mass loss (Mean \pm SEM; ng s⁻¹ per g initial mass of rock grains; N = 13 tree species) for carbonate (chalk, oolite, dolomite and marble) and silicate rock grains for burial periods of 0-3, 0-7 and 0-14 months (91.0 \pm 3.9 days; 215.6 \pm 3.9 days; 425.6 \pm 3.9 days respectively). Results of Tukey HSD test are shown as superscripts, where values sharing the same letter are not significantly different (2-way ANOVA; Weathering rate \sim Harvest time \times Rock type; $P > 0.05$). Interaction terms were not significant and have not been included in this table.

	Weathering rates (Mean \pm SEM; ng s ⁻¹ g ⁻¹)		
	3 months	7 months	14 months
Chalk	0.78 \pm 0.14 ^{abcd}	1.53 \pm 0.38 ^a	1.35 \pm 0.11 ^{ab}
Oolite	0.82 \pm 0.11 ^{abcd}	1.45 \pm 0.18 ^a	1.23 \pm 0.09 ^{ab}
Dolomite	0.54 \pm 0.1 ^{bcd}	0.89 \pm 0.32 ^{abcd}	1.11 \pm 0.12 ^{abc}
Marble	1.12 \pm 0.15 ^{abc}	1.12 \pm 0.33 ^{abc}	1.31 \pm 0.12 ^{ab}
Silicate	0.11 \pm 0.08 ^d	0.29 \pm 0.08 ^{cd}	0.12 \pm 0.02 ^d

Table 3.6 Average molar weathering rates normalised by BET surface area of unweathered rock grains (Mean \pm SEM; $\times 10^{-12}$ moles m⁻² s⁻¹; N = 13 tree species) for carbonate and silicate rock grains for burial periods of 0-3, 0-7 and 0-14 months. Results of Tukey HSD test are shown as superscripts, where values sharing the same letter are not significantly different (2-way ANOVA; Weathering rate \sim Harvest time \times Rock type; $P > 0.05$). Interaction terms were not significant and have not been included in this table.

	Surface area normalised weathering rates (Mean \pm SEM; $\times 10^{-12}$ moles m ⁻² s ⁻¹)		
	3 months	7 months	14 months
Chalk	7.72 \pm 1.37 ^b	15.23 \pm 3.74 ^{ab}	13.47 \pm 1.12 ^{ab}
Oolite	7.87 \pm 1.06 ^b	14.02 \pm 1.75 ^{ab}	11.87 \pm 0.83 ^{ab}
Dolomite	6.98 \pm 1.25 ^b	11.51 \pm 4.15 ^{ab}	14.36 \pm 1.54 ^{ab}
Marble	215.29 \pm 29.27 ^c	215.26 \pm 63.67 ^c	252.51 \pm 23.02 ^c
Silicate	9.25 \pm 6.22 ^{ab}	24.07 \pm 6.26 ^a	9.81 \pm 1.55 ^{ab}

Table 3.7. Net molar weathering rates for chalk and dolomite (Mean \pm SEM; $\times 10^{-12}$ moles m⁻²s⁻¹), normalised to surface area and adjusted for changing SA using mass loss dependence relationships from BET data (Section 4.3.4.2)

	Surface area normalised net weathering rates (Mean \pm SEM; $\times 10^{-12}$ moles m ⁻² s ⁻¹)		
	0-3 months	3-7 months	7-14 months
Chalk	7.72 \pm 1.37 ^a	23.07 \pm 6.27 ^a	12.95 \pm 4.51 ^a
Dolomite	6.98 \pm 1.25 ^a	25.03 \pm 13.32 ^a	31.78 \pm 10.83 ^a

Carbonate weathering rates and phosphorus biogeochemical cycling

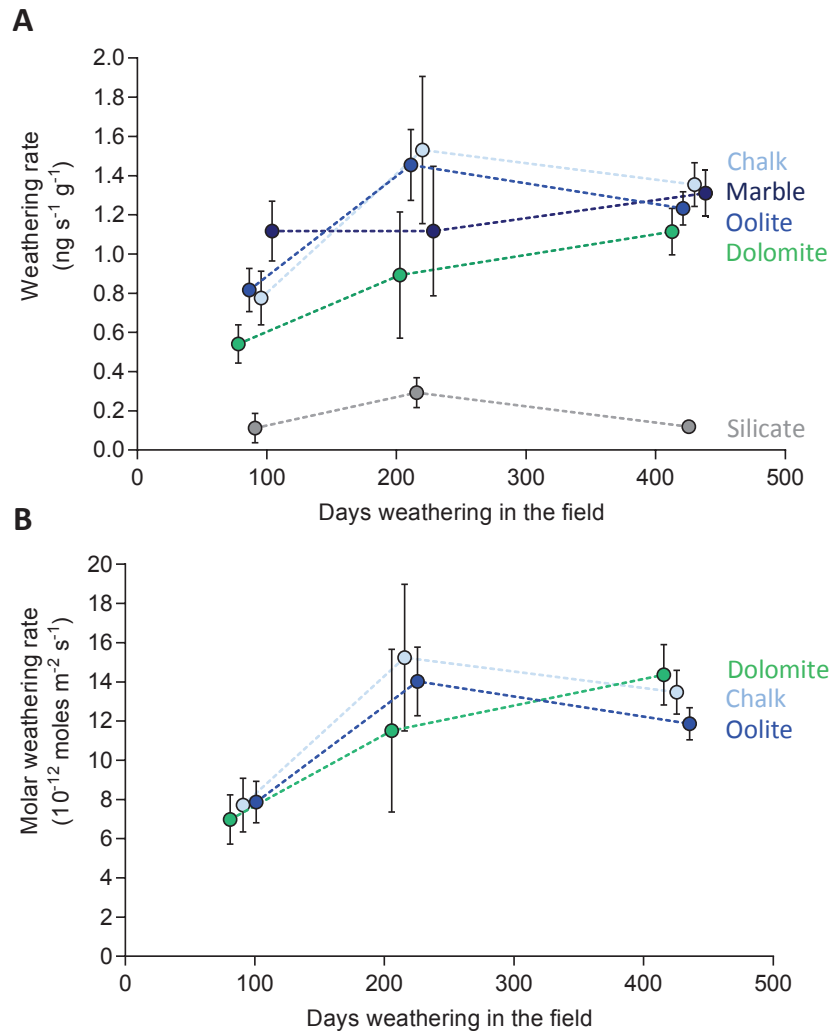


Figure 3.9. Overall cumulative weathering rates for 0-3, 0-7 and 0-14 months by rock type: chalk (light blue), oolite (mid-blue), marble (dark blue), dolomite (green) and silicate (grey). **A)** Cumulative weathering rates in terms of mass loss ($\text{ng s}^{-1} \text{g}^{-1}$ of initial rock grains buried; **Table 3.5**); **B)** Molar weathering rates normalised by initial sample BET surface area. In the lower panel, only rates for carbonate rock grains (chalk limestone and dolomite) are displayed. Marble had very high molar weathering rates due to small initial BET surface area (Table 3.6, Figure 3.8). In both panels data points are offset for clarity to prevent error bars overlapping. In reality, there are 3 weathering durations, 91.0 ± 3.9 days; 215.6 ± 3.9 days and 425.6 ± 3.9 days.

Chapter 3

3.3.3 Effect of tree-mycorrhizal functional group on calcite weathering rates

After 3 months sample incubation in the field, the most intense weathering of calcite containing rock grains (marble, chalk and oolite) occurred beneath EM angiosperms (Two-way ANOVA, Table 3.8; Figure 3.10B). Both tree group (Angiosperm/Gymnosperm) and mycorrhizal type (AM/EM) significantly affected calcite-weathering rate, however, this pattern may be primarily driven by the far higher 3-month weathering rates beneath EM angiosperms (Figure 3.10). There was no significant effect of tree-mycorrhizal functional group on the weathering of either dolomite or silicate rock grains (Two-way ANOVA, Table 3.8). After subsequent harvests there was no longer any effect of tree type and only a significant effect of mycorrhizal type on calcite weathering (Table 3.8, Figure 3.11) with EM fungi exhibiting faster weathering rates than AM fungi.

Table 3.8. Results of 2-way ANOVAs showing the F statistic and significance for weathering rates in terms of mass loss ($\text{ng s}^{-1} \text{g}^{-1}$ initial mass) of calcite-containing, dolomite and silicate rock grains. ANOVAs were used to test the effects of tree functional group (Angiosperm/Gymnosperm) and associated mycorrhizal type (AM/EM) for each rock grain type at each time point mesh bags were recovered from the field. The interactions between these tree and mycorrhizal type are also included; however, they were never statistically significant. * Indicates significance level $P < 0.05$

Harvest	Rock grain type	Mycorrhizal type (AM/EM)	Tree type (Ang/Gym)	Interaction Myc:Tree type
3 months	Silicate	$F_{1,9} = 0.466$ $P = 0.512$	$F_{1,9} = 0.020$ $P = 0.892$	$F_{1,9} = 0.060$ $P = 0.813$
	Dolomite	$F_{1,9} = 0.019$ $P = 0.8937$	$F_{1,9} = 3.916$ $P = 0.0792$	$F_{1,9} = 1.831$ $P = 0.2091$
	Calcite	$F_{1,9} = 8.169$ $P = 0.0188^*$	$F_{1,9} = 5.181$ $P = 0.0489^*$	$F_{1,9} = 1.058$ $P = 0.3306$
7 months	Silicate	$F_{1,9} = 0.348$ $P = 0.570$	$F_{1,9} = 0.240$ $P = 0.636$	$F_{1,9} = 1.811$ $P = 0.211$
	Dolomite	$F_{1,9} = 0.510$ $P = 0.493$	$F_{1,9} = 0.775$ $P = 0.401$	$F_{1,9} = 2.391$ $P = 0.156$
	Calcite	$F_{1,9} = 9.612$ $P = 0.0127^*$	$F_{1,9} = 0.716$ $P = 0.4193$	$F_{1,9} = 1.811$ $P = 0.253$
12 months	Silicate	$F_{1,9} = 0.645$ $P = 0.4426$	$F_{1,9} = 4.797$ $P = 0.0562$	$F_{1,9} = 0.027$ $P = 0.8724$
	Dolomite	$F_{1,9} = 7.151$ $P = 0.0254^*$	$F_{1,9} = 1.476$ $P = 0.2553$	$F_{1,9} = 1.861$ $P = 0.2056$
	Calcite	$F_{1,9} = 3.512$ $P = 0.0937$	$F_{1,9} = 0.249$ $P = 0.6300$	$F_{1,9} = 0.101$ $P = 0.7574$

Carbonate weathering rates and phosphorus biogeochemical cycling

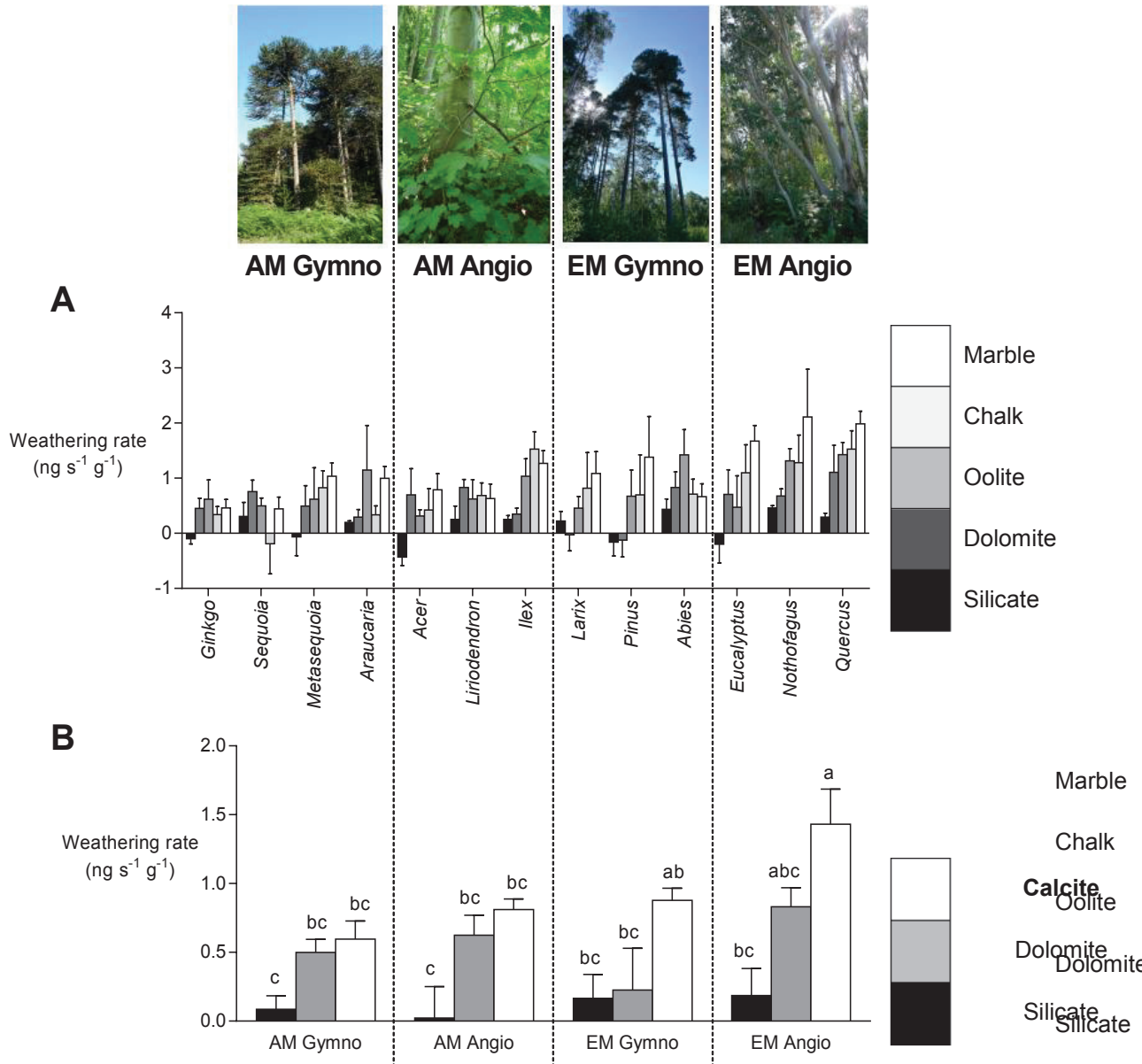


Figure 3.10. Weathering rates of rock grains (Mean \pm SEM) after 3 months burial under established stands of mature trees at Bedgebury Pinetum, Kent, UK (May-August 2013). Results sorted by **A**) tree species (N = 3 replicate trees of each of 13 species, Table 3.1) and **B**) tree-mycorrhizal functional group for each calcite (chalk, oolitic limestone and marble), dolomite and silicate minerals (N = 3 tree species of each functional group, except arbuscular mycorrhizal (AM) gymnosperm where N = 4). Lettering shows results of Tukey HSD test, where bars sharing the same letter are not significantly different (P > 0.05)

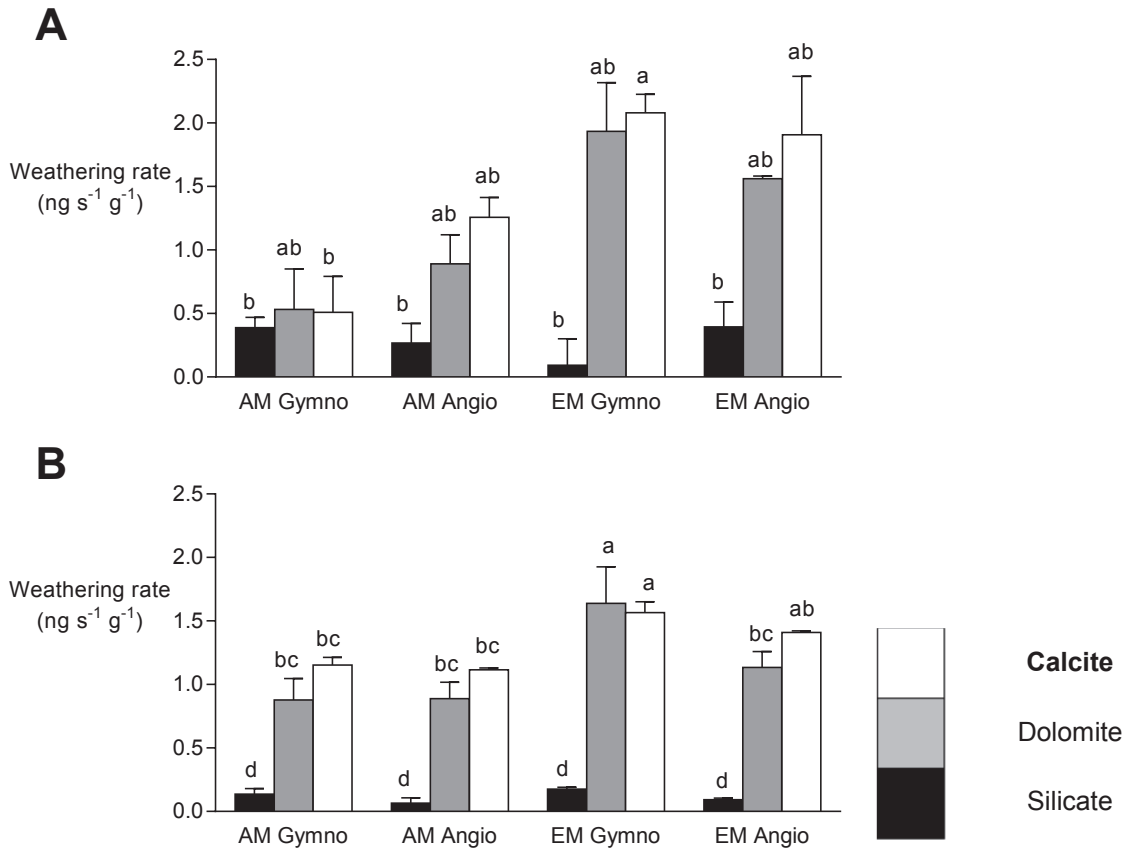


Figure 3.11. Mass loss weathering rates of rock grains (Mean ± SEM) buried in root-excluding mesh bags after **A**) 7 and **B**) 14 months, grouped by tree–mycorrhizal functional group for each calcite (chalk, oolitic limestone and marble), dolomite and silicate minerals (N = 3 tree species of each functional group, except arbuscular mycorrhizal (AM) gymnosperm where N = 4) **Calcite**

3.3.3.1 Tree-mycorrhizal functional group affects SA-normalised weathering rates Dolomite

Because after 7 and 14 months there was no effect of tree type (angiosperm/gymnosperm) on weathering rates (Table 3.8), in this section, SA normalised molar rate data are grouped only by mycorrhizal type. Molar weathering rates are normalised to BET surface area and relative to molar masses calculated from XRF data, their calculation is described in the methods section (Section 3.2.3). In general, carbonate weathering within EM tree stands was consistently faster than that under AM species, although this effect was often not significant (Figure 3.9, Figure 3.10). The most significant impact of mycorrhizal type was for the weathering of calcite-containing rock grains after 3 and 7 months weathering (Figure 3.11, Table 3.9).

Calcite
Dolomite
Silicate

Carbonate weathering rates and phosphorus biogeochemical cycling

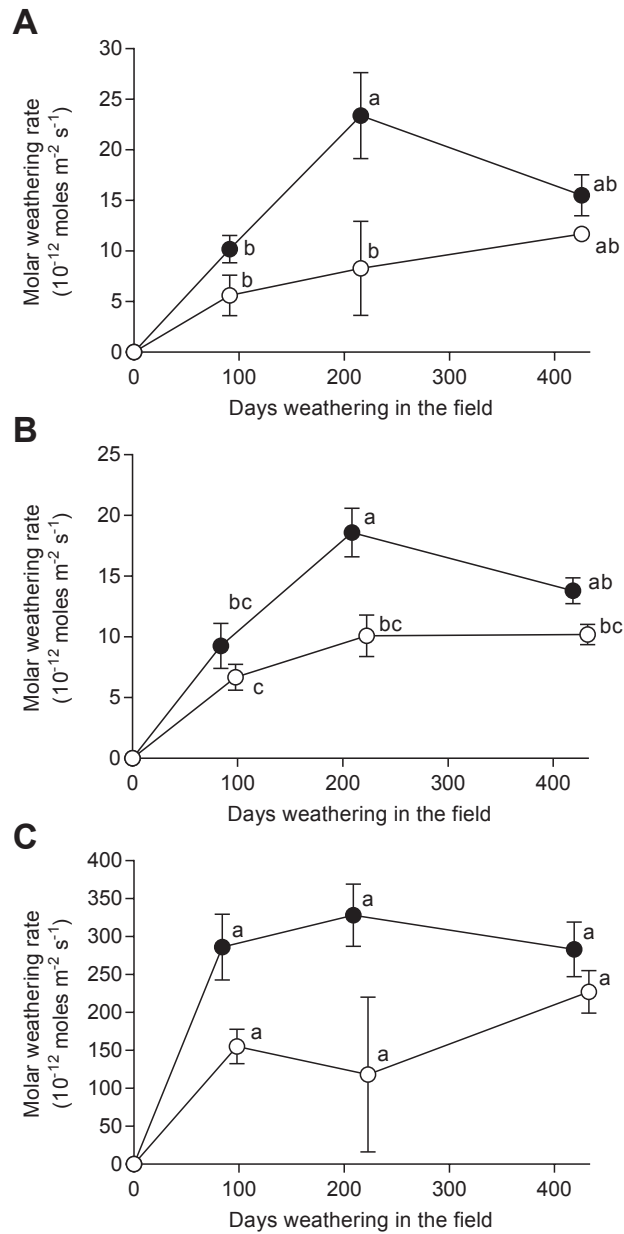


Figure 3.12. Molar weathering rates for calcite-containing rocks, grouped by mycorrhizal type (Mean \pm SEM; EM species, closed symbols, mid blue, N = 6; AM trees, open symbols, light blue, N = 7) for **A**) chalk, **B**) oolite and **C**) marble. Lettering beside data points shows the results of Tukey HSD testing based on a 2-way ANOVA investigating the effect of mycorrhizal type and weathering duration (Table 3.9). Note difference in scales between 3 panels, in B and C data points are slightly offset to avoid overlapping error bars, the precise weathering durations are 91, 215.6 and 425.6 days, respectively.

Chapter 3

Table 3.9. Results of 2-way ANOVAs showing the F statistic and significance for molar weathering rates of calcite-containing samples normalised to BET surface area of unweathered rock grains (Figure 3.11). The ANOVAs tested the effects of mycorrhizal type (AM/EM) for each grain type at each time point mesh bags were recovered from the field. The two-way interactions between mycorrhizal type and harvest time are also included but were never statistically significant. * $P < 0.05$ ** $P < 0.01$ (N = 13 tree species, 7 AM, 6 EM). There was no effect of mycorrhizal type on molar weathering rates of dolomite or silicate rock grains, and these are not included in this table.

	Mycorrhizal type (AM/EM)	Harvest (3/7/14 Months)	Myc type:Harvest
Chalk	$F_{1,35} = 8.93$ $P = 0.0051$	$F_{1,35} = 2.38$ $P = 0.13$	$F_{1,35} = 0.16$ $P = 0.69$
Oolite	$F_{1,9} = 11.55$ $P = 0.0017^{**}$	$F_{1,9} = 3.41$ $P = 0.073$	$F_{1,9} = 0.002$ $P = 0.97$
Marble	$F_{1,9} = 8.74$ $P = 0.0057^{**}$	$F_{1,9} = 0.31$ $P = 0.074$	$F_{1,9} = 0.98$ $P = 0.38$

3.3.4 Phosphorus changes over weathering

In this section, sample phosphorus content (Table 3.4) is described in two ways, both as a concentration (Table 3.10) and as a total quantity (Table 3.11). Two measures are used as a difference in total P of a sample may or may not result in a change in overall concentration, depending on the corresponding change in sample mass throughout weathering. Phosphorus concentration data is required to establish if changes in P occur at the same rate as bulk changes in rock grain characteristics, such as mass loss. For instance, if there is a decrease in P concentration this means there has been a selective depletion, and if there is an increase in concentration, a selective accumulation.

In this study, chalk and silicate samples had the highest initial P content, dolomite and marble the lowest, and oolite intermediate (Table 3.10, Table 3.11). At a glance, weathering carbonate and silicate rock grains appear to have contrasting behaviour in terms of changes in phosphorus content. In silicate samples, P is gradually depleted, however, all carbonate samples exhibit rapid accumulation of P (Figure 3.13). In particular, over the course of weathering, chalk grain P content is elevated above that of silicate samples, both in terms of total P and P-concentration. These observations are discussed in more detail in the following sections.

Carbonate weathering rates and phosphorus biogeochemical cycling

Table 3.10. Phosphorus content per unit mass of rock samples, measured after total sample solubilisation by aqua regia digest. Both for unweathered rock grains (Mean \pm SEM; 5 samples per rock type) and after 3, 7 and 14 months weathering in the field (Mean \pm SEM; N = 13 tree species). Superscripts show the results of Tukey HSD test for each rock type individually to show significant differences between Phosphorus concentrations within each row.

	Unweathered	Weathered ($\mu\text{g P g}^{-1}$ dry rock)		
	($\mu\text{g P g}^{-1}$ dry rock)	3 Months	7 Months	14 Months
Silicate	107.8 \pm 0.52 ^a	106.79 \pm 2.38 ^a	102.19 \pm 2.36 ^a	89.92 \pm 2.8 ^b
Chalk	94.38 \pm 0.21 ^a	112.97 \pm 2.01 ^b	109.28 \pm 1.81 ^b	111.93 \pm 1.3 ^b
Oolite	30.65 \pm 0.68 ^a	36.45 \pm 0.85 ^a	37.51 \pm 1.34 ^a	36.02 \pm 1.54 ^a
Dolomite	8.78 \pm 0.48 ^a	12.53 \pm 0.52 ^a	12.41 \pm 0.48 ^a	19.72 \pm 1.72 ^b
Marble	5.88 \pm 0.65 ^a	8.66 \pm 0.29 ^{ab}	9.43 \pm 0.61 ^b	10.26 \pm 0.65 ^b

Table 3.11. Total P content of rock samples adjusted by total sample mass before (Mean \pm SEM; 5 samples per unweathered rock type) and after 3, 7 and 14 months weathering in the field (Mean \pm SEM; N = 13 tree species. Phosphorus content of unweathered samples was scaled to their original mass of 2.5g, and that of weathered samples were individually scaled to the mass of each recovered sample.

	Unweathered	Weathered ($\mu\text{g P sample}^{-1}$)		
	($\mu\text{g P sample}^{-1}$)	3 Months	7 Months	14 Months
Silicate	269.49 \pm 1.3 ^a	266.74 \pm 2.38 ^a	253.65 \pm 2.36 ^a	223.66 \pm 2.8 ^b
Chalk	235.96 \pm 0.53 ^a	279.94 \pm 2.01 ^b	265.27 \pm 1.81 ^b	266.52 \pm 1.3 ^b
Oolite	76.62 \pm 1.7 ^a	90.51 \pm 0.85 ^a	91.19 \pm 1.34 ^a	85.55 \pm 1.54 ^a
Dolomite	21.96 \pm 1.19 ^a	31.09 \pm 0.52 ^a	30.38 \pm 0.48 ^a	47.27 \pm 1.72 ^b
Marble	14.7 \pm 1.62 ^a	21.46 \pm 0.29 ^{ab}	22.99 \pm 0.61 ^b	24.38 \pm 0.65 ^b

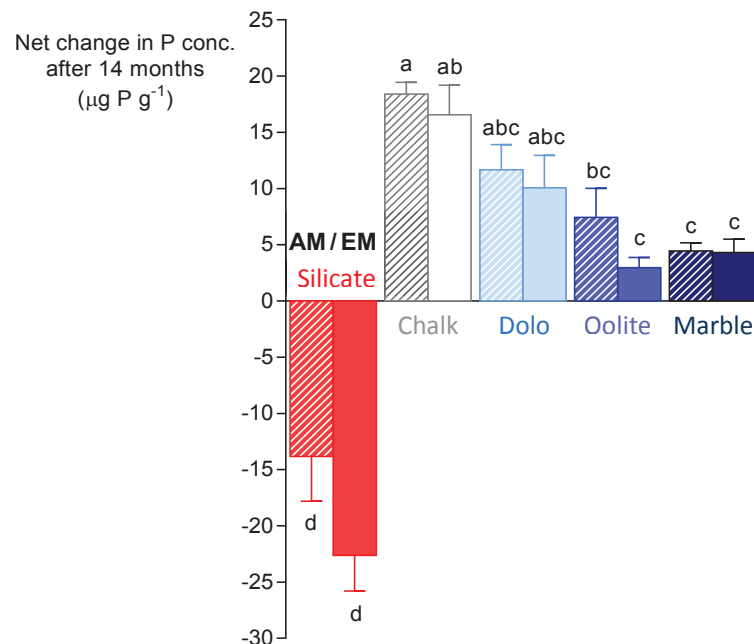


Figure 3.13. Net P change per unit mass after 14 months weathering for silicate (red) and carbonate rock grains (chalk, white; dolomite, light blue; oolite, mid blue; marble, dark blue), separated by mycorrhizal association (Mean \pm SEM; EM species, solid coloured bars, N = 6; AM trees, patterned bars, N = 7). Letters denote results of Tukey HSD for 2-way ANOVA testing the effect of rock and mycorrhizal type on the net change in P concentration over 14 months weathering. Where bars share the same letter the means are not significantly different.

Chapter 3

3.3.4.1 Selective depletion of phosphorus in silicate samples

As silicate rock grains weather, they lose phosphorus (Table 3.12). This is a selective depletion as there is a decrease in concentration as well as in total P, showing the loss of P outweighs the corresponding mass loss. There was a significant effect of weathering duration, on both total P and its concentration, as the P-content of silicate grains decreased over time (Figure 3.14; Effect of weathering duration on P Concentration: 1-way ANOVA, $F_{3,38} = 9.19$, $P = 0.00011^{***}$). There is marginally greater depletion of P in silicate samples below EM than AM tree species (Figure 3.13, Figure 3.14), however, this was not significant (2-tailed T-test with Welch's modification for unequal variances; $t = 1.77$; $df = 10.7$; $P = 0.11$).

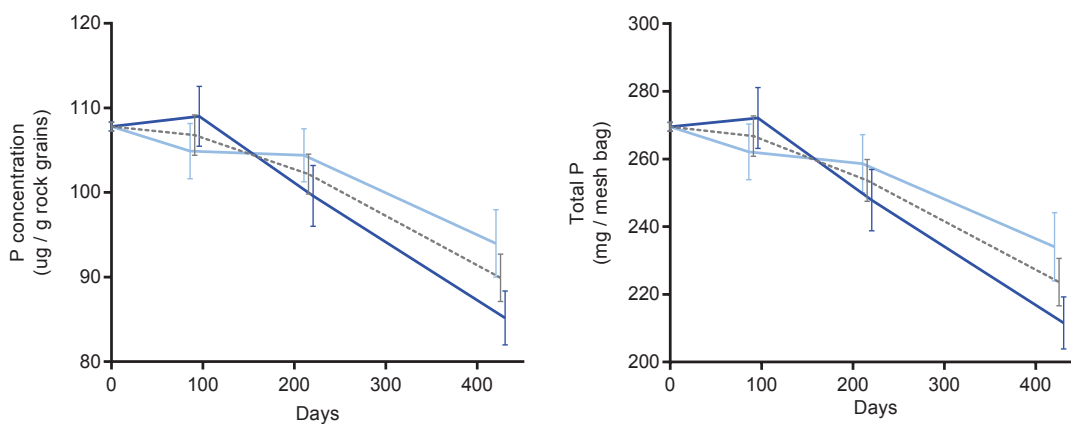


Figure 3.14. A) Per unit mass and **B)** total phosphorus content (Mean \pm SEM) of silicate rock grains over a time course of 0, 3, 7 and 14 months weathering in the field, split by mycorrhizal type (AM, light blue lines, $N = 7$; EM, dark blue lines, $N = 6$; overall average, grey dashed lines, $N = 13$ tree species).

3.3.4.2 Accumulation of phosphorus in carbonate samples

Samples of all carbonate rock types increased total P-content over the course of weathering (Table 3.12; Figure A. 1). This P accumulation was accompanied by concurrent mass loss, so the concentration of P also increased over time (Figure 3.15). Carbonate samples buried within stands of EM trees tended to accumulate marginally less P; however, this was not significant for any rock type (Figure 3.13).

Carbonate weathering rates and phosphorus biogeochemical cycling

Table 3.12. Net % change in total and per unit mass phosphorus content of rock grains after 3, 7 and 14 months weathering (Mean \pm SEM). Negative values, in red, represent an overall decrease in either total or per unit mass P content, whereas positive values show P accumulation. Superscript * denotes where results are significantly different from unweathered total P content or concentration for each rock type (Tukey HSD, **Table 3.10**, Table 3.11).

	Net % change in P concentration			Net % change in total P		
	3 months	7 months	14 months	3 months	7 months	14 months
Silicate	-0.9 \pm 5.6	-5.2 \pm 5.7	-16.6 \pm 6.5*	-1.0 \pm 0.9	-5.9 \pm 0.9	-17.0 \pm 1.0*
Chalk	19.7 \pm 5.5*	15.8 \pm 3.8*	18.6 \pm 3.5*	18.6 \pm 0.9*	12.4 \pm 0.8*	13.0 \pm 0.6*
Oolite	18.9 \pm 6.7	22.4 \pm 10.4	17.5 \pm 11.5	18.1 \pm 1.1	19.0 \pm 1.8	11.7 \pm 2.0
Dolomite	42.8 \pm 15.3	41.4 \pm 13.2	124.6 \pm 47.6*	41.6 \pm 2.4	38.4 \pm 2.2	115.3 \pm 8.0*
Marble	47.3 \pm 12.1	60.4 \pm 25.3*	74.6 \pm 25.3*	46.0 \pm 2.0	56.4 \pm 4.1*	65.8 \pm 4.4*

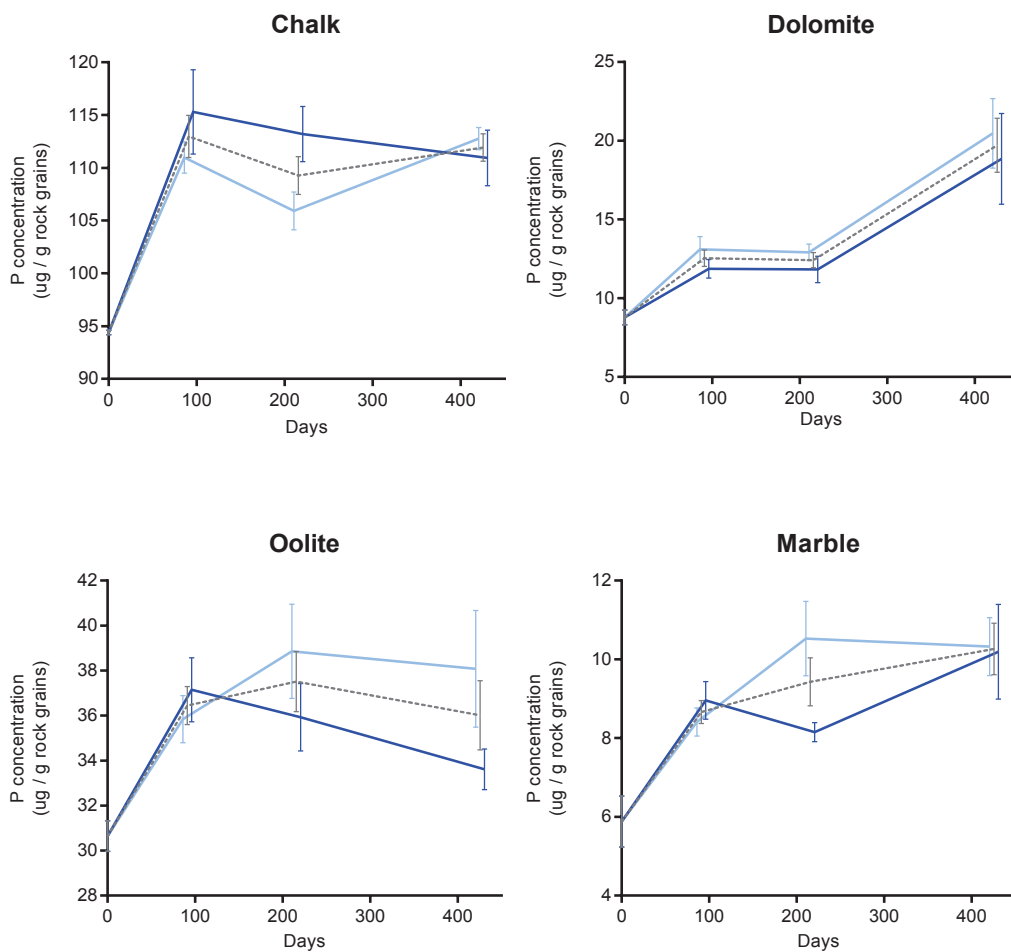


Figure 3.15. Phosphorus content per unit mass (Mean \pm SEM) of chalk, dolomite, oolite and marble grains over a time course of 0, 3, 7 and 14 months weathering in the field, separated by mycorrhizal type (AM, light blue lines, N = 7; EM, dark blue lines, N = 6; overall average, grey dashed lines, N = 13 tree species). For total P content taking account of sample mass loss over weathering see appendix Figure A. 1).

Chapter 3

3.3.4.3 Hyphal colonisation determined by initial P concentrations in rock samples

After 3 months, hyphal colonisation was closely linked to the initial P content of both carbonate and silicate samples (Figure 3.16; 1-way ANOVA, $F_{4,59} = 6.834$, $P < 0.0009$). Silicate and chalk rock grains had the highest initial P concentration, and also the greatest degree of hyphal colonisation with 6.3 ± 1.1 m and 5.5 ± 0.9 m per gram of sample respectively.

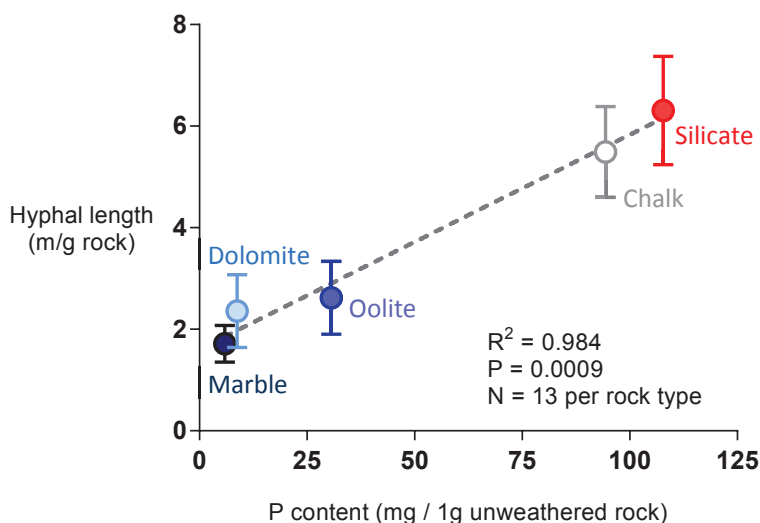


Figure 3.16. Hyphal count data (Mean \pm SEM; N = 13 tree species) after 3 months weathering for silicate (red) and carbonate rock grains (chalk, white; dolomite, light blue; oolite, mid blue; marble, dark blue), plotted against initial P concentration (Mean \pm SEM; 5 samples per unweathered rock type).

3.3.5 Investigating origins of P accumulated by carbonates

3.3.5.1 Influence of soil P content on P accumulation in carbonates

To understand the accumulation of phosphorus by carbonate samples, several follow-up analyses were performed to investigate possible sources of this P. As reviewed in the introduction, the most likely origin of additional P in weathered samples is that it had adsorbed from soil solution. Exchangeable P was measured through soil extractions followed by Murphy-Riley spectrophotometric P determination. Olsen's extractions were carried out to measure phosphorus content of fresh and dried soil samples from Bedgebury (Table 3.4). Microbial biomass P, of fresh soil samples, was also estimated by determining soil P content before and after 24 hours of CHCl_3 fumigation to lyse microbial cells and mobilise phosphorus from soil microbial biomass.

P extracted from fresh soil ranged from $0.097 \pm 0.041 \mu\text{g P g}^{-1}$ from Liriodendron stands to $2.34 \pm 1.49 \mu\text{g P g}^{-1}$ for Larix (Figure 3.17A; measured relative to 1 g dry soil). There was larger variation in P-content measured after extractions of

Carbonate weathering rates and phosphorus biogeochemical cycling

air-dried and powdered soil, ranging from $0.079 \pm 0.006 \mu\text{g P g}^{-1}$ to $5.87 \pm 1.74 \mu\text{g P g}^{-1}$, again with the extreme values being taken by *Liriodendron* and *Larix*. Despite some variation, there was significant correlation between these two measures of soil P (Figure 3.17B; Linear regression, $F_{1,11} = 6.14$, $P = 0.031^*$; $N = 13$ tree species), however, the strongest relationship is that between fresh and fumigated soil P-contents (Figure 3.17C; Linear regression, $F_{1,11} = 77.5$, $P < 0.0001^{***}$; $N = 13$ tree species). After subtracting the baseline value for fresh soil, the extra P in fumigated samples follows the same trend as P-content of control samples (Linear regression of log-log transformed data; $F_{1,11} = 15.9$, $P = 0.002$, $R^2 = 0.59$, $N = 13$ tree species). Data points for soil P-extractions cluster at low-P with a few outliers, so log transformation of data was used to remove positive skew and permit the use of ANOVA statistics.

P accumulation in carbonates does not appear to be linked to either soil P content or microbial activity. There is no relationship between carbonate P-accumulation and soil P content (Figure 3.18, Table 3.13) or microbial P (Figure 3.18, Table 3.13) for any of the rock types surveyed. There is still no significant relationship between either fresh, or fumigated, soil P-content and carbonate P-accumulation when soil P-extraction data are log-transformed, as above.

Table 3.13. Results of linear regressions for effect of soil extractable P (Figure 3.18) and microbial P (Figure 3.19) on P accumulation by carbonate rock grains weathering under mature stands of each tree species ($N = 13$). ^{n.s.} indicates no significant relationship

Carbonate Rock	Fresh soil P content	Extra P in fumigated soil
A Chalk	$F_{1,11} = 1.80$; $P = 0.21^{\text{n.s.}}$ $R^2 = 0.14$	$F_{1,11} = 0.24$; $P = 0.63^{\text{n.s.}}$ $R^2 = 0.021$
B Oolite	$F_{1,11} = 0.50$; $P = 0.49^{\text{n.s.}}$ $R^2 = 0.044$	$F_{1,11} = 2.09$; $P = 0.18^{\text{n.s.}}$ $R^2 = 0.16$
C Marble	$F_{1,11} = 0.0025$; $P = 0.96^{\text{n.s.}}$ $R^2 = 0.00023$	$F_{1,11} = 0.00015$; $P = 0.99^{\text{n.s.}}$ $R^2 = 0.000014$
D Dolomite	$F_{1,11} = 2.12$; $P = 0.17^{\text{n.s.}}$ $R^2 = 0.16$	$F_{1,11} = 1.43$; $P = 0.26^{\text{n.s.}}$ $R^2 = 0.11$

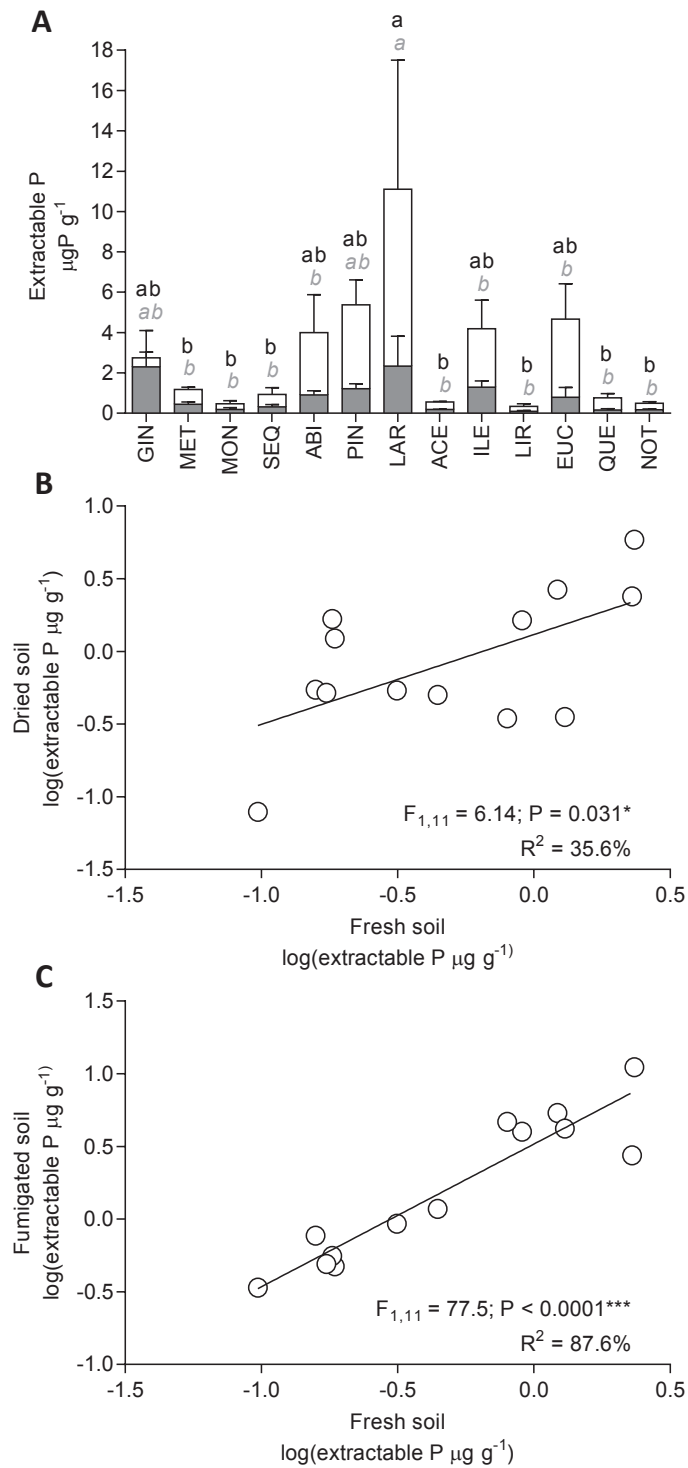


Figure 3.17. A) Average (Mean + SEM) of P content of each tree species soil in December 2013 at Bedgebury Pinetum (grey, extracted from fresh soil; white; extracted after CHCl₃ fumigation). Tukey HSD test results displayed, black letters for fumigated samples and grey italics for unfumigated samples. Log-log plot of P-extracted from fresh soil versus **B)** air dried and powdered soil and **C)** CHCl₃ fumigated soil, showing results of linear regression.

Carbonate weathering rates and phosphorus biogeochemical cycling

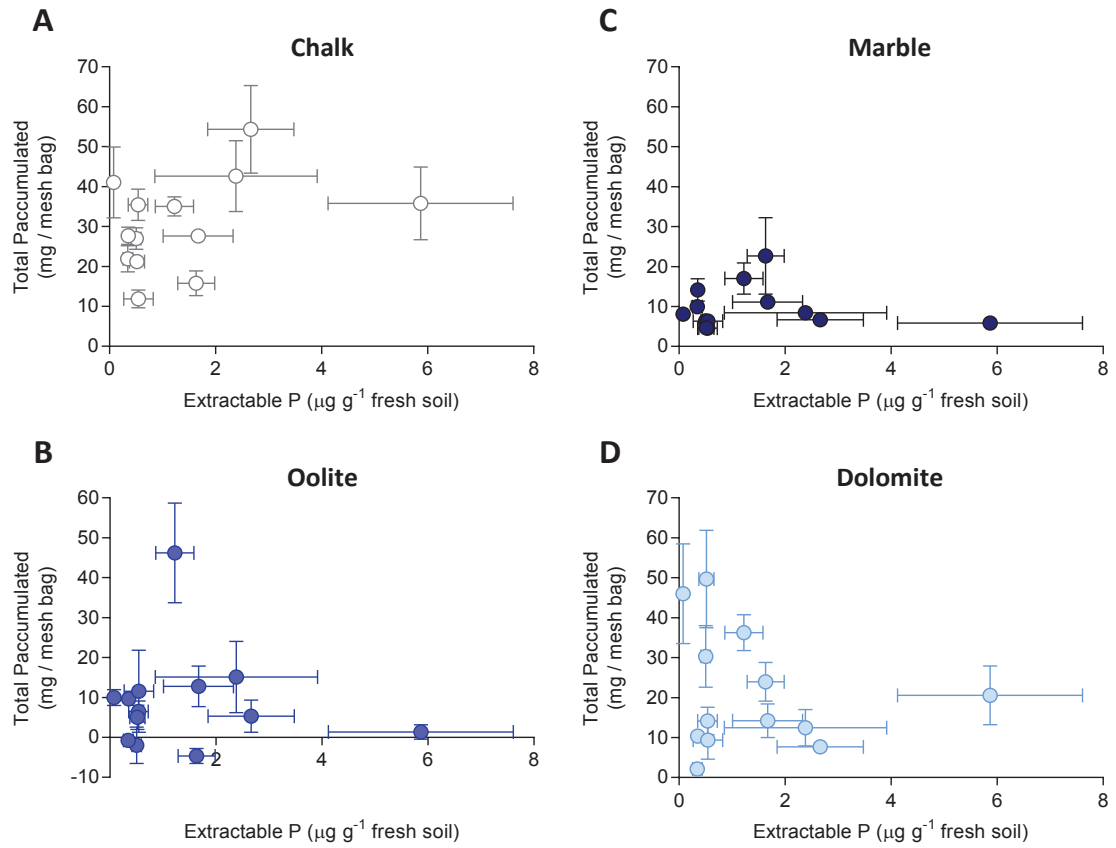


Figure 3.18. Fresh soil extractable P-content does not influence P accumulation of **A)** chalk (white), **B)** oolite (mid blue) **C)** marble (dark blue) or **D)** dolomite (light blue). All values shown are Mean \pm SEM, for N = 13 tree species. Note the different scale used for oolite due to P-depletion in some samples of *Abies*, *Metasequoia* and *Eucalyptus*.

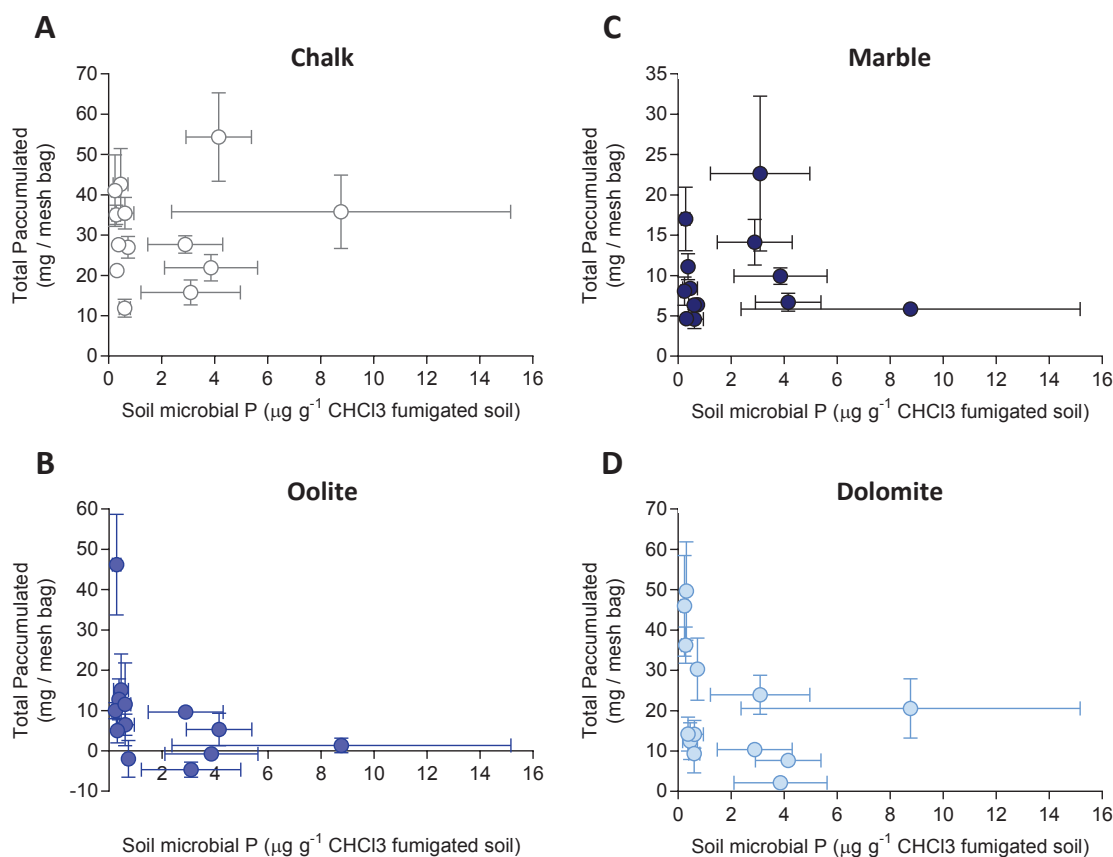


Figure 3.19. P-accumulation (Mean \pm SEM, N = 13 tree species) in carbonate samples plotted against P extracted from CHCl_3 fumigated soil as a proxy for soil microbial activity (Mean \pm SEM). A) Chalk (white), B) oolite (mid blue) C) marble (dark blue) and D) dolomite (light blue). All values are Mean \pm SEM with N = 13 tree species and soil microbial P is the net P-content after subtracting P recovered from control soil from that in fumigated soil.

3.3.5.2 Phosphorus in lipids extracted from weathered carbonates

The second follow-up analysis to investigate the origin of the P that accumulated on carbonate rock grains attempted to provide an estimate of the relative quantity of biological P within each sample by measuring P contained in extracted lipids. This analysis was only performed for chalk and silicate rock grain samples after 14 months of weathering, as according to hyphal length results (Figure 3.16), these were the most likely to contain measureable quantities of lipid-P (Table 3.4).

Phosphorus contained within extracted lipids on both carbonate and silicate rock was negligible compared with total sample P extracted during AR digests (Section 3.3.4.2, Table 3.10, Table 3.11). After 14 months weathering, on average there was $112.8 \pm 1.1 \mu\text{g P g}^{-1}$ measured in chalk grains following aqua regia digests (Table 3.10), but only $0.17 \pm 0.04 \mu\text{g P g}^{-1}$ extracted during $\text{NaCl}:\text{CHCl}_3$ direct extractions (Figure 3.20A; Mean \pm SEM, N = 13 tree species). For silicate rock grains after the same period of weathering total phosphorus was $89.9 \pm 2.8 \mu\text{g P g}^{-1}$ (Table 3.10) and the lipid soluble surface fraction was $0.090 \pm 0.033 \mu\text{g P g}^{-1}$ (Figure 3.20B; Mean \pm SEM,

Carbonate weathering rates and phosphorus biogeochemical cycling

N = 13 tree species). Lipid-P measured in silicate samples was slightly lower in silicate than carbonate rock grains, however this was not statistically significant (Figure 3.21).

There was no relationship between the lipid-P contents of each chalk sample, and total P determined following aqua regia digests (Figure 3.20). There was also no correlation between lipid-P and either weathering rate after 14 months (linear regression: $F_{1,11} = 1.90$, $P = 0.20^{\text{ns}}$); hyphal length after 3 months ($F_{1,11} = 0.098$, $P = 0.76^{\text{ns}}$) or fumigated soil P content ($F_{1,11} = 1.32$, $P = 0.28^{\text{ns}}$).

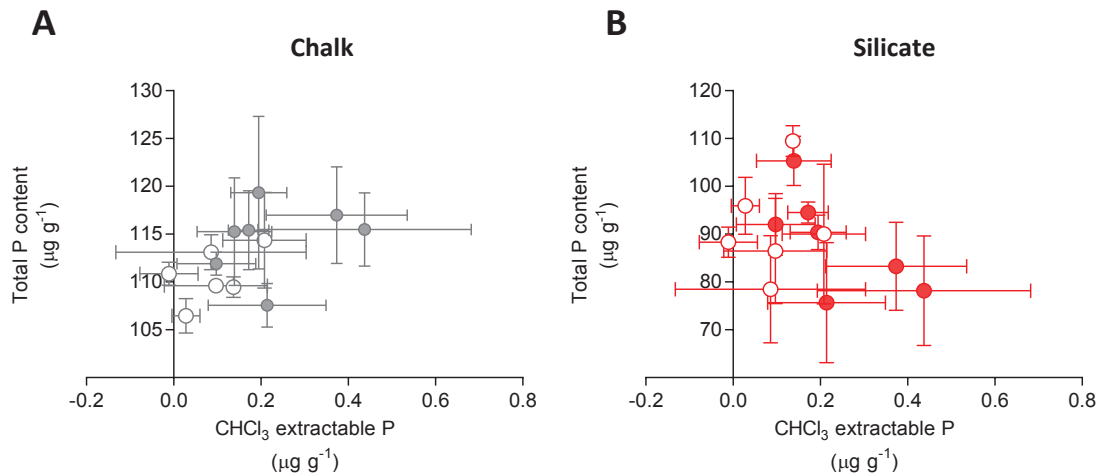


Figure 3.20. Total and lipid-P contents (Mean \pm SEM, N = 13 tree species) measured after aqua regia digest and CHCl₃:NaCl extractions respectively of **A**) chalk (Linear regression: $F_{1,11} = 4.52$, $P = 0.057^{\text{ns}}$) and **B**) silicate (Linear regression: $F_{1,11} = 1.83$, $P = 0.20^{\text{ns}}$) rock grains. Closed symbols used for gymnosperm and open symbols for angiosperm tree species. Results of linear regressions are not displayed for chalk or silicate samples as neither were significant.

There was a significant effect of tree group (angiosperm/gymnosperm), but not of mycorrhizal association on the quantity of lipid-P, both per unit mass of rock grains (Table 3.14A) and scaled by sample mass taking account of mass losses during weathering (Table 3.14B). There was little difference between total lipid P and that per unit mass (Table 3.14), so in further analyses only concentration per unit mass is investigated. Both rock types showed greater accumulation of lipid-P in samples incubated under gymnosperm than under angiosperm trees (Figure 3.21). This trend was significant for chalk (2-tailed T test with Welch's modification for unequal variances; $t = -2.28$, $df = 32.0$, $P = 0.030^*$), but not for silicate rock grains ($t = -1.97$; $df = 32.0$; $P = 0.057$).

Chapter 3

Table 3.14. Results of 2-way ANOVAs investigating the effect of tree-mycorrhizal functional group on lipid P content of chalk and silicate rock grain samples, both **A)** per unit mass and **B)** adjusted for total sample mass at 14 months. Interaction terms were included but were not significant and not detailed here.

		Rock type	Ang/Gym	EM/AM
A	Per unit mass	C	$F_{1,30} = 4.91, P = 0.034^*$	$F_{1,30} = 0.027; P = 0.87$
		S	$F_{1,30} = 3.34; P = 0.077$	$F_{1,30} = 0.59; P = 0.45$
B	Per total sample	C	$F_{1,30} = 4.96, P = 0.034^*$	$F_{1,30} = 0.024; P = 0.88$
		S	$F_{1,30} = 3.33, P = 0.078$	$F_{1,30} = 0.60; P = 0.44$

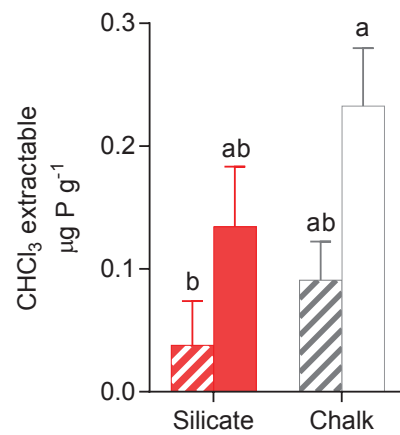


Figure 3.21. CHCl₃ extractable, 'lipid-P' content per unit mass of chalk (grey bars) and silicate rock grains (red bars), separated by mycorrhizal type (Gymnosperm = closed bars, Angiosperm = patterned bars). All values are mean \pm SEM (N = 7 tree species for gymnosperm and N = 6 for angiosperm) and letters show results of Tukey HSD test after 2-way ANOVA to find the effect of rock and tree type on lipid soluble P fraction. Bars sharing the same letter are not significantly different from one another at $P < 0.05$.

3.4 Discussion

3.4.1 Discussion of evidence related to research hypothesis 1

In forest soils, carbonate weathering rates exceed those of silicate minerals and are most intense below EM Angiosperm tree species

3.4.1.1 Calcite mass loss exceeds that of silicates

As expected, in terms of mass loss, calcite weathering is faster than silicate weathering (Table 3.5). This is likely due to the slower weathering kinetics of silicate minerals, with higher activation energies, E_a , for dissolution (reviewed in White 2003; Palandri and Kharaka 2004), and the susceptibility of carbonates to dissolution in acidic environments (Cubillas *et al.* 2005) such as those found at Bedgebury (Figure 2.11).

In terms of SA-normalised molar weathering rates, by far the greatest rates are exhibited by marble (Table 3.6). Although the mass loss of marble grains is not dissimilar to that of other calcite-bearing rocks, rates are faster due to the very low initial BET SA of marble used for normalisation (Figure 3.8). Similarly, in terms of molar rates, silicate dissolution is not always slower than that of carbonate, because of the low BET SAs measured for silicate grains (Figure 3.8, Table 3.6). For marble, it is questionable whether the use of initial BET is appropriate for normalising weathering rates, as due to the crystalline structure of this rock, grains disintegrated rapidly, far more than for any of the other carbonates (observations only).

Due to the slow weathering kinetics of silicates, it is difficult to accurately determine dissolution rates from mass changes. A more appropriate method would be to investigate elemental changes after sequential extraction of some tracer elements, using a technique such as ICP-MS. For instance, Quirk *et al.* (2012) measured the rate of Ca-release from both carbonate and oxide fractions of basalt grains.

3.4.1.2 Intensification of calcite and silicate weathering over initial 7 months

Both calcite-containing, chalk and oolite, and silicate rock grains showed an initial intensification of weathering, from 3-7 months (Figure 3.9), followed by a plateau or decline, both in terms of total, 0-3, 0-7, 0-14 months (Table 3.5, Table 3.6), and net weathering, 0-3, 3-7, 7-14 months (Table 3.7).

This observation may be explained by a lag-phase, where hyphal colonisation of newly buried mesh bags is slow. Firstly, time will be needed to repair any disruption to roots and hyphal networks that was undoubtedly caused whilst inserting samples. Secondly, immediate colonisation is unlikely as hyphae require time to grow and explore the potential of new mineral resources (Leake *et al.* 2008).

Chapter 3

These biological factors may be exacerbated by environmental conditions. The initial 3 months of this study, April/May – August 2013, were especially dry, with the south of England receiving less than half the 1981-2010 average summer rainfall (MET office 2013). Low soil moisture will hinder rhizosphere microbial activity and limit the water-mineral contact time required for dissolution. So, faster weathering at 3-7 months, compared to 0-3 months may in part be due to more established hyphal colonisation, but could also result from increased soil water in the autumn (Met Office 2014).

3.4.1.3 Weathering rate decrease from 7-14 months

Over the period 7-14 months, calcite and silicate weathering rates slow. This decline is probably linked to decreasing surface reactivity of weathering rock grains, which could occur for several reasons. Firstly, surfaces are gradually occluded by adsorbed organic matter (OM) or metal oxides. This is suggested by the discolouration of rock grains, especially an accumulation of orange residue, which may be Fe oxide (Table 4.10, Section 4.4.3). Accumulation of surface OM and oxides may both prevent hyphal access and reduce surface reactivity to abiotic weathering.

The second possibility is that after 7 months, the most weatherable features may have been already dissolved, potentially leaving less weatherable components. This may either be accompanied by a change in surface area characteristics, which is investigated in the following chapter, or a change in chemical composition, especially at the grain surface.

3.4.1.4 Dolomite weathering increases throughout the 14 month burial period

The sustained increase in weathering rate of dolomite from 7-14 months, over the period where calcite weathering was either plateauing or decreasing, is probably due to the slower weathering kinetics of dolomite compared to calcite (reviewed in Morse and Arvidson 2002). Another possibility is that there is slower hyphal colonisation, and therefore fungal weathering, of dolomite as a result of its lower phosphorus content than chalk, oolite or silicate grains (Figure 3.16). This is discussed in more detail in a following section.

3.4.1.5 Mass gain of samples and net weathering rates

Occasionally, samples gained mass over the period they were buried (Figure 3.10A). This mass gain was generally only seen after 3 months and is probably due to the accumulation of organic matter and secondary precipitates, as well as ingrowth of hyphae. All samples of all rock types were discoloured to some extent (Table 4.10). Samples were sometimes colonised by dark brown rhizomorph forming fungi (Figure 3.2) or white fungi, visible to the naked eye or under dissecting microscope, and are certainly colonised by other soil micro-organisms not visible except at higher magnification.

Because most samples decreased in mass over the weathering period, it is reasonable to assume that where samples gained mass overall, is because the increase in mass, from hyphal accumulation, OM adsorption or secondary precipitates, outweighs any loss of material through weathering. It follows from this that where samples have lost mass, in reality the mass loss of original material will exceed that measured as it is offset by accumulated surface material (Eqn 12).

Equation 12 describes the observed changes in mass of carbonate rock grain samples weathering in the field. M_{WL} signifies weathering mass loss, and $(M_{OG} + M_{IG})$ the sum of organic (OG; hyphal/bacterial ingrowth, OM accumulation) and inorganic (IG; secondary mineral precipitates, metal oxides) mass gain.

$$Final\ mass = Initial\ mass - M_{WL} + (M_{OG} + M_{IG}) \quad (12)$$

While this study has investigated net changes in carbonate mass, key terms of this equation still need to be investigated to split these mass changes into their component parts and aid understanding of the weathering process. The most likely terms for future study are weathering mass loss, M_{WL} , and OM accumulation, M_{OG} . Identification of suitable trace elements (Gaillardet *et al.* 2003) or stable isotopes present in initial rock grains, but not in secondary carbonate precipitates would aid quantification of M_{WL} . Thermogravimetric analysis (TGA) could be used to measure M_{OG} . TGA tracks mass loss over a gradual increase in temperature. This method is used for organic carbon determination in calcareous soils as all volatiles and organic mass components would be lost at temperatures below that required for the thermal decomposition of carbonate or dolomite minerals occurring above 600°C (Pallasser *et al.* 2013).

Chapter 3

3.4.1.6 Comparison of SA normalisation with Thorley *et al.* (2015)

Molar weathering rates in Thorley *et al.* (2015) were scaled relative to molar mass, estimated from the bulk mineral composition before normalising to geometric surface area calculated from average particle size and experimentally determined density (Section 3.2.2.1). This method introduced several sources of uncertainty in the calculation of weathering rates.

Firstly, it excluded the possibility that any carbonate rock type contained traces of multiple minerals, and assumed that all shared the same empirical formulae, either CaCO_3 for calcite, or $\text{CaMg}(\text{CO}_3)_2$ for dolomite. The three calcite-containing rocks, marble, chalk and oolite were assumed to have identical compositions of pure CaCO_3 . In reality this is quite close and they contain 96.5%, 95.6% and 93.9% CaCO_3 by weight, respectively, so this estimation made little difference to calculated weathering rates.

On the other hand, use of a molar mass based on the empirical formula of dolomite resulted in underestimation of its weathering rate in Thorley *et al.* (2015). Pure dolomite contains roughly 50% Ca and 50% Mg, making its empirical formula CaMgCO_3 . This is associated with a molar mass of 184, nearly double that of CaCO_3 ($M_r = 100$). Use of this high M_r artificially reduced dolomite molar weathering rates relative to those of calcite-containing rocks. For instance, a weathering mass loss of 100 mg would equate to 0.001 moles CaCO_3 , but only 0.00054 moles of $\text{CaMg}(\text{CO}_3)_2$, making molar weathering rates misleading.

The second source of uncertainty in Thorley *et al.* (2015) is the normalisation of weathering rates to geometric surface area. Subsequent BET data collection shows that SA of all rock types was previously underestimated. Remarkably, whilst different greatly in magnitude, BET and geometric SA were almost proportional (Figure 3.8), so whilst the absolute weathering rates have changed between then and the current study, there actually very little change when considering the relative rates of each rock type. The interplay of weathering and surface area has since been investigated in greater detail, and this forms the focus of Chapter 5.

3.4.1.7 Effect of tree-mycorrhizal functional group on carbonate weathering rates

During the initial 3 months of weathering, there was a significant effect of both tree and mycorrhizal functional group on weathering rates of calcite-containing rock grains (chalk, marble and oolite). Calcite dissolution was most rapid under EM angiosperm species (Figure 3.10B), an effect that was established in the work of Quirk *et al.* (2012) who discovered that Ca-release from the carbonate fraction of basalt grains

Carbonate weathering rates and phosphorus biogeochemical cycling

was greater under EM angiosperm than AM gymnosperm tree species. This weathering intensification of carbonate inclusions within silicate rocks must have an important indirect effect on silicate weathering rates through increasing vulnerable surface area.

After longer weathering durations, there was no longer any effect of tree type, however, EM species continued to promote faster calcite weathering, although this was only significant after 7 but not 14 months (Figure 3.11, Figure 3.12; Table 8). Tree-mycorrhizal functional group had no effect on silicate weathering rates, and the only effect of mycorrhizal type on dolomite weathering was seen after 14 months, where faster weathering occurred in EM than in AM tree stands (Table 8, Figure 3.11). As seen earlier, dolomite has slower dissolution kinetics than calcite, and it may be that the difference between AM and EM species would become more distinct after longer weathering durations.

3.4.1.8 Carbonate weathering intensification by EM fungi

Rapid weathering under trees hosting EM associations may be achieved through a combination of direct and indirect effects. One direct effect could be increased weathering by mycorrhizas for plant and fungal mineral nutrition. EM fungi have a broader range of weathering strategies than AM fungi, including the secretion of LMWOAs and chelating anions (Section 1.5.3) that can chemically destabilise mineral surfaces, making them more susceptible to dissolution. Indirect weathering may occur through modification of the soil environment, such as acidification through proton extrusion. It is likely that at Bedgebury, the low soil pHs measured below stands of EM trees is the primary driver of rapid carbonate weathering after 3 months; this has been investigated in more detail in Chapter 4.

No sustained weathering intensification by angiosperm trees

Initial weathering of calcite was faster under angiosperm than gymnosperm trees. This could be due to greater carbon flux belowground, promoting mycorrhizal activity. On the other hand, this pattern is primarily driven by rapid weathering below EM angiosperms (Figure 3.10), and could result from the combination of season and specific tree species chosen, rather than a more generalizable effect of angiosperms.

Seasonal variation in belowground C-allocation

Radiolabelling experiments using ^{13}C have shown belowground allocation of carbon for microbial respiration in grassland (Leake *et al.* 2006) and forest ecosystems (reviewed in Hogberg and Read 2006; Subke *et al.* 2009; Hogberg *et al.* 2010; Epron *et al.* 2011). Belowground carbon allocation, and therefore its promotion of rhizosphere microbial activity are seasonal (Hogberg *et al.* 2010; Epron *et al.* 2011). This is clear

Chapter 3

for deciduous species, which require aboveground C-allocation for leaf growth in late spring and belowground storage in late summer before leaf senescence, however, is also significant for evergreen trees.

One study in a Swedish *P.sylvestris* forest measured a five-fold increase in carbon allocation belowground at the end of the summer, in August, compared to earlier in the year, in June (Hogberg *et al.* 2010). Epron *et al.* (2011) studied seasonal variation of belowground C-allocation, also using $^{13}\text{CO}_2$ canopy labelling, in the same beech, oak, pine system. The lag time until ^{13}C to appear in soil $^{13}\text{CO}_2$ efflux measurements was 0.5 - 1.3 days for angiosperms, and longer in pine, ranging from 1.6–2.7 days in the active growing season, and >4 days in the winter. Both pine and beech, but not oak trees, showed significant seasonal variation in belowground C-allocation (Epron *et al.* 2011).

It may be that less carbon is allocated belowground in the summer over the first 3 months, particularly for deciduous species included in this study. There was no obvious effect of leaf habit on weathering rates; however, the split of evergreen and deciduous species within each tree-mycorrhizal functional group is unbalanced (Table 3.1) and data not suited to accurately investigate this effect. The increase in belowground C-allocation toward the end of the growing season may be a better explanation for why, after 3 months, tree type no longer significantly affected calcite weathering rate, rather than for the differences observed in initial weathering rates.

Phloem transport rates differ between tree species

The amount of carbon that can be allocated belowground depends on the speed of transport from the site of photosynthesis, through the phloem to the roots and then soil. Radiolabelling experiments using ^{14}C showed phloem transport rates in angiosperms can be up to twice as fast than in gymnosperms, with a shorter delay between canopy labelling and $^{14}\text{CO}_2$ efflux from the soil (reviewed by Kuzyakov *et al.* 2010). Phloem velocity is partly determined by sap viscosity, and also by phloem anatomy, most importantly tube diameter and sieve plate anatomy. Considering phloem anatomy, there are structural differences between that of angiosperms and gymnosperms. Gymnosperm phloem lacks companion cells, which play a role in loading and unloading photosynthates into and from the sieve elements. Temperature and water availability are the main environmental factors affecting phloem transport velocity, however, the precise mechanisms of this are still uncertain.

Intrinsic factors influencing phloem velocity not only vary from angiosperms to gymnosperms, but also between individual species. A ^{13}C radiolabelling study of small

beech, oak and pine trees found all to have different carbon transport rates relative to trunk diameter. Phloem transport rates for both angiosperm species, but not for pine, increased proportional to trunk diameter, however, for a given diameter was faster in beech than in oak (Dannoura *et al.* 2011). Although selected trees all had approximately the same trunk diameter, variation existed both within and between species (Table A. 2).

3.4.2 Discussion of evidence related to research hypothesis 2

Mycorrhizal dissolution of carbonate rock grains in forest soils increases access to mineral phosphorus, which is selectively depleted over the course of weathering.

3.4.2.1 Hyphal colonisation proportional to rock grain P-content

After 3 months incubation in the field, mesh ingrowth bags of different carbonate and silicate rock grains were, on average, colonised by fungal hyphae in proportion to their initial P content (Figure 3.16). Silicate and chalk had the longest hyphal lengths measured, and also the highest initial P-concentrations. Dolomite and marble had both the lowest initial P and the shortest hyphal lengths, whilst oolite grains were intermediate for both.

EM hyphal colonisation in response to inorganic-P supply has been seen before in both microcosm (Leake *et al.* 2008), and field experiments (Hagerberg *et al.* 2003; Wallander and Thelin 2008). The positive relationship between P-content and hyphal length indicates fungi colonise rock grains to access mineral sources of limiting nutrients, in this case phosphorus. In this study, it is not possible to say whether hyphae were from AM, EM or saprotrophic species, and in reality it is likely to be a mixture, especially considering the close proximity of plots and probable overlap of tree root systems and soil fauna (Section 2.4.3.2).

Initial P was used for this analysis, rather than P-content after 3 months weathering, as colonising hyphae were presumably attracted by historical P-content, and the sample preparation method does not distinguish between recently active and dead hyphae. As weathering progresses, hyphal colonisation will be responding dynamically to changing phosphorus concentrations and that of other potentially limiting nutrients.

In this study, sample P-content was derived from aqua regia digestion, which totally dissolved carbonate samples (Table 3.4). Because the relationship between total rock grain P and hyphal colonisation is so strong (Figure 3.16), it is likely that hyphae

Chapter 3

can sense-P resources throughout carbonate grains, not only at their surface, lending weight to the assumption that fungal hyphae can tunnel into rocks.

3.4.2.2 Phosphorus depletion in silicates

Over time, the decline in both total phosphorus, and its concentration in silicate rock grains (Figure 3.14, Table 3.12) indicates it is being selectively removed. Phosphorus is often a plant growth-limiting nutrient in forests, and may be being extracted from silicate grains by soil micro-organisms, in particular, mycorrhizal fungi.

Several field experiments have indicated that EM hyphal colonisation of mineral P-sources increases with host plant nutrient demand, in particular P, K Mg and Ca (reviewed in Rosenstock 2009). Sand-filled mesh in-growth bags buried under stands of *P. abies* in Sweden showed consistently greater EM hyphal colonisation when sand was amended with apatite (Hagerberg *et al.* 2003), except where forests were concurrently P-fertilised (Wallander and Thelin 2008). In a boreal forest podsol, weathering intensity was greatest where soil fertility lowest (Hoffland *et al.* 2003). This study measured the density of tunnels within feldspar grains, presumably formed by EM fungi to access mineral nutrient resources.

3.4.2.3 Phosphorus accumulation by carbonates

Weathering of carbonate and silicate rock grains appears to have contrasting behaviour in terms of changes in phosphorus content. Whilst P is depleted from silicate rock grains, it accumulates in carbonate samples (Figure 3.15, Table 3.12). This accumulation is especially rapid over the first 3 months burial in the field (Figure 3.15).

P-accumulation could arise from a variety of sources, which are not fully resolved within this study. These include passive absorption of P from the surrounding soil solution, or active biological import of P, possibly via fungal hyphae. Sample P change is summarised in Eqn 13 as the net outcome of both P-accumulation through passive (P_p) and active P_A processes, and P-depletion through rock dissolution or microbial weathering (P_{loss}).

$$\Delta P = (P_p + P_A) - P_{loss} \quad (13)$$

3.4.2.4 Limitations of total rock grain phosphorus measurements.

For all of the above phosphorus measurements, carbonate samples were totally solubilised by aqua regia digestion before P-determination (Table 3.4). Silicate samples were treated in the same way, however due to their resistance to acid treatment, silicate grains were not totally dissolved, as they were for carbonates. This aggressive method was chosen as a way to solubilise all phosphorus that could possibly be available to fungal hyphae, even if acidic exudates permitted tunnelling into rock grains.

However, if most chemical modifications occur at mineral surfaces, aqua regia digestion has one major limitation. Total digestion effectively dilutes the altered portions of each sample, because material from the interior of each grain is likely to have been altered to a much lesser extent. This may reduce the significance of any localised changes in P content. In addition to this, total dissolution of carbonates prevents us partitioning any phosphorus changes between the grain surface and its interior. This is not the case for silicate grains, where P-changes must be occurring at the surfaces accessible to acid digestion.

In this study, there were many limitations on the measurements of both inorganic and organic phosphorus accumulated by carbonate rock grains. These included the inability to isolate elemental changes only on mineral surfaces, and compromise in measuring total sample P to avoid issues with rock grain splitting or internal modifications. Another limitation was the difficulty in quantifying very limited lipid-P, the large variation in these measurements, and uncertainty whether this gives a relative measure of organic P associated with samples. In particular, it would be very informative if it was possible to distinguish between original mineral P present in rock grains, and secondary deposits of inorganic P, possibly in insoluble complexes with Ca, Mg, Fe and Al.

Chapter 3

3.4.3 Discussion of evidence related to research hypothesis 2

Additional phosphorus in weathering carbonate grains accumulates passively from inorganic phosphate in the immediate soil environment.

3.4.3.1 Possible origins of accumulated phosphorus in weathered carbonates

This is the first time that phosphorus accumulation in weathering carbonates has been observed. There is no literature precedent for this, and previously only P-depletion has been observed in weathering silicates (Leake *et al.* 2008). Most studies on phosphorus adsorption focus on sediments in aquatic environments (Wang *et al.* 2010), in order to assess the impacts of P from fertiliser in agricultural runoff or from sewage effluent. In this section I have examined two possible explanations for the origin of this additional phosphorus:

1. Accumulation of P from soil
2. Import of P by soil biota

3.4.3.2 Passive accumulation of P from soil

The environment immediately surrounding dissolving carbonate rock grains will contain high concentrations of basic cations, most notably Ca and Mg. These can form complexes with inorganic phosphate, and orthophosphate may be adsorbed to, or co-precipitated with CaCO_3 at rock grain surfaces (Boström *et al.* 1988; Kuo and Lotse 1972). In order for P to adsorb from soil solution, there must be some interaction between rock grain surfaces and available P. This will depend both on the availability of P in the immediate soil environment and on the surface area of rock samples that it can adsorb to. The kinetics of phosphate adsorption to CaCO_3 depend on initial phosphorus concentration; at low concentrations, P adsorption is directly proportional to concentration, and at higher concentrations, it is more likely to precipitate as dicalcium phosphate, CaHPO_4 (Kuo and Lotse 1972).

Influence of carbonate sample SA on P-accumulation

There is a slight indication that P adsorption depends on rock grain surface area, as chalk and dolomite which had the greatest P accumulation (Figure 3.13) also had large initial BET SA (Figure 3.8). Evidence to the contrary also exists, as oolite samples accumulated equivalent P to marble samples despite their far greater initial SA, which exceeds even that of dolomite and chalk. Due to the incomplete understanding of BET SA changes throughout weathering of either marble or oolite (Chapter 4) and their differences in rock structure and composition, it is not possible to say for certain

whether SA is an important factor in their P accumulation, and it is probably more appropriate to only compare data for a single rock type.

Soil P availability

Elutable-P was measured for fresh; CHCl₃ fumigated and air-dried soil samples using Olsen's extraction method (Table 3.4). Contrary to expectations, there is no indication that high concentrations of either extractable (Figure 3.18, Table 3.13) or microbial P (Figure 3.19, Table 3.13) in soils leads to greater accumulation of P by carbonate rock grains.

Olsen's P was consistently higher for air-dried than for fresh soil (Figure 15B). Drying and powdering probably releases P through damage or lysis of microbial cells. There was loose correlation between P extracted from paired samples of fresh and air-dried soil (Figure 3.17B). This indicates that where it is not possible to rapidly analyse fresh samples, air-dried soil may be used as an alternative, however, the precise change in P-content during drying depends on the tree species (Figure 3.17). Fresh soil extractions better represent the field situation and give a more realistic indication of P available to plants and for this reason this measure was used for subsequent analyses.

Soil extractable P (Table 3.4) varies considerably between tree species (Figure 3.17A), *L. tulipifera* soils had the lowest P-content, and *L. decidua* the highest. Low soil P under *Liriodendron* may be due to soil waterlogging and gleying in this plot. Waterlogging potentially limits soil oxygen availability and inhibits microbial activity and associated organic phosphorus mineralisation. This is supported by the minimal increase in P extracted from *Liriodendron* soil after CHCl₃ fumigation (Figure 3.17A), indicating that there is little microbial activity.

High soil P content for *Larix*, as well as *Abies*, *Pinus*, *Ilex* and *Eucalyptus*, might be due to the large seasonal input from litter, coupled with rapid mineralisation of organic matter by abundant soil micro-organisms, which is supported by the strong correlation between phosphorus eluted from fresh and fumigated soil (Figure 3.17C).

The point lying furthest from the regression line in Figure 3.17C is from *Ginkgo*. This also had relatively high extractable P, but was little changed by fumigation. This may be due to the positioning of *Ginkgo* specimens within the landscaped section of the arboretum, rather than in single-species stands. Management of this landscaped section could have included soil amendment with fertiliser, as this site is known to be P-limited (Ovington 1958). Alternatively, the close proximity to other plant species might provide a broader range of soil microorganisms and faster P release from organic sources.

Chapter 3

Although soil samples were processed as soon as possible after sampling and kept cool prior to analysis, there was certainly some sample degradation that might result in a slight over-estimation of field-available P. Storage likely caused microbial death or decomposition and soil coring would have severed fine roots and fungal networks. This may be especially damaging for mycorrhizal fungi which become disconnected from their host tree carbon supply.

3.4.3.3 *Active import of organic P*

An alternative origin for the phosphorus accumulated by carbonate samples is biological import, possibly by mycorrhizal fungi. Organic phosphorus could be contained either within biological matter, such as fungal hyphae, or in substances secreted for other purposes, for instance, adhesion.

The quantity of P in lipids was estimated using a modified Bligh and Dyer extraction method, followed by acid digestion and Murphy-Riley P-determination. This extraction method is gentler than aqua regia digestion (Table 3.4), and should only elute lipid-P that can be desorbed from the surface of rock grains. P measured by this procedure includes that in cell wall components, such as phospholipids and is likely to scale with other forms of organic P such as nucleic acids. Only silicate and chalk rock grains after 12 months weathering were studied as these had the highest phosphorus content, and a pilot of other rock grain types (dolomite, oolite and marble) showed that they fell below detection limits.

Overall, the minimal quantities of P extracted from lipids were too small to be of consequence for total P accumulation: on average chalk grains accumulated a total of $112.8 \pm 1.1 \mu\text{g P g}^{-1}$, only $0.17 \pm 0.04 \mu\text{g P g}^{-1}$ of which was extracted as lipid-P (Table 3.10, Figure 3.21). This is supported by the lack of correlation between total sample P and lipid-P for either chalk or silicate rock grains (Figure 3.20). There was high variation in lipid-P, which may result, in part, from sampling issues. Hyphae tended to clump together within in-growth mesh bags, preferring to grow along the interface between mesh and rock grains. To avoid inaccuracies in sampling fungal material, which was analysed separately by hyphal counting, sub-samples only including rock grains were used when possible. The same sub-sampling technique was used for both aqua regia digests and lipid extractions, so this cannot explain the lack of correlation between these datasets.

Slightly higher lipid-P was measured in chalk than in silicate grains, but this is not significant and cannot account for the much greater accumulation of P by chalk grains because P extracted from lipids is comparable between these rock types (Figure

3.21). Significantly more lipid-P was recovered from rock grain samples weathering under gymnosperm than angiosperm trees, however there was no effect of mycorrhizal type. This may be explained by the earlier observation of particularly high extractable P after CHCl_3 fumigation of some gymnosperm soils, notably *Larix*, *Pinus* and *Abies* (Figure 3.17A), although there was no overall correlation between lipid-P and the extra P released from soil micro-organisms upon fumigation (Section 3.3.5).

The minimal quantities of lipid-P measured suggest that within carbonate samples, accumulated P is unlikely to be contained wholly within biological material. However, although this analysis only attempts to estimate the relative differences in organic P-content of weathered samples, there are serious methodological limitations. Firstly, only P contained in lipids and not within other organic molecules such as nucleic acids can be measured. Secondly, the minimal quantities and high variation in lipid-P measured suggest that the extraction used may not be the optimal technique for measuring any accumulation of organic P.

3.5 Conclusions

In this thesis we present the first comparative study of carbonate and silicate weathering rates, by an evolutionarily diverse group of trees and their mycorrhizal symbionts. While silicate weathering has been investigated previously in the field (Quirk *et al.* 2012), this approach contrasts with previous work on carbonate dissolution which is studied in batch reactors or continuous-flow laboratory systems under controlled conditions (Arvidson *et al.* 2003; Chou *et al.* 1989; Cubillas *et al.* 2005; Kirstein *et al.* 2016).

3.5.1 Research hypothesis 1

Evidence from a 14-month study at the UK's national pinetum confirms that weathering rates of carbonate rocks are greater than those of silicates and are increased by a wide range of mature EM and AM angiosperm and gymnosperm tree species. All types of carbonate rock grains studied (chalk, oolite, marble, dolomite) weather faster than those of a primarily quartz silicate. After 3 months weathering (May–August 2013), especially rapid weathering was observed within EM angiosperm forest soils, potentially due to the broader range of weathering strategies available to EM than to AM fungi (Section 1.5). It is likely that at Bedgebury, the greatest single factor influencing carbonate weathering rates is the low soil pH below EM species, and this forms the focus of the first part of Chapter 4.

From 3-7 months, weathering rates of calcite-containing samples (chalk, oolite, marble) continue to increase, before plateauing or slightly decreasing, between 7-14 months. After the initial 3 months, EM fungi continued to promote faster carbonate weathering, however there was no longer any rate enhancement by angiosperm compared to gymnosperm trees. The later decline or stabilisation of calcite weathering rates is potentially due to decreased surface reactivity of weathering carbonates. This might arise from accumulation of adsorbed organic matter or secondary precipitates on rock grain surfaces, decreasing their susceptibility to further weathering. Also might be due to most weatherable components already having dissolved. Unlike calcite-containing rock grains, after 14 months incubation, dolomite weathering rates continue to increase due to the slower dissolution kinetics of this mineral.

Carbonate weathering rates and phosphorus biogeochemical cycling

3.5.2 Research hypothesis 2

Over the course of weathering, P is selectively depleted from silicate samples, but accumulated by carbonates. Depletion is likely due to selective P-mobilisation as a nutrient source supplying trees and their associated soil microbial community, particularly mycorrhizas. There was no significant impact of mycorrhizal type on either P-depletion from silicate or P-accumulation by carbonate rock grains.

After 3 months sample incubation in the field, hyphal colonisation of rock grains is proportional to their initial P content. Both field and microcosm studies have shown that where plant growth is P-limited, EM fungi are able to biosense P sources within minerals. Hyphae preferentially colonise minerals with high phosphorus content or small grain size allowing greater phosphorus accessibility (Leake *et al.* 2008; Quirk *et al.* 2012).

Considering two results, first that carbonate samples in EM forest soils accumulated slightly less P than under AM trees; and second that P depletion of silicates was greatest in EM forests; it is likely that P is simultaneously being removed, as it is from silicates. However, due to accumulation rates exceeding those of depletion, the resultant effect is a net accumulation of P.

3.5.3 Research hypothesis 3

The final section of this chapter investigates the origin of phosphorus accumulated by carbonate samples during weathering. This P may originate from a combination of sources: passive adsorption from surrounding soil or active import by a biological agent.

There is no evidence from soil extractions that P-accumulation in carbonates is determined by soil P-content, and in reality, there is bound to be complex interplay between available phosphorus and rock grain surface characteristics, as well as the effect of surrounding pH environment on the favourability metal-phosphate precipitation. Dissolving carbonates release basic cations; in particular Ca and Mg, which will initially be concentrated in close proximity to the mineral surfaces, before diffusing or leaching into the soil solution. This basic environment immediately surrounding dissolving carbonate grains is favourable for the precipitation of sparingly soluble metal-phosphorus complexes.

Accumulated P is more likely to be in inorganic complexes rather than organic compounds as only minimal quantities of P were measured following lipid extraction as a proxy for biological P. Due to measurement limitations, it is still possible that organic phosphorus may be actively imported by micro-organisms and adsorbed. Given the

Chapter 3

very small quantities of phosphorus measured in lipid extractions, this unlikely, but may be the case if input of resources were required to enable access some other even more growth limiting nutrient. This is possible for chalk, however, unlikely for marble, which had a slight P-accumulation, despite containing no biologically interesting trace elements.

Since mycorrhizal hyphae can mobilise P from rock grains (Leake *et al.* 2008), carbonate weathering in soil may be important, not only for release of P contained within mineral, but for its ability to act as an effectively renewable P-source, filtering and concentrating P from the surrounding environment. Current evidence suggests a new model of soil P cycling in weathering carbonates, described by the following equation and in Figure 3.22. Net change in carbonate phosphorus content (ΔP) is the product of P-depletion through rock dissolution or microbial weathering (P_{loss}) and P-accumulation through passive (P_P) and active (P_A) processes. In the case of carbonates, there is an imbalance between these processes and $(P_P + P_A) > P_{loss}$, resulting in phosphorus accumulation.

$$\Delta P = (P_P + P_A) - P_{loss} \quad (13)$$

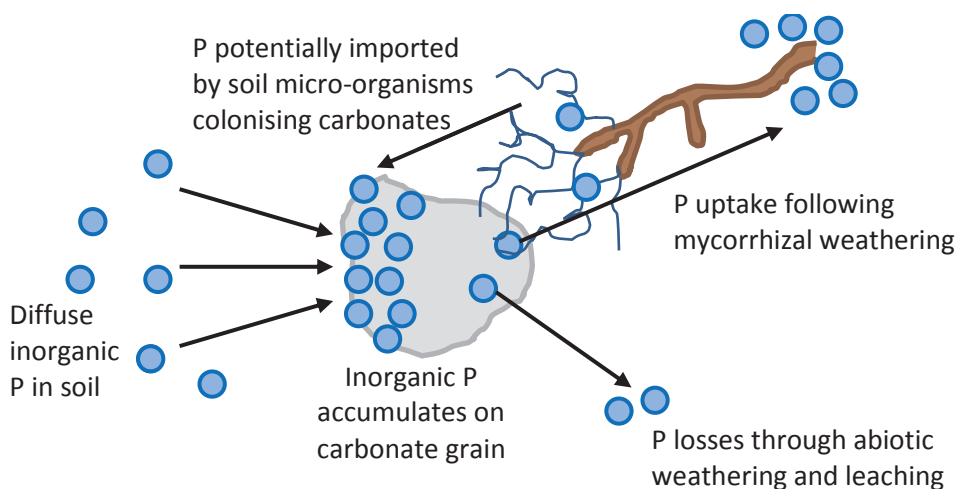


Figure 3.22. Proposed model of interactions between biota and weathering carbonate rock grains in soil, concerning transfer of inorganic phosphorus.

Chapter 4

Carbonate weathering rate dependence on soil acidity and grain surface area

4.1 Introduction

This chapter was originally planned to investigate the impacts of environmental pH on carbonate weathering rates in the field; integrating experimental weathering results with those expected based on theoretical calculations using constants derived in laboratory-based studies of calcite and dolomite dissolution. However, there was a large difference between calculated and experimental carbonate weathering rates in the field. As a consequence of this, this chapter adopts a two-step approach, firstly investigating environmental pH control on weathering, followed by an examination of carbonate grain surface area and its evolution throughout weathering. Some of the material covered in this chapter was previously included in Thorley *et al.* (2015).

Understanding this “laboratory-field discrepancy” (Brantley and Mellott 2000; Brantley 2003) is key to successfully integrating field- and laboratory-derived rates with models describing weathering dynamics at larger spatial scales, however, as yet there is no consistent method to accurately compare these different rates (Navarre-Stitchler and Brantley 2007). The laboratory-field discrepancy has been characterised most thoroughly for silicate minerals where laboratory dissolution rates can be 2-5 orders of magnitude faster than in the field (White and Brantley 2003), but until now has not been investigated for carbonates. Consistent overestimation of field weathering rates when using laboratory data is thought to be due to an incomplete understanding of mineral surface area (Brantley and Mellott 2000), which is investigated in this chapter for a selection of carbonate rock types. A more robust understanding of field weathering controls in relation to surface area will facilitate the use of mineral surface-area-normalised data, representative of the field situation, in global-scale modelling studies which currently use geographic-surface-area-normalised weathering rates calculated from laboratory-derived kinetic constants.

Chapter 4

Within the introduction, each hypothesis for this chapter is posed in the context of relevant literature. Following this, the main aims are detailed, along with a description of the techniques used to test these hypotheses. Theoretical information relevant to each method and their major limitations are included at this point. The results section is structured to first discuss the environmental pH effects on weathering rate, continuing to the more thorough investigation of surface area evolution in order to probe weathering feedbacks. Some of the material covered in this chapter was previously included in Thorley *et al.* (2015).

4.1.1 Soil pH is a major control on carbonate weathering rate

The following section focuses on the dissolution of calcite and dolomite in acidic conditions (Eqn 6, Section 1.4.1.2), such as those found in most European forest soils, and almost all soils in the UK (Figure 1.3). In soils, different chemical agents contribute to determining the rate of carbonate dissolution reactions. Key acidic weathering strategies of mycorrhizal fungi that may influence carbonate weathering, are the production of low molecular weight organic acids (LMWOAs) and formation of carbonic acid, catalysed by carbonic anhydrase (CA). Biologically-produced acidic agents, such as oxalic acid, are known to be important drivers of silicate mineral dissolution (Reviewed in Berner 1992; Brady and Carroll 1994) and are discussed more fully in Chapter 1 (Section 1.5.3).

One way to investigate the pH dependence of weathering rates in the field is by comparison to theoretical relationships calculated from rate equations and constants derived from laboratory studies. Theoretical carbonate weathering rates can be calculated using Equation 6; the temperature dependant rate constants k_1 , k_2 and k_3 of the three possible dissolution reactions detailed in Chapter 1 (Eqns 6-8) and s , an constant signifying reaction order. For example, the dissolution of calcite, $CaCO_3$, in acidic environments is first order and uses $s = 1$. Compared to calcite, dolomite, $CaMg(CO_3)_2$, dissolution has both a different stoichiometry, as 2 moles of acid are required to fully dissolve 1 mole of dolomite, and follows a different reaction order with fractional s , often quoted as $s = 0.5$ (Palandri and Kharaka 2004) or $s = 0.75$ (Chou *et al.* 1989).

$$Rate = k_1[H^+]^s + k_2[H_2CO_3]^s + k_3 \quad (14)$$

Carbonate weathering rate dependence on soil acidity and grain surface area

Carbonate dissolution kinetics makes them most vulnerable in acidic conditions, and is almost linearly dependant on pH between pH 3.5-5.5 in laboratory-dissolution experiments (Reviewed in Arvidson *et al.* 2003; Cubillas *et al.* 2005). Although most laboratory experiments are performed at relatively high temperatures and with much greater fluid-mineral ratios than in the natural environment, it is still reasonable to expect that carbonate weathering in the field will be most rapid where pH is lowest. This leads to the first hypothesis of this chapter:


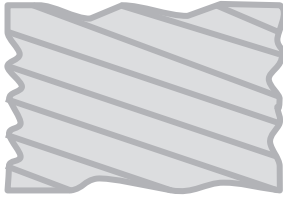
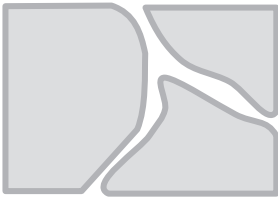

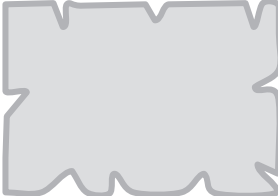
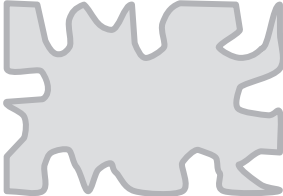
Research hypothesis 1

Soil acidity is the main driver of carbonate dissolution in the field, and its effect parallels that of calculated theoretical weathering rates and those determined in laboratory studies.

4.1.2 Physical properties of minerals affect weathering rates

The properties of rocks that are important during weathering can be split into two main categories: their mineralogy and their structure. Mineralogy affects weathering rates as it determines the solubility of the rock. Rocks with mineralogies that make them susceptible to acid dissolution would be expected to weather fastest, if all other factors relating to rock structure were constant. Structural properties of rocks that influence weathering rate are those which effectively control the surface area of mineral that can be in contact with water and other weathering agents. These include grain size, surface texture and whether the rock is massive or has some internal organisation such as bedding planes in a sedimentary rock. These properties are summarised in Table 4.1, overleaf.

Table 4.1. Structural properties of rocks that influence weathering rates

Rock structural property	Slower weathering	Faster weathering
Rocks which contain grain boundaries, bedding planes or fractures will weather faster than those with massive structure as these boundaries provide a line of weakness that can be exploited. The spacing of these features will affect weathering rate.		
Smaller grain sizes will have greater surface area to volume ratios and therefore faster weathering rates. For this reason, weathering rates are normalised to some measure of surface area.		
Rocks with greater pore sizes or more pores will have a larger surface area for a given mass of rock. Pores can also retain water by capillary action, prolonging water-mineral contact time and promoting dissolution		

4.1.2.1 Rock structure affects carbonate weathering mechanisms

Evidence for the impact of rock structure on carbonate weathering rates comes from the work of Kirstein *et al.* (2016). This study compared the dissolution of two calcite-based rocks, micrite and spartic limestone at low-temperatures and pH 4.7 in batch and flow-through reactors. Despite their almost identical mineralogy, dissolution of spartic limestone required lower activation energy, E_a . These differences in E_a required suggest some alteration of dissolution mechanism and show the importance of knowing accurate rate constants for the particular lithology under investigation.

This variation may be due to the in structure of the rock samples, and differential dissolution of different sized calcite crystals present in this rock type. Spartic limestone is composed of varying sizes of calcite crystals, and in the experimental conditions presented, the finer crystals dissolved first. This could lead to the formation of channels, increased water penetration into the interior of the rock grain and may, in turn, facilitate further dissolution.

Vertical scanning interferometry (VSI, see Section 5.2.5 for background information on this technique) has been used to map surface evolution of crystal faces of dolomite and calcite during dissolution (Dolomite, Lüttge *et al.* 2003; Calcite, Arvidson *et al.* 2003). Quantification of calcite and dolomite dissolution rates using these VSI measurements yielded far slower rates than those from studies on the dissolution of powders (Lüttge *et al.* 2003; Arvidson *et al.* 2003). This variation in rates is seen frequently across studies measuring carbonate dissolution, and is well over an

Carbonate weathering rate dependence on soil acidity and grain surface area

order of magnitude across published studies of dissolution at $\text{pH} \geq 6$, compiled by Arvidson *et al.* (2003). Rates derived from crystal surface observations such as these VSI studies are 5-100 times slower than those measured from bulk powder dissolution experiments. This is likely to result from the increased density of grain boundaries, steps and defects exposed by crushing, however, is not fully understood. Alongside increased overall surface area, this increased availability of highly reactive surface features would lead to faster dissolution rates as grain size decreases.

4.1.2.2 Biological activity targeted to smaller grain sizes

Acquisition of growth-limiting inorganic nutrients is possibly one of the primary benefits for enhanced weathering by plants and micro-organisms, as has been previously reviewed in Section 1.4.3. Microcosm studies with *P. sylvestris* in association with *P. involutus* showed that ectomycorrhizal fungi are able to discriminate between inorganic nutrient sources supplied as crushed minerals with different grain sizes (53-90 μm and 500-1000 μm). Radiotracing experiments showed more carbon was allocated to EM respiration where fungi were foraging from minerals richest in P, and also favoured those growing on the finest rock grains (Leake *et al.* 2008). Small rock grains have the greatest surface-area to volume ratio, so fungi can maximise their interaction with mineral surfaces and foraging potential for inorganic nutrients.

In soils, chemical weathering requires contact between mineral surfaces and weathering agents in soil solution. From the diagrams in

Chapter 4

Table 4.1, it can be seen that in general, rock structural properties that facilitate water-mineral contact and are expected to increase weathering rates also increase surface area. Surface area may therefore be used as a proxy measurement to describe changes in weatherability related to rock structure, and rock samples with the greatest surface area would be expected to weather most rapidly. Additionally, mycorrhizal fungi are an important functional group in forest soils and are able to target inorganic nutrient sources in a grain-size dependant manner. From this, it could be expected that higher weathering rates will be observed where surface area is greatest. This leads to our second hypothesis:

Research hypothesis 2

Carbonate weathering rates are proportional to sample surface area.

4.1.3 Surface area evolution through weathering

Overall weathering is a net outcome of two main processes, chemical and physical weathering. Physical weathering can promote chemical weathering by increasing surface area and access to water. Likewise, chemical weathering can enhance physical weathering through destabilising the rock matrix through removal of cations, and making the rock more vulnerable to disintegration. Overall changes in particle size distribution and rock surface characteristics observed throughout field weathering studies are likely to result from a combination of both physical and chemical weathering and feedback on future weathering dynamics. Throughout silicate weathering, physical and chemical changes feedback on one another as mineral surfaces roughen and porosity increases (White and Brantley 1995). Part of this chapter aims to investigate whether the same mechanisms dominate grain-scale carbonate weathering in the field.

Time-lapse VSI imaging was used by Lüttge *et al.* (2003) to follow the surface dissolution of dolomite crystals at pH 3. Weathering progressed via two main mechanisms, firstly, through the formation of shallow etch pits, and secondly by the entire surface receding. Etch pits were much wider than they were deep, and grew in both dimensions over time at a consistent rate, regardless of which crystal face was examined. The gradual dissolution of the entire surface was confirmed by comparison of heights of a dolomite surface exposed to the acidic solution, with a reference surface prevented from reacting by a covering of rubber. The progress of this overall surface recession has been modelled as a dissolution stepwave, probably originating from defects such as the etch pits. Calcite surface dissolution at pH 8.8 also progressed via the formation of etch pits, these had a common orientation, and coalesced as they grew. The formation of etch pits and steps during dissolution of crystal faces is likely to increase surface area, however, this has not yet been investigated in detail.

Surface area evolution throughout weathering is likely to be a balance between mass loss through dissolution and overall particle size reduction, and changes in surface roughness. Surface changes could result in increased surface area through the formation of new surface features such as etch pits and dissolution steps. On the other hand, there could be a decrease in surface area during weathering as the most soluble components selectively dissolve. This may be this due to more soluble mineralogy caused by the presence of impurities, or vulnerability in rock structure, as seen by preferential dissolution of finest crystals in spartic limestone studied by Kirstein *et al.* (2016).

Chapter 4

The net effect of these processes will determine whether surface area increases or decreases overall during weathering. Silicate mineral surfaces roughen during dissolution (White and Brantley 1995), however, most studies of mineral surfaces are performed on initially flat surfaces and do not use crushed rock grains, which will have a very different initial surface topography. The carbonate rock grains used in the current study contain a range of size fractions, with diameters initially between 500-1000 μm , and are likely to have a high density of defects from crushing during sample preparation. In this complex situation, it is assumed that overall surface roughness will stay the same. So, working only from the expectation that as carbonate mineral surfaces retreat during weathering, particles should decrease in size, this leads to the formation of the third hypothesis of this chapter.

Research hypothesis 3

Surface area decreases throughout weathering as carbonate rock grains dissolve and shrink.

4.1.4 Overall aims of chapter 4

The aims of this chapter are to first characterise the soil pH environment of forest plots at Bedgebury pinetum. This was done over the course of several field sampling excursions and laboratory soil analyses. To investigate the effect of soil acidity on carbonate dissolution, this soil pH dataset will be combined with weathering rate results from mass-balance calculations in the previous chapter. This section specifically investigates whether there is evidence of any mineral or tree functional group specific influences.

Following this, field weathering responses to pH are integrated with theoretically derived carbonate dissolution rates. Calculating weathering rates from mass balance measurements requires normalising to surface area. In this chapter particle surface area was first approximated using an estimation of particle geometry and bulk rock grain characteristics. These values were later refined after characterising rock grain surface areas in more detail using BET gas adsorption surface area measurements and particle size distributions by laser diffraction techniques.

As mentioned previously, field weathering rates were far lower than those expected based on laboratory-derived rate constants and theoretical calculations. In laboratory studies there will be less complex fluid chemistry than in the soil environment. For instance, in the field there is variable hydrology and less well defined fluid-mineral contact time compared to in a batch or flow reactor. There may also be effects of deposition on mineral surfaces, for instance, soluble iron or humic substances

Carbonate weathering rate dependence on soil acidity and grain surface area

are probably deposited on carbonate substrates in the field, which will have relatively high local pH environments. This deposition will impact on the effective surface area available for carbonate dissolution reactions.

Reactive surface area is known to be a major control on mineral dissolution rates and uncertainties in its measurement have been proposed as one cause of the discrepancy between weathering rates measured in field and laboratory studies and those calculated theoretically. The second half of this chapter investigates the evolution of surface area throughout rock grain incubation in the field in an attempt to understand precise weathering mechanisms of carbonates, and reduce the discrepancy between theoretical weathering rates and those measured in the field.

Chapter 4

4.2 Methods

4.2.1 Soil sampling and pH measurement

Soils at Bedgebury pinetum were sampled within each tree stand in July (N = 3 per tree species) and December 2013 (N = 5 per tree species). At each point where mesh ingrowth bags were buried, soil samples were collected from the surface organic-rich soil horizon near the base of each tree at approximately 5 cm depth. These samples were stored in a cool box until it was possible to process and analyse them back in the laboratory. Air-dried and ball-milled soil was mixed with water in a 1:1 ratio v/v and pH measured using a pH meter (Jenway 3540 pH meter; calibrated at pH 4, pH 7 and pH 10).

4.2.2 Calculation of theoretical weathering rates for calcite and dolomite

Theoretical weathering rates were calculated according to Eqn 14 at both 25°C and at field air-temperature, 13.4°C (hourly weather station data, May – August 2013; Bedgebury Pinetum). There are few laboratory studies of carbonate dissolution at low temperatures, such as those found in the field in the UK, and kinetic constants are only available at 298K, 25°C. Reaction rate is highly temperature dependant (Section 1.4.1.4, Eqn 9), and constants from literature must be scaled to make them appropriate for this study at lower temperatures, where reaction rates will be slower.

Weathering rate constants for 13.4°C were estimated using the Arrhenius equation (Eqn 9) in combination with temperature-dependant rate constants, k_1 , k_2 and k_3 (Chou *et al.* 1989; Palandri and Kharaka 2004) and the activation energy, E_a . Initially theoretical curves were scaled to field temperature using $E_{a,s}$ of for sedimentary dolomite = 36.1 kJ mol⁻¹ and for calcite = 14.4 kJ mol⁻¹, compiled by Palandri and Kharaka (2004). These curves have been recalculated more recently using $E_{a,s}$ for micrite = 51.0 kJ mol⁻¹, spartic limestone = ~21 kJ mol⁻¹ and dolomite = 22.3 kJ mol⁻¹ published in a new study of natural carbonate rock dissolution at low temperatures (Kirstein *et al.* 2016).

Scaling was performed using Eqn 15, as in Brady and Carroll (1994), Kirstein *et al.* 2016 and reviewed in White (2003). In this equation, k^T the rate constant at temperature T is calculated relative to that at a reference temperature, k^0 at temperature T^0 ; again E_a is the activation energy and R the molar gas constant.

$$\frac{k^T}{k^0} = e^{\frac{E_a}{R} \left(\frac{1}{T^0} - \frac{1}{T} \right)} \quad (15)$$

Carbonate weathering rate dependence on soil acidity and grain surface area

As all soils sampled in both July and December 2013 at Bedgebury Pinetum fell in the pH range 3-6 it was assumed that the acid dissolution reaction (Eqn 6) dominates carbonate weathering and $k_1[\text{H}^+]$ is the dominant term in the rate equation. Theoretical weathering curves were subsequently calculated without accounting for the effect of soil pCO_2 , included in the neutral term $k_2[\text{HCO}_3^-]$ (Eqn 9). This assumption was made as overall field soil pH includes acidity contributions from all sources of soil CO_2 , carbonic acid and organic acids and inclusion of another $k_2[\text{HCO}_3^-]$ rate term would be likely to result in an overestimation of theoretical weathering rates.

Field weathering rates from Thorley *et al.* (2015) estimated using the assumption that all rock grains were spherical (average diameter of 0.84 mm) are revised in (Figure 4.7) by normalisation using BET surface area (Brunauer-Emmett-Teller; Figure 4.8), similar to many laboratory dissolution studies (Brantley and Mellott 2000; White and Brantley 2003; Navarre-Stitchler and Brantley 2007).

4.2.3 Brunauer-Emmett-Teller surface area determination

4.2.3.1 BET theory

BET is the most widely used technique for determining the surface area of solids. This method uses the properties of adsorption by the test solid. Adsorption is the adhesion of any molecule, atom, or ion from a solid, liquid or gas to a solid surface. In the case of BET analysis, the quantity of inert gas, typically nitrogen, adsorbed to the surface of a test solid is calculated via the construction of an adsorption isotherm. For this isotherm, nitrogen is gradually injected in controlled increments to the previously evacuated test vial containing the solid sample. This is then allowed to equilibrate before each measurement of pressure or relative pressure (P/P_0). Relative pressure is calculated from P , the equilibrium pressure and P_0 the adsorbate saturation pressure at the temperature of adsorption, here 77K for N_2 .

There are 6 main types of adsorption isotherm defined by the International Union of Pure and Applied Chemistry, IUPAC (Brunauer *et al.* 1938), however, only the 2 relevant for BET theory are discussed in this section. Adsorption isotherms of types II and IV can be divided into three sections, shown in Figure 4.1. Gas is gradually injected into the test vial containing the sample. The first section of the isotherm corresponds to the initial completion of the monolayer of gas particles around pores and particle surfaces. Here, gas particles are held in proximity to the rock grain surface by the temporary dipole-induced dipole interactions of Van der Waals force. This type of physical particle interaction has a very low binding energy. For a given quantity of gas introduced, the pressure will decrease as the sample and gas equilibrate in the test vial

Chapter 4

as gas molecules sorb to the rock particle surfaces. Performing BET measurements requires measuring the amount of N_2 gas required to bring P/P_0 to a specific value. Surface area is then calculated by determining the total area covered by the monolayer (n_m , Eqn 16) of adsorbed gas molecules. This calculation uses the cross sectional area of nitrogen, which is 0.1620 nm^2 at 77K for the conditions used in this analysis.

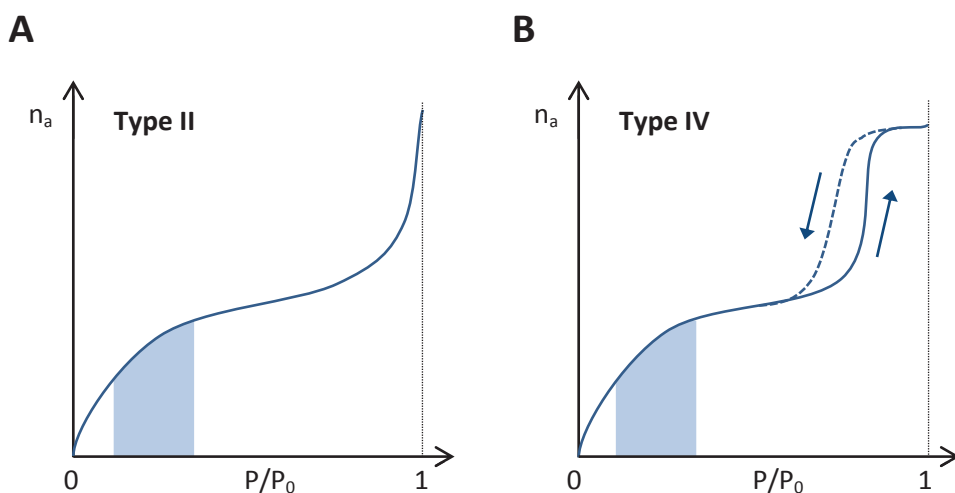


Figure 4.1. BET method is appropriate to use for solids which obey **A)** Type II or **B)** Type IV adsorption isotherms. Typical ranges of relative pressures used during BET analysis are shaded. Type I solids are generally nonporous or have macropores. Type IV solids are mesoporous with pore diameters ranging from 2-50 nm and may exhibit hysteresis, illustrated by the dashed blue line. The chalk used in this investigation is likely to have a type IV isotherm based on measurements of its pore diameter, see below. P/P_0 is relative pressure and n_a is adsorbed gas quantity

When N_2 gas is introduced into the previously evacuated test vial containing the rock sample, random collisions occur between the gas molecules and the rock surface. As the pressure increases, the frequency of these random collisions increases, as does the number of these gas particles adsorbed to the rock surfaces by coulombic interactions (Figure 4.2). Eventually the first monolayer of gas molecules surrounding the rock grains is completed. When pressure is increased beyond this point, the second phase identified in the isotherm is reached. This section of the isotherm has a constant gradient produced by the formation of multiple layers of particles on the surface, and may include second, third and fourth layers. It is this formation of multiple layers that is used in the derivation of the BET equation (Eqn 16) from Langmuir theory, as equilibrium constants for 1, 2, 3, ..., n successive monolayers are calculated.

Above this point the gradient of the isotherm again increases as capillary action causes more particles to condense into pores in the test solid due to the narrowing of pores. This causes the quantity of gas adsorbed to increase disproportionately to the increase in relative pressure, P/P_0 , until saturation is reached at $P/P_0 = 1$.

Carbonate weathering rate dependence on soil acidity and grain surface area

Type IV solids reach saturation pressure at pressures below P_0 due to capillary action filling pores. Adsorption hysteresis also occurs in this type of mesoporous solids as the decrease in pressure required to desorb gas molecules held in narrow pores by capillary action is greater than the increase in pressure that was required to adsorb them (Figure 4.1B).

$$\frac{p}{n_a(p_0-p)} = \frac{1}{n_m C} + \frac{p}{p_0} \cdot \frac{(C-1)}{n_m C} \quad (16)$$

The inputs to the BET equation above are n_a the volume of adsorbed gas; p , equilibrium and p_0 , saturation pressure of N_2 adsorbant at the adsorption pressure, 77K. The terms n_m , the monolayer capacity, and the BET constant, C , are calculated using the gradient and intercept of the adsorption isotherm.

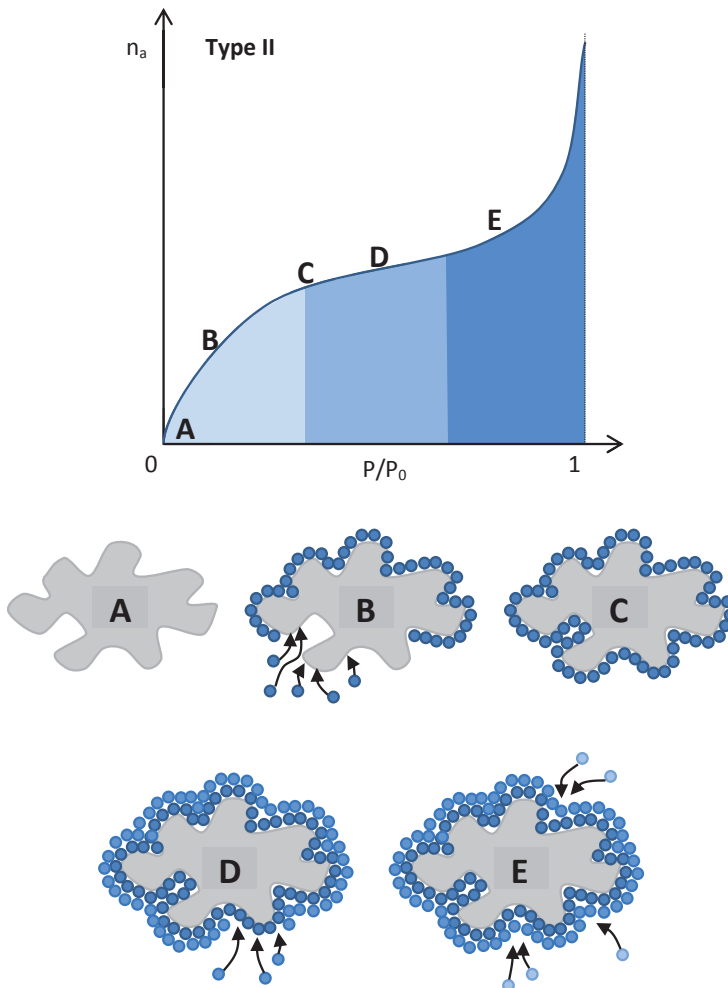


Figure 4.2. Adsorption isotherm for BET surface area analysis, starting with sample in an evacuated test vial (A). BET analysis is performed during the first section of the curve (B), as a monolayer of N_2 gas molecules adsorb to the rock grain surfaces. When monolayer formation is complete (C), further layers of gas molecules adsorb to the particle surfaces, surrounding the existing monolayer (D). This results in a constant gradient in the adsorption isotherm. The gradient increases again in the final stage in the adsorption isotherm (E) as gas molecules fill pores via capillary attraction and the rock grains reach saturation, where $P/P_0 = 1$.

Chapter 4

4.2.3.2 *Sample selection for BET*

Freeze-dried samples were used for BET analysis. In each case, an entire sample used to avoid biasing results by size-selective subsampling techniques such as pouring rock grains. Samples were selected to represent the entire range of weathering mass changes observed after both 7 and 14 months. Data were ordered by ascending value for dry mass according to the cumulative frequency distribution in Figure A. 2. Six equally spaced samples were selected from each of the 7 and 14 month datasets. The highly weathered range of the 14-month samples was underrepresented in the original sampling because the most highly weathered samples were part of the tail of the distribution, where few samples span quite a large mass range (Figure A. 3) and there is a lack of overlap in weathered mass between 7 and 14 month samples at this end of the scale (Figure A. 3).

4.2.3.3 *BET analysis methodology*

Rock grains were transferred to clean, pre-weighed BET sample tubes (Ohaus Pioneer Analytical Balance; 120 g x 0.0001 g; Ohaus Europe GmbH, Switzerland), reweighed then degassed with N₂ overnight (>16h) at 100°C using a micromeritics FlowPrep 060 sample degas system (Figure 4.3; Micromeritics U.K. Ltd., Hexton, UK). Degassing ensures an accurate surface area measurement by reducing the possibility of any phase changes by heating. The flow of inert gas whilst heating removes any gas molecules that are weakly adsorbed to the surface of the rock grains and ensures rock grains are totally dry.

Glassware was prepared by washing with methanol and a fine brush, followed by 3 minutes sonication (U300 Ultra BT Ultrasonic Bath; Ultrawave Precision Ultrasonic Cleaning Equipment, Cardiff, UK) and two further methanol rinses.

Prior to analysis, degassed samples were re-weighed and individually analysed using a micromeritics surface area and porosity analyser (micromeritics Gemini VII Surface Area Analyser; Micromeritics U.K. Ltd., Hexton, UK). Nitrogen at its boiling point, 77.3K, was used as the BET adsorbent. All analyses were performed at the School of Earth and Environment, Leeds University.

4.2.3.4 *Standard reference material*

A standard reference material with a known surface area was analysed before running samples, in order to check the sensitivity of the equipment (Table 1; α -Alumina for nitrogen BET specific surface area; BCR® – 169 and BCR® – 170 Certified Reference Materials). This is especially important when analysing substances with very small surface areas, less than 10 m²g⁻¹, such as the rock samples used in this study. The

Carbonate weathering rate dependence on soil acidity and grain surface area

BET surface area obtained from the standard reference material fell within the expected range and gives an indication of the measurement precision.

Table 4.2. Measured and expected BET surface areas and uncertainties of two certified reference materials α -Alumina BCR® – 169 and BCR® – 170. Expected measurements are the certified values from the European Commission Institute for Reference Materials and Measurements certificates of analysis. Observed values were obtained from 5 repeat measurements of a single sample, using the same BET equipment at the School of Earth and Environment, Leeds University. Experimental values in this table are the work of Andy Connelly.

Certified Reference Material	Surface area \pm measurement error (m^2g^{-1})		
	Expected	Expected range	Measured
BCR® – 169	0.104 ± 0.012	0.092 - 0.116	0.098 ± 0.011
BCR® – 170	1.05 ± 0.05	1.00 - 1.10	1.02 ± 0.05

4.2.3.5 Replicate measurements of a single weathered sample

To understand the uncertainty in each measurement of a single sample, one weathered sample was measured 3 times. This chalk sample had been buried in *Araucaria araucana* woodland for 231 days. The mean surface area of this sample, with standard error, is $0.902 \pm 0.013 \text{ m}^2\text{g}^{-1}$. Due to time and cost restrictions, this measurement of error has been used for all weathered chalk samples.

4.2.3.6 Limitations of BET analysis

Surface area measured by BET depends on the adsorbent gas used. Observed surface area for several laboratory-ground silicate samples were up to 50% greater when using N_2 than with Kr as the adsorbent (Brantley and Mellott 2000). Kr may be used as an adsorbent when measuring very low surface areas, however, in the present study, N_2 has been used throughout as the surface areas measured were within the operating range using N_2 , despite being at the lower end of that range.

Also, higher SAs can be observed where there is greater hysteresis in the adsorption-desorption isotherm, as occurs when there mesopores present (2-50 nm diameter). It is likely that pores of this size are also present in the rock grains measured in this study, as they have been shown to be of importance in many weathered silicate minerals (Reviewed in Brantley and Mellott 2000). These pores contributed significantly to total specific surface area. And while we cannot totally disregard that this may impact on results, this effect is likely to be similar between rock samples of a single rock type, and SAs have not been compared between rock types.

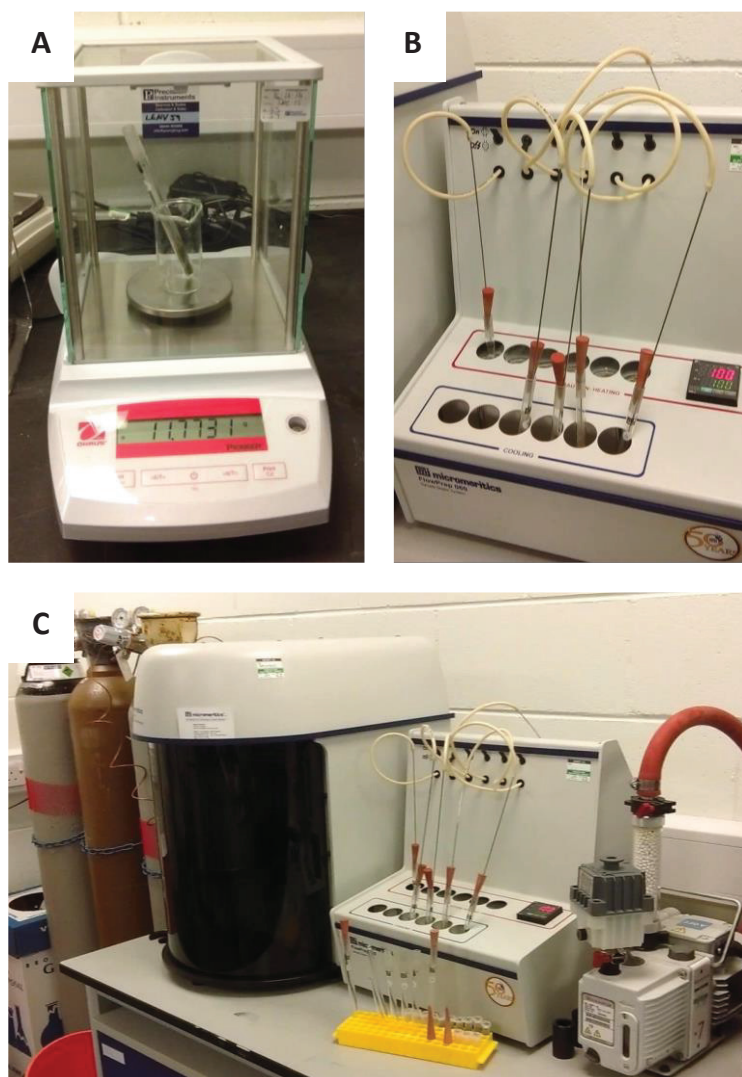


Figure 4.3. BET analysis equipment setup. **A)** Weighing samples into BET test vials with Ohaus Pioneer analytical balance. **B)** Degassing samples with N_2 overnight at $100^\circ C$ using micrometrics FlowPrep 060 sample degas system. **C)** Entire BET setup with micrometrics Gemini VII surface area analyser; sample degas unit and compression pump.

4.2.4 Laser Diffraction Particle Size Analysis (PSA)

4.2.4.1 PSA Theory

Laser diffraction uses the properties of scattered light to analyse particle size. As particles suspended in a dispersant pass through a narrow chamber, called the optical bench, particle edges interfere with the light path, causing it to diffract and scatter (Figure 4.4A). Large particles scatter light at small angles, but generally at high intensity. On the other hand, light scattered from smaller particles ($<20 \mu m$), is measured at much greater angles, but lower intensities. Light of two wavelengths is used in a particle size analyser. Red light (632.8 nm) is used for larger particles and blue light (470 nm) with a smaller wavelength for smaller particles. Red and blue light to measure the entire particle size range of 10 nm up to 3.5 mm .

Carbonate weathering rate dependence on soil acidity and grain surface area

The intensities of scattered light are measured by an array of detectors spanning different angles relative to the angle of incident light. Particles are modelled as spheres and the Mie theory of light scattering is then used to calculate the particle size distribution (PSD) of rock grains passing through the optical bench. For this analysis, water was used as a dispersant, and particles were assumed to possess the optical properties of calcite as this is the main constituent of the material present is calcite (96.39% calcite; XRF data of unweathered chalk; appendix). PSD is then used to estimate overall sample surface area, using the assumption of spherical particle geometry.

4.2.4.2 PSA analysis methodology

Particle size distribution of chalk samples was measured by wet dispersion before and after weathering. This analysis was performed after measurement of BET surface area, giving paired samples which had undergone both analyses. Analyses were performed with a Laser Diffraction Particle Size Analyser (Figure 4.4B; Malvern Mastersizer 3000; Malvern Instruments Ltd, Malvern, UK) in the Department of Materials Science and Engineering Characterisation laboratory, with much help and advice from Ben Palmer

Samples were dispersed for 10 s in distilled water before commencing measurements (Hydro EV; Malvern Instruments Ltd, Malvern, UK). Five repeat measurements each of 10s duration were made for each sample and the average calculated. Measurements were interspersed by 5 s pauses. Sample dispersion by stirring is in order to achieve an appropriate flow rate of particles to optimally obscure the laser beam. As these chalk samples are quite delicate, they tended to break up with extensive stirring, as very fast stirring was required in order to suspend such large particles. To avoid this substantially influencing results, particle size measurements were performed as soon as possible after dispersion had commenced.

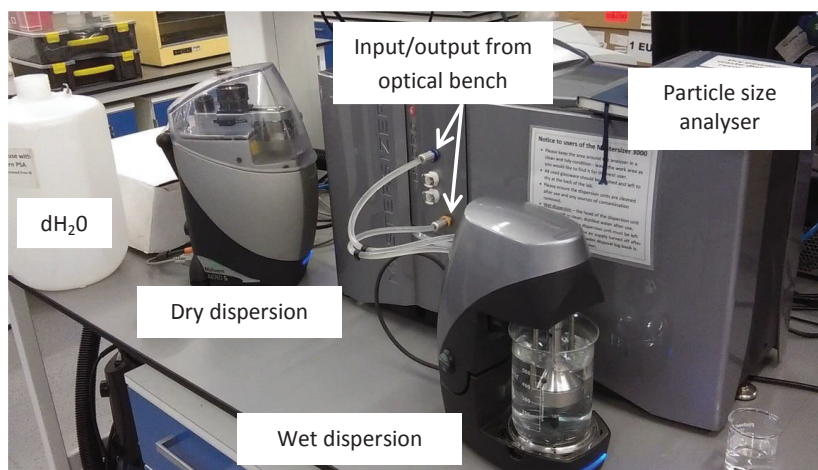
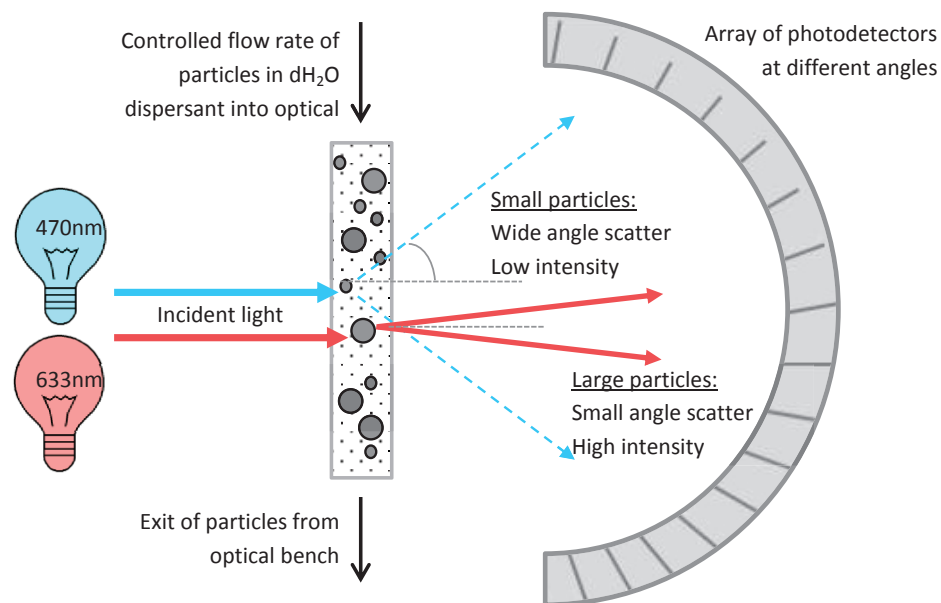


Figure 4.4. A) Schematic of particle size measurement by differential scattering of blue and red laser light from large and small sample particles. Smaller particles produce greater angles of light deflection by edge diffraction than larger particles do, so these light scattering patterns are measured by different photodetectors in the array. **B)** Mastersizer 3000 unit used in this study with wet dispersion unit attached. Sample is added directly to beaker containing 500 ml of dH₂O dispersant when propeller of wet dispersion unit is in place agitating the contents of this beaker.

4.2.4.3 Limitations of PSA analysis

The relatively large size of particles used in this study (>250 μm) and small total sample mass decreased the accuracy of this technique when compared to very fine samples. This is partly due to the difficulty in achieving optimal laser obscuration with the relatively few particles in each. To improve obscuration, the stirring speed within the dispersion unit needed to be increased to suspend large chalk particles, making this a tricky balance between remaining within laser obscuration limits and avoiding excessive damage to rock grains.

Carbonate weathering rate dependence on soil acidity and grain surface area

The major challenge faced during PSA analysis was the disintegration of carbonate grains as they collide with the walls of the beaker during wet dispersion. Dry dispersion (Aero S; Malvern Instruments Ltd, Malvern, UK) was trialled as an alternative to suspending particles in dH₂O. In this variation, particles are drawn through the optical bench with aid of a vacuum, thus avoiding the breakup of particles observed during violent stirring with a propeller in water. However, the size of field weathered samples was insufficient to make 5 replicate measurements as the sample is not re-circulated as it is during wet dispersion. For this reason, wet dispersion was selected as the most appropriate technique, and measurements were performed as soon after sample addition as possible.

A more minor inaccuracy in particle size distribution may have been introduced by the approximation of sample mineralogy and using refractive index data for pure calcite and dolomite respectively. Whilst the chalk and dolomite used are almost pure, there are, of course slight variations in chemical composition as can be seen in the XRF analysis (Table A. 3), which are likely to be more divergent after weathering. The refractive index acts as a scaling factor and amendment may slightly alter particle size distributions or calculated surface area. This limitation prevented the use of PSA for silicate rock grains in this study as their precise mineralogy is not known. For these silicate grains, the best approximation would be to model as quartz, which is the dominant component, however, thin section images show clearly traces of other minerals (Section 5.3.1).

4.2.4.4 Comparison of wet and dry dispersion techniques and limitations of PSA

When analysing unweathered chalk, the particle distributions obtained using both dispersion techniques were very similar. The main peaks of particle volume were coincident with a modal particle size of 1110 µm, however, with the dry dispersion method, there was a loss of resolution in the data for the finest particles. In addition to this, weathered samples were too small to be measured using the dry dispersion technique and a larger volume of sample would be required. For these reasons, dispersion in dH₂O is used for comparison of weathered and unweathered samples.

There is some overestimation of the maximum particle sizes present in this study, potentially due to clumping of larger rock grains as they pass through the analytical chamber, especially as the maximum size of particles measured is approaching the 2 mm operating limit of the equipment used. This is because it is difficult to resolve the small scattering angles produced by large particles.

Chapter 4

4.2.5 Software and statistics

Theoretical carbonate dissolution curves investigating pH dependency were calculated in Microsoft Excel 2010 (Version 14.0.7173.5000; Microsoft Corporation) and scaled for field temperature using the Arrhenius relationship as described in Section 4.2.2. Particle size distribution data were modelled using nonlinear log-Gaussian regressions using GraphPad Prism (Prism 6 for windows; version 6.05; GraphPad Software Inc.; La Jolla, CA, USA). All graphs were drawn in GraphPad Prism and statistical analyses performed using R (R version 3.1.2, 2014), RStudio (Version 0.98.1091, 2014).

4.3 Results

4.3.1 Soil acidity as a driver of carbonate weathering

4.3.1.1 Soil acidification and enhanced carbonate dissolution under EM trees

All tree stands surveyed for this study at Bedgebury pinetum had acidic soils (Figure 2.11, Figure 2.12). In July and December 2013 soil pH was within the range 3-6 for all tree species surveyed. Soil pH was significantly affected by the type of mycorrhizal association (AM/EM: three-way ANOVA; $F_{1,5} = 8.76$; $N = 13$; $P = 0.032$), with tree species partnered with EM fungi generally exhibiting lower soil pH ($\text{pH } 3.50 \pm 0.04$, $N = 6$; mean \pm SEM) than those forming AM fungal associations ($\text{pH } 4.30 \pm 0.22$, $N = 7$; mean \pm SEM). Neither leaf habit (evergreen/deciduous: three-way ANOVA; $F_{1,5} = 1.92$; $N = 13$; $P = 0.22$) nor tree type (angiosperm/gymnosperm: three-way ANOVA; $F_{1,5} = 0.008$; $N = 13$; $P = 0.79$) had any measurable effect on soil pH at the time these measurements were performed.

At Bedgebury Pinetum from May – August 2013, the greatest weathering rates of calcite rock types were observed below EM tree stands (Section 2.8.3; Figure 3.10). Unsurprisingly, given the susceptibility of carbonate minerals to acid dissolution, calcite rocks weathered fastest at lowest pH (Figure 4.5A; $F_{1,11} = 6.16$; $P = 0.030$; $R^2 = 0.36$). The same significant relationship was seen in linear regressions for both chalk ($F_{1,11} = 6.24$; $P = 0.032$; $R^2 = 0.384$) and marble ($F_{1,11} = 9.801$; $P = 0.0096$; $R^2 = 0.471$) individually, but the relationship with pH was not significant for oolitic limestone ($F_{1,11} = 3.883$; $P = 0.0745$; $R^2 = 0.261$). After the initial stages of weathering in the first 3 months there still a significant, but less marked impact of average soil pH on weathering rate after 7 months (Figure 4.5B; $F_{1,11} = 5.80$; $P = 0.035$; $R^2 = 0.35$). The pH

Carbonate weathering rate dependence on soil acidity and grain surface area

effect on calcite dissolution rates seen when considering all tree species is not evident when analysing results for each mycorrhizal type (Figure 4.5).

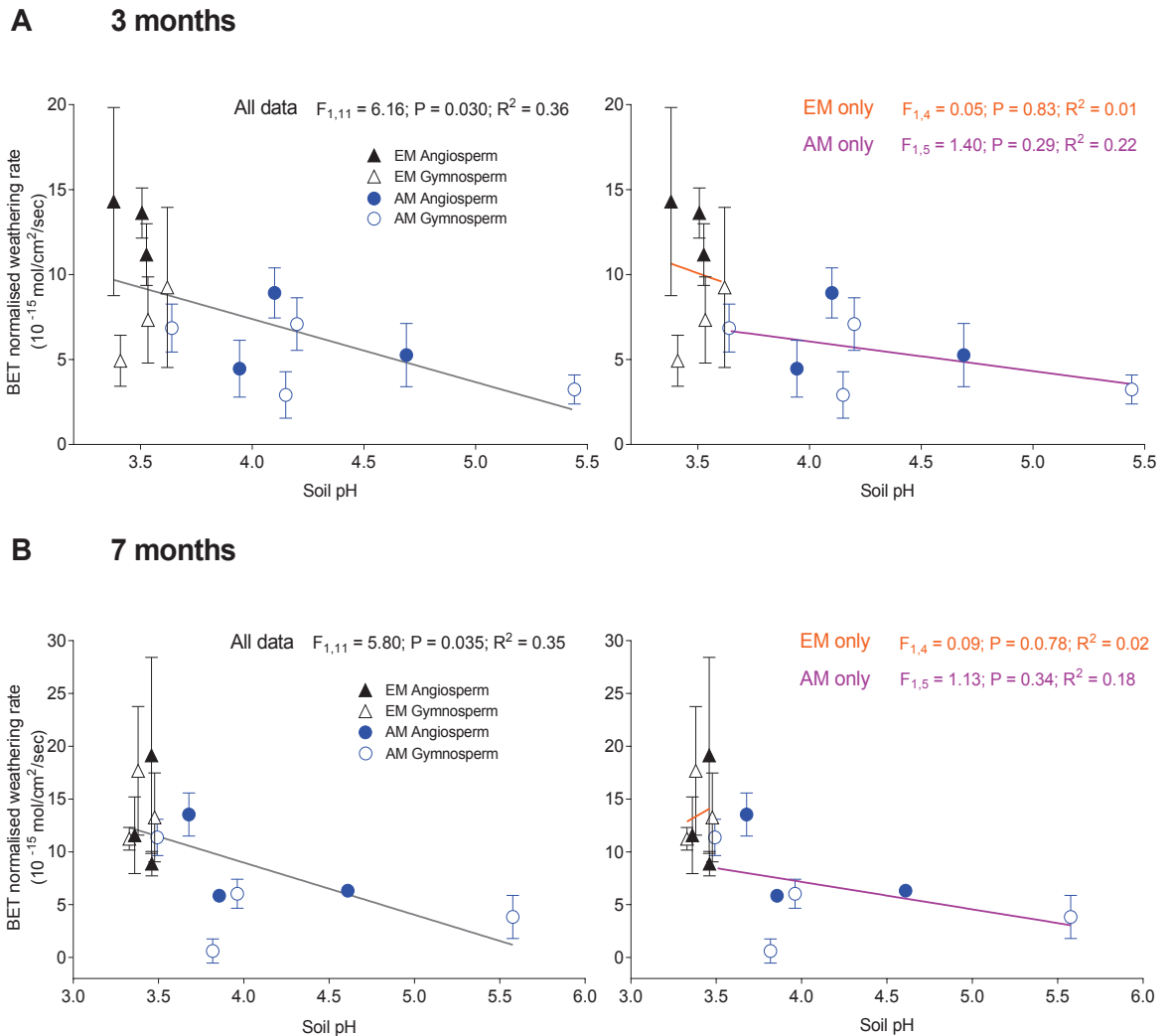


Figure 4.5. Effect of soil pH on field calcite weathering rates (mean \pm SEM, N = 3) at Bedgebury Pinetum, Kent, UK after **A**) 3 months (soil pH: July 2013) and **B**) 7 months (soil pH: mean of July 2013 and December 2013). Weathering rates normalised for BET surface area and mineralogy (Appendix A3) of individual rock types. Left panels show results of linear regression for all data, and right panels for each mycorrhizal types, AM (purple) and EM (orange), individually. Y-axis scales are the same for both left and right panels.

4.3.2 Comparison between field and theoretical rates for calcite and dolomite

In this section, field data are compared to theoretical weathering rates of calcite and dolomite, in order to understand the observed dependency on pH. Within the pH range 3-6, calculated theoretical weathering rate curves at 298K lie close to experimental values from Chou *et al.* (1989; Figure 4.6). There is a slight underestimation of dissolution rate for dolomite at 298K as the curve lies below Chou *et al.*'s published experimental results. This may partly be due to a lack of experimental

Chapter 4

data within the pH range investigated; alternatively, correspondence may be improved by inclusion of the k_2 term.

Carbonate weathering rate dependence on soil acidity and grain surface area

When normalised for particle surface area, estimated field weathering rates for both calcite and dolomite follow the same general pattern as theoretical dissolution rates (Figure 4.7, Figure 4.8). However, in the field, carbonate rocks weather up to several orders of magnitude slower than expected based on theoretical calculations and experimental observations during laboratory studies. The correspondence between field and theoretical dissolution rates is closest when calculated using the thermodynamic constant, E_a , from Kirstein *et al.* (2016; black lines, Figure 4.8) and much more disparate when using E_a from Palandri and Kharaka (2004; blue lines, Figure 4.8).

After 3 months incubation of rock grains in the field, soil pH was the most obvious driver of carbonate rock weathering when normalised by BET surface area (Figure 5), especially for those rocks containing calcite (Linear regression using $\log(\text{weathering rate})$; $F_{1,11} = 7.53$; $N = 13$; $P = 0.019$; $R^2 = 0.41$). Dolomite also exhibited the same general pattern of greater mass loss in more acidic environments, however, this was not significant (Linear regression; $F_{1,9} = 2.52$; $N = 11$; $P = 0.147$; $R^2 = 0.22$).

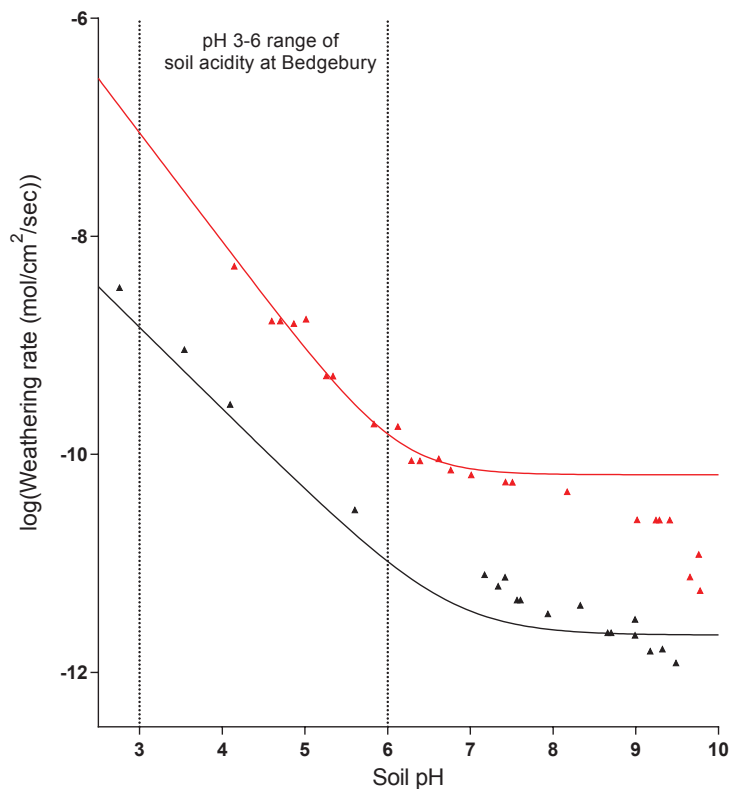


Figure 4.6. Theoretical calcite (red line) and dolomite (black line) weathering rates calculated from pH 2-10 at 298 K showing range of close agreement with experimental results (red and black data points) of Chou *et al.* (1989). Dotted vertical lines highlight the measured range of Bedgebury soil pH, and this section is enlarged alongside field study results in **Figure 4.7** and **Figure 4.8**.

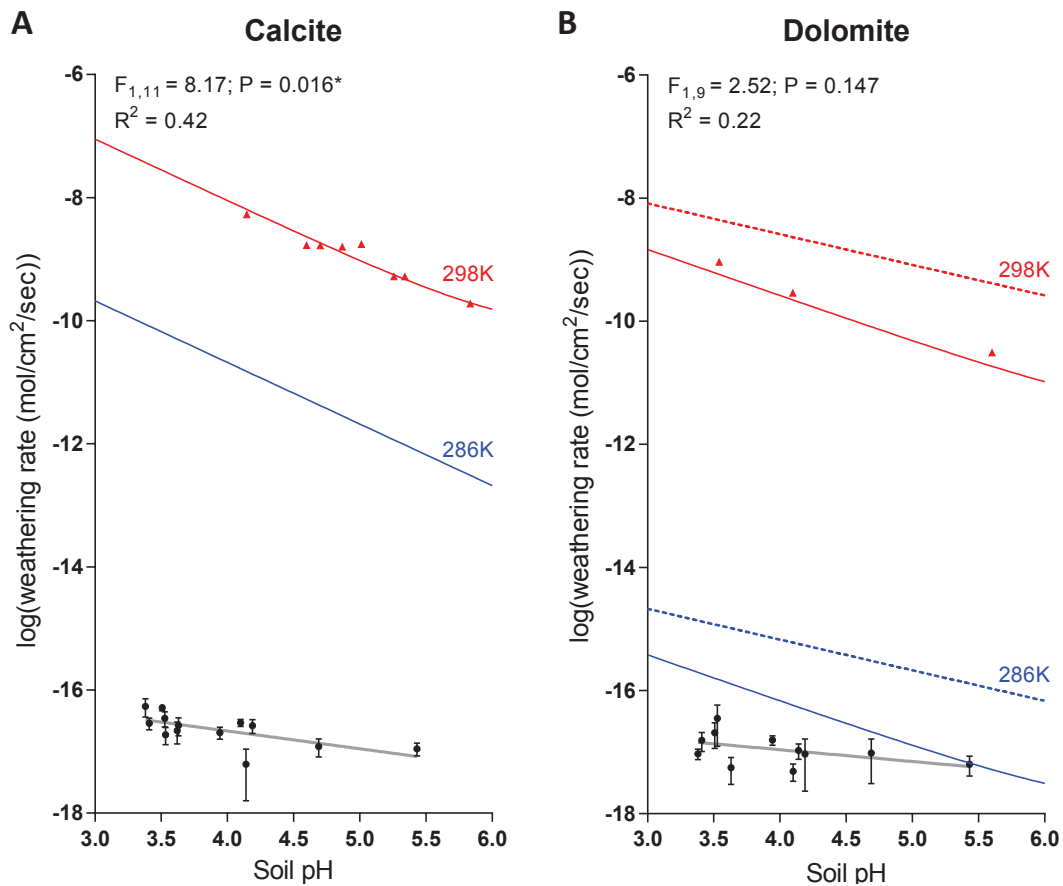


Figure 4.7. Comparison of experimental results from carbonate weathering field study at Bedgebury Pinetum from May - August 2013 (mean \pm SEM; black points; dark grey lines) with theoretical calcite and dolomite weathering rates, over the measured range of Bedgebury soil pH. Theoretical rates calculated at 298K (red lines; red points from experimental work of Chou *et al.* 1989 at 298K) and field temperature, 286.4K (blue lines) for **A**) calcite (N = 13 tree species) and **B**) dolomite (N = 11 tree species). For dolomite dissolution, dashed and solid lines represent different reaction orders (Eqn 14; dashed lines, $s = 0.5$; solid lines, $s = 0.75$ as used in Chou *et al.* (1989)). Rate constants were adjusted for 286.4K using the Arrhenius equation and activation energies from Palandri & Kharaka (2004). Outputs of two-way ANOVA to demonstrate pH dependence of field weathering rate for both calcite and dolomite are displayed on each graph panel. This figure is reproduced in part from Thorley *et al.* (2015).

Carbonate weathering rate dependence on soil acidity and grain surface area

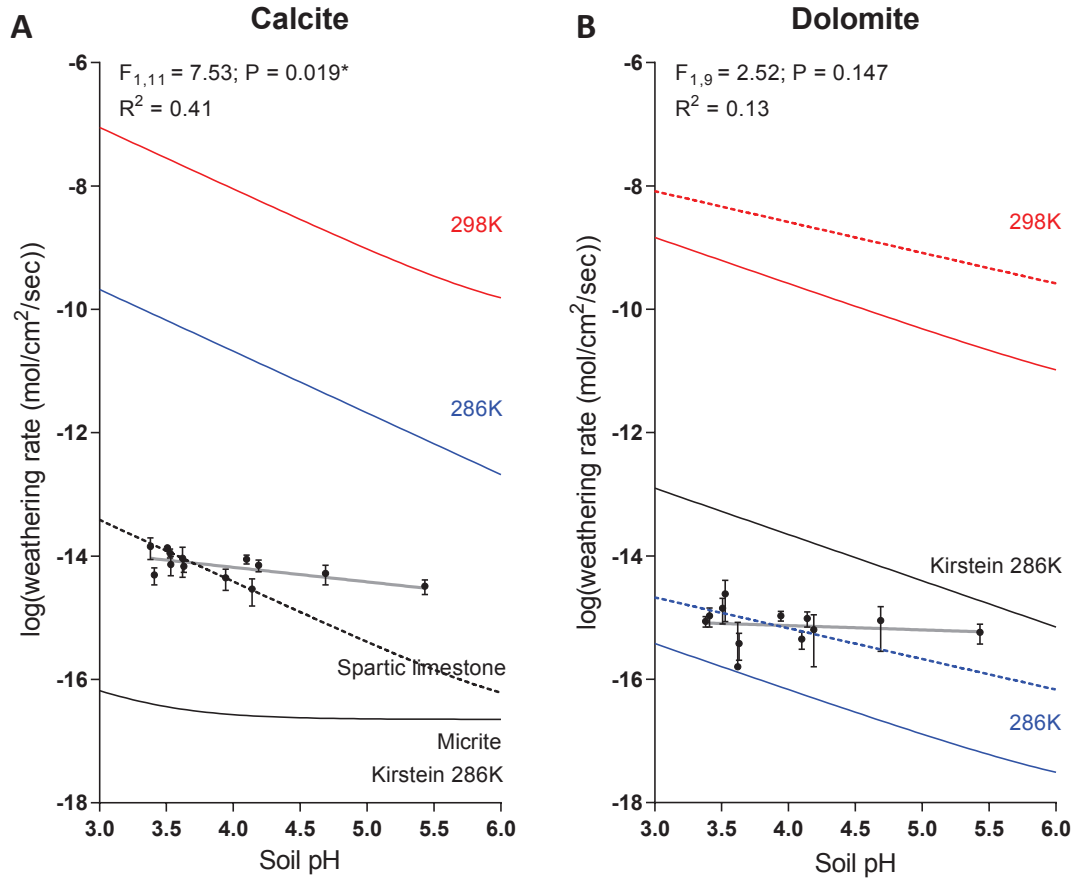


Figure 4.8. Comparison of experimental results from carbonate weathering field study at Bedgebury Pinetum from May - August 2013, as in Figure 4.7, but with weathering rates for **A**) calcite and **B**) dolomite rock grains normalised by BET surface area and mineralogy (Table A. 3). Black lines represent theoretical pH dependence at 286K with rate constant k_1 calculated using $E_{a,s}$ for calcite (Micrite, solid line; Spartic limestone, dashed line) and dolomite (solid line) from Kirstein *et al.* (2016)

Chapter 4

4.3.3 BET and PSA Results

4.3.3.1 Surface area of unweathered rock grains measured by BET analysis

Mean BET surface areas per unit mass dry unweathered rock grains are shown in Table 4.3 below. BET plots for these unweathered samples showing the region over which P/P_0 was measured; the BET constant (C) and equipment measurement uncertainty are shown below (Figure 4.9, Table 4.4).

Table 4.3. BET surface area \pm SE (m^2g^{-1}) of unweathered rock grains. Analysis focussed on chalk, dolomite and silicate, and for these samples, $N = 3$. For oolite and marble, $N = 1$. Full results and sample masses are found below in Figure 4.9, Table 4.4 and in Table A. 4

Rock Type	BET surface area \pm SE (m^2g^{-1})
Silicate	0.175 ± 0.020
Dolomite	0.848 ± 0.015
Chalk	1.024 ± 0.023
Oolite	1.062
Marble	0.053

Table 4.4. BET values, the BET constant, and correlation coefficients for representative unweathered rock grain samples. Rock grain types are identified with letters A-E and correspond to plots in Figure 4.9.

Sample	Analysis date	Degassed mass (g)	BET \pm equipment error (m^2g^{-1})	C	Correlation coefficient
A Chalk	03/06/2015	1.7745	1.0386 ± 0.0060	183.5	0.99987
B Oolite	19/06/2015	3.4157	1.0620 ± 0.0092	111.6	0.99971
C Marble	19/06/2015	3.8810	0.0526 ± 0.0017	180.0	0.99576
D Dolomite	19/06/2015	3.5116	0.8331 ± 0.0048	105.8	0.99987
E Basalt	03/06/2015	2.0267	0.1950 ± 0.0024	51.3	0.99939

Carbonate weathering rate dependence on soil acidity and grain surface area

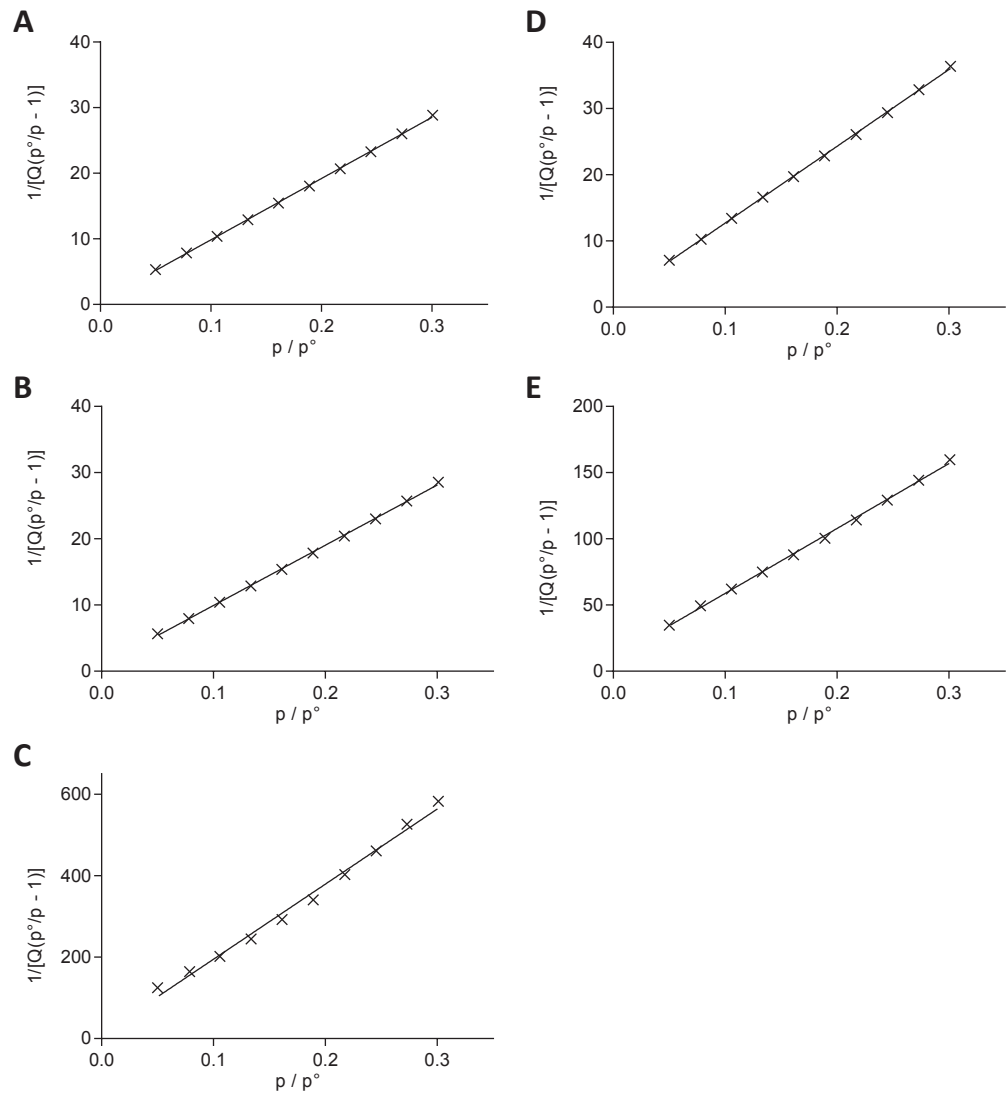


Figure 4.9. Representative BET isotherm plots to show region of linearity for **A)** chalk, **B)** oolite and **C)** marble, **D)** dolomite and **E)** silicate rock grains. Note different y-axis scales required for different rock types. For each of silicate, chalk and dolomite, more than one sample of unweathered rock was analysed and the additional data on sample masses, the BET constant, C , and equipment measurement uncertainties can be found in Table A. 4.

4.3.3.2 Unweathered chalk particle size distribution

When measured using laser diffraction techniques, unweathered chalk gives a log-normal distribution of particles with the main peak of the distribution corresponding to particles measuring $1110 \mu\text{m}$ diameter. In addition to this main distribution, there is another small peak far to the left of particles measuring $1.65 - 5.21 \mu\text{m}$ diameter (Figure 4.11C). This peak only composes 0.0005% of the total sample volume and is seen consistently across all 5 measurements of unweathered chalk.

Chapter 4

Table 4.5. Summary of particle distribution and surface area characteristics for unweathered chalk and samples recovered after 7 (blue shading; 4 samples) and 14 months (green shading; 6 samples) weathering beneath mature stands of AN = *A. nordmanniana*; LD = *L. decidua*; PS = *P. sylvestris*; EC = *E. coccifera*, ND = *N. dombeyii* and AA = *A. araucana*. Two measures of surface area are included, BET measured by gas adsorption and that calculated from the particle size distribution during wet dispersion of each sample.

Sample	Mass loss (mg)	Surface area (m ² g ⁻¹)		% of particles in size range			Modal particle size within category (µm)		
		BET (±SEM)	Dispersion	0-25	25-240	>240	0-25	25-240	>240
Chalk	0	1.02 ± 0.02	0.0104	0.001	0.000	99.999	2.13	0	1110
AN	110.97	1.01 ± 0.02	0.0676	0.020	0.384	99.596	4.03	127	976
LD	59.67	0.94 ± 0.02	0.0146	0.002	0.008	99.991	3.55	98	976
PS	43.86	0.92 ± 0.02	0.0389	0.008	0.164	99.828	3.12	111	859
AA	11.08	0.90 ± 0.02	0.0266	0.003	0.144	99.853	2.75	98	859
ND	87.74	1.04 ± 0.02	0.0584	0.018	0.436	99.545	4.03	127	859
EC	220.48	1.15 ± 0.02	0.0665	0.024	0.257	99.719	4.58	127	976
PS	326.11	1.24 ± 0.02	0.0833	0.033	0.476	99.492	5.57	127	976
PS	126.17	1.09 ± 0.02	0.0993	0.028	0.115	99.857	3.12	111	756
ND	142.51	1.20 ± 0.02	0.1113	0.035	0.907	99.058	4.03	127	859
AN	39.12	0.94 ± 0.02	0.0258	0.004	0.064	99.932	2.75	86.4	859

4.3.4 Evolution of surface area and particle size distribution during weathering

4.3.4.1 Change in particle size distribution with weathering

The main peak of large particle size distribution were modelled by nonlinear log-Gaussian regressions and the mean and S.E. of these distributions compared (Figure 4.10; Table 4.6). The fits of log-Gaussian curves to each dataset were very robust with $R^2 > 99\%$ in all cases, however there was a slight tendency to overestimate the particle diameter at which the peak of the distribution occurred in comparison with the peak amplitude from measured data in Table 4.5. However, this is likely to be due to the relatively low resolution of original data with only 20 data points lying within the >240 µm diameter range used in this section of the analysis. A better estimate of the mode can be calculated by interpolating between the particle diameters, x_1 and x_2 with the two greatest amplitudes of % volume, y_1 and y_2 , weighted as in Eqn 17 (Table 4.6).

$$\text{Interpolated mode} = \frac{(x_1 \times y_1) + (x_2 \times y_2)}{(y_1 + y_2)} \quad (17)$$

Additional curves have been plotted with PSA normalised relative to the mass loss of each sample during weathering. To achieve this, curve amplitudes were scaled in relation to proportional mass change, as volume \propto mass. This method emphasises the shift in the main curve upon weathering, as this is the part of the curve which represents most volume and therefore sample mass.

Carbonate weathering rate dependence on soil acidity and grain surface area

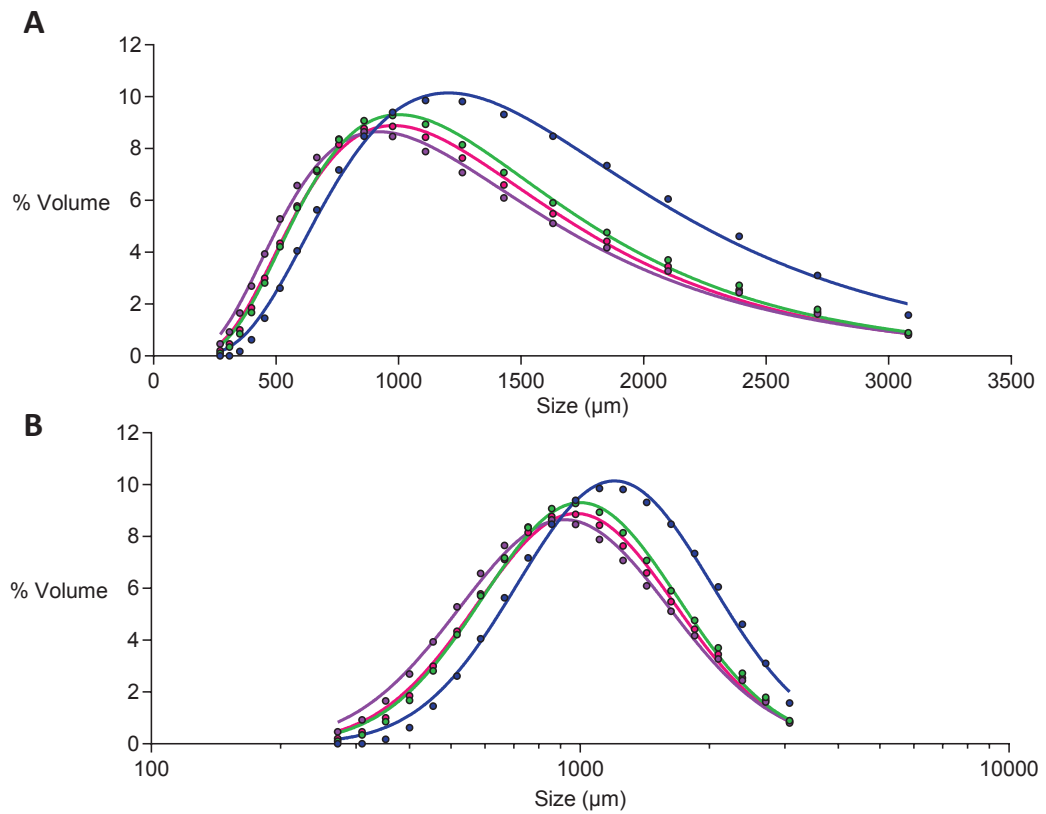


Figure 4.10. Particle size distribution of particles $>240 \mu\text{m}$ diameter for one unweathered (blue line) and 3 weathered chalk samples (14 months), *P. sylvestris* (pink), *E. coccifera* (green) and *N. dombeyii* (purple) measured by wet dispersion. **A)** Curves are log-Gaussians fitted by least squares method to each dataset, displayed on with a log scale for the x-axis in **B)**.

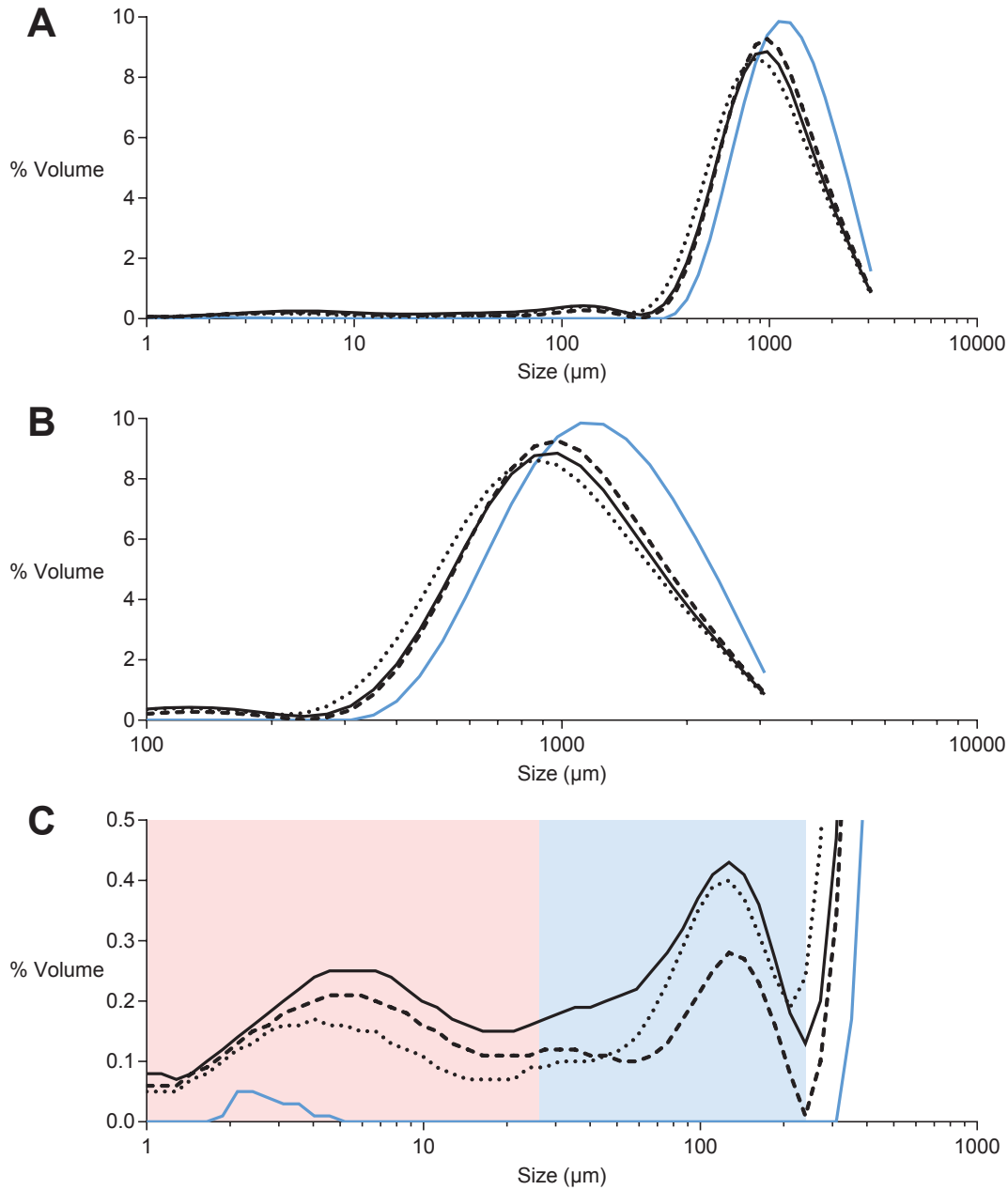


Figure 4.11. Particle size distribution of 1 unweathered (blue line) and 3 weathered chalk samples, *P. sylvestris* (black continuous line), *E. coccifera* (long dashes) and *N. dombeyii* (dotted line) measured by wet dispersion. **A)** Overall view of particle size distribution. Expanded sections of **B)** only particles >100 µm diameter and **C)** particles <1000 µm diameter (note the difference in scale). Pink shading represents the range defined for small particles, 0-25 µm and blue shading that for medium particles, 25-240 µm. Above 240 µm particles are classed as large. Each trace is an average of 5 measurements of 10s duration.

Carbonate weathering rate dependence on soil acidity and grain surface area

Loss of largest particles

As rock grains weather over the course of 14 months, there is a noticeable shift in the main peak of log particle size distribution toward smaller particle diameters, and also reduces in amplitude (Table 4.5, Figure 4.11, Figure A. 4). Over the course of weathering, the main change in particle size distribution is in the loss of larger particles with diameter, $d > 810 \mu\text{m}$, and accumulation of particles $240 > d > 810 \mu\text{m}$ towards the left tail of the distribution of large particles (Figure 4.12).

Table 4.6. Comparison of distribution characteristics of particles $>240\mu\text{m}$ diameter for unweathered chalk and three weathered samples recovered after 7 (blue shading; 4 samples) and 14 (green shading; 6 samples) months burial beneath mature stands of AN = *A. nordmanniana*; LD = *L. decidua*; PS = *P. sylvestris*; EC = *E. coccifera*, ND = *N. dombeyii* and AA = *A. araucana*. Interpolated modal particle size is based on data from wet dispersion of samples, and calculated from modal values in Table 4.5 using Eqn 17. Other columns describe log-Gaussian distributions fitted to data using a least squares method shown in Figure 4.10.

Sample	N	Interpolated modal diameter of particles $>240\mu\text{m}$ diameter (μm)	Results of non-linear regression for log Gaussian distribution of particles $>240\mu\text{m}$ diameter			
			Centre \pm SE (μm)	Amplitude (% volume)	R ² (%)	Degrees of Freedom
Chalk	20	1185	1203.0 \pm 10.2	10.2 \pm 0.1	99.34	17
AN	20	917	994.2 \pm 10.0	9.4 \pm 0.2	98.99	17
LD	20	1042	1049.0 \pm 11.9	10.2 \pm 0.2	98.75	17
PS	20	917	941.7 \pm 10.6	10.1 \pm 0.2	98.70	17
AA	20	808	848.1 \pm 6.8	10.9 \pm 0.2	99.33	17
ND	20	918	919.3 \pm 8.7	8.6 \pm 0.1	99.08	17
EC	20	817	1001.0 \pm 8.4	9.3 \pm 0.1	99.29	17
PS	20	918	978.5 \pm 8.3	8.9 \pm 0.1	99.27	17
PS	20	807	833.8 \pm 9.7	8.4 \pm 0.2	98.69	17
ND	20	917	926.7 \pm 5.2	7.4 \pm 0.1	99.67	17
AN	20	917	917.3 \pm 10.8	10.3 \pm 0.2	98.56	17

Accumulation of small and mid-sized particles

The second most noticeable change in particle size distribution was that of accumulation of mid-sized particles. Samples recovered after 12 months of weathering had an additional peak in their particle size distributions. This lay between 25-240 μm and represents medium-sized particles that were not present in unweathered chalk.

Finally, after weathering, there is a slight accumulation of dust $< 25 \mu\text{m}$ diameter. This still only accounts for only a small proportion of total volume as dust is so fine, and the relative volume that this group represents rises from 0.0005% to 0.0016-0.035% after weathering (Table 4.6).

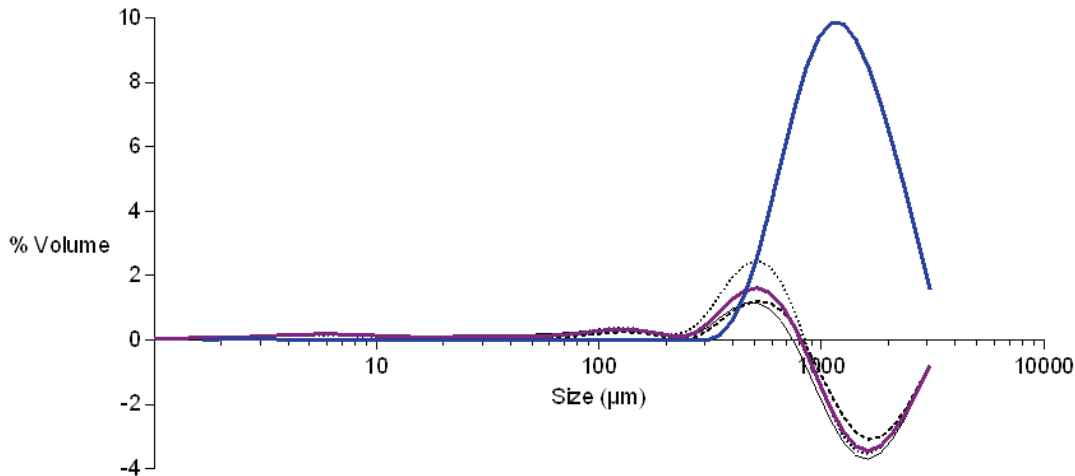


Figure 4.12. Change in chalk particle size distribution of particles after 14 months weathering for *P. sylvestris* (black continuous line), *E. coccifera* (long dashes) and *N. dombeyii* (dotted line), in comparison to unweathered grains (blue line). Purple curve is the mean change, calculated from all weathered samples ($N = 6$) after data was normalised relative to sample mass loss.

4.3.4.2 Change in BET surface area with weathering

Increase in BET surface area of silicate rock grains after 14 months weathering

All weathered silicate samples analysed had greater surface area than unweathered silicate grains (Unpaired 2-tailed T-test with Welch's correction, assuming unequal variances: $T = 4.32$; d.f. = 5.50; $P = 0.0061$). The mean BET surface area after weathering was $0.321 \pm 0.027 \text{ m}^2\text{g}^{-1}$ (mean \pm S.E.), which is over 180% higher than the unweathered surface area of $0.175 \pm 0.020 \text{ m}^2\text{g}^{-1}$.

Although there is an overall increase in surface area with weathering, there is no statistically significant relationship between BET values and sample mass loss (Figure 4.13; BET surface area per unit mass: general linear model; $F_{1,6} = 0.25$; $N = 8$; $R^2 = 4.03\%$; $P = 0.63$). In contrast to the carbonate rocks investigated, weathering mass loss was minimal for all silicate samples. For this reason, BET surface area is only plotted relative to unit mass (Figure 4.13), and is not also calculated for total sample mass as it was for carbonates.

Carbonate weathering rate dependence on soil acidity and grain surface area

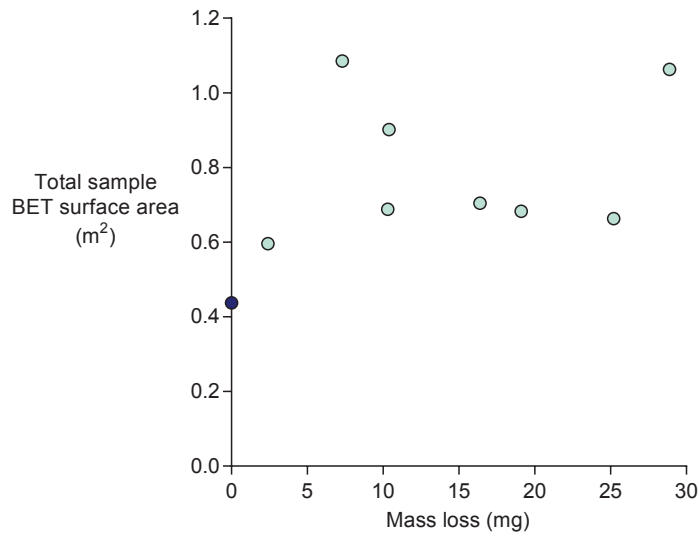


Figure 4.13. BET surface area of unweathered (dark blue) and 14-month weathered (light blue) silicate rock grains relative to total weathering mass loss. BET surface area per unit mass of 1 g.

Initial surface area reduction of chalk and dolomite grains

Some chalk samples recovered from the field after 7 and 14 months showed little change in terms of rock grain mass loss. These samples, however, did exhibit a sharp reduction in surface area by $0.1 \text{ m}^2\text{g}^{-1}$ ($N = 4$; Table 4.7), relative to the initial, unweathered surface area of chalk, $1.024 \pm 0.023 \text{ m}^2\text{g}^{-1}$ (Table 4.3). This reduction amounts to $9.80 \pm 0.03 \%$ of the total initial surface area per unit mass and an $11.20 \pm 0.07 \%$ reduction in total chalk grain surface area within each mesh bag. Overall, this initial decrease in surface area occurs at an average rate of 0.0075 m^2 per mg of mass loss through weathering.

Unweathered dolomite had a BET surface area of $0.848 \pm 0.015 \text{ m}^2\text{g}^{-1}$, and similarly to chalk, exhibited an initial reduction in surface area during weathering. Calculating the effective unweathered surface area based on the BET surface area per unit mass (Figure 4.14A) it is $0.482 \pm 0.063 \text{ m}^2\text{g}^{-1}$. Alternatively, calculation based on the BET surface area for entire samples (Figure 4.14B), the effective unweathered surface area is $1.22 \pm 0.146 \text{ m}^2$ for a 2.50 g sample, equivalent to $0.488 \pm 0.058 \text{ m}^2\text{g}^{-1}$.

Chapter 4

Table 4.7. BET surface area comparison of unweathered chalk (N = 3), with a selection of samples that showed a sharp reduction in surface area during initial weathering. Samples are identified by tree species and followed by sample harvest in brackets (7 or 14 months). AA = *A. araucana*; PS = *P. sylvestris*; AN = *A. nordmanniana*; LD = *L. decidua*. The chalk sample from AA after 7 months was used for determining the accuracy of BET measurement of a single sample (N = 3). This error has been used for all weathered chalk samples.

Chalk Sample	Sample mass (mg)	BET (m^2g^{-1})	Reduction in BET during initial weathering	
			By unit mass	By total mass
Chalk	2500	1.024 ± 0.023		
AA (7)	2488.92	0.902 ± 0.013	$11.90 \pm 0.03 \%$	$12.29 \pm 0.07 \%$
PS (7)	2456.14	0.921 ± 0.013	$10.06 \pm 0.03 \%$	$11.64 \pm 0.07 \%$
AN (14)	2460.88	0.935 ± 0.013	$8.67 \pm 0.03 \%$	$10.10 \pm 0.07 \%$
LD (7)	2440.33	0.936 ± 0.013	$8.59 \pm 0.03 \%$	$10.77 \pm 0.07 \%$
Average	2461.57	0.924 ± 0.013	$9.80 \pm 0.03 \%$	$11.20 \pm 0.07 \%$

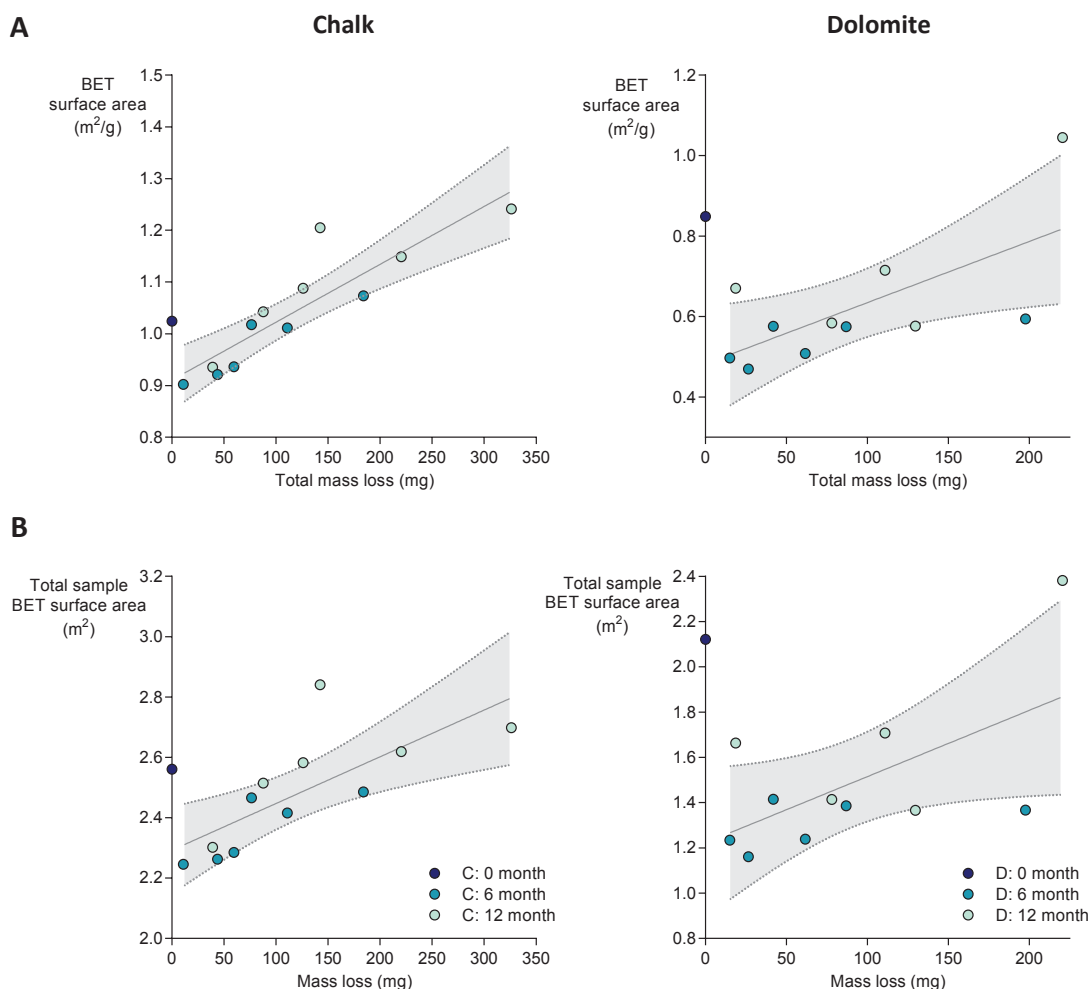


Figure 4.14. BET surface area of chalk (left panel), and dolomite (right panel) grains relative to total weathering mass loss. **A)** BET surface area per unit mass of 1 g, and **B)** total BET surface area of weathered sample with an initial, unweathered mass of 2.5 g. Dark blue symbols are unweathered chalk grains, mid blue are samples after 7 months of weathering and light blue after 14 months burial at Bedgebury. Shaded area indicates 95% confidence interval for all weathered samples.

Carbonate weathering rate dependence on soil acidity and grain surface area

Increase in carbonate surface area with further weathering

As weathering mass loss progresses, chalk grain surface area increases linearly after the initial reduction in surface area, regardless of the time point samples when were harvested (Figure 4.14A; BET surface area per unit mass: general linear model; $F_{1,10} = 38.45$; $N = 12$; $R^2 = 79.36\%$; $P = 0.0001$) (Figure 4.14B; Total BET surface area per sample: general linear model; $F_{1,10} = 12.17$; $N = 12$; $R^2 = 54.89\%$; $P = 0.0058$). The rate of BET surface area relative to mass loss is calculated from the gradient of the regression in Figure 4.14A. For chalk, surface area per unit mass is reduced by $0.00112 \pm 0.00018 \text{ m}^2\text{g}^{-1}$ for every mg weathering mass loss. And, taking into account the effect of the change in total sample mass on surface area, the total surface area is reduced by $0.00155 \pm 0.00044 \text{ m}^2 \text{ mg}^{-1}$ mass loss. This latter measure considers an entire sample with an initial mass of 2.50 g, contained within a mesh bag.

From these relationships we can extrapolate to find the effective initial surface area of chalk, disregarding the rapid surface area reduction upon first burying the mesh sample bags. When calculated from the intersect in Figure 4.14A, BET surface area per unit mass, this effective initial surface area is $0.910 \pm 0.002 \text{ m}^2\text{g}^{-1}$ for unweathered chalk grains. If using the total BET surface area, the effective initial surface area is $2.292 \pm 0.065 \text{ m}^2$ per sample of 2.50 g, which equates to $0.917 \pm 0.026 \text{ m}^2\text{g}^{-1}$. The value calculated using the total sample BET surface area is slightly higher than that calculated using unit mass, however, this is not significantly different, and the estimates lie within the same range when the considering measurement error of either these values, or the standard error calculated from analysis of 3 individual unweathered chalk samples, which was $\pm 0.023 \text{ m}^2\text{g}^{-1}$ (Table 4.3).

Similarly to chalk, as weathering progresses, dolomite surface area again increases from its theoretical minimum, the effective initial surface area, calculated above. For dolomite the surface area change equates to an $0.00152 \pm 0.00056 \text{ m}^2\text{g}^{-1}$ increase per mg weathering mass loss when calculated based on BET surface area per unit mass (Figure 4.14A). This value is $0.00117 \pm 0.00052 \text{ m}^2\text{g}^{-1}$ increase per mg weathering mass loss when calculated from total BET surface area per sample (Figure 4.14B) and scaled by initial sample mass (2.50 g), however, this linear regression is not statistically significant at $P < 0.05$ (Table 4.8). There was no statistically significant difference between the mean 7 and 14-month samples (Unpaired 2-tailed T-test with Welch's correction, assuming unequal variances: $T = 2.06$; d.f. = 4.48; $P = 0.10$), and these have been treated as the same population for the purpose of these analyses.

Chapter 4

Table 4.8. Results of linear regressions showing response of dolomite BET surface area to weathering mass loss. All dolomite samples are used in each regression (N = 11). Neither regression includes data for unweathered dolomite. Results significant at $P < 0.005$ are highlighted by *.

	Slope	Intercept	R ² (%)	F _{1,9}	P
Whole samples (m ² sample ⁻¹)	0.0029 ± 0.0013	1.22 ± 0.146	35.90	5.04	0.051
Unit mass (m ² g ⁻¹)	0.0015 ± 0.0006	0.482 ± 0.063	44.93	7.34	0.024*

Chalk BET surface area is influenced by weathering rate

In this section, the burial time of samples is used to compare their weathering behaviour. For simplicity, these are referred to as 7 and 14 month samples, however, in reality, 7-month samples were buried for 203-231 days, and 14 month samples for 413-440 days (Section 2.7.1).

In general, both total and unit mass BET surface areas of chalk grains are greater for those samples recovered after 14 months than after 6 months (Unpaired 2-tailed T-test with Welch's correction for unit mass BET surface area, assuming unequal variances: $T = 2.49$; d.f. = 8.15; $P = 0.037$). These data come from different distributions (Table 4.9; Wilcoxon rank sum test, $W = 31$, $P = 0.041$) and is a result of the overall distribution of sample masses after each time point, which is demonstrated in Figure 4.15.

Table 4.9. Results of linear regression for response of chalk BET surface area (m²g⁻¹) to weathering rate of whole samples (mg day⁻¹). F_{1,4} for each 7 and 14 month samples individually where N = 6, and F_{1,10} for all chalk samples combined where N = 12. Neither regression includes unweathered chalk data. Results significant at $P < 0.005$ are highlighted by *.

	Slope	Intercept (m ² g ⁻¹)	R ² (%)	F	P
7 months	0.24 ± 0.05	0.89 ± 0.02	84.92	22.52	0.009*
14 months	0.39 ± 0.12	0.96 ± 0.05	74.12	11.46	0.028*
All weathered chalk	0.32 ± 0.11	0.93 ± 0.05	46.63	8.738	0.014*

Carbonate weathering rate dependence on soil acidity and grain surface area

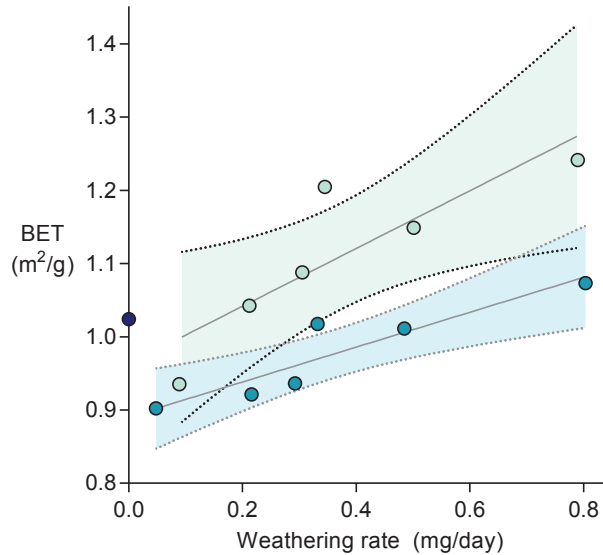


Figure 4.15. BET surface area of chalk grains relative to rate of weathering mass loss. Dark blue symbols are unweathered chalk grains, mid blue are samples after 7 months of weathering and light blue after 14 months burial at Bedgebury. Shaded area indicates 95% confidence interval for 7 month and 14 month samples individually

4.3.5 Chalk grain porosity measured by gas adsorption

Within the pressure range used for BET analysis, saturation pressure was not reached, so it is not possible to say for certain whether the rock types studied would have Type II or Type IV isotherms. However, based on a pilot investigation of chalk pore size, it is likely that this rock type would have a Type IV isotherm as pores were roughly 150-350 Å diameter (15-35 nm; Figure 4.17), meaning they fall in the class of mesoporous solids.

The pore size study was not continued due to time constraints; however, preliminary results indicate that over the course of 14 months, there may be an increase in pore size as chalk grains weathered (Figure 4.16). Currently there is insufficient data on pore size to draw any robust conclusions, so this topic is not discussed in detail outside this section.

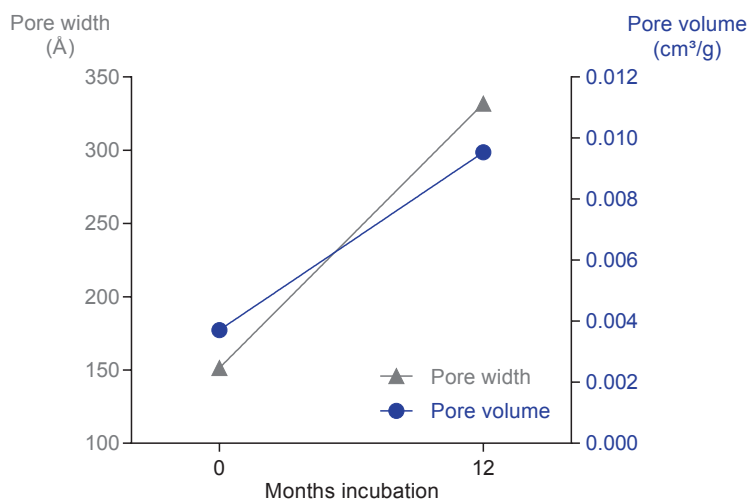


Figure 4.16. Pore width (left y-axis) and pore volume (right y-axis) of chalk grains before and after 14 months of weathering in the field. Pore width and total pore volume both increase during weathering. Further data were not collected due to the time consuming nature of this measurement.

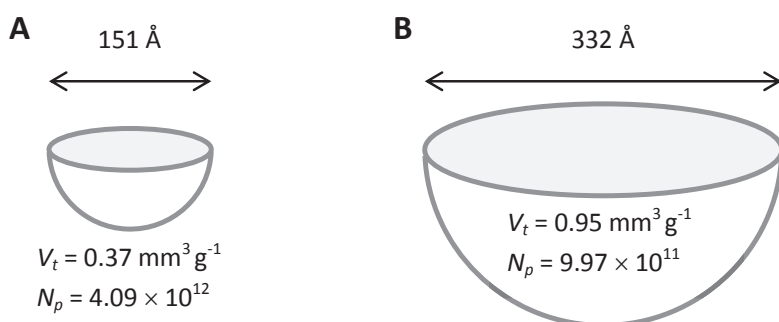


Figure 4.17. Scale illustration of pore size differences, **A)** before and **B)** after 14 months of weathering under a stand of *E. coccifera* trees. Average pore width (Å) is indicated above diagrams. Total pore volume per unit mass rock grains, V_t ($\text{mm}^3 \text{g}^{-1}$), and average pore width are used to estimate total number of pores, N_p , before and after weathering, assuming hemispherical pore geometry.

4.3.6 Comparison of measured BET and calculated PSD surface areas

BET and PSA surface area results for 7 and 14-month weathered samples of chalk correlate ($F_{1,8} = 21.1$, $P = 0.0018$, $R^2 = 0.725$; Figure 4.18A). There is no significant relationship between PSA and BET surface area for dolomite rock grains ($F_{1,4} = 1.2$, $P = 0.33$, $R^2 = 0.232$, Figure 4.18B), however, less data are available than for the chalk samples.

Carbonate weathering rate dependence on soil acidity and grain surface area

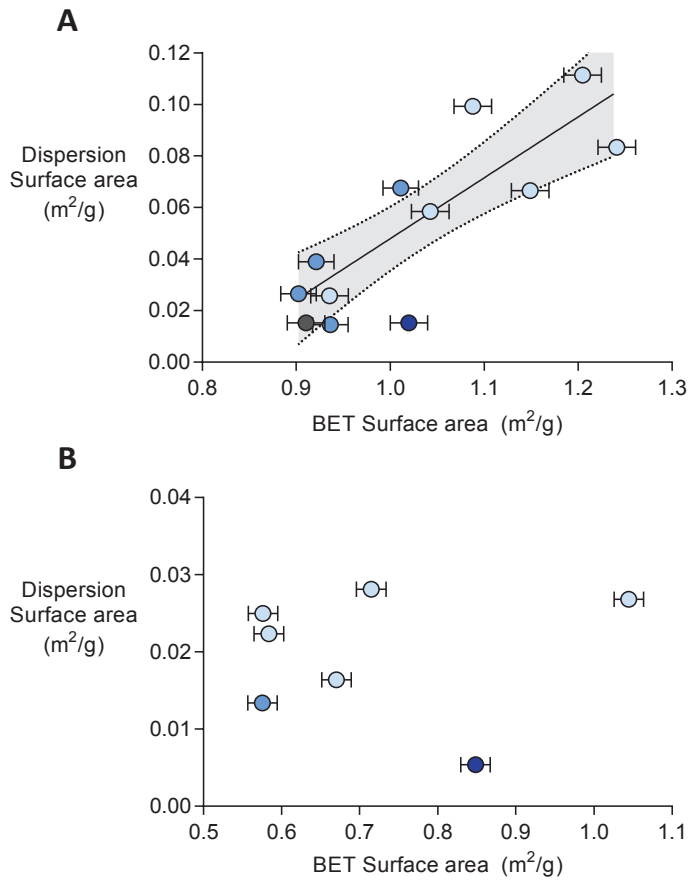


Figure 4.18. Comparison of chalk surface area calculated from PSA by wet dispersion with that measured by BET analysis for unweathered (dark blue is BET surface area; grey is calculated effective initial surface area), 7-month (mid blue) and 14-month (light blue) weathered rock grains of **A) Chalk** and **B) Dolomite**.

4.4 Discussion

4.4.1 Carbonate weathering rate dependence on environmental pH

During the sampling periods in 2013 at Bedgebury, the total range of soil pH was 3-6, with the most acidic soils occurring below EM species. Calcite weathering rates, as estimated from mass balance calculations, were significantly correlated with soil acidity when both AM and EM species were analysed together. The fastest weathering samples were those incubated under EM tree stands, which is unsurprising as carbonate minerals, particularly calcite, are susceptible to acid dissolution (Eqn 6; Section 1.4.1.2). The lack of any significant pH dependency when considering the subset of either AM or EM species individually (Figure 4.5) may indicate that mycorrhizal type, and not pH, is the overarching factor controlling dissolution rates. This may be realised via their influence over soil acidity, which co-varies with mycorrhizal type.

Soil acidification by all tree groups may result from a combination of proton extrusion, leaching and plant uptake of base cations, humus accumulation and organic acid secretion (Arvieu *et al.* 2003; Casarin *et al.* 2003, 2004; Sandnes *et al.* 2005). One of the most important factors determining soil pH, and associated weathering, may be rhizosphere acidification by direct and indirect effects of mycorrhizal fungal activity. Rhizosphere acidification may be especially significant below EM tree stands, and account for the large pH differences observed and associated higher weathering rates. This result differs from historical conclusions that coniferous (gymnosperm) trees cause the greatest soil acidification at Bedgebury (Ovington 1953), as there was no measureable effect of tree group (angiosperm/gymnosperm), or leaf habit (evergreen/deciduous) on soil pH.

When analysed individually this correlation between pH and weathering rate was significant for both marble and chalk, but not for the other calcite rock, oolitic limestone. One factor that may contribute to the lack of any significant relationship for oolite weathering is the lower calcite content of oolite compared to chalk or marble. This is indicated by the lower Ca and marginally higher SiO₂ contents identified in XRF analysis (Table A. 3), and will make mass balance calculations based on calcite slightly less accurate, combined with the lower weatherability of SiO₂. Another reason oolite weathering may differ is due to its greater heterogeneity in both structure and mineralogy compared to both chalk and marble. The presence of shelly fragments and ooids make oolite samples naturally more variable than either of the other calcite-containing rocks, despite crushing and thorough mixing during sample preparation. The

Carbonate weathering rate dependence on soil acidity and grain surface area

precise composition of each oolite sample analysed will impact on the weathering rate recorded.

4.4.2 Why is calcite weathering rates different in field and laboratory studies?

Calcite weathering dependence on soil pH follows the same trend as expected based on theory, with higher weathering rates within more acidic soils. However, despite normalising field weathering rates by BET surface area, calcite weathering rates are still up to several orders of magnitude slower than expected based on theoretical calculations. Using E_a from a study of carbonate dissolution at low temperatures (Kirstein *et al.* 2016; black lines Figure 4.8) yields closer correspondence between field and theoretical dissolution rates than when using E_a values from an earlier compilation (Palandri and Kharaka 2004; blue lines Figure 4.8).

This gap between observed and expected weathering rates has been discussed in the literature in relation to silicate minerals and makes it difficult to scale results from laboratory experiments to predict mineral weathering rates in the field. White and Brantley (2003) observed that in the field, Panola granite weathered 1-2 orders of magnitude slower than the experimental rate measured in the laboratory. However, the discrepancy between field and laboratory results are slightly greater for calcite weathering, which is approximately 4 orders of magnitude slower in the field than calculated theoretically. In contrast, there is fairly good correspondence between theoretical and field dolomite weathering rates (Figure 4.8B), despite there being no significant pH dependency in the field results.

The most commonly proposed source of this discrepancy is the uncertainty in measurement of reactive surface area of weathering rock grains in field and laboratory studies (Brantley and Mellott 2000). This is known to be an important factor for silicate minerals (White and Brantley 2003), and is likely to also affect carbonate weathering. Weathering rates are therefore usually normalised for surface area, which is often measured by BET gas adsorption analysis, yet this is thought to be imperfect and potentially leads to underestimation of weathering rates (Arvidson *et al.* 2003). Other factors that may contribute to this discrepancy between observed and expected dissolution rates are discussed in the following section. This study utilises BET and PSA techniques to probe the mechanics of carbonate rock grain weathering in forest soils.

Chapter 4

4.4.2.1 Inappropriate thermodynamic constants

In this study, theoretical weathering rates were calculated using thermodynamic constants obtained from literature (Chou *et al.* 1989; Palandri and Kharaka 1994; Kirstein *et al.* 2016). There are some indications that these literature values may not be ideal when applied to the weathering of natural rocks in field conditions. With the exception of Kirstein *et al.*, rate constants are derived in studies using pure minerals rather than natural rocks and at relatively high temperatures in systems far from equilibrium using batch or flow reactors.

For instance, the rate constant, k , used in calculations in this chapter (Chou *et al.* 1989) was determined using hydrothermal carbonate minerals, crystallised from high temp aqueous solution, and not sedimentary rocks as used in this study, in addition to a smaller grain size (0.1-0.3 mm diameter). The presence of impurities, common in natural rocks, and present in the samples used in this study (Table A. 3) may also affect solubility and modify thermodynamic constants as has been seen for SO_4^{2-} , PO_4^{3-} , Sr and Mg (reviewed in Kirstein *et al.* 2016).

In studies far from equilibrium, dissolution is rapid and primarily limited by how quickly reagents can be transported to the mineral surface and dissolution products can be removed. Close to equilibrium, reaction rates decrease, however this has not been investigated thoroughly at low temperatures, or in the natural environment. In these natural systems, there are much smaller solute:carbonate ratios and complex fluid chemistry, which will impact on dissolution behaviour. There is some indication from the literature that in conditions close to equilibrium, carbonate dissolution may have higher E_a as a result of rate limitation by surface reactions (reviewed in Gutjahr *et al.* 1996 and Kirstein *et al.* 2016).

The closest correlation between theoretical and field experimental results were obtained using published activation energies, E_a , in Kirstein *et al.* (2016) compared with those from Palandri and Kharaka (2004). Rate constants from the work of Kirstein *et al.* (2016) are most likely to represent our samples, as their study investigated natural carbonate rocks prepared with a similar grain size (0.5-1 mm) to that in the current study (0.5-1.18 mm) at low dissolution temperatures (5, 12.5 and 25°C), which lie closer to conditions in the field (~13.4°C average air temperature), however, there are still large differences in experimental setup. The dissolution studies of Kirstein *et al.* were performed far from equilibrium in a pH 4.7 solution of sulphuric acid, with a volume sufficient to maintain continual fluid-mineral contact and ensure rapid dissipation of dissolution products.

Carbonate weathering rate dependence on soil acidity and grain surface area

One other outcome of Kirstein *et al.*'s work is to highlight the major impact rock structure can have on rate constants, as shown by the disparate activation energies of two calcite-based rocks micrite and spartic limestone. Chalk used in the current study is probably most structurally similar to the micrite used by Kirstein *et al.* (2016), as it is predominantly composed of coccoliths distributed throughout micrite. When viewed in thin section, the chalk used in this study has a fairly homogenous structure (Section 5.3.1), however, there may be differences in dissolution when compared to pure micrite.

4.4.2.2 *Incomplete understanding of weathering agent dynamics in the field*

In the field, carbonate minerals will be interacting with a suite of weathering agents, including soil CO₂, carbonic acid, organic acid exudates and potentially stronger inorganic acids. The relative importance each acidic soil component is likely to vary drastically both spatially and seasonally, responding to biological activity, climatic conditions and soil hydrology. The effects of these soil acidifying agents has not been separated within theoretical weathering rate calculations, which were determined purely on the basis of pH, and inclusion of separate terms may decrease the gap between field and theoretical results.

4.4.2.3 *Transport limitation*

As discussed in Section 1.4.1.1, theoretical relationships between pH and dissolution rates are derived from laboratory experiments performed far from equilibrium. In these studies, there is generally a high mineral:fluid ratio, allowing dissolution products to be rapidly transported away from the site they were produced, thus reducing their concentration and allowing further dissolution to occur. For this reason, many laboratory weathering studies are performed in through-flow reactors, or batch reactors whilst stirring to maintain a high diffusion gradient.

In the field situation, transport limitation will be prevalent due to the relatively long residence times of soil water (2 weeks – 2 months; Stewart and McDonnell 1991). The slow movement of water and hydrological complexity of soils will retain weathering products close to their parent mineral, potentially trapped in pores in the rock surface or adsorbed to nearby soil particles. Where weathering products are not removed, this will slow the rate of further mineral dissolution as the system approaches equilibrium (Eqns 1, 2), and may even result in a mixture of carbonate dissolution and re-precipitation. For these reasons, even at pHs where theoretically weathering rate would be limited by the interface reaction, they may be transport limited in a natural system close to equilibrium (Brantley 2003; White and Brantley 2003).

Chapter 4

4.4.2.4 Incomplete understanding of reactive surface area

In weathering studies where reaction rates are normalised to surface area it is vital to have an accurate measure for reactive surface area of the mineral available for weathering. The consensus in literature is that problems in defining reactive surface area are one of the major sources of discrepancy between natural and experimental or theoretical weathering rates.

Currently there is no solution on how to accurately measure reactive surface area. Several techniques have been used, across a range of studies, to normalise weathering rates to surface area, most commonly BET analysis or geometric estimations, both of which have significant limitations (Arvidson *et al.* 2003). Normalisation using BET measurements may underestimate weathering rates as it includes internal surfaces which may have a different dissolution environment than external surface or may be inaccessible to weathering agents. Geometric measurements on the other hand, could overestimate weathering agents by disregarding much surface roughness and internal surfaces. Other techniques such as VSI or AFM are able to map mineral surface topography in detail, however, are time consuming and not appropriate to use for bulk samples.

The importance of understanding reactive surface area is demonstrated by the many studies reviewed by Brantley and Melott (2000) have shown that naturally weathered silicate rock grains in soils have greater specific surface areas compared to laboratory ground samples. This increase in SA in weathered samples has been attributed to increased roughness of grain surfaces and may also be partly due to etching of internal surfaces or development of porosity. If the weathering rate of fresh minerals is faster than that of already weathered minerals (White and Brantley 2003), despite the surface area of weathered rock grains being generally greater than that of freshly prepared samples, there must be a mismatch between total surface area and active surface area.

One method used to understand reactive surface area splits the total rock grain surface into two contributing fractions, the external surface area, and the internal surface area, which is that contained within pores, channels and voids within the rock grain. White *et al.* (1996) proposed an expression for the specific surface area of a spherical rock grain, measured by absorption, in terms of the external surface roughness, λ_{ext} , and the internal surface area, SSA_{int} , where d signifies diameter, ρ density and a is a dimensionless constant. Eqn 18 can be applied to varying grain sizes if surface roughness and internal surface area are independent of grain size:

$$SSA_{ads} = \lambda_{ext} \frac{a}{(\rho d)} + SSA_{int} \quad (18)$$

The two components contributing to total SA, described by White *et al.* (1996) may be of particular importance in field weathering studies as there may not be equivalent weathering of internal and external surfaces. Understanding the ratios of these two types of surface area and dissolution kinetics in these two weathering environments is essential and may contribute to the discrepancies observed between field and theoretical weathering rates (White and Brantley 2005). For example, internal surfaces may not be accessible by water, or larger organic molecules, or there may be transport limitation trapping solutes in pores. On the other hand, water retention in rock pores may promote dissolution by increasing mineral-water contact time. For these reasons, it is appropriate to use caution when comparing BET SA with dissolution rates (Brantley and Mellott 2000).

Kirstein *et al.* (2016) used only PSA and geometric calculation to estimate reactive surface area, assuming spherical particle geometry. Their reasoning behind this assumed that internal SAs measurable by BET will be occupied by solution that is saturated with respect to the products of carbonate dissolution. Solution within pores would therefore reach equilibrium with the carbonate pore walls and slow exchange of solution within rock pores would inhibit further dissolution. On the other hand, at the external surface of rock grains there is expected to be more exchange of solution and less transport limitation so the majority of weathering is expected to take place here.

4.4.2.5 Reduced reactive surface area in the field

Even where weathering minerals undergo identical preparation, there are a variety of reasons why reactive surface area may be different in the field than in laboratory studies. There is likely to be more physical weathering of test minerals as they are in close proximity to surrounding soil and rock particles and can be contacted by microorganisms and other soil fauna, whereas in a laboratory experiment, weathering minerals are typically surrounded only by fluid. Secondly, in the field, organic material and clays will sorb to weathering minerals, potentially reducing the surface area available for dissolution reactions. This has been suggested by an experiment by White and Brantley (2003) where the weathering rate of fresh Panola granite plagioclase was an order of magnitude higher than that of already weathered granite plagioclase in the laboratory when normalised for surface area and mineralogy.

To summarise, many factors may be contributing to the observed discrepancies between field and laboratory or theoretical weathering rates. These include both intrinsic reasons related to the weathering minerals themselves, in addition to

Chapter 4

differences in the external environment. One factor highlighted of particular importance is the reactive surface area of dissolving minerals which is currently not fully understood (Brantley 2003) and will be investigated in the remainder of this chapter using gas adsorption, BET, surface area and particle size analysis, PSA, techniques.

4.4.3 Evolution of surface area and particle size distribution during weathering

4.4.3.1 Unweathered carbonate particle size distribution

PSA showed unweathered chalk particles to have a log-normal distribution, peaking at 1110 μm diameter (Figure 4.10). This is within the range expected based on the sample preparation technique of sieving and collection of the fraction falling between 1180 μm and 500 μm sieves. A far smaller peak, representing 0.0005% of total sample volume, was consistently observed far to the left of the main distribution of large particles and is probably the result of dust particles that were not removed by repeated rinsing during preparation of rock grains for filling mesh bags.

Despite remaining within the quoted operating limits for the equipment (capable of measuring particles 10 nm - 3.5 mm), there is a slight overestimation of the size of the largest particles within each sample in this study. This may potentially be attributable to low numbers of particles at this extreme, clumping of rock grains leading to artificially high measurements; or deviation from the assumption that particles are approximately spherical when irregularly-shaped, angular particles cause unusual laser diffraction

4.4.3.2 Surface area of unweathered carbonate grains

Of the three predominantly calcite rock types, chalk was chosen for further analysis from and the other two calcite-containing rocks, oolite and marble, were not included in any further analysis. Marble was excluded as based on a preliminary analysis (Table 4.3) the grains were found to have very small surface areas, at the very lowest operating point of the BET equipment used. Chalk was used in preference over oolite for this fine scale surface area measurement as the physical structure of oolite is quite heterogeneous due to the presence of ooids and shelly fragments, also identified in thin sections (Section 5.3.1).

Of the rock samples measured, chalk and oolite had the highest initial surface areas prior to weathering (Table 4.3); dolomite had a lower surface area than chalk, despite its superficial similarity of appearance. Unsurprisingly, silicate rock grains had a lower surface area than all of the carbonates, except marble, which has a very crystalline texture, accounting for its lack of porosity.

4.4.3.3 Modelling log-Gaussian distribution of particles in chalk samples

To compare the distributions of the largest chalk particles before and after weathering, the main peak of each distribution (>240 µm diameter) was modelled by nonlinear log-Gaussian regressions. The original fits to this dataset were improved when interpolation was used to provide a more accurate estimation of mean particle size, and reduce the impact of using a small number of data points to model each curve. After this treatment there are still slight discrepancies between the actual distribution and that calculated. These which are likely to partly result from enforcing an artificial cut-off point at 240 µm between two overlapping distributions: that of particles generally >240 µm, and the tail of the distribution of those that would fall in the mid-size particle range of approximately 25-240 µm (Figure 4.11). The estimate for unweathered chalk is one of the most accurate, because the curve for large particles reaches 0% volume before the next curve begins, whereas, for most weathered samples the minimum point lies between 0.1-0.2% of total volume, where there is greater overlap between the distributions of mid and large-sized particles, as is illustrated in Figure 4.19.

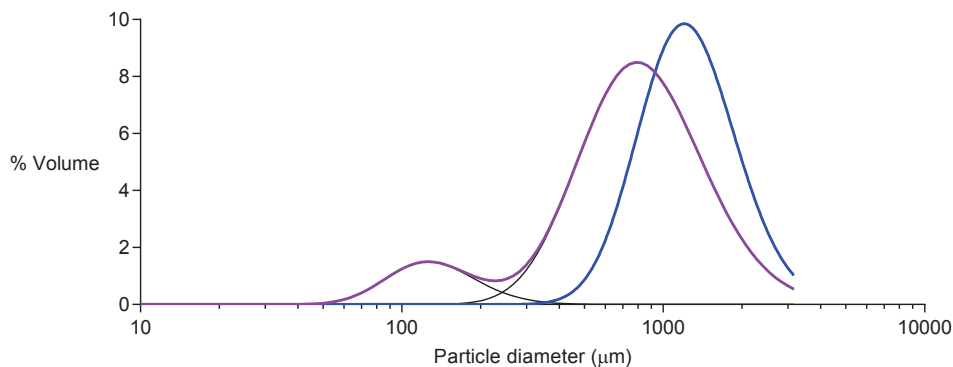


Figure 4.19. Illustration of uncertainty produced by overlap when modelling with log Gaussian curves for weathered samples where distributions of large and mid-sized particles overlap significantly. Weathered samples are represented in purple and unweathered samples with no overlap in blue. This figure does not include actual data, and the amplitude of the peak for mid-sized particles is exaggerated to demonstrate the effect of this overlap.

4.4.3.4 Silicate rock grain weathering behaviour

Increase in BET surface area of silicate rock grains after 14 months weathering

Unlike chalk and dolomite, silicate rock grains do not show an initial decrease in surface area. This may be due to only having data for samples recovered after 14 months, or may be because there were few easily weatherable surface features or rock dust attached to surfaces. It was easier to clean silicate rock grains during the preparation of mesh ingrowth bags than it was for dolomite, chalk and oolite. Distilled

Chapter 4

water used to wash rock grains usually ran clear after a few rinses, whereas it took far more rinses to reach the same result for the carbonate rocks.

4.4.3.5 Chalk and dolomite particle weathering behaviour

Over the course of weathering in the field, the surface area of chalk grains increases linearly in proportion to mass loss, after an initial sharp decline, accompanied by shifts in particle size distribution. This same pattern is seen during dolomite weathering, but not for the non-carbonate rock grains investigated.

This section compares measures of surface area and particle size distribution using different techniques, in order to evaluate possible carbonate weathering mechanisms that could produce these observations in the field. Possible weathering scenarios are illustrated in Figure 4.20 below.

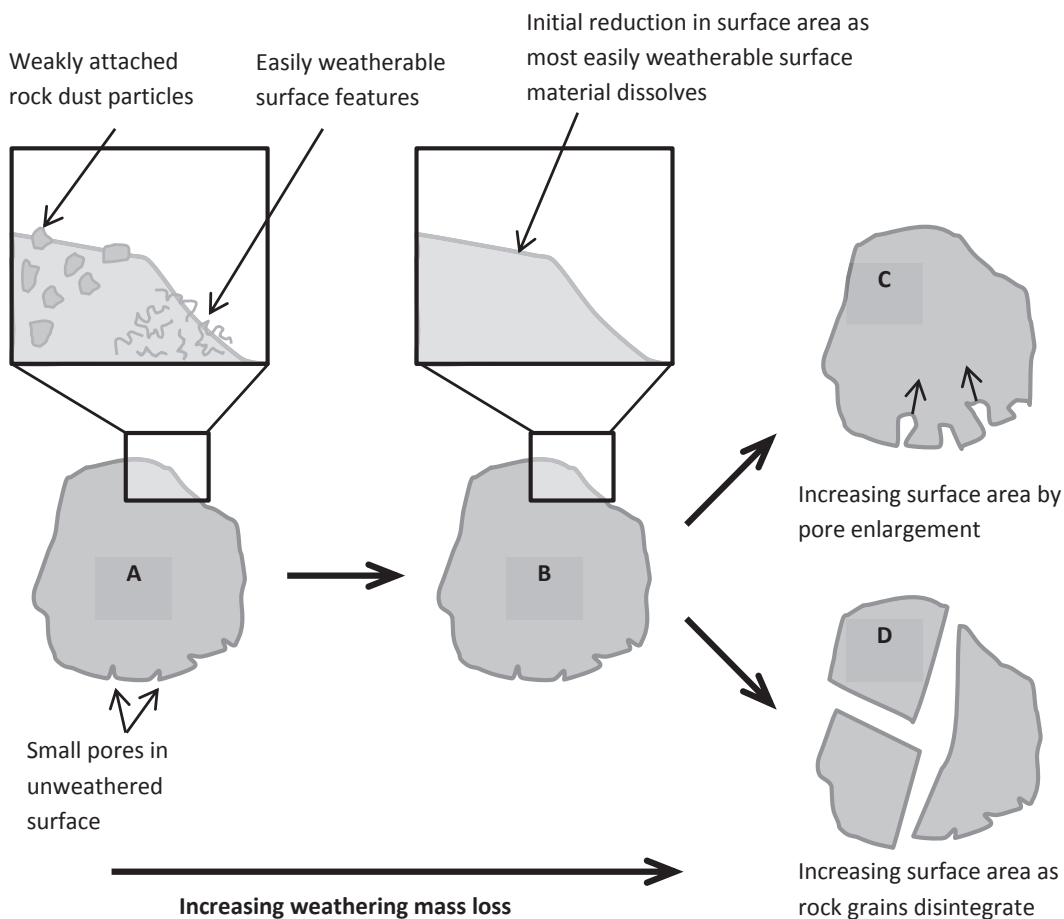


Figure 4.20. Illustration of possible weathering scenarios for chalk and dolomite rock grains, based on interpretation of BET surface area data. **A,B**) The initial reduction in surface is most likely due to dissolution of chalk/dolomite dust not removed by washing, or of easily weathered features with a high surface area, such as coccoliths. **B**) This results in a large reduction in surface area for a very small mass loss. In this study, this new state is called the 'effective initial surface area'. As weathering progresses, the surface area steadily increases. This is either due to **C**), an enlargement of surface area contained within pores; **D**) disintegration of rock grains or more likely, a combination of these processes.

Carbonate weathering rate dependence on soil acidity and grain surface area

Initial decline in chalk and dolomite surface area

When buried in the field, both dolomite and chalk samples exhibited an initial sharp decline in surface area, corresponding to minimal total mass loss. Laser diffraction PSA detected the presence of small particles 1.65 – 5.21 μm diameter in samples of unweathered chalk. This dust makes up only 0.0005% of the total sample volume, however, may well account for the sharp initial drop in chalk BET surface area, for minimal loss of sample mass (Figure 4.14A). For this reason, effective initial surface areas were calculated, to decrease the influence of this rapid initial loss of loosely attached dust on surface area results. It is likely that the initial striking decline in surface area occurs as a result of the most reactive sites on the chalk surface weathering. For instance through rapid dissolution of weakly attached carbonate dust or easily weatherable surface features (Figure 4.20) with a relatively high surface area susceptible to acidic weathering reactions.

Before burial, rock grains were thoroughly washed with multiple rinses of distilled water, until the water ran clear. If it is the case that the initial loss of surface area is due to the loss of weakly attached chalk dust, then a different preparation method would be recommended for future work. After thorough rinsing with distilled water, a wash with very dilute HCl might be appropriate, followed by further dH_2O rinses.

A similar effect was seen in a previous study by Kirstein *et al.* (2016). In the first batch of their dissolution experiments, carbonate rocks had been prepared with a size distribution of 0.5-1 mm diameter, and despite washing ultrasonically in acetone, some much finer particles (diameter 0.5-2 μm) were present. These fine particles contributed to the initial measured surface area, however, then rapidly dissolved, causing a sharp rise in pH from 4.7 to 6 and coincidentally reducing the geometric SA from 0.011 to 0.0057 m^2g^{-1} , or by 52% (Kirstein *et al.* 2016). This observation parallels one result of our current study where the reduction in BET surface area attributable to dissolving carbonate fines, $\Delta\text{SA}_{\text{fine}}$, was calculated (Eqn 19). For chalk this fraction equates to a 10.7 ± 0.4 % reduction in surface area and a more dramatic 42.8 ± 0.7 % for dolomite.

$$\Delta\text{SA}_{\text{fine}} = 1 - \frac{\text{Effective initial SA}}{\text{Total unweathered BET SA}} \quad (19)$$

Subsequent increase in carbonate surface area

After the initial decline, the linear increase in BET surface area with further weathering could be due to two processes; rock grains splitting to reveal unweathered surfaces; enlargement or roughening of existing pore or crack features, or formation of new ones; or some combination of these (Figure 4.20). The correlation between BET

Chapter 4

surface area and sample mass loss for chalk and dolomite show that on average, samples that have been in the soil longer have weathered more and have a larger surface area as a result of this.
















PSA data shows an accumulation of mid-sized and small particles that must have previously started as larger rock grains, accompanied by an overall shift in the peak of the log-Gaussian distribution of larger particles ($> 240 \mu\text{m}$) towards slightly smaller particles. This shift in distribution may be caused by slight weathering and shrinking of larger particles, or their splitting into fragments, whilst maintaining diameter $>240 \mu\text{m}$.

Particles in the small size category ($< 25 \mu\text{m}$ diameter) are likely to be remnants of broken rock grains and dust produced during particle splitting. There will also be uncertainties introduced by particles of fine organic matter that were weakly adsorbed to chalk particles during incubation in the field, as the rock grains were discoloured over the course of the field study (Table 4.10). However, only particles such as this that could be easily detached by dispersion in water would be measured by this PSA method. In addition to this, there is likely to be some flux of particles in this size group out of buried mesh bags, as these particles have a smaller diameter than the mesh weave of $35 \mu\text{m}$.

Mid-sized particles ($25\text{-}240 \mu\text{m}$) are small enough that they would have been removed by sieving during initial sample preparation, yet not so small that they could remain unnoticed and attached to larger particles, such as the very fine dust also seen in the particle size analysis of unweathered chalk. The peak for mid-sized particles is still small in comparison with that for large particles, and represents only up to 0.5% of sample material, by volume (Figure 4.11B). Prior to weathering, samples contained no mid-sized particles and these are probably produced by the splitting of larger particles that were originally in the main part of the PSA distribution.

Carbonate weathering rate dependence on soil acidity and grain surface area

Table 4.10. Samples of chalk, dolomite, oolitic limestone, marble and silicate rock grains before and after 7 and 14 months of weathering in the field for. Note discolouration of chalk particles during weathering.

	Unweathered	7-months	14-months
Chalk			
Dolomite			
Limestone			
Marble			
Silicate			

4.4.3.6 Effect of organic matter adsorption on carbonate weathering

Chemical stabilisation of SOM can reduce weathering through restricting access of weathering agents to mineral surfaces (Figure 4.21). Charge dense metal cations, including Al^{3+} and Fe^{3+} , can interact to form SOM-metal complexes bridging between negatively-charged organic matter and mineral surfaces, thus reducing availability of organic substrates for soil micro-organisms. High availability of trivalent Al and Fe cations have been found coincident with reduced microbial biomass and soil respiration (Hobbie *et al.* 2007).

Organic matter in soils flocculates due to electrostatic interactions; hydrogen bonding between carboxyl groups; and through weak, temporary, dipoles known as Van der Waals interactions. The tendency to flocculate strengthens at low pH and these processes eventually lead to aggregate formation. The permanence of aggregation is

Chapter 4

enhanced by high concentrations of cementing agents, such as Al, Fe and clays. It is also likely to occur in the vicinity of dissolving carbonates due to high Ca^{2+} and Mg^{2+} concentrations, in addition to trace levels of Al and Fe (Table A. 3).

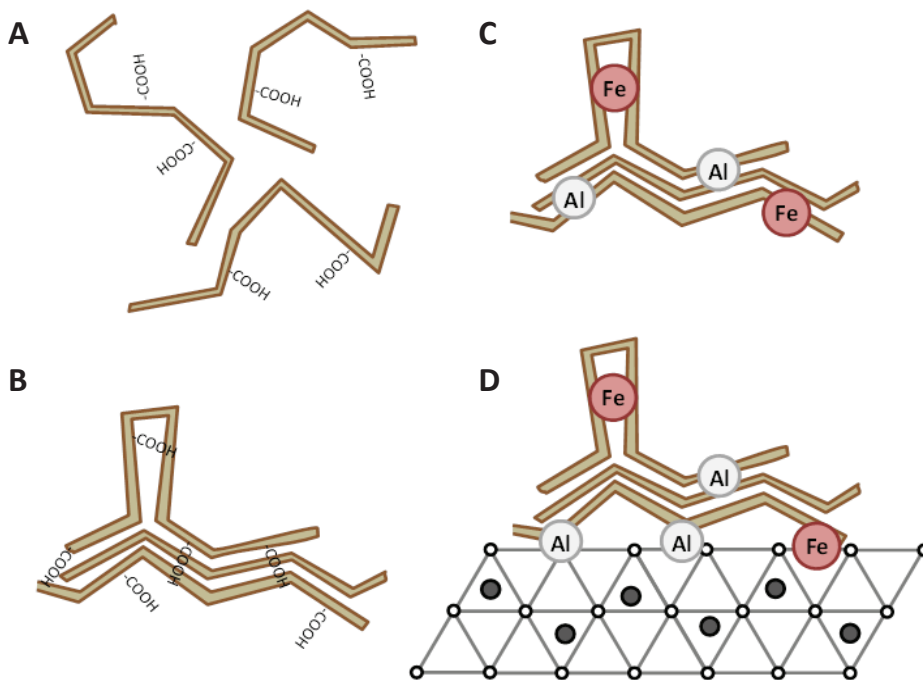


Figure 4.21. OM complexation by coagulation and cation bridging. **A)** Dispersed soil OM; **B)** Temporary flocculation of OM by hydrogen bonding; **C)** Stabilisation of microscopic aggregate by Al^{3+} and Fe^{3+} ; **D)** further stabilisation by bonding with clay minerals.

4.4.3.7 Chalk grain porosity measured by gas adsorption

Another factor that could contribute to an increasing surface area is an increase in pore size. Larger pores will have a greater internal surface area than small pores. However, if adjacent pores are enlarged, this is likely to result in them merging, and so, the overall increase in surface area may not be as great as there would be fewer pores in total. Whilst it was not possible to gather sufficient pore-size data using BET analysis (Figure 4.16), this hypothesis has been investigated by comparing surface area measures from BET gas adsorption with those calculated from the particle size distribution, assuming spherical particle geometry.

4.4.3.8 Comparison of measured BET and calculated PSD surface areas for chalk

Surface areas calculated from PSA results depend purely on particle geometry using the assumption of sphericity and do not take account of any porosity. BET surface area measurements, on the other hand, depend on measuring gas adsorption to all available surfaces, disregarding the size of individual particles in the sample. Because of these properties, a comparison of BET and PSA surface areas can give a

Carbonate weathering rate dependence on soil acidity and grain surface area

more complete understanding of particle weathering and apportion surface area changes to changes in particle size or surface topography.

If there is good correlation between particle size SA and that of BET SA for the experimental results in this study, and points lie close to a line $y = kx$ (Figure 4.22) which passes through the value for unweathered material, then it can be said that grain roughness or porosity does not change significantly throughout weathering, and surface area is mainly determined by particle geometry, given an appropriate scaling constant to account for surface texture. If, however, these two measures of SA do not follow a linear relationship, it would be expected that other changes happened to mineral surfaces during weathering, such as differing porosity. If the point lies above the line $y = kx$ (Figure 4.22) then the actual SA is lower than would be expected from that particle size distribution and particles are smoother, or have lost surface roughness. If points lie below this line, then particles are rougher than expected, or have increased porosity.

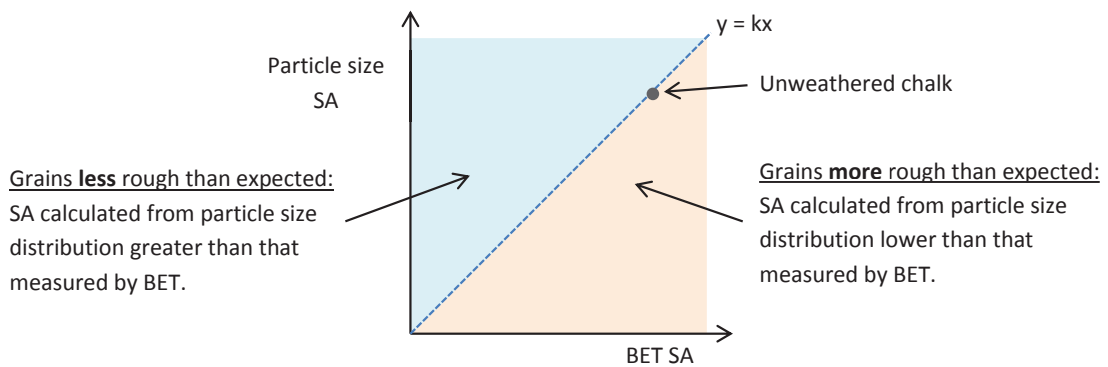


Figure 4.22. Theoretical relationship between surface areas measured by BET and calculated based on particle size distribution. $y = \text{BET SA}$, $x = \text{SA determined from particle size distribution}$ and k is a dimensionless roughness constant.

Whilst there is correlation between PSA and BET-derived surface areas for weathered chalk samples, data points are widely spread (Figure 4.18) and all lie above the line $y = kx$ defined by the relationship between PSA and BET measurements for unweathered chalk grains. This means that weathered chalk samples fall in the blue sector of the graph in Figure 7, and are smoother than expected based on their particle geometry. This will result in gradual particle shrinking and is partly due to the high initial BET surface area of unweathered chalk, which is predicted to be due to the presence of fine rock dust or easily weatherable surface features. PSD results give evidence for fine rock dust ($<25 \mu\text{m}$, which is present in both unweathered chalk and dolomite samples. As fine dust is also present in weathered chalk samples, despite them having typically higher PSD:BET surface area ratios, this might point towards the loss of easily weatherable surface features as a contributing factor in the initial high reduction in weathering chalk surface area.

Chapter 4

The correlation between BET and particle size distribution measures of surface area for chalk particles indicate that it is possible to estimate BET surface area based on particle size distribution statistics using the assumption of sphericity, given an appropriate roughness conversion factor. This roughness conversion factor differs from that which would apply to unweathered chalk, and a good approximation may be to use the 'effective initial surface area' calculated in Section 4.3.4.2. There is of course, quite a wide spread of data points for weathering chalk samples, where samples have either a higher or lower BET surface area than would be predicted from their particle size distribution, and therefore have either higher or lower surface roughness or porosity. For dolomite, however, there is no such correlation and it may be the case that there is far more variation in the surface topography of rock grains throughout weathering.

4.5 Conclusions

In this section we have seen that, as expected from theory, soil acidity is one of the main drivers of calcite weathering, especially during the initial few months of sample incubation in the field. This pattern is linked to the divide between EM and AM species, as both the most acidic soils and the highest weathering rates were observed below EM tree stands. Dolomite weathering rates, on the other hand, did not appear to be significantly affected by soil pH. When field experimental results were compared to those calculated theoretically from rate equations and constants, they were found to differ considerably. Dolomite weathering in the field did not exhibit the pH dependence predicted based on kinetic theory, but the most striking discrepancy was seen for calcite weathering. Here, the dissolution rate of calcite containing rock grains in the field, after normalising to BET surface area, was approximately 4 orders of magnitude slower than predicted by theory. The same effect has been seen in previous studies of silicate mineral weathering, and is most likely to result from the increased complexity of fluid chemistry in the soil environment compared to in the laboratory experiments from which the theoretical constants and relationships are derived.

After both 7 and 14 month harvests, weathering rate was proportional to BET surface area, however, given the strong correlation between sample mass loss during weathering, and surface area increase, it is more likely that higher weathering rates are driving large surface areas, and not the other way around. To investigate this hypothesis more fully, it would be necessary to compare weathering rates between samples of the same rock type with different initial grain sizes, as it is inappropriate to compare between the different rock types in this study given their different mineralogy and structure.

Upon initial burial, there was a rapid decline of chalk grain surface area, associated with very little mass loss, this is likely to be due to the dissolution of fine carbonate dust or easily-weatherable surface features. Following this, both BET and PSD surface area measurements show that the surface area of carbonate rock grain samples increases as they lose mass. This is contrary to the initial hypothesis that surface area would decrease throughout weathering. Two possible explanations for the observed SA changes were either that particles split, or that there was an increase in surface roughness or porosity. The PSA results show an accumulation of small and mid-sized particles, indicating that there is a degree of rock grain splitting during weathering. For chalk, there is good correlation between PSD and BET surface areas, suggesting that evolution of surface topography is consistent between samples under different tree species. However, a more reliable method of quantifying rock grain

Chapter 4

porosity, such as further BET analysis, would provide more information and could confirm this. Results from this section confirm that for chalk there is both shrinking and fragmentation of chalk rock grains during weathering in forest soils.

Although carbonate rock grain surface areas increase during weathering, this does not necessarily lead to a positive feedback on rates. Whilst there may be a greater total SA, the proportion of this which is in contact with water-mineral contact and available for further chemical dissolution may be reduced. Processes that may decrease surface reactivity over time are likely to be especially prevalent in a field environment with complex fluid chemistry. Reduced reactivity may be realised partly through preferential dissolution of the most easily weatherable features, rendering the remainder of the mineral surface relatively less soluble. Another contributing factor could be the occlusion of surfaces by the adsorption of clays, iron, Al-oxides organic compounds. These may form a barrier to the transport of reagents to the minerals surface or dissolution products from the surface, thus reducing reactivity.

Chapter 5

Physical surface alteration of carbonate rocks during weathering

5.1 Introduction

Most chemical weathering by mycorrhizal fungi (reviewed in Chapter 1) is thought to be only effective in immediate proximity to hyphae, the area known as the mycorrhizosphere. In this region, chemical weathering exudates, including LMWOAs and chelating anions, may reach high enough concentrations to promote mineral dissolution via localised secretion or through biofilm formation.

This chapter focuses on the weathering dynamics of carbonate and silicate mineral surfaces over the course of a field experiment at Bedgebury Pinetum. In particular, I investigate the effect of tree-mycorrhizal functional group on mineral surface alteration during carbonate weathering. The first part of this chapter gives a brief overview of the field experimental setup at Bedgebury Pinetum. This is followed by a description of experimental techniques and investigation addressing methodological limitations within this, and similar studies.

SEM and VSI analysis are used to observe and quantify bulk surface weathering characteristics, and the formation of putative hyphal channel features described in the introduction to this chapter. SEM imaging provides insight into in-situ hyphal colonisation and surface modification of the same rock grain samples used in different analyses throughout this thesis. VSI analysis maps mineral surface topography, giving a more easily quantifiable measure of surface characteristics. However, VSI measurements must be performed on specially-prepared mineral chips, making this less representative of bulk mineral weathering within in-growth mesh bags. Both techniques are used to provide hyphal width measurements, and the relative merits of these two methods discussed

Chapter 5

5.1.1 *The role of biofilms in mineral weathering*

Both AM and EM fungi radiate through the soil from host plant root tips, in a mesh-like network of hyphae, surrounding rock particles. Physical contact between rock grains and the mycelium can promote mineral weathering by a variety of mechanisms reviewed in detail in Chapter 1. In the vicinity of hypha, weathering may be enhanced by development of a biofilm or localised micro-environment favourable to mineral dissolution.

EM fungi colonising mineral surfaces produce a range of exudates, both LMWOAs (reviewed in Chapter 1, Section 1.5.3), and a wider group of higher molecular weight compounds collectively known as Extracellular Polymeric Substances (EPS). When a hyphal tip contacts a mineral surface it produces exudates, causing a gradual accumulation of EPS along the hyphal-mineral interface. EPS can extend from the hypha by up to 6 μm in a layer approximately 30 nm thick. Adjacent accumulations of EPS can fuse to form a more extensive organic layer, or build up over successive generations of hyphal colonisation. This layer has been observed using AFM on biotite and chlorite in microcosm studies containing *P. sylvestris* seedlings inoculated with *P. involutus* (Saccone *et al.* 2012; Gazzè *et al.* 2013).

The biofilm has several roles, reviewed by Gazzè *et al.* (2013); these include hyphal adhesion; buffering from dehydration by providing of a water reservoir; nutrient accumulation and also protection from a range of physiochemical changes and biocides. The EPS layer is predicted to enhance mineral weathering of silicates both by lengthening water-mineral contact time and accumulating of LMWOAs and other weathering agents close to the mineral surface. The same is likely to be the case for mycorrhizal carbonate weathering, however, this has not hitherto been investigated, which leads to the first hypothesis of this chapter.

Research hypothesis 1

Carbonate weathering is promoted by direct contact with mycorrhizal fungal hyphae and associated biofilm formation

5.1.2 *Mycorrhizal hyphae can etch channels on mineral surfaces*

Fungal tunnelling into rock grain interiors may allow hyphae exclusive access to inorganic nutrients, however, due to its energy-intensive nature, this process contributes only a small proportion to total mineral weathering (Smits *et al.* 2005; reviewed in Chapter 1, Section 1.5.1.1). Where possible, it may yield better returns on energy invested for mycorrhizas to source nutrients from more accessible external surfaces of rock grains. This may lead to the formation of surface weathering channel

features, which have been seen on a range of different carbonate (calcite marble) and silicate minerals (chlorite, biotite, muscovite). The main evidence for these features on carbonates is from the work of Rosling (2003), who identified channels proceeding from colonising hyphae, on a polished marble surface after 4 months incubation in a *H. crustaliniforme*, *P. sylvestris* microcosm experiment.

Similar surface channels have been noted for a variety of silicates in weathering experiments at a range of scales. In the laboratory, trenching of biotite surfaces has been seen after incubation in liquid culture experiments with EM *Suillus tomentosus* (Balogh-Brunstad *et al.* 2008) and on both chlorite and biotite in *P. involutus* microcosms growing with EM tree seedlings (Bonneville *et al.* 2009; Gazzè *et al.* 2012). Etching and dissolution of naturally weathered K-feldspars colonised by fungal hyphae, and other microbial fragments, was observed using Transmission Electron and Focussed Ion Beam Microscopy (Lee *et al.* 2007), however it is uncertain whether micro-organisms associated with mineral surfaces exert much influence in these laboratory bioweathering studies (Ward *et al.* 2013). similar processes have been studied in the field, under both AM and EM forests, on a variety of silicate minerals (Hoffland *et al.* 2003; Smits *et al.* 2005; Quirk *et al.* 2012; Koele *et al.* 2014).

Quirk *et al.* (2014) reported the formation of channels measuring 2-5µm wide on muscovite chips exposed to the rhizosphere of AM tree saplings. In actuality, this range might be wider, and will no doubt, be affected by specific mycorrhizal species, in addition to other saprotrophic fungi found in the soil. The exact width of channels will likely be influenced by the incubation time of each mineral chip in the rhizosphere, as well as the nutrient demand of host plants and potential requirements for mineral weathering. There is some indication that trenching provides a larger contribution to total weathering under EM than AM tree species (Quirk *et al.* 2012, 2014), however, this has been investigated using a limited range of tree species. The second part of this chapter seeks to expand this dataset, leading to our second hypothesis:

Research hypothesis 2

Mineral weathering by surface alteration including trenching or channelling is more prevalent under EM than AM species

Chapter 5

5.2 Methods

5.2.1 *Field experiment design*

To investigate changes in mineral surface features over the course of weathering, a field experiment was set up at Bedgebury Pinetum, Kent, UK. Hyphal in-growth bags containing pre-scanned mineral chips alongside crushed and sieved silicate rock samples (Particle size of 0.5–1.18 mm diameter; total mass 2 g) were incubated for 7 months under stands of mature trees at Bedgebury Pinetum. Tree species were selected to represent the four main functional groups found in northern Hemisphere forests: AM gymnosperms, AM angiosperms, EM gymnosperms and EM angiosperms, and surface weathering quantified under each. Further details on experimental setup and sampling can be found in Section 2.7.1.

5.2.2 *Mesh bag pH*

Quartz rock grains (1 g, N = 3 per tree species) recovered from mesh bags containing VSI chips were mixed with 10ml UHP dH₂O and pH measured (Jenway 3540 pH meter; calibrated at pH 4, pH 7 and pH 10).

5.2.3 *Rock thin sections*

For each rock type used to make mesh in-growth bags, thin sections were prepared (Ocean and Earth Science, National Oceanography Centre, University of Southampton) and viewed under plain polarised light (PPL) and crossed polars (XPL) using a petrographic microscope (Leica DM2700 P; Leica Microsystems (UK) Ltd, Milton Keynes, UK).

5.2.4 *SEM imagery*

Freeze-dried weathered carbonate rock grains, recovered from mesh in-growth bags after 3 months burial under stands of mature trees at Bedgebury Pinetum, were selected for SEM imaging. Rock grains were mounted on a graphite SEM stub, taking care to handle gently with fine forceps to avoid dislodging surface material. Prior to imaging, samples were gold sputter coated, no other pre-treatment was performed.

Samples were imaged using an electron beam with 20kV accelerating voltage, at 50-8000× magnification in secondary electron imaging mode (Philips XL-20, Philips, Eindhoven, Netherlands; Department of Biomedical Science, Sheffield University). Image processing was performed in Corel PHOTO-PAINT 9 (Corel Inc. 2000, Ottawa, Canada).

5.2.4.1 Hyphal width measurements from SEM images

Hyphal width data were extracted from SEM images using ImageJ software (Schneider 2012). Hyphal cross sections were produced from transects spanning the shortest possible dimension across each hypha. A plot of the grey values for each profile was calculated in ImageJ, and the width of the hypha extracted as in Figure 5.1. For each of 4 images, 10 measurements of hyphal width were made and an average calculated (N = 4).

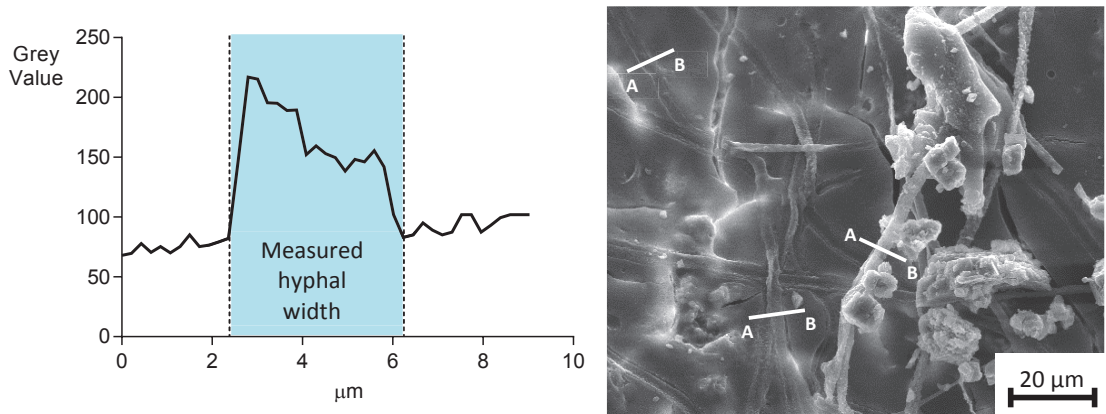


Figure 5.1. Example of method used to extract hyphal width data from SEM images. **A)** Profile of grey values for one transect with measurement used for hyphal width shaded in blue. **B)** Example transects across hyphae on an image of a dolomite grain buried below *L.decidua*, 800× magnification.

5.2.5 Vertical scanning interferometry (VSI)

5.2.5.1 VSI Theory

To quantify weathering features and hyphal channels seen in SEM images, changes in mineral surface topography were examined using VSI imagery (Figure 5.2; Wyko, NT 9100; Bruker, WI, USA). VSI allows for non-contact investigation of surface topography at the μm scale using laser scanning to chart surface heights. This technique has previously been used to measure biological dissolution of mineral surfaces by mycorrhizal fungal hyphae (Quirk *et al.* 2012, 2014), and by etch-pit forming bacterial siderophores (Buss *et al.* 2007).

During VSI measurements, a beam of white light is passed through a neutral density filter and split. Half the beam reflects from the sample and the remainder from a reference mirror, causing the two beams to have slightly different intensity modulation. Each scan starts above focus and as the objective descends vertically, the resulting interference signal between the split beams is measured at each point. VSI is an appropriate method for analysing quite rough surfaces, as the maximum vertical range for VSI scans is approximately 2 mm, with a vertical scan error of <0.1 nm (Wyko NT 9100)

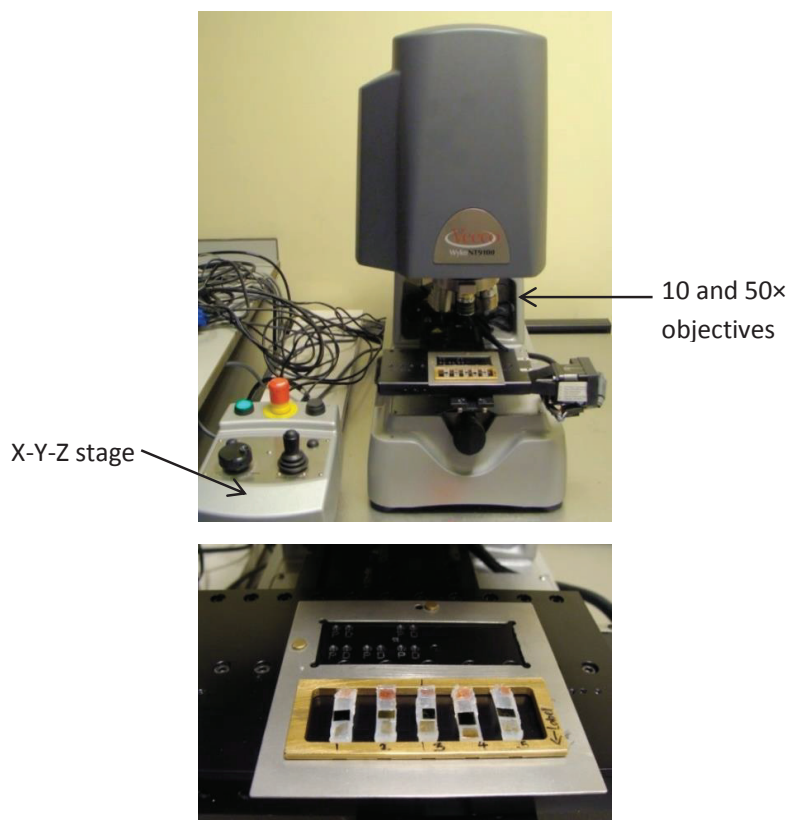


Figure 5.2. Vertical scanning interferometry (VSI) of minerals surfaces. **A)** WYKO NT 9100 VSI analyser. **B)** 5 VSI slides mounted on stage below objective. Photos by Joe Quirk, Sheffield

5.2.5.2 Mineral chip preparation for VSI analysis

Cleaved muscovite, calcite dolomite and polished marble (approx. 4×4 mm; Table 5.1) were mounted in silicone and backed with a labelled glass slide (26×4 mm; Figure 5.3). After drying, mineral chips were checked individually by gentle probing with a blunt plastic tip to ensure they were firmly embedded in silicon, before cleaning with lens polishing cloth and dilute detergent (1% SDS) to remove surface dust. This method has been used before and shown to have no damaging effect on the surface of muscovite (Quirk 2012). Pre scanned slides were sealed in mesh ingrowth bags ($35 \mu\text{m}$ pore size) containing 1.0 g crushed and dH_2O rinsed quartz ($0.5 - 1.18$ mm grain size). After recovery, slides were not cleaned before re-analysis to avoid damaging any delicate surface features or dislodging adhered hyphae if present.

Physical surface alteration of carbonate rocks during weathering

VSI analysis requires very smooth, flat surfaces, so it was not always possible to use the same rock types as elsewhere in this study. Rock grains prepared for in-growth mesh bags are all different sizes and shapes, within the range determined by sieving (500-1180 μm diameter), with irregular sides as a result of rock crushing sample preparation. The exception to this was marble, which used the same rock as in the mesh bags, as this was originally a polished marble slab. Intact chips with polished surfaces were used for VSI slide preparation. Whilst marble surface prior to weathering looks shiny and smooth to the naked eye, under magnification with VSI, the polishing is obvious as straight sided scratches and grooves.

Table 5.1. Origin of rocks and minerals used for VSI analysis.

Chip	Description and origin	Photo	Supplier
Muscovite	Muscovite mica, Norway		Geology Superstore http://www.geologysuperstore.com/
Calcite	Cubic cleavage, white, Morocco		Geology Superstore http://www.geologysuperstore.com/
Dolomite	Clusters of rhomboidal, pink dolomite crystals, Morocco		Geology Superstore http://www.geologysuperstore.com/
Marble	White, Carrara		Pisani, Matlock

5.2.5.3 VSI scanning methodology

Duplicate scans of two well-spaced areas of each mineral chip were performed, in case one scan area could not be re-identified after weathering (N = 2 for each mineral per slide). The location of each scan was recorded in a stage file so that the VSI microscope stage could be automatically adjusted to locate the same point in later analysis of the same VSI slide. When re-locating scan areas some fine manual adjustment was usually required, because although the stage usually adjusted to very close to the original scan area it was necessary to ensure the images were exactly aligned. This was especially the case after weathering where some mineral chips had moved slightly or been dislodged.

Chips were first scanned at 100 \times magnification (620 \times 464 μm scanned area), and then at 500 \times (126 \times 94 μm scanned area) in the centre of the area recorded at 100 \times .

Chapter 5

Scanning at lower magnification was to aid relocation as there are often few recognisable features at 500×. The 100× scan covers a larger area, so there is more chance of locating the same area of rock surface (Figure 5.4). All VSI scans for characterisation of mineral surfaces, and associated measurements were collected using Vision software package (Vision 4.10; Veeco Instruments Inc; Woodbury, NY, USA).

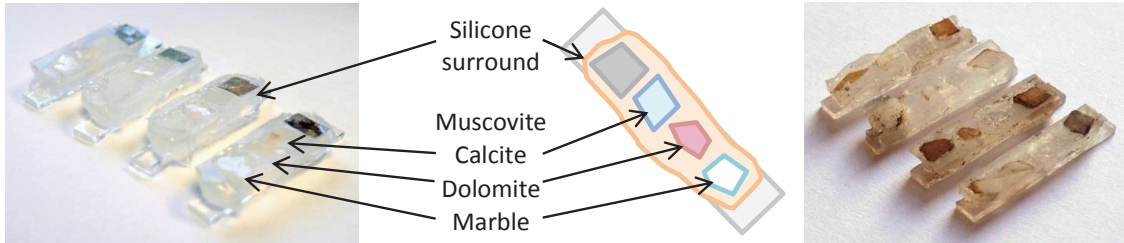


Figure 5.3. Pre-scanned VSI chips (26 × 4 mm) with muscovite and 3 carbonate mineral chips embedded in silicone. VSI slides showing discolouration after 6 months burial shown on right.

5.2.5.4 Roughness measurement

To quantify changes in bulk surface characteristics throughout weathering, surface roughness of mineral chips was characterised by VSI at 500× magnification. R_a , average roughness, and R_q , roughness quotient, are both measures of surface roughness that can be calculated during VSI analysis. R_a (Eqn 20) is the arithmetic mean of deviation from the mean height of the surface, whereas R_q is the geometric mean, or root mean squared (Eqn 21) of the same height deviation, and is sometimes referred to in literature as R_{RMS} . For historical reasons, R_a is the most frequently used roughness measure, and the one used in this study.

$$R_a = \frac{1}{n} \sum_{i=1}^n |x_i - \bar{x}| \quad (20)$$

$$R_q = \sqrt{\frac{1}{n} \sum_{i=1}^n (x_i - \bar{x})^2} \quad (21)$$

Physical surface alteration of carbonate rocks during weathering

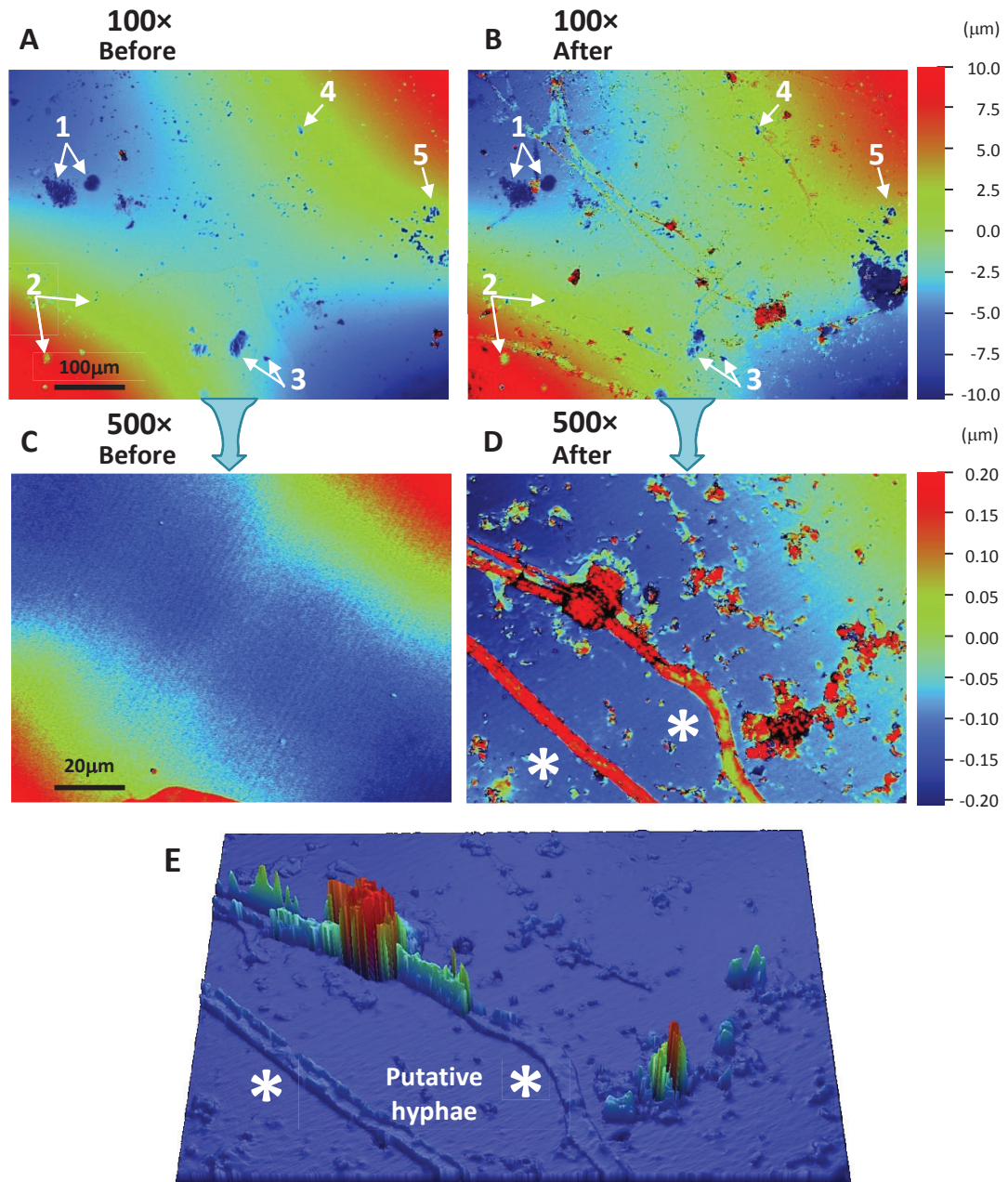


Figure 5.4. VSI scans of one muscovite chip before and after burial at Bedgebury. 10× scan **A)** before, and **B)** after weathering used to ensure the same area is used for analysis on both occasions. Scans are annotated 1-5 to demonstrate the type of features used to ensure correct relocation. 50× scans made in the centre of the larger, 10× region, **C)** before and **D)** after weathering. These contain a much higher level of detail and are used for quantitative analysis. Surface features that potentially correspond to the presence of hyphae are identified by asterisks in D and E) a 3D interpretation of 50× scan post-weathering to show putative hyphae standing slightly proud of mineral surface. Red/green regions of this plot are spikey due to poor digital rendering of very raised (or sunken) regions. Examples used in this figure are pre- and post-scans of VSI chips incubated under *L. tulipifera*.

Chapter 5

Errors produced by mineral chip misalignment

For muscovite, VSI scanning is likely to underestimate roughness changes over weathering due to imprecise pre-scan data. Slight misalignment of some mineral chips means that the surface is not exactly horizontal and the sample may be slanted with respect to its mounting. Where this is the case, sometimes the resulting scan appears as though overall sample depth is greater than in reality due to interference from underlying mineral layer/s. To reduce this, scan length was decreased for these samples to minimise interference, but it occasionally still occurs, both before and after weathering. Where this is the case the surface appears rougher than it actually is (Figure 5.5).

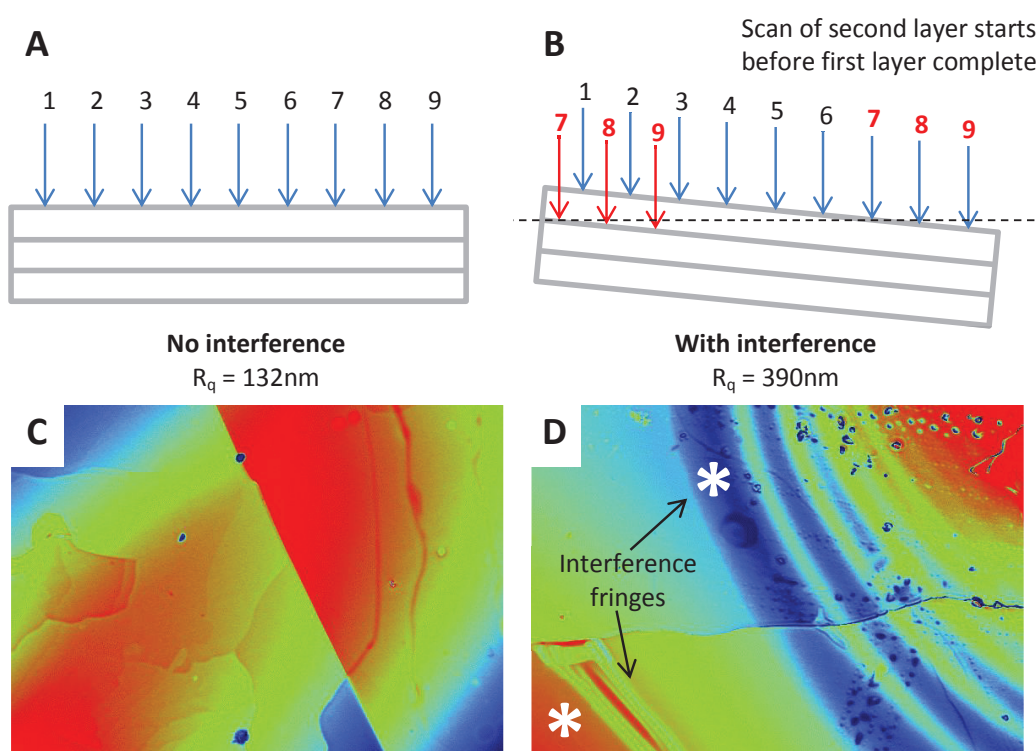


Figure 5.5. Illustration of interference in VSI scans due to commencement of VSI scanning of underlying mineral layer/s before scan of top layer is complete. This was particularly an issue for muscovite samples with transparent layered mineral sheets. **A)** Scan of flat mineral surface, the entire scan of only the top layer is completed, represented by blue arrows 1-9. **B)** Slanted mineral, scan of underlying mineral layer commences before scan of top layer is completed (red arrows 7-9), making sample surface appear rougher than in reality. Corresponding examples of VSI scans of unweathered muscovite **C)** without interference, R_q (roughness quotient) = 132 nm and **D)** with interference fringes, R_q = 390 nm. In D, asterisks indicate interference fringes. All scans performed at 500 \times magnification.

5.2.5.5 Quantifying biological surface weathering features

Surface weathering features potentially produced by hyphae were identified based on their morphology. Candidates for biological features were distinguished from scratches made by mechanical abrasion using the conditions that they must have some curvature and not lie parallel to other scratches or grooves (Figure 5.6).

Physical surface alteration of carbonate rocks during weathering

Cross sections of both curved channels and remaining hyphal fragments were measured from 4-6 evenly spaced transects crossing each hyphal trace identified in VSI scans of muscovite (Figure 5.14A). The total number of transects used was variable and depended on the length of feature available to measure (Figure 5.7; Figure A. 5). Average track width was defined as the distance between the first point where there was a sharp increase in gradient to the final point where there was a sharp gradient decrease, thereby spanning the entire width of a hypha. Start and end points were identified as the first and last significantly non-zero values from the first differential of the x-y curve. Measurements of hyphae and channels were made from multiple VSI scans of weathered muscovite and overall average calculated.

Hyphal cross sectional area is calculated as the integral of the curve of the hyphal transect. The surface of the mineral chip was used as a baseline for integration of each curve. The baseline value was defined as the average of the first and last 5 values of each transect, which extended onto the chip surface either side of the hypha. Channel depths are calculated from the cross sectional area and channel width, and as such, represent the average channel depth across its profile.

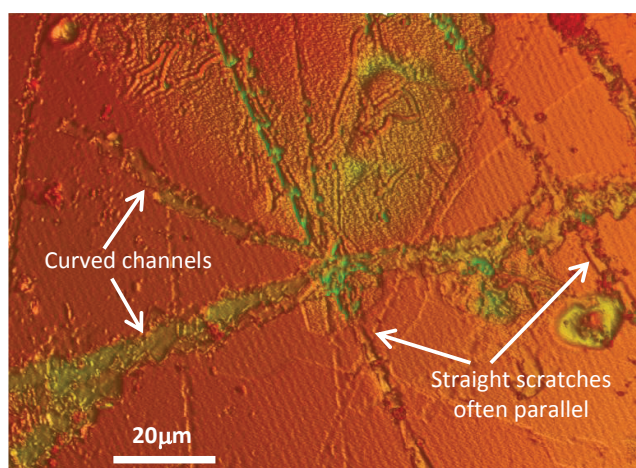


Figure 5.6. Identifying curved channels of possible biological origin and straight scratches from mechanical abrasion on muscovite chip surfaces after weathering. VSI scan used in this example is from a VSI chip buried under *Q. petraea* under 500× magnification.

5.2.6 Software and statistics

Statistical analyses were performed using R (R version 3.1.2, 2014), RStudio (Version 0.98.1091, 2014) and GraphPad Prism (Prism 6 for windows; version 6.05; GraphPad Software Inc.; La Jolla, CA, USA). When processing roughness quotient data from VSI scans, it was necessary to log transform data prior to statistical analysis as raw data were strongly negatively skewed. After log transformation, all datasets are normally distributed (D'Agostino & Pearson omnibus normality test; $P > 0.05$).

5.3 Results

5.3.1 Unweathered Thin Sections

Investigation of rock thin sections using a petrographic microscope showed the chalk, dolomite and marble used in this study to be relatively homogeneous. Marble was almost entirely composed of angular calcite crystals, which reflects its chemical composition determined by XRF (Table A. 3), which contained 54.07% CaO by weight, equating to over 96% calcite. The remainder of mass is split between SiO₂ and MgO, which both represent <1% of the marble by mass. These might form part of the cement surrounding each calcite crystal, which can be seen under PPL (Figure 5.7A). Chalk contained numerous Radiolaria, seen as small white discs in both PPL and XPL (Figure 5.7B). Dolomite was relatively uniform in texture with few crystals measuring >100 µm across, and occasional calcite crystals marked by faint red staining.

The oolitic limestone crushed for this study had a more varied structure and contained numerous shells and ooids (Figure 5.8A). Partial and complete bivalves were the most common shell component (Figure 5.8B), and these measured up to 5 mm in length. Gastropods were also present and one is shown in Figure 5.8C. Most shells had undergone secondary mineralisation of calcite, which could be identified from the large calcite crystals within the shell boundary. When this rock was crushed to prepare mesh in-growth bags, most of the shells will have been broken and this detail lost as rock grains were sieved to 0.5-1.18 mm diameter.

The silicate rock used in this study is most likely to be an arenite with a high proportion of quartz (>75% SiO₂ from XRF analysis, Table A. 3), with occasional crystals of plagioclase, microcline and muscovite mica (Figure 5.9). Mica is identifiable by its high birefringence, plagioclase has parallel black and white stripes under XPL, however, some crystals are quite highly weathered and these parallel lines are less distinct. Microcline crystals look very similar to those of plagioclase, with white and black banding, but with some crosshatching under XPL.

Physical surface alteration of carbonate rocks during weathering

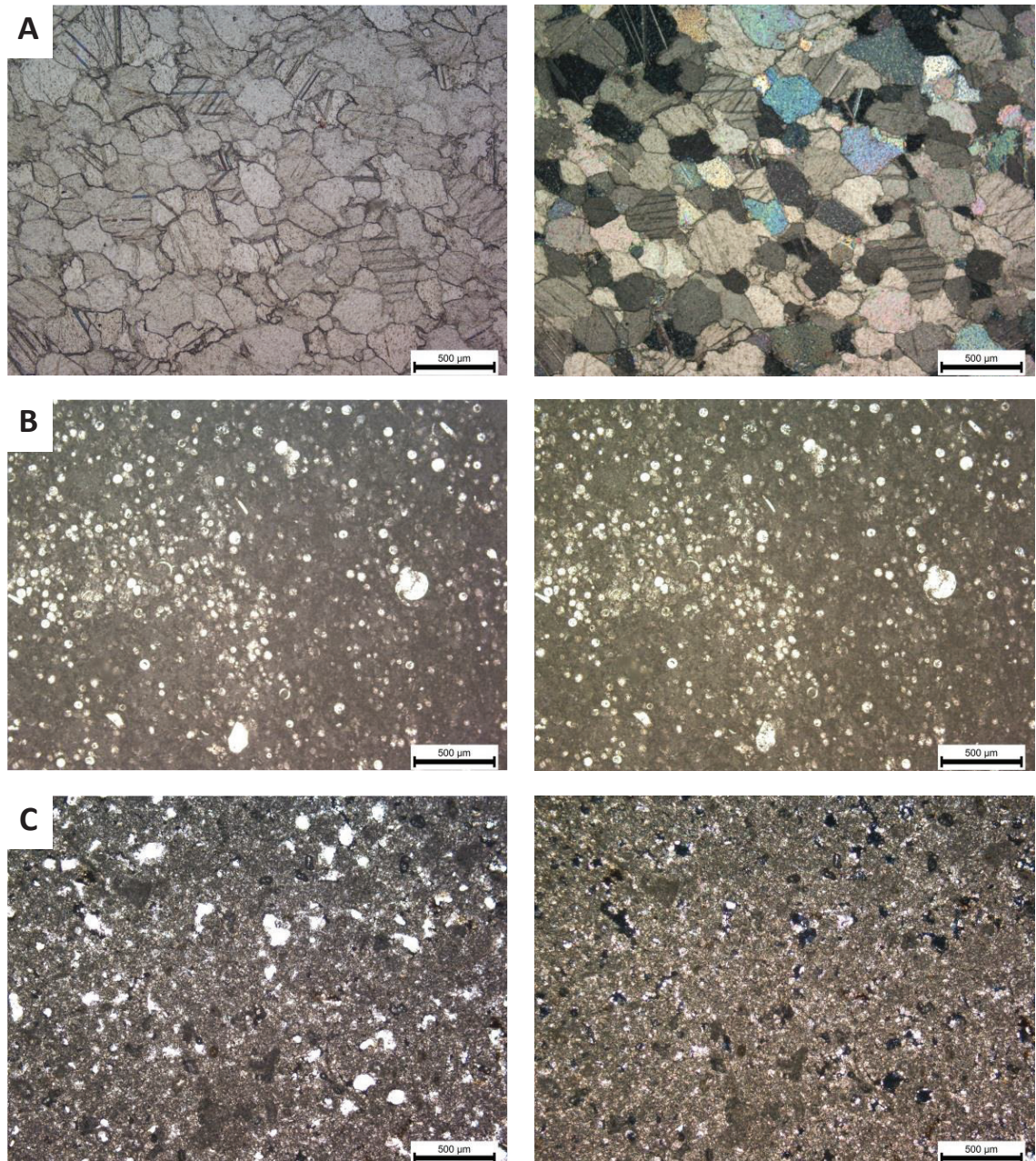


Figure 5.7. Thin sections of unweathered **A)** marble, **B)** chalk and **C)** dolomite imaged using plain polarised light, PPL (left panel) and cross polarised light, XPL (right panel) at 50× magnification.

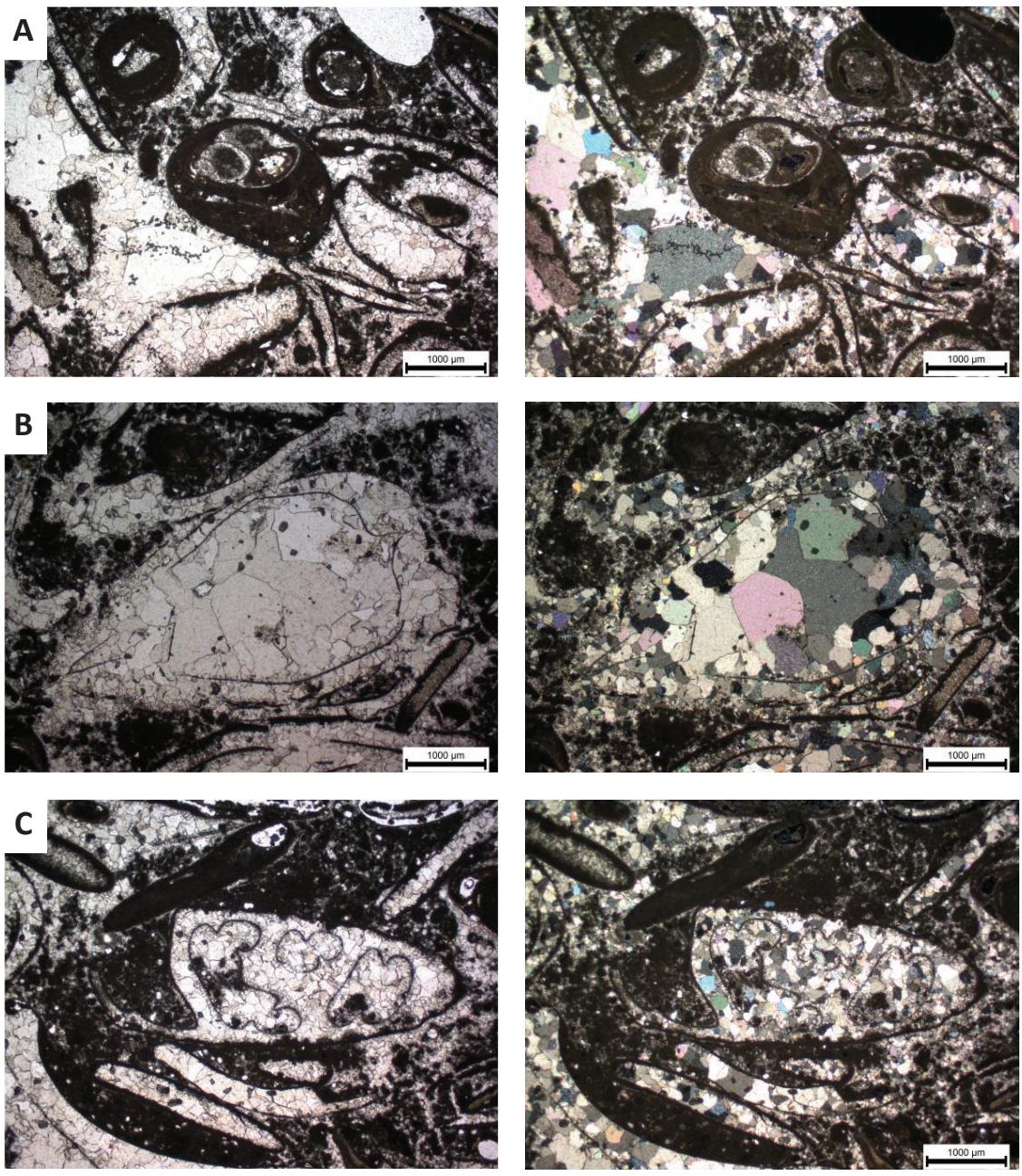


Figure 5.8. Thin sections of unweathered oolitic limestone used in this study, with images of representative features in PPL (left panel) and XPL (right panel) at 25× magnification. **A)** Ooids and shell fragments, one oolite has formed around a small shell. **B)** Bivalve shell where calcite has been replaced by secondary mineralisation in-situ, with one micritised shell fragment in bottom right corner. **C)** Gastropod undergone secondary mineralisation of calcite.

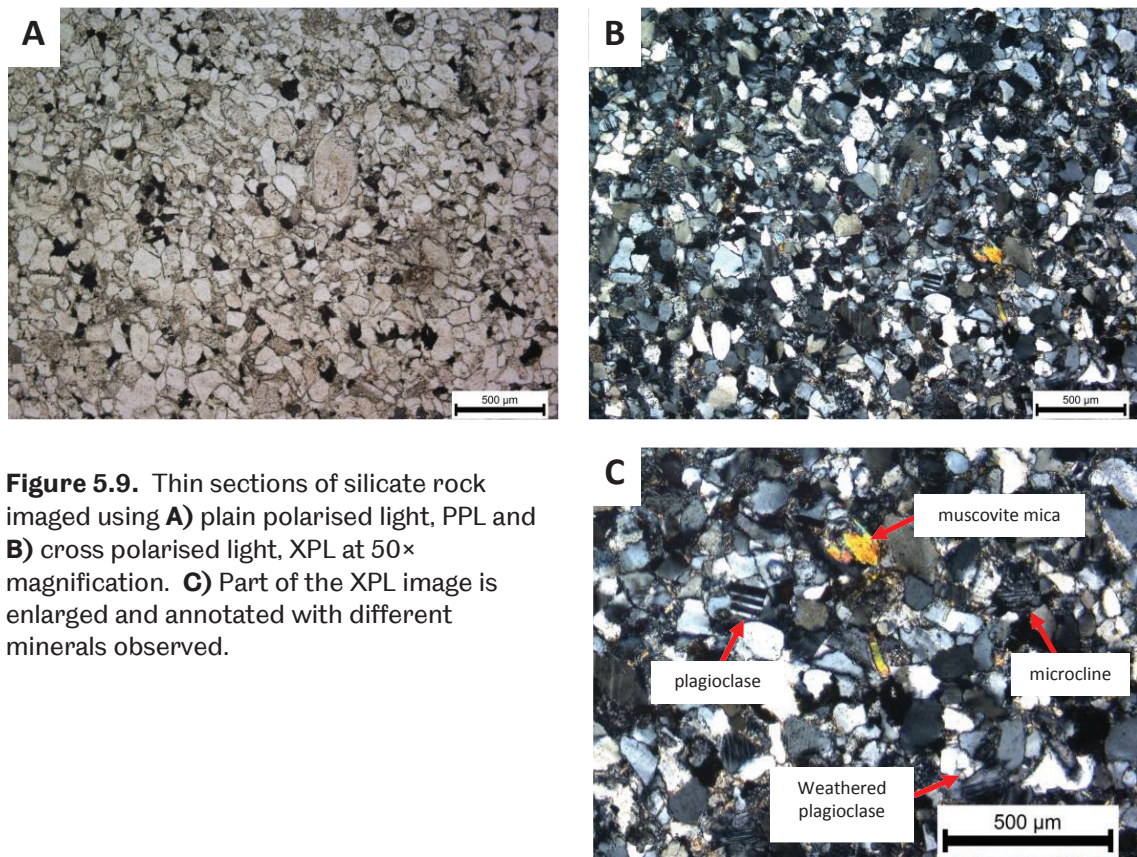


Figure 5.9. Thin sections of silicate rock imaged using **A)** plain polarised light, PPL and **B)** cross polarised light, XPL at 50× magnification. **C)** Part of the XPL image is enlarged and annotated with different minerals observed.

5.3.2 SEM Imagery of weathered carbonates

Carbonate grains imaged after 3 months burial beneath mature tree stands were generally surrounded by material of biological origin, hyphae and possibly other soil micro-organisms. Most of this material took the form of long strands, which were either loose, surrounding rock grains (Figure 5.10A) or formed a mesh in close contact with the rock surface (Figure 5.10B).

After recovery from the field, hyphae were common on carbonate rock grain surfaces. These were identified as strands with approximately constant width, some of which had roughly cylindrical shape. Other organisms did not have constant width, appeared flatter, and were sometimes pattered with surface protrusions (Figure 5.11). These were probably also hyphae, but may have been affected by sample desiccation and the harsh conditions during SEM imaging. The width of hyphae determined from SEM imagery was $3.36 \pm 0.52 \mu\text{m}$ (mean \pm SEM; N = 4 SEM images, 10 hyphal measurements taken from each; Figure 5.1). Hyphal diameters sometimes change across a junction, and branching hyphae are often slightly narrower.

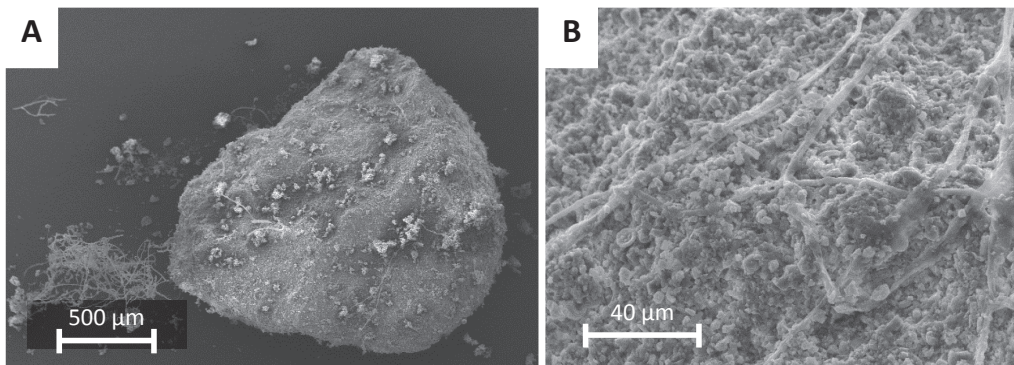


Figure 5.10. SEM images of chalk grains showing **A)** loose hyphae at 50× magnification and **B)** mesh of hyphae attached to rock surface at 800× magnification.

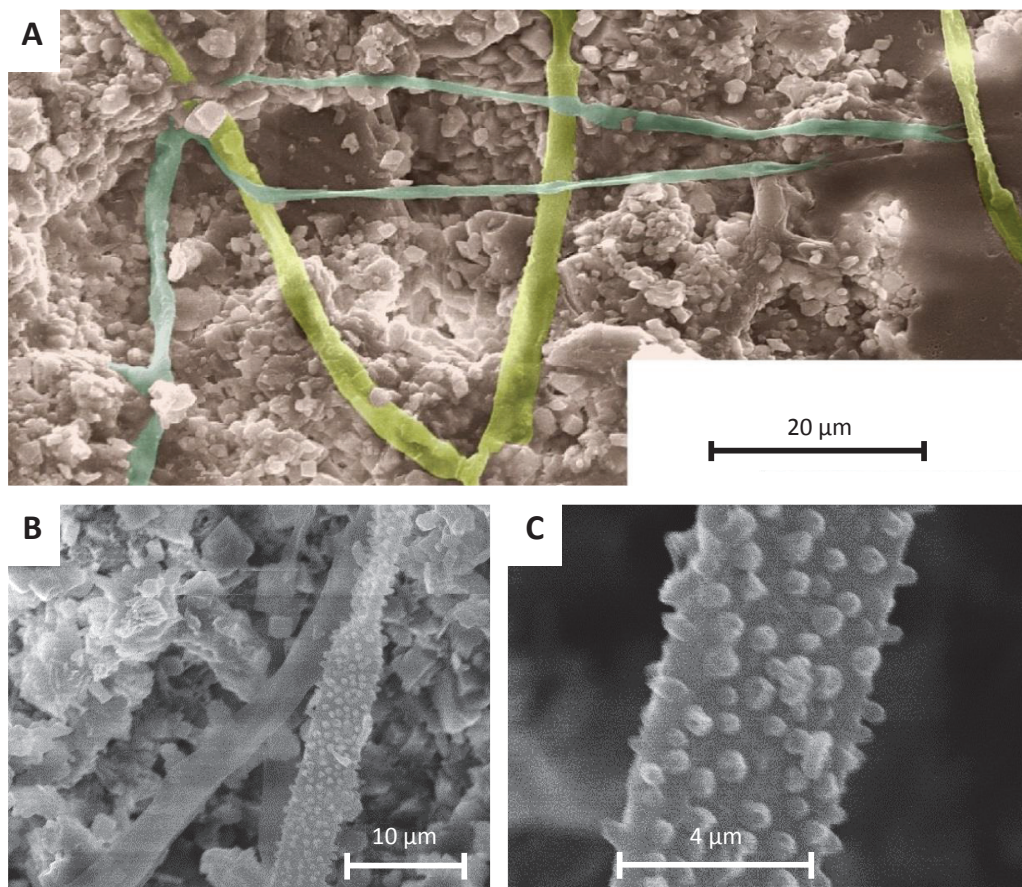


Figure 5.11. **A)** SEM images of typical filamentous hyphae (blue and green), 1600× magnification, with a close-up of filamentous hypha showing surface texture at **B)** 2000× and **C)** 8000× magnification.

Hyphae wind between surface features and possibly enter the rock matrix, shown by the narrower, branching hyphae highlighted in Figure 5.12. They sometimes co-occur with what appear to be channels or grooves in the rock surface. These features are most obvious where hyphae have been dislodged, or have deflated in-situ (Figure 5.13). This deflation may occur due to freeze-drying, or as some side effect of SEM gold sputtering pre-treatment or vacuum microscopy conditions. Channels are slightly wider ($6.01 \pm 0.13 \mu\text{m}$) than hyphae ($3.36 \pm 0.52 \mu\text{m}$), and have a rougher texture than

Physical surface alteration of carbonate rocks during weathering

elsewhere on the rock surface. These features may be result from acid etching, or the action of other fungal exudates. Similar pitting is also seen further from hyphae on dolomite samples (Figure 5.13B), these might be etch pits. These features have not been identified in images of chalk as the surface is too granular to see this kind of detail. Some amorphous material at the end of hyphae has been observed (Figure 5.13D). This may be for adhesion, anchoring hyphae to rock grains by a biofilm of organic exudates.

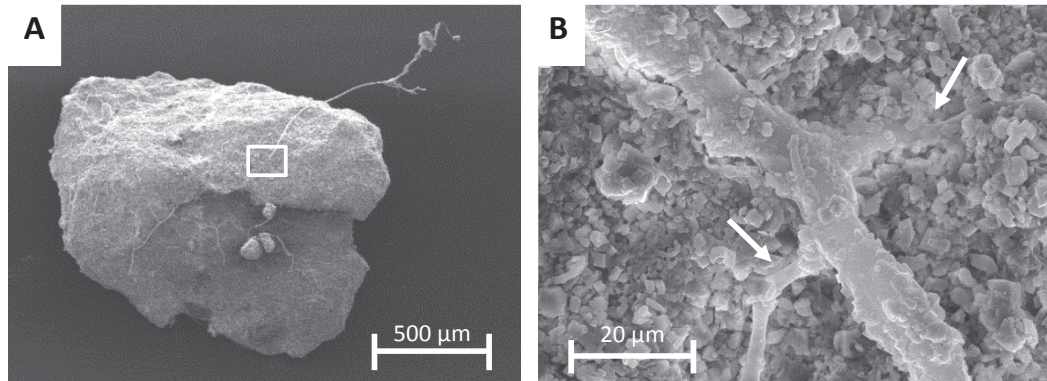


Figure 5.12. **A)** Hyphae growing on the surface of a chalk grain buried under EM *P. sylvestris*, 50× magnification. Area highlighted enlarged in **B)** where branching hyphae are indicated by arrows, 1500×.

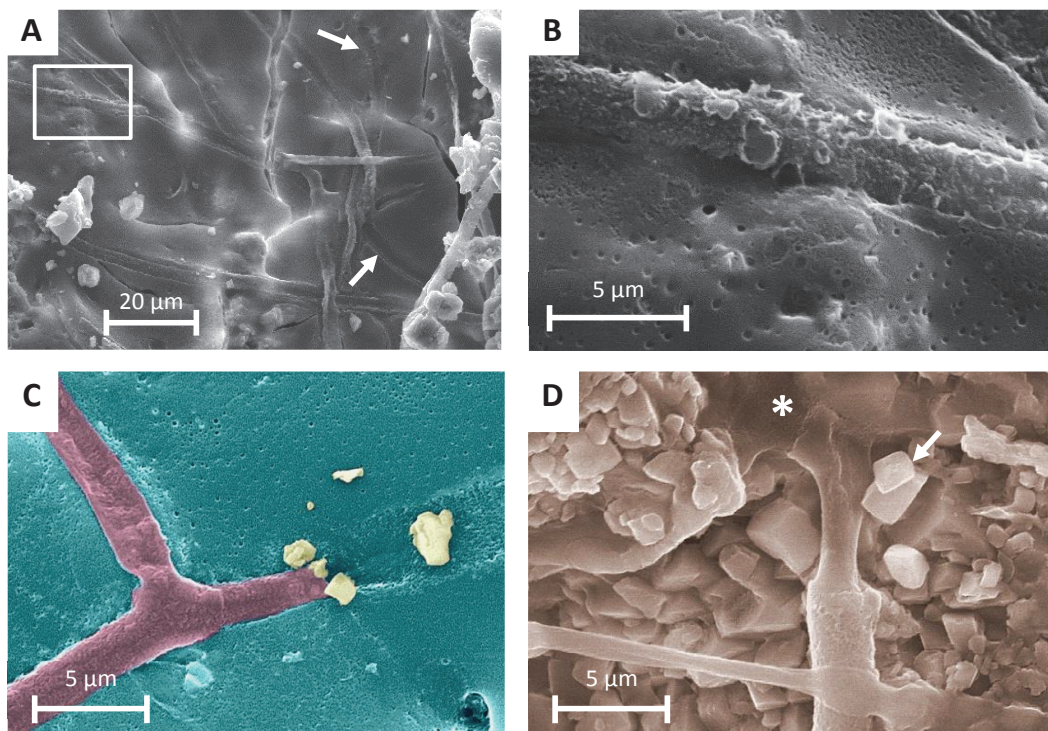


Figure 5.13. **A)** Indications of hyphal channelling on the surface of a dolomite grain under *L. decidua* at 800× magnification. Arrows indicate location of possible channels where hyphae may have detached from surface or deflated in-situ. **B)** Enlargement of highlighted area in A at 6400× magnification. **C)** Channel following path of partially detached hypha, showing pitted surface and putative calcium oxalate crystals. **D)** Hypha anchoring to a chalk surface highlighted by *, and calcium oxalate crystals with an arrow, 5000× magnification.

Chapter 5

5.3.3 VSI topography analysis of weathering carbonate and silicate surfaces

5.3.3.1 Difficulties in identifying pre-scanned areas on VSI chips

Due to extensive damage to VSI chips during incubation in the field, in addition to loss of several bags containing chips, some samples were unusable once recovered. There are several reasons why a chip may be unusable after recovering from the field. Firstly, the glass slide itself might have been broken, either by the glass backbone snapping, or one or more chips being dislodged. Where chips were missing from a slide, these could sometimes be re-inserted into the silicone moulding which originally surrounded them. Sometimes, however, mineral chips themselves were damaged, and were no longer the right shape to fit in the silicone surround. Such samples could not be used as it was impossible to re-locate exactly the same point surveyed before burial.

Another issue results from intense weathering of mineral surfaces, which can make the chip unrecognisable during VSI scanning. For some samples, it was not possible to re-locate the original area surveyed, even at the lowest magnification, of 100×. Where the original area could be recognised after weathering at 100×, but not after changing the turret to 500×, the slide position was not adjusted and a measurement taken at this point, assuming that the surface had undergone significant alteration.

5.3.4 Biological surface weathering features

Putative hyphae identified based on their morphology, were found on several rock and mineral chips after weathering. Figure 5.14 shows these features on muscovite chips, as this type of VSI chip typically had smoother surfaces which aided identification. Hyphal features were similar to those seen in SEM images of weathered rock grains: both imaging techniques showed long, thin, curved features with raised edges and a lower section in the centre (Figure 5.14B). Approximate width 3.36 ± 0.52 μm from SEM images, however, this could be quantified with greater accuracy from 2D analysis of VSI scans (Figure 5.14, Table 5.2).

5.3.4.1 Dimensions of channels and hyphae in muscovite

Hyphal width observed in this study ranged from 2.48 – 8.19 μm , and channels from 2.83 – 7.05 μm (Table 5.2). Over all samples, the mean width of hyphae was 5.66 ± 0.58 μm and that of channels was slightly narrower at 4.55 ± 0.38 μm (mean \pm SEM), however, the observation that channels are generally narrower than hyphae is not significant (One-tailed T-Test with Welch's correction for unequal variances; $T = 1.60$; d.f. = 20.73; $P = 0.063$). The width of channels and residual hyphal material are

Physical surface alteration of carbonate rocks during weathering

significantly correlated (Figure 5.15A; Linear regression; $F_{1,11} = 9.62$; $R^2 = 46.7\%$; $P = 0.010$).

Cross-sectional areas (CSA) of both hyphae and channels were also correlated (Figure 5.15C; Linear regression; $F_{1,11} = 5.40$; $R^2 = 32.9\%$; $P = 0.040$), however, this relationship was weaker, and not significant if data were not first log-transformed, probably due to data clustering with a few values lying very far from the majority of points.

5.3.4.2 Comparison of hyphal channels formed under AM and EM tree stands

On average, both channel width (Unpaired 2-tailed t-test with Welch's correction; $t = 2.40$, $P = 0.044$, $R^2 = 42.2\%$) and hyphal width (Unpaired 2-tailed t-test with Welch's correction; $t = 3.24$, $P = 0.0089$, $R^2 = 51.0\%$) are greater under in muscovite chips buried in AM forest stands than those incubated under EM trees (Table 5.2). The distribution of points is shown in Figure 5.15A, and summary of averages in Figure 5.15B. One EM data point, that for *Q. petraea*, lies separately from the majority of EM data for *N. dombeyii*, *E. coccifera*, *A. nordmanniana* and *P. sylvestris* (Figure 5.15C).

Table 5.2. Mean width and CSA of hyphae and channels measured on VSI scans of muscovite chips buried under EM and AM (below dotted line) tree stands, with overall means for each AM and EM species. AN = *A. normanniana*; EC = *E. coccifera*; ND = *N. dombeyii*; PS = *P. sylvestris*; QP = *Q. petraea*; LT = *L. tulipifera*; IA = *I. aquifolia*

Tree	Hyphae			Channels		
	Mean width \pm SEM (μm)	Mean CSA \pm SEM (μm^2)	N	Mean width \pm SEM (μm)	Mean CSA \pm SEM (μm^2)	N
AN	3.42 \pm 0.31	9.89 \pm 0.57	6	3.62 \pm 0.43	2.60 \pm 0.52	5
AN	2.84 \pm 0.24	0.89 \pm 0.08	6	2.83 \pm 0.44	0.37 \pm 0.03	5
EC	4.19 \pm 0.46	0.94 \pm 0.36	5	2.83 \pm 0.40	0.14 \pm 0.01	5
EC	7.12 \pm 0.70	0.39 \pm 0.09	4	3.85 \pm 0.16	0.42 \pm 0.03	4
ND	4.41 \pm 0.41	1.15 \pm 0.14	5	5.06 \pm 0.53	1.49 \pm 0.31	5
ND	7.06 \pm 0.38	3.71 \pm 0.36	6	4.04 \pm 0.54	1.28 \pm 0.61	4
ND	4.56 \pm 0.40	0.68 \pm 0.1	5	3.59 \pm 0.12	0.44 \pm 0.02	4
PS	2.48 \pm 0.28	0.8 \pm 0.14	6	3.84 \pm 0.31	0.51 \pm 0.08	4
QP	7.42 \pm 0.46	46.48 \pm 6.74	4	7.02 \pm 0.87	1.53 \pm 0.42	5
Average EM	4.83 \pm 0.64	7.21 \pm 5.00	9	4.08 \pm 0.43	0.98 \pm 0.27	9
LT	5.93 \pm 0.29	2.36 \pm 0.14	6	5.15 \pm 0.35	4.20 \pm 1.44	4
LT	8.19 \pm 0.58	2.75 \pm 0.75	6	5.15 \pm 0.35	4.20 \pm 1.44	4
IA	7.96 \pm 0.74	2.98 \pm 0.37	7	7.05 \pm 0.38	2.16 \pm 0.23	4
IA	7.96 \pm 0.74	2.98 \pm 0.37	7	5.10 \pm 1.13	1.21 \pm 0.29	3
Average AM	7.51 \pm 0.53	2.77 \pm 0.15	4	5.61 \pm 0.48	2.94 \pm 0.75	4

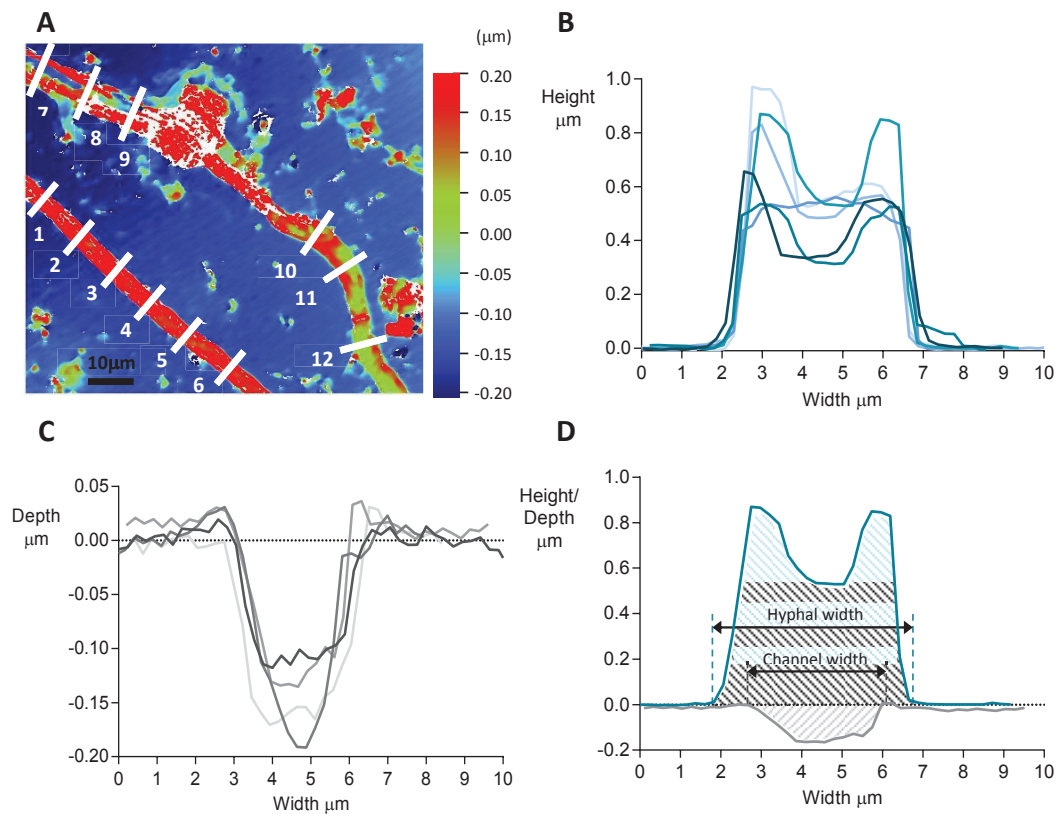


Figure 5.14. **A)** Illustration of transects used for analysis of hyphal profile. Each hypha, transects 1-6, and 7-12 were analysed separately. Example used in this figure is post-scan of *L. tulipifera*. Example profiles from measurement of **B)** residual hyphal material and **C)** curved grooves in muscovite chips. Each line on plots B and C are superimposed transect profiles measured from the same muscovite chip. These individual traces were averaged to produce summary statistics (**Table 5.2**) of hyphal/channel width for each VSI slide. **D)** A single transect for each of hyphal and channel profile to illustrate relative dimensions and measurements collected. Blue shaded area = hyphal cross sectional area (CSA) and grey shaded area = channel CSA.

Physical surface alteration of carbonate rocks during weathering

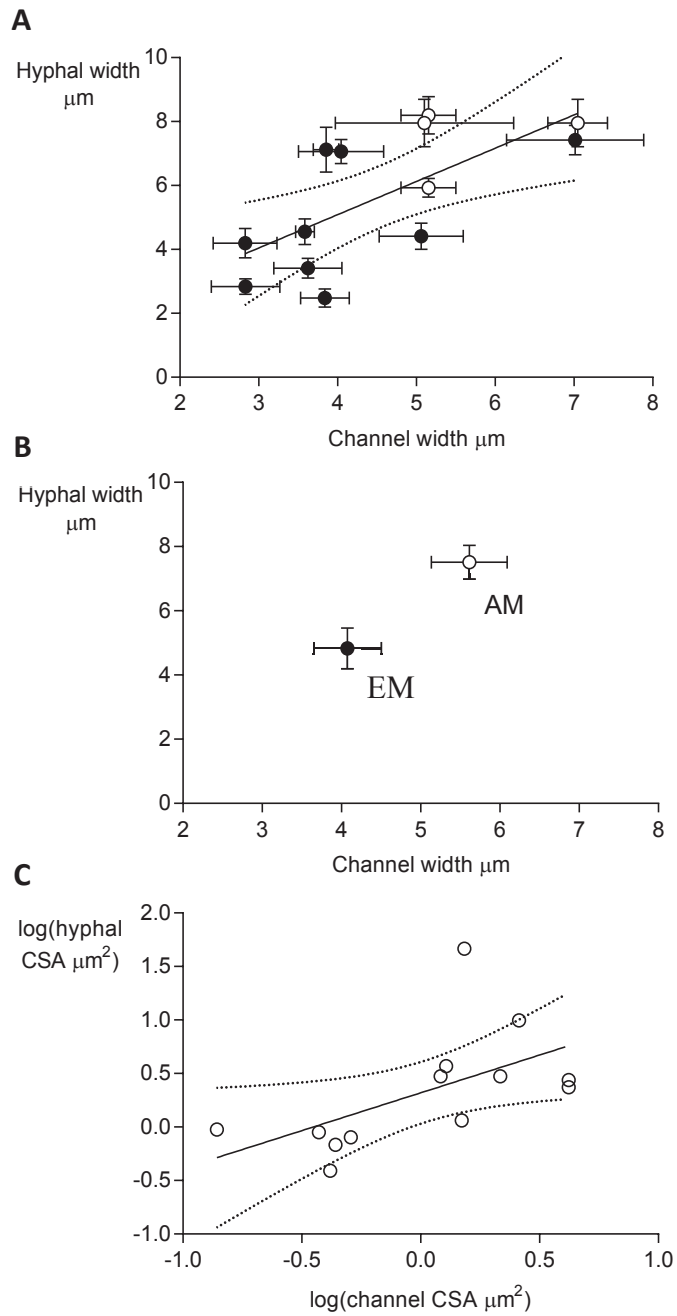


Figure 5.15. Scatter plot of summary measurements for **A**) average hyphal and channel width. Each point represents average values \pm SEM for a single muscovite chip. AM tree species shown with open symbols and EM species with filled symbols. **B**) Mean \pm SEM of hyphal and channel widths in muscovite for each AM (open symbols) and EM (closed symbols) species. **C**) Log-log plot of cross sectional area (CSA) for both hyphae and channels. Both plots show results of linear regression with 95% confidence limits.

Chapter 5

5.3.5 Mineral surface roughness

5.3.5.1 R_a scales with scan area

Concentric subsampling VSI scan datasets, to emulate a range of smaller scan areas (Figure 5.16D) showed logarithmic scaling between R_a and scan area for marble, calcite and muscovite (Figure 5.16A-C). As scan area increased up to the maximum extent possible using VSI equipment available ($12,000 \mu\text{m}^2$), R_a also increased in a manner that could be modelled with a log-log fit. After log-log transformation all datasets for all calcite, muscovite and marble chips showed significant positive correlation between scan area and R_a (Figure A. 7). There was, of course, some variation around this log-log fit; this depends on exact subsampling routine and topography of the mineral chip scanned. For some VSI chips, R_a measurements approached a plateau, and there was little subsequent change in R_a , despite further increase in sub-sampled area. This plateau was reached for all unweathered marble chips and for 2 of the 3 muscovite chips measured (Figure 5.16A-C).

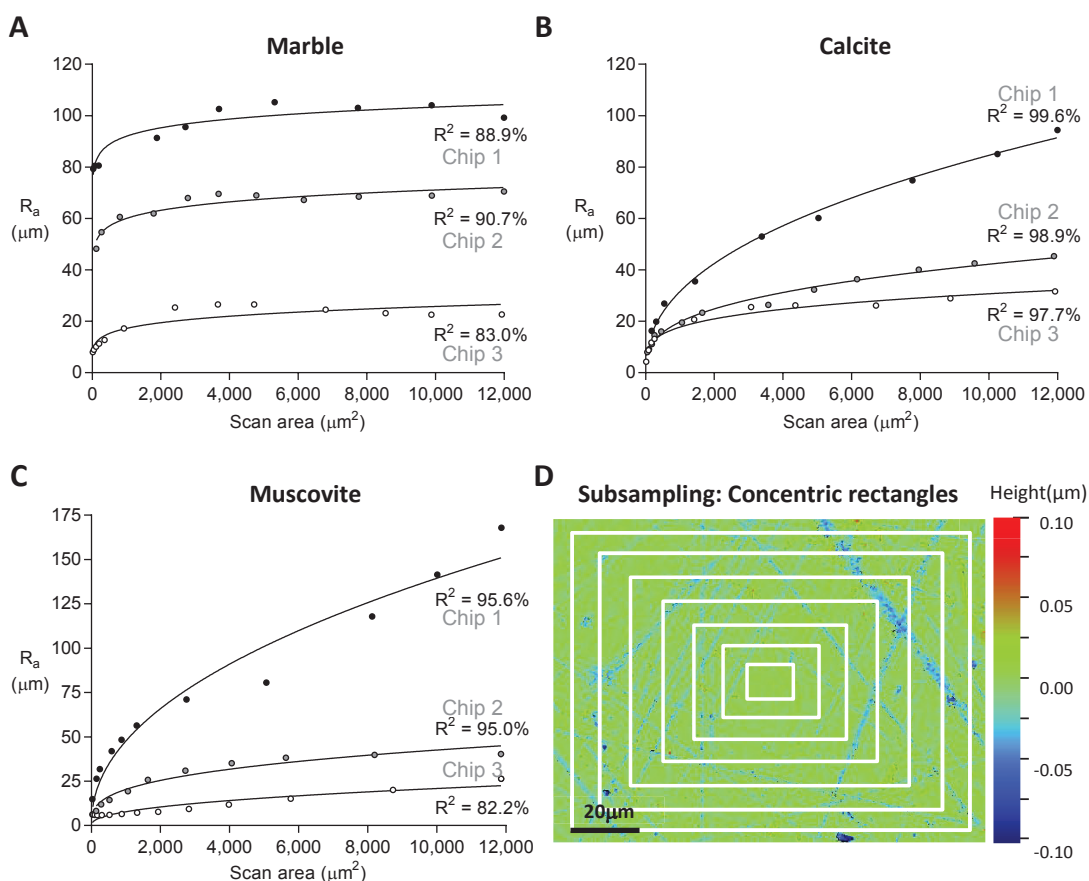


Figure 5.16. Average roughness as a function of VSI scan area measured for at 500 \times for 3 different unweathered chips each of **A)** marble **B)** calcite and **C)** muscovite. Goodness of fit, R^2 , for a log-log curve is indicated beside each dataset. **D)** Concentric rectangle method used for subsampling.

Physical surface alteration of carbonate rocks during weathering

5.3.5.2 Increase in average roughness over 7 months weathering

Prior to weathering, scans of each type of mineral chip exhibited a wide range of surface roughness, represented by R_a (Figure 5.17, Table 5.3). Muscovite had the lowest mean surface roughness prior to weathering (1.61 ± 0.07 ; Mean \pm SEM, for log R_a data), and dolomite the highest roughness (2.53 ± 0.06 ; Mean \pm SEM, for log R_a data). Average roughness, R_a , is significantly different for each rock type both before and after weathering, as is the interaction between these conditions (Figure 5.17, Table 5.3; 2-way-ANOVA; rock type $F_{3,170} = 49.1$, $P < 0.001$; un/weathered $F_{1,170} = 126.0$, $P < 0.001$; rock type:un/weathered $F_{3,170} = 4.2$, $P = 0.007$). R_a increased significantly during weathering when considering paired samples of VSI chips before and after weathering (Table 5.3, Table 5.4).

The majority of VSI chip surfaces become rougher over the course of weathering, lying above the 1:1 line when weathered R_a is plotted against unweathered R_a (Figure 5.18). In addition to this, samples that have higher initial roughness, on average, also have greater roughness after weathering, a relationship which is significant for all types of rock chip assessed, except dolomite (Table 5.4; Figure 5.18B-E). Dolomite could be an exception because scans were typically very poor quality with many missing pixels where topography lay beyond the maximum vertical scan range. This is partly due to naturally curved crystal surfaces and the small size of crystals in the specimens used to prepare VSI chips. Dolomite has therefore been excluded from subsequent analyses.

As R_a after weathering was related to R_a prior to weathering, the following analyses that investigate the effect of tree-mycorrhizal functional group, consider only relative changes in roughness over weathering as a proportion of original average roughness in an attempt to reduce the effects of this correlation.

Table 5.3. Range and average (mean \pm SEM) R_a measured for dolomite, marble, calcite and muscovite mineral chips before and after weathering. Data have been log-transformed prior to analysis. Range is calculated using Tukey method, and represents the entire span of measurements for all minerals except calcite, where one outlier with unusually high R_a is excluded (Figure 5.17)

VSI chip	Log(Unweathered R_a (nm))		Log(Weathered R_a (nm))	
	Range	Mean \pm SEM	Range	Mean \pm SEM
Calcite	1.44 – 2.79	2.01 \pm 0.09	2.27 – 3.19	2.80 \pm 0.06
Dolomite	2.00 – 3.22	2.53 \pm 0.06	2.49 – 3.36	2.92 \pm 0.06
Marble	1.36 – 2.62	1.86 \pm 0.08	1.60 – 3.26	2.65 \pm 0.11
Muscovite	1.09 – 2.23	1.61 \pm 0.07	1.50 – 2.57	2.04 \pm 0.06

Chapter 5

Table 5.4. Results of 2-tailed paired T-tests to compare R_a of samples before and after weathering. Asterisk denotes significance at 5% level or above. T-test performed on log-transformed data of R_a , originally measured in nm.

VSI chip	t	N (pairs)	P	R^2 (%)	Difference in means \pm SEM
Calcite	9.62	24	<0.001*	80.1	0.79 \pm 0.08
Dolomite	5.17	21	<0.001*	57.2	0.39 \pm 0.08
Marble	10.21	21	<0.001*	83.9	0.79 \pm 0.08
Muscovite	6.17	23	<0.001*	63.4	0.43 \pm 0.07

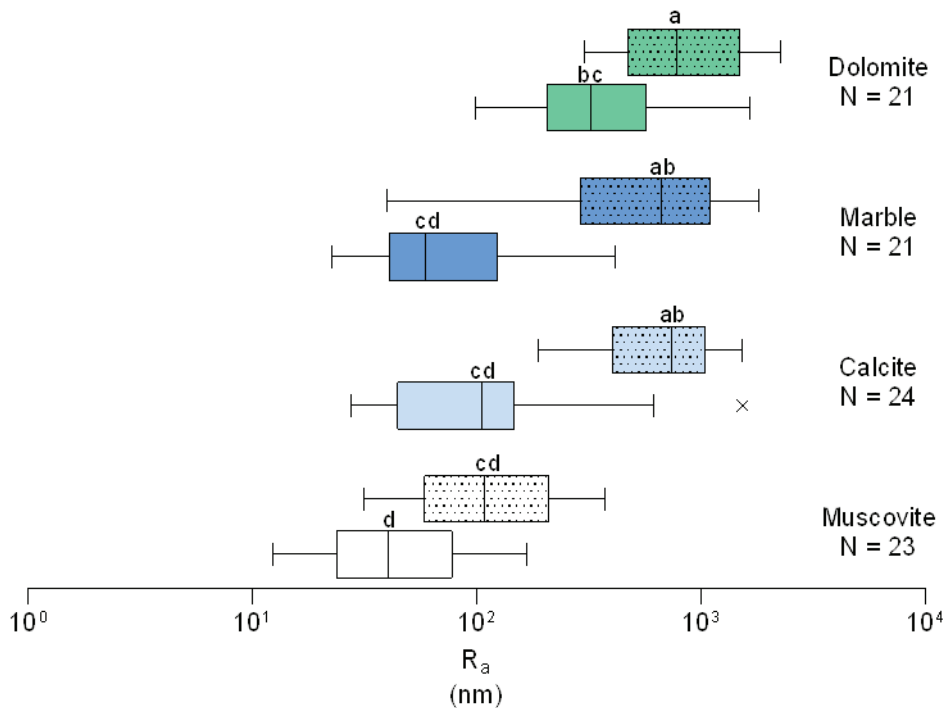


Figure 5.17. Overall summary statistics for average roughness, R_a , of unweathered (lower, unpatterned) and weathered (top, dotted) VSI chips of each mineral or rock type. Median, 25% and 75% quartiles marked. Whiskers are drawn using the Tukey method and the outlier identified lies further than $1.5\times$ the distance of the interquartile range above the upper quartile or below the lower quartile. Lettering above means shows results of Tukey HSD test, where values sharing the same letter are not significantly different (2-way ANOVA; $R_a \sim$ Rock type \times Weathering status (weathered/unweathered); $P>0.05$).

Physical surface alteration of carbonate rocks during weathering

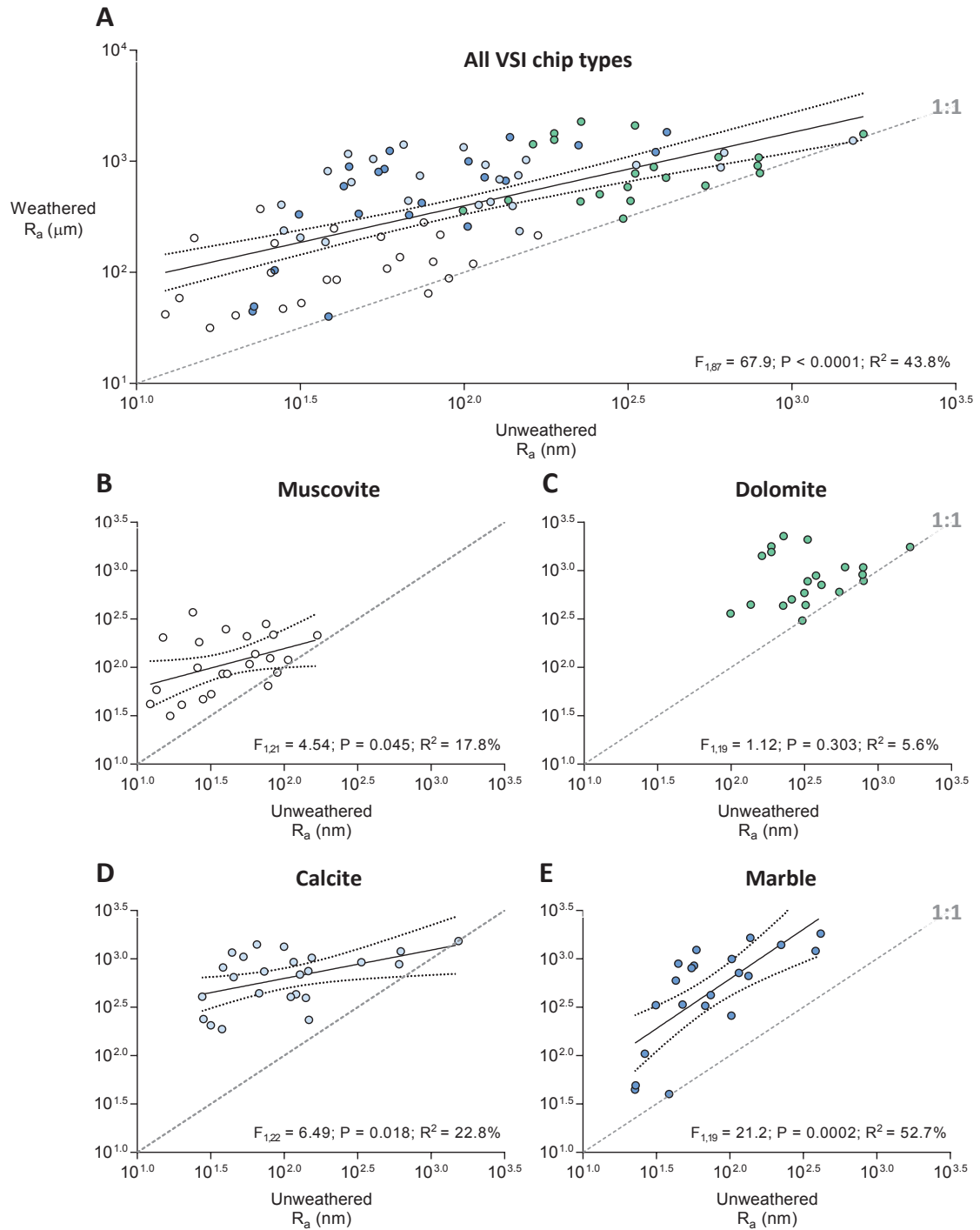


Figure 5.18. Log-log scatterplots of average roughness, R_a , of paired samples before and after weathering, with results of linear regressions (95% confidence interval shown). **A)** All samples included in top panel, then separated by rock type: **B)** muscovite = white, **C)** dolomite = green, **D)** calcite = light blue and **E)** marble = mid blue. The same colouration is used for each type of mineral chip throughout. 1:1 line marked on each plot (dotted grey line), the majority of points lie above this line and have become rougher over the course of weathering. Points lying below this line would indicate smoothing and decreasing R_a over the weathering period.

Chapter 5

5.3.5.3 Influence of tree-mycorrhizal functional type on R_a evolution

There is no consistent pattern of the effect of tree-mycorrhizal functional group on the surface roughness of different mineral chips. For muscovite (Figure 5.19A), there is a much larger increase in roughness over the period of weathering for EM gymnosperm trees than for EM angiosperm trees and then AM trees, however, the means were not significantly different (Unpaired 2-tailed T-test with Welch's correction; $t = 1.78$, $P = 0.13$, $R^2 = 37.9\%$). However, when the change in R_a for EM gymnosperm and angiosperm trees is averaged, there is no significant difference between this and the average for AM trees (Unpaired 2-tailed T-test with Welch's correction; $t = 0.43$, $P = 0.67$, $R^2 = 1.5\%$). There are insufficient data to compare angiosperm and gymnosperm trees with AM fungal associations.

For Marble (Figure 5.19C), again there is a greater increase in % R_a for chips weathered under EM trees than those under AM trees (Unpaired 2-tailed T-test with Welch's correction; $t = 2.62$, $P = 0.017$, $R^2 = 26.7\%$), however, when EM trees are split into gymnosperm and angiosperm groupings, there is no significant difference between these, although it appears as if there is a marginally higher increase in R_a under gymnosperms, as there was for muscovite (Unpaired 2-tailed T-test with Welch's correction; $t = 1.46$, $P = 0.19$, $R^2 = 23.1\%$).

Contrastingly, calcite (Figure 5.19B) shows no significant differences between the relative change in roughness between EM and AM species (Unpaired 2-tailed T-test with Welch's correction; $t = 0.10$, $P = 0.92$, $R^2 = 0.11\%$), or between EM angiosperms and gymnosperms (Unpaired 2-tailed T-test with Welch's correction; $t = 0.75$, $P = 0.47$, $R^2 = 5.0\%$).

5.3.5.4 Influence of pH and field weathering rates on surface roughness changes

The proportional change in R_a of calcite containing chips, rhomb calcite and marble, correlates significantly with calcite molar weathering rates, measures in mesh ingrowth bags, over the same incubation period of 7 months (Figure 5.20A; $F_{1,14} = 4.9$; $P = 0.044$; $R^2 = 26.0\%$). This relationship is driven by the contribution of calcite VSI chips, as these showed highly significant correlation ($F_{1,6} = 19.4$; $P = 0.005$; $R^2 = 76.4\%$), whereas marble did not ($F_{1,6} = 0.15$; $P = 0.71$; $R^2 = 2.4\%$). There was no significant influence of pH, measured within mesh bags containing VSI chips and inert, quartz grains, on R_a for calcite-based VSI chips (Figure 5.20B; $F_{1,14} = 0.006$; $P = 0.94$; $R^2 = 0.04\%$).

Physical surface alteration of carbonate rocks during weathering

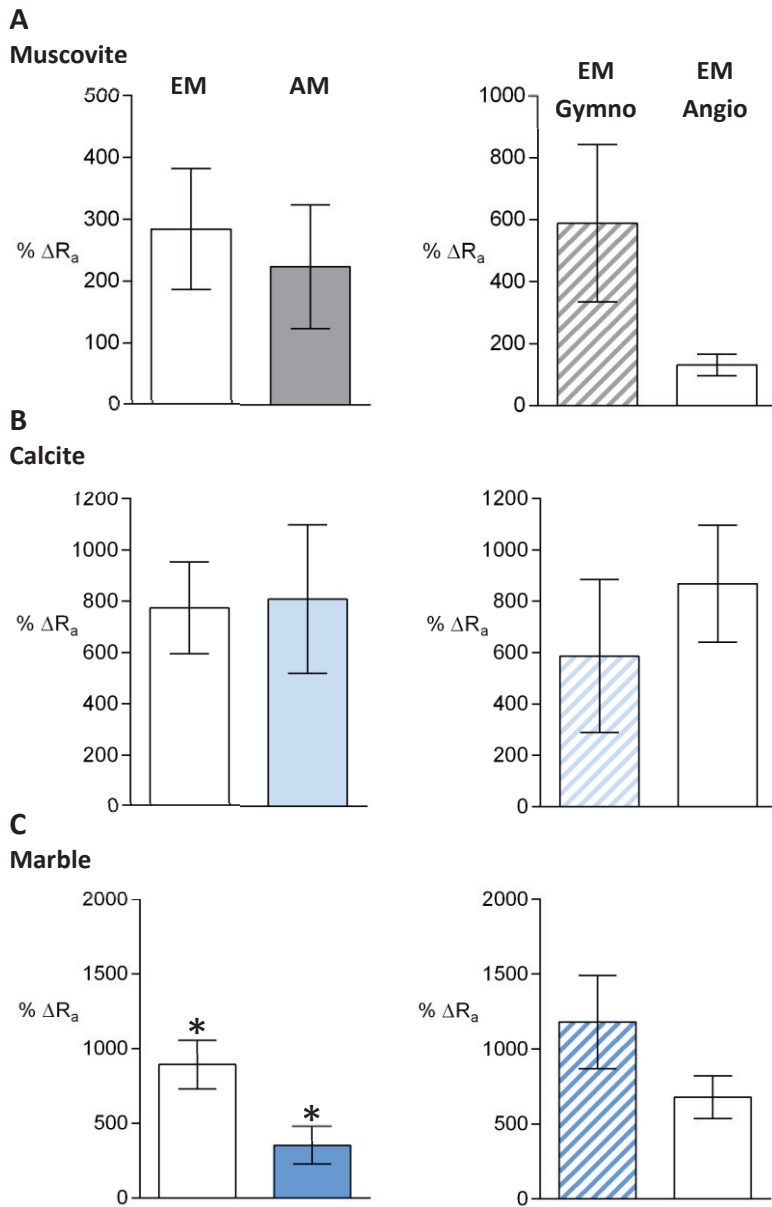


Figure 5.19. Mean % Increase in Ra (average roughness) \pm SEM over weathering for **A)** muscovite = grey, **B)** calcite = light blue and **C)** marble = mid blue. Left panel: AM (solid coloured bars) versus EM (white bar). Right panel: EM-gymnosperm (striped bars) versus EM angiosperm (white bars) trees. For AM trees, N = 5. For EM trees, N = 18 trees, 6 of which were gymnosperms, and 12 angiosperms. Bars marked * are those where the outcome of an unpaired 2-tailed T-test with Welch's correction was significant at $P < 0.05$

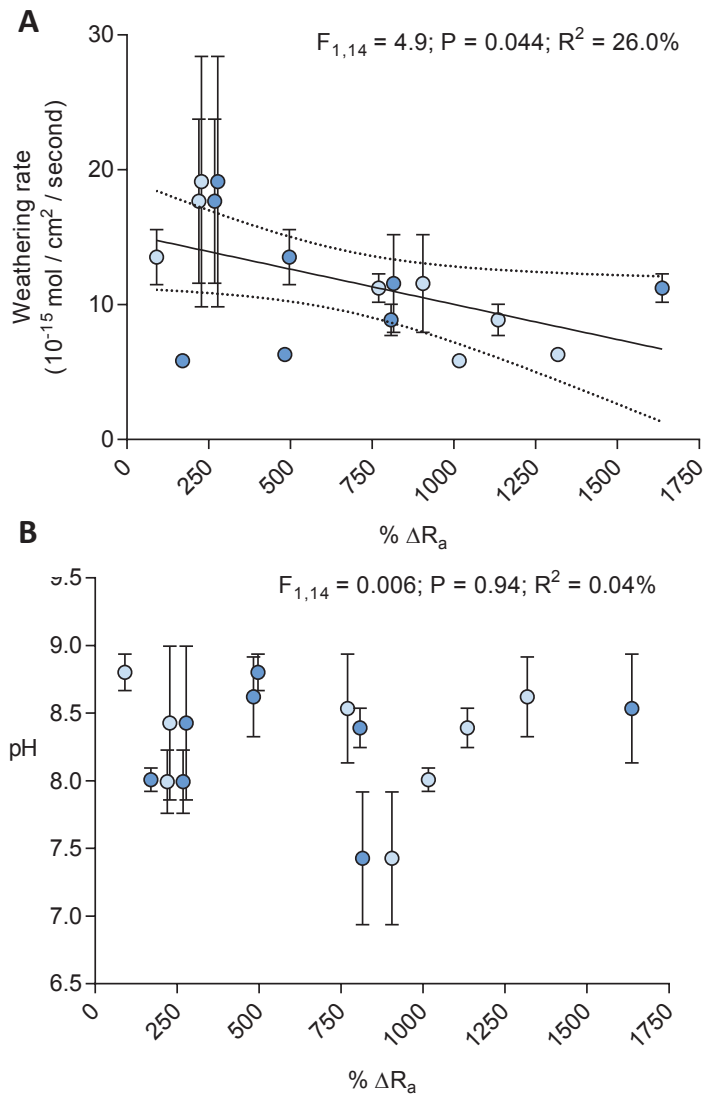


Figure 5.20. Scatterplots of **A**) bulk calcite weathering rates over 7 months incubation in the field (Mean \pm SEM) and **B**) pH measured within VSI chip mesh bags (Mean \pm SEM); versus the proportional change in surface roughness, R_a , over the same period. VSI data plotted for marble (mid blue) and calcite (light blue).

5.4 Discussion

5.4.1 Micro-organisms observed on weathering surfaces

Within forest soil a wide range of micro-organisms will be in contact with rock grains. Different types of fungi have been identified in this study (Figure 4), and similar work using atomic force microscopy (AFM), has yielded images of smaller bacteria on biotite flakes incubated in the field (Figure 5.21; AFM work by Loredana Saccone, Sheffield University). These organisms are all interacting with mineral surfaces and this section investigates their contribution to mineral weathering in the field.

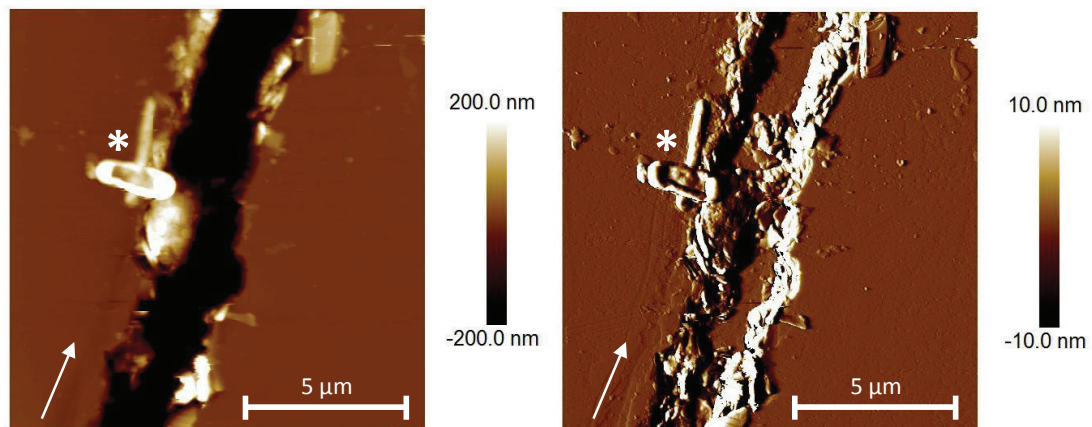


Figure 5.21. AFM images of biotite alteration after burial beneath mature stand of *Quercus* trees in the field. **A)** Surface topography; **B)** deflection shows that the surface is different where the colour is different. White areas are likely to be organic residue at channel edges, possibly exudates deposited by a fungal hypha, or remains of a deceased hypha. To the left of the channel are a couple of bacteria, one of which has made a shallow channel over the surface where it has travelled, just to the right of the white arrow. Images taken by Loredana Saccone

5.4.2 Comparison of hyphal width measurements using SEM and VSI techniques

The width of hyphae measured from SEM images of chalk and dolomite ($3.36 \pm 0.52 \mu\text{m}$; mean \pm SEM) is within the typical range for both EM ($3\text{--}10 \mu\text{m}$; Hoffland *et al.* 2003) and AM hyphae ($<5 \mu\text{m}$; Staddon *et al.* 2003). The width of hyphae observed on carbonate minerals in this study were slightly greater those seen in microcosm experiments using polished marble incubated with EM *H. crustaliniforme* in symbiosis with *P. sylvestris* ($2\mu\text{m}$; Rosling 2003). It cannot be determined from these results whether organic material on rock grains originates from mycorrhizal or saprotrophic fungi.

The range of hyphal widths measured on a muscovite surface using VSI imaging was slightly wider, than when using SEM, at $2.48\text{--}8.19 \mu\text{m}$, with a mean of $5.66 \pm 0.58 \mu\text{m}$ (mean \pm SEM), again falling within the range for mycorrhizal fungi. Differences between SEM and VSI measurements are likely to be methodological.

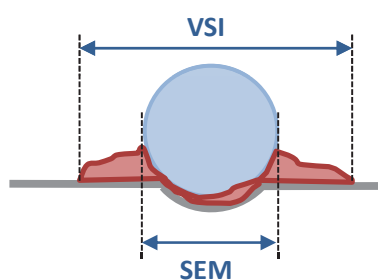
Chapter 5

The harsh conditions in SEM with an energetic electron beam and vacuum sample chamber might damage delicate biological material, and cause hyphae to distort or deteriorate. In some cases, it was more difficult to measure hyphal widths from SEM images as the rock surface was less uniform than the specially prepared VSI chips of muscovite. The granular surface texture of rock grains made it challenging to find edges of hyphae as sometimes occluded by small mineral crystals, particularly for chalk. To avoid this, only hyphae where both sides could be seen clearly were measured.

On the other hand, hyphae were generally easier to identify during SEM compared with VSI, which just provides a height profile. During VSI analysis, hyphal width may have been overestimated as the measurement technique assumed that where a hypha was identified; all material occurring above the mineral surface was fungal. Whereas, in reality some might have been accumulated organic matter or biofilm either side of hyphae (Figure 5.22). Successive layers of biofilms can build up over time and have previously been seen surrounding fungi growing on biotite flakes (Gazzè *et al.* 2013).

One other advantage of using SEM is that it can show hyphae growing on realistic mineral surface environments, whereas VSI uses specially prepared mineral chips with smooth surfaces. These flat surfaces are less likely to occur in soils, particularly for carbonate minerals, due to the need to artificially polish marble to achieve a flat surface, and the rapid weathering kinetics of carbonate minerals.

VSI topographic measurements may include biofilm
or organic matter accumulation



Hyphae more easily identified by SEM, which may result
in narrower measurements

Figure 5.22. Hyphal width may be overestimated during VSI analysis, compared with SEM, if exuded organic matter or biofilm is included in measurements.

5.4.3 Hyphal channels observed on muscovite surfaces and carbonate rock grains

Channel widths in muscovite measured by VSI in this study ($4.55 \pm 0.38 \mu\text{m}$) have similar dimensions to those measured during a field study by Quirk *et al.* 2012 (Figure 5.24); and lie within the range of 3-10 μm identified for hyphal tunnels in feldspar grains (Hoffland 2002, 2003; Jongmans 1997; Smits *et al.* 2005). The variation in widths, and especially depths, of channels in muscovite, compared to those observed in feldspars and hornblendes is minimal, and may be attributed both to methodological differences, and also to the varying susceptibilities of these minerals to weathering (Cochran and Berner 1996).

5.4.4 Correspondence between hyphal and channel widths

Channel and hyphal widths in muscovite were related (Figure 5.15), and best represented by a linear regression with the formula $y = 1.040x + 0.925$. This significant correlation makes it likely that these features are associated with each other. Channels may result from fungal hyphae attempting to directly absorb inorganic nutrients from mineral surfaces, without them first entering the soil pool, an effect which may be especially pronounced in nutrient poor soils (Blum *et al.* 2002; Finlay *et al.* 2009; Hoffland *et al.* 2003).

There is an almost 1:1 correspondence between change in hyphal width and change in channel width (Regression gradient 1.040). The regression intersect is, however, non-zero, so at the point where there are no channels (channel width = 0), we could still theoretically expect to find fine hyphae, with a diameter of approximately 1 μm . This theoretical limit may have limited biological relevance, because the smallest hyphae observed in this study had a diameter of $2.4 \pm 0.1 \mu\text{m}$ (mean \pm SEM), and the narrowest type of mycorrhizal hyphae, those from AM fungi, have an average diameter of 2-20 μm (Friese and Allen 1991).

On muscovite, hyphae ($5.66 \pm 0.58 \mu\text{m}$) have a slightly greater average width than channels ($4.55 \pm 0.38 \mu\text{m}$). One possible explanation for this is that the entire diameter of a single hypha is not in contact with the mineral surface. Hyphae have a roughly cylindrical cross section, and as the hyphal channels are generally shallower than the average hyphal radius, it is reasonable to assume that there is a limited area of contact between rock surface and hypha (Figure 5.23). On dolomite, the opposite was observed, and a channel partially occupied by a hypha had a slightly greater width ($6.01 \pm 0.13 \mu\text{m}$) than hyphae ($3.36 \pm 0.52 \mu\text{m}$; SEM image, Figure 5.13). This could be due to the typically faster weathering rates of carbonate minerals compared with that of silicates. Carbonate minerals are particularly susceptible to dissolution in acidic

Chapter 5

conditions (Cubillas *et al.* 2005), such as those that will surround hyphae exuding protons or LMWOAs (reviewed in Chapter 1).

Unfortunately channel dimensions in muscovite cannot be compared qualitatively with those in calcite in this study, as it is not possible to reliably identify such features from VSI data for calcite or marble, due to severe surface alteration. This data can only be used for observing changes in bulk surface characteristics, such as R_q .

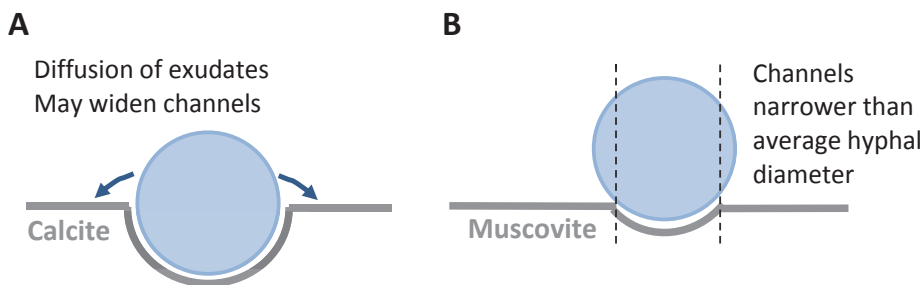


Figure 5.23. Channels in **A)** calcite/dolomite containing rocks may be wider than those in **B)** muscovite due to lower weatherability of silicate-containing minerals such as muscovite. Width of channels measured from VSI scans of muscovite chips were slightly lower than the width of residual hyphal material. Channels observed on dolomite using SEM imagery appeared wider than associated hyphal fragments, possibly due to rapid carbonate weathering or diffusion of weathering agents.

5.4.5 Correspondence between width and depth of hyphal channels

VSI analysis of muscovite chips, weathered in the field, reveals a positive correlation between channel width and depth (Figure 5.15B), regardless of mycorrhizal type, as was found by Quirk *et al.* (2012, 2014). When data from a later, controlled environment study were included (Figure 5.24A, Quirk 2014), this relationship persists, but is less significant. This is possibly partly due to the need to estimate channel depth from CSA as data were not reported in the same format as either field study, or due differences in experimental setup.

Experimental conditions impact channel morphology, and differences have been observed between muscovite when exposed to mature stands of *S. sempervirens* or to saplings in a pot experiment. In the field, channels measured $2.2 \pm 0.2 \mu\text{m}$ wide and $0.12 \pm 0.02 \mu\text{m}$ deep (Mean \pm SEM; Quirk *et al.* 2012), but in the pot experiment they were larger: $2.7 \pm 0.2 \mu\text{m}$ wide and $0.2 \pm 0.2 \mu\text{m}$ deep (Mean \pm SEM; Quirk *et al.* 2014).

5.4.5.1 Weathering duration and hyphal colonisation rate

The correlation between channel width and depth may be because wider hyphae are able to etch deeper channels; however, this is probably too simplistic. Alternatively, this could result from differing weathering durations, and wider and deeper channels

may just be those which formed earliest. Although all VSI chips were incubated over the same period, hyphae will have colonised them at different times. As silicate minerals weather, porosity and surface roughness increases (White and Brantley 1995), thus, initial hyphal etching will increase surface area and facilitate future weathering. Channel formation also exposes different mineral faces, which will increase the amount of surface area that is highly reactive, as was proposed by Arvidson and Luttge (2003) in their study of calcite dissolution.

In addition to this, the mesh bags prepared for the current study may have taken longer to colonise due to use of different minerals. The rock grains included alongside the VSI chips in this study are of a predominantly quartz silicate, whereas in Quirk *et al.* (2014, 2014) bags were filled with basalt which has a different elemental makeup and may contain more micronutrients. This depends on the interaction between the weathering minerals, soil nutrient status and plant and fungal nutrient requirements which are not catalogued by either study in a way that would help us work this out. Channels may be deeper where there is greater nutrient limitation, mirroring what was seen in Section 1.4.3 where more tunnels, potentially produced by foraging mycorrhizal hyphae, were counted where nutrients including K were limiting in a northern Swedish podsol forest (Hoffland *et al.* 2002).

In the current study, two muscovite chips exhibited particularly deep channels with correspondingly high CSAs; one of these had been incubated below *A. nordmanniana* and the other under *L. tulipifera* (Figure A. 6). This may be due to measurement of an existing channel or groove in the muscovite surface, perhaps formed by abrasion after the initial scan. It may be the case that a hypha has enlarged an existing crack, giving it the same shape as other hyphal channels, or that these features have been misidentified, and have hyphal association and these two points were excluded from subsequent analyses (Figure 5.24).

5.4.6 Comparison of hyphal channel morphology under AM and EM tree stands

There are fewer data points for AM channel width and depth than for EM as the prevalence of channels was lower on VSI slides recovered after incubation in AM forests (Table 5.2). This is consistent with previous experimental observations both in the field (Quirk *et al.* 2012) and pot-based studies (Quirk *et al.* 2014), where basalt grains showed lower hyphal colonisation under AM than EM tree species, after the same incubation period.

Quirk *et al.* (2012) found that in the field, putative hyphal channels on muscovite incubated under mature stands of AM *S. sempervirens* were narrower and

Chapter 5

shallower than those under EM *P. sylvestris* or *B. pendula* (Figure 5.24). A later experiment growing saplings in a controlled environment chamber (Quirk *et al.* 2014), found that channels on muscovite beneath EM *B. pendula* saplings were significantly wider and deeper than on chips buried below AM Acer or Sequoia (Figure 5.24A). However, in the current study, the opposite was observed, and channels on muscovite chips buried under AM *I. aquifolium* had greater dimensions than under any of the EM species investigated (*N. dombeyii*, *A. nordmanniana*, *P. sylvestris* and *E. coccifera*) (Figure 5.24).

Putative hyphal channels on muscovite buried under EM trees at Bedgebury were both narrower and shallower than those measured under EM *P. sylvestris* by Quirk *et al.* 2012. Channel depth and width will depend on contact time between hyphae and the mineral surface. Although the VSI slides in both studies were both buried for comparable lengths of time (9 months: November 2009 - May 2010, Quirk *et al.* 2012; 10 months: August 2013 – July 2014, current study) they were at different locations in the UK and may have been subject to different weathering conditions. These may include different growing season lengths, average soil temperature, pH and moisture content. For instance, soil at Bedgebury is very acidic, especially below EM tree stands, however, Westonbirt, where Quirk *et al.* (2012) performed their field study is situated over Cotswold limestone which produces more alkaline soils.

5.4.6.1 Climatic factors might cause different hyphal channelling behaviour

Bedgebury pinetum

Summer 2013 (June – Aug) was the warmest summer since 2006 with a prolonged heatwave throughout most of July, and exceptionally dry conditions with the south of England, where our study site is located, receiving less than half the 1981-2010 average summer rainfall (MET office 2013). Soil moisture content would have been low, both reducing the mineral-water contact required for dissolution, and possibly hindering mycorrhizal activity or increasing mortality. It may be that in summer, the most active mycorrhizal species are stress-tolerant and potentially not very active in weathering.

The following winter was very stormy with temperatures 1.5-2°C higher than the 1981-2010 average and >200% of the average rainfall for the study region (MET Office 2015). After the dry summer, this may have offset any slowing in weathering caused by droughted soil, however, would be more likely to increase bulk mineral weathering rates through leaching, rather directly affect hyphal channelling. Such heavy rainfall and soil waterlogging may actually be detrimental to mycorrhizal growth

(Mendoza *et al.* 2005). Some sites, particularly those for *Acer* and *Liriodenron*, would have been particularly prone to flooding as soil was more gleyed indicating poor drainage.

Westonbirt arboretum

In the region of the UK where Westonbirt Arboretum is located, spring 2010 was the driest spring since 1984 with approximately half the average rainfall (1971-2000). However, the impact of this may have been less than the summer drought during the current study. There are two reasons this may be the case: firstly, despite comparable proportional reduction in rainfall over the two periods, Spring 2010 and Summer 2013, there soil moisture content would have still been greater in spring, because spring is generally wetter than summer. Secondly, this unusually dry period occurred toward the end of Quirk *et al.*'s (2012) study, whereas, the dry summer in the current study may have potentially hindered initial hyphal colonisation of minerals.

5.4.6.2 Plant growth conditions and fungal colonisation affect channelling

In addition to differences in water-mineral contact time, biotic factors including hyphal colonisation rates and host plant nutrient requirements may produce differences in hyphal channel formation between studies. Mesh bags prepared for the current study may have taken longer to colonise than those of Quirk *et al.* (2012), because of both climatic factors, and the use of different minerals. In the current study, VSI chips are surrounded by grains of a predominantly quartz silicate, whereas in Quirk *et al.* (2012, 2014) filled his with basalt. The basalt used contains 0.29% P₂O₅ by weight, which may make it more attractive for mycorrhizal weathering than rock grains in our study (quartz silicate: 0.056% P₂O₅).

Channel formation will depend on the interaction between the weathering minerals, soil nutrient status and plant and fungal nutrient requirements. Although, this interaction has not been directly catalogued in this or any other study, there are indications that larger channels form where there is greater nutrient limitation and therefore more demand for inorganic nutrients from mineral weathering. This is supported by the observations of Hoffland *et al.* (2002) who found more putative hyphal tunnels in feldspar grains where K was limiting in Swedish podsol forest soils. Secondly, channels with significantly smaller CSA formed in muscovite when buried under saplings grown under low, 200ppm CO₂, than when those under high CO₂ at 1500ppm (Quirk *et al.* 2014). This may be due to increased host plant demand for mineral nutrients as a result of CO₂ fertilisation.

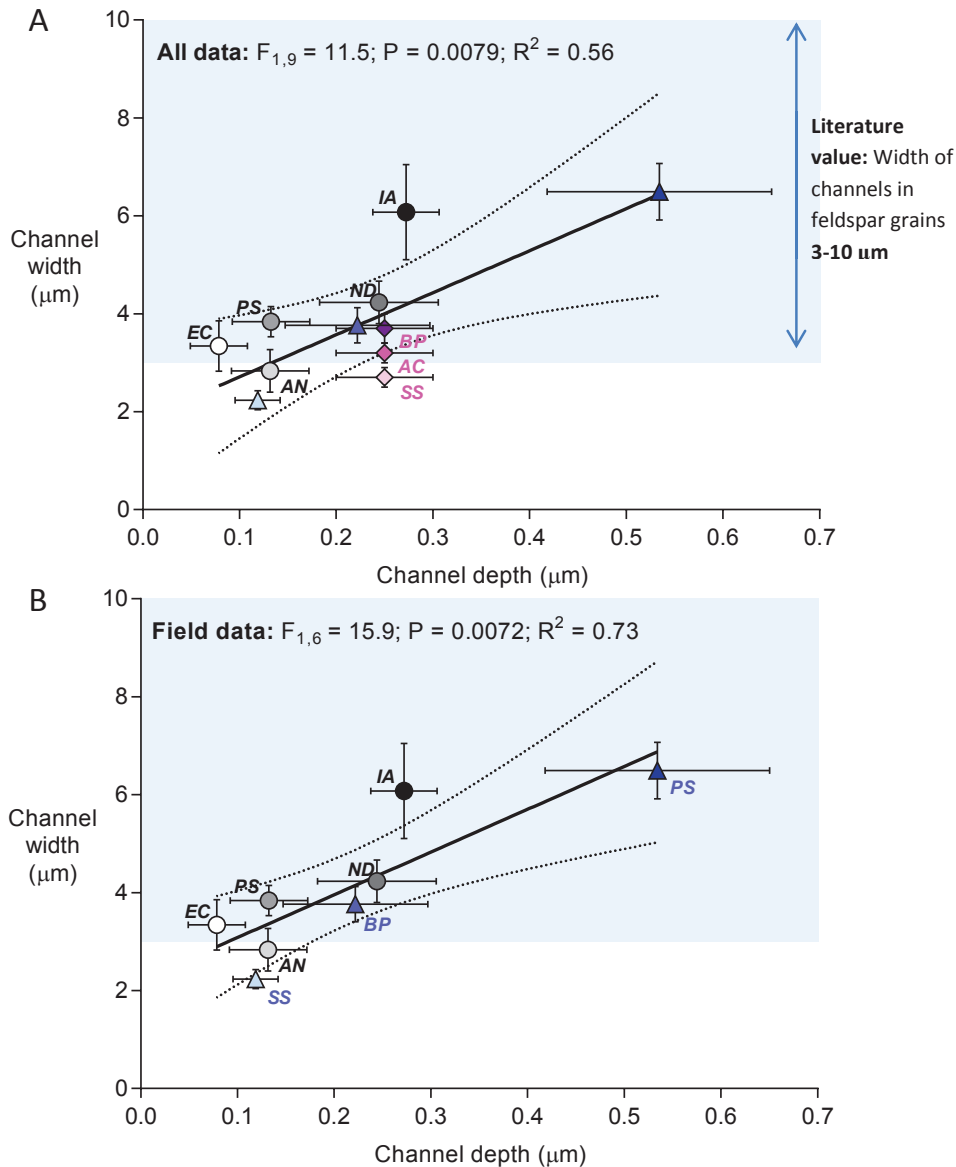


Figure 5.24. Cross plot of measured channel width and depth on muscovite (Mean \pm SEM) from this study alongside those from field and controlled environment studies by **A)** Quirk *et al.* (2012) and Quirk *et al.* (2014) respectively ; and **B)** with field study results from Quirk *et al.* (2012) only. Results of linear regressions for **A)** all data, and **B)** field study data only are shown with 95% confidence interval. Shaded area between 3-10 μm channel width corresponds to the diameter of channels found in feldspar grains in a Swedish podsol (Hoffland 2002, 2003, Jongmans 1997).

Data from **this study** shown as labelled circles: EC = *E. coccifera* (white); AN = *A. nordmaniana* (light grey); PS = *P. sylvestris* (mid grey); ND = *N. dombeyii* (dark grey); and IA = *I. aquifolium* (black) (N = 5 measurements of 2 muscovite chips for each AN, IA, PS and EC and 5 measurements from 3 muscovite chips for ND). Data from **Quirk *et al.* (2012)** as triangles: SS = *S. sempervirens* (light blue), BP = *B. pendula* (mid blue) and PS (dark blue) (N = 4 scans of 2 muscovite chips). Data from **Quirk *et al.* (2014)** are plotted as diamonds: BP (purple), AC = *A. campestre* (dark pink) SS (light pink). For Quirk 2014, the same depth is used for all channels measured $0.25 \pm 0.05 \mu\text{m}$, based on the measurement for channels under sequoia measuring 0.2-0.3 μm .

5.4.7 Evidence of organic exudates or biofilm formation

EM and other fungi excrete considerable quantities of LMWOAs, of which the most important is thought to be oxalic acid (reviewed in chapter 1). This LMWOA can chelate Ca^{2+} ions, leading to the formation of calcium oxalate. Some angular crystals observed on mineral surfaces in this experiment have the correct morphology and were consequently identified as calcium oxalate (Figure 5.13C,D). These secondary precipitates form as a weathering product of Ca-containing soil minerals (Kolo *et al.* 2007; Schmalenberger *et al.* 2010; Verrecchia *et al.* 2006) and are often found in the vicinity of ectomycorrhizas including *Piloderma* (Arocena *et al.* 2001; Casarin *et al.* 2003), *Paxillus* (Lapeyrie *et al.* 1987) and some non-mycorrhizal oxalate-producing fungi on chalk (Verrecchia and Dumont 1996).

5.4.8 Etch pit formation and changes in mineral surface texture observed with SEM

On dolomite, surface pitting often occurs adjacent to hyphal channels seen using SEM (Figure 6B,C). These may be etch pits extending beyond the area occupied by a hypha, perhaps formed under a biofilm used for hyphal adhesion, or by fungal exudates such as LMWOAs (Saccone *et al.* 2012; Gazzè *et al.* 2013). The amount of this pitting might depend on rock type, and has only been seen for dolomite, but not chalk in this study. This may be because fine surface features are obscured on the very granular chalk. Pitting is not seen on polished marble either, and in contrast with our observations, the rock surface within a hyphal track was thought to be smoother than the surrounding rock face (Rosling 2003), however, the image resolution and perspective makes this difficult to say with certainty.

5.4.8.1 Increase in average roughness over 7 months weathering

Muscovite had the lowest roughness measured during VSI analysis, both before and after weathering. Before weathering, this is due to its phyllosilicate mineral structure, as it easily cleaves into sheets with smooth surfaces. After weathering, low R_a is probably due to a combination of perfect cleavage between sheets, and its silicate mineralogy, compared with the other three types of chip which are all carbonates, which typically have faster dissolution kinetics.

Dolomite has the highest roughness both before and after weathering, which mostly results from the structure of the chips used in this experiment. The pink Moroccan dolomite generally split along cleavage planes, however, these are not flat as they are for both calcite and muscovite. There was a much greater range of heights in each dolomite VSI scan due to this curvature, which accounts for its high R_a . Dolomite roughness has not been included in all analyses as the large range of heights produced

Chapter 5

very low-quality VSI scans, and it was challenging to re-locate original scan areas at 500× magnification as the surface had often changed beyond recognition and identifying features were lost (Figure 5.25A).

Unweathered marble and calcite both have intermediate R_a , they both form chips with flat surfaces, marble, because it was prepared as a polished slab, and calcite as it has perfect rhombohedral cleavage. Neither of these carbonates is as smooth as muscovite; calcite has microscopic steps following different cleavage planes, and the marble polishing produces an array of parallel scratches and grooves (Figure 5.25B).

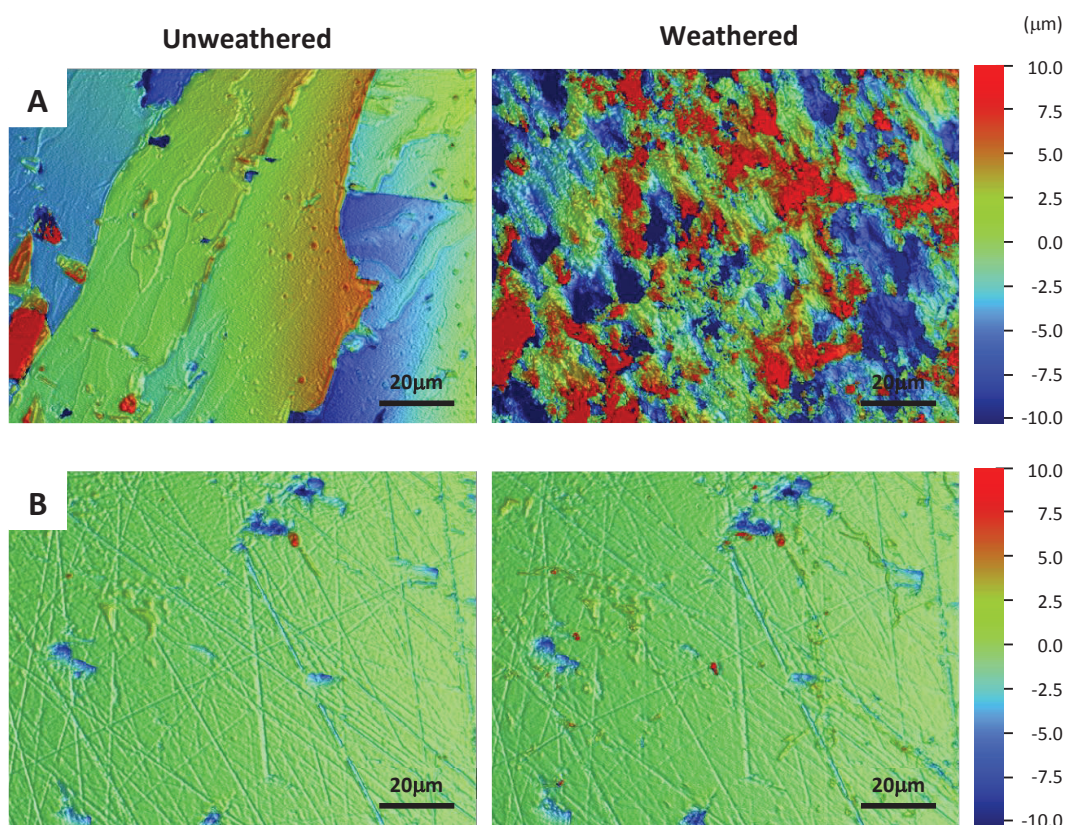


Figure 5.25. VSI images of same areas of unweathered (left panel) and weathered (left panel) surfaces of **A**) dolomite and **B**) marble, showing scratches and grooves resulting from polishing, 500× magnification.

Over weathering, surface roughness increased for all mineral chips and the greatest increases were seen for those chips which also had the highest initial roughness (Figure 5.18). This relationship was significant overall, for all samples, and for calcite, marble and muscovite individually. Rougher surfaces are those with large variation in heights, this can be caused by surface features such as etch pits, scratches or grooves, or by microscopic steps between mineral cleavage planes. These features lead to a higher overall surface area vulnerable to weathering, more intense dissolution and greater increases in roughness (Arvidson and Lüttge 2003).

5.4.8.2 Influence of tree functional group on surface roughness changes

Tree-mycorrhizal functional group had no consistent, significant effect on the evolution of R_a throughout weathering. Of the rock types investigated, only marble VSI chips exhibited significantly higher % R_a increase for EM than AM trees, neither was there any correlation between R_a increase and in-bag pH (Figure 5.20B). This contrasts with the expectation that the larger range of weathering strategies available for EM rather than AM fungi (Section 2.8.3) and typically more acidic soil environments below EM trees (Figure 4.5) would facilitate greater weathering intensities below these species.

Angiosperm and gymnosperm tree groups were only compared for EM species, as there were insufficient data to analyse this for AM trees. Here, there were no significant differences between these tree groups, for proportional change in R_a , for any mineral chip. This is similar to results for weathering rate as the mycorrhizal status was the only factor influencing soil pH (Section 2.3.2.2, Section 4.3.1.1).

5.4.8.3 Influence of field weathering rates on surface roughness changes

There was a significant negative correlation between proportional change in R_a and weathering rate over the 7 month period mesh bags and VSI slides were buried at Bedgebury Pinetum. This relationship was driven by calcite VSI chips, as there was no correlation for marble when rock types were analysed independently. This result indicates that the evolution of surface roughness of calcite is less where field weathering rates are higher.

This result is surprising as I would have expected that surface roughness measured by VSI would increase most where weathering rates of bulk calcite were fastest; potentially through formation of etch pits or accumulation of surface hyphal matter promoting weathering, as well as contributions from mechanical abrasion and acid surface dissolution. However, Figure 5.20A shows the inverse relationship, especially for calcite. There may be larger increases in R_a where weathering rates are slowest as a result of deposition of secondary mineral precipitates, or adsorption of organic matter, providing some protection from weathering. Where calcite dissolution is slowest, there is likely to be a more favourable environment for calcite precipitation and potential formation of secondary minerals on surfaces.

Chapter 5

5.4.8.4 Limitations of VSI roughness measurements

VSI analysis is sensitive and measuring average roughness, R_a , may not be the best technique to assess mineral weathering in the field. Changes in surface roughness can occur as a result of many factors. R_a will be increased not only as a result of biological or abiotic weathering in the field, but simply by sample handling as VSI chips are abraded by rock grains sharing the same mesh in-growth bag (Saccone *et al.*, personal communication). VSI results presented in this chapter provide an indication of what is happening with mineral surfaces in the field and could be improved by performing a larger experiment as many samples were damaged during burial in the field.

Roughness parameters R_a and R_q are known to scale logarithmically with scan size (Koyuncu *et al.* 2006); however, the exact relationship depends on the exact material scanned. This relationship depends on not only the mineral type, but the exact area of the scan and subsampling technique used. Data collected to illustrate this point was collected by subsampling randomly selected scans of each mineral type and subsampling using concentric rectangles as shown in Figure 5.16D.

Above a certain point, the logarithmic relationship between R_a and scan area plateaus, and ideally measurements would be made for scan sizes of this area or above, to avoid statistical misrepresentation of the sample (Koyuncu *et al.* 2006). Physically, this is because as scan size gets larger, there is a higher likelihood the surveyed area will include unusually high or low topography, thus increasing scan roughness. Even at maximum scan size, the point at which R_q and scan area are decoupled is not consistently reached in this study, apart from for marble (Figure 5.16C). Ideally, measurements would be made at scan areas at or greater than the point where this plateau is reached, to avoid statistical misrepresentation of the samples (Koyuncu *et al.* 2006).

Theoretically, the average roughness could increase dramatically at low areas if the area subsampled contained a large range of surface heights. Clearly, the probability that the area sampled is representative of the entire chip increases with increasing area, so to minimise the effect of area on roughness, the same VSI scan size was used for each sample, and where possible, change in average roughness during weathering (ΔR_a) is calculated. With the VSI setup at Sheffield, the best that can be achieved is to use the maximum possible scan area, as in this study. However, this investigation shows the importance of ensuring that both the mineral type and each individual VSI chip is appropriate to measure using this technique. The relationship between scan area and roughness may well be different for weathered and unweathered samples.

5.5 Conclusions

This chapter has shown evidence of surface alteration of carbonate minerals by fungal hyphae. SEM images showed channels likely to be formed by fungal weathering; the width of these channels was measured from both SEM and VSI images. Measurements of hyphae from VSI images were slightly greater than those from SEM images. As VSI measures only topography, this could indicate the presence of a layer of exudates either side of each hypha, and might account for the tapering in hyphal cross section towards each side (Figure 5.14, Figure 5.22). Other indications that exudates might be implicated in fungal weathering are the slight difference in width between channels observed in SEM images, and hyphae that had been partially dislodged; and probable calcium oxalate crystals (Figure 5.13). In this study, EM and saprotrophic hyphae cannot be distinguished from one another, as is the case in other studies using SEM images (Koele *et al.* 2014).

Calculating channel width and channel depth from VSI data indicated that muscovite chips incubated under AM trees had slightly wider and deeper channels than those under EM trees. However, when contrasted with the results of Quirk *et al.* (2012, 2014) where the opposite result was seen, it is more likely that there are a wide range of channel width and depths depending on tree species and the soil environment. There is insufficient evidence to support my hypothesis that the contribution of surface channelling to mineral weathering is more prevalent under EM than AM species.

It is probably not currently possible to say conclusively whether hyphae in soils below AM or EM tree species form the deepest or widest channels on a mineral surface. Measurements for both functional groups fall within a tight range (Figure 5.24), and there are likely to be many factors that contribute to this weathering process, both biotic and abiotic, these may include climate; mineral incubation time; water-mineral contact time; rate of hyphal colonisation; growth conditions and nutrient requirements of mycorrhizal host plants. Alternatively, channel width and depth may not be indicative of AM/EM characteristics and may be more a measure of the timing of hyphal colonisation, and subsequent channel enlargement by biotic and abiotic dissolution. Future studies measuring the timing and rate of hyphal colonisation are required to detangle this confounding factor.

Relative increase in surface roughness was significantly greater for EM than for AM species for marble, however, this was not the case for calcite or muscovite, the other minerals where this parameter was measured. Calcite surface roughness and bulk weathering rates measured in mesh bags were inversely correlated; however, there was no relationship between roughness and pH, pointing towards the involvement of process

Chapter 5

other than dissolution, perhaps precipitation of secondary minerals or accumulation of surface organic matter. There are however, numerous other factors that can contribute to surface roughness, for instance, physical abrasion during sample handling, and this may not be a reliable method to use in future studies.

The use of VSI analysis to investigate bulk mineral surface alteration during weathering may be limited if not performed appropriately. Both measures of roughness, R_a and R_q , scale logarithmically with scan area. This relationship plateaus above a certain scan area, and ideally roughness measurements should be made only on scan areas above the point of this plateau. However, to ensure this condition is fulfilled will be both labour and time intensive using our current methodology. The exact relationship depends not only on the mineral type, but also on the exact area scanned, and may well be different before and after weathering.

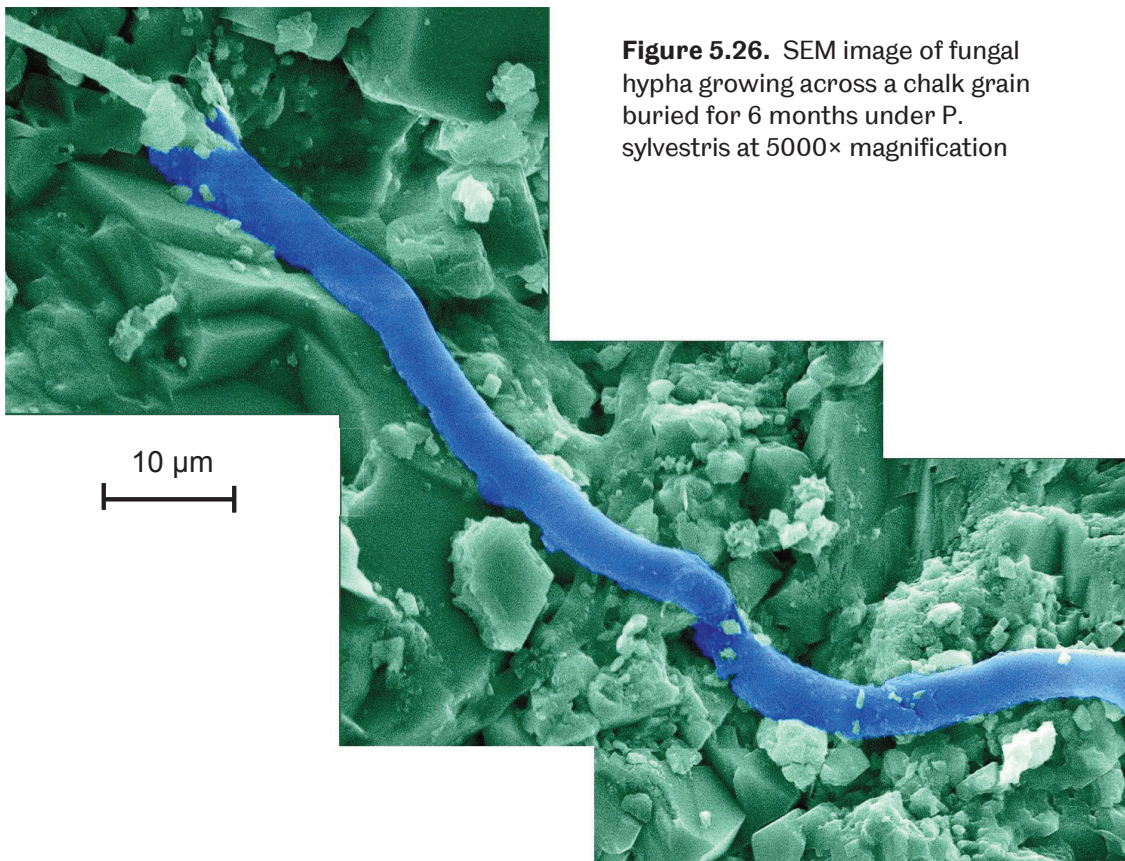


Figure 5.26. SEM image of fungal hypha growing across a chalk grain buried for 6 months under *P. sylvestris* at 5000× magnification

Chapter 6

General discussion

6.1 Introduction

Throughout the last century, anthropogenic CO₂ emissions have escalated dramatically, causing rapid climate change and ocean acidification (NOAA/ESRL 2016; Schmidt *et al.* 2016). Although anthropogenic emissions are slowing, atmospheric CO₂ concentrations are set to continue rising for the foreseeable future (Jackson *et al.* 2016). This presents two critical priorities for scientific research: first, to improve understanding of Earth processes and reduce uncertainty in future climate scenarios. Secondly, to devise strategies to both reduce atmospheric CO₂ concentrations and increase surface ocean pH.

Urgent action is required if we are to be able to limit the global temperature rise to 2°C by 2100, as agreed at the convening of the United Nations Framework Convention on Climate Change in Paris last December. Many strategies have been proposed to remove CO₂ from the atmosphere (Williams 2016), two of which are highly relevant in the context of this thesis. As discussed in Chapter 2, forests provide a natural CO₂ sink, and in the UK alone store 790 Mt C, removing about 15 Mt CO₂ per year. Creation of 230 km² new woodland annually could produce emissions abatement of 25% CO₂ from fossil fuels by 2030 or 10% of total greenhouse gas emissions by 2015 (Read *et al.* 2009).

Secondly, enhancement of silicate weathering by applying pulverised rocks, such as olivine, to the soil surface in highly active, mainly tropical, weathering regions has the potential to reduce global CO₂ levels by up to 50 ppm (Taylor *et al.* 2015). Silicate mineral weathering plays a vital role in the long-term global carbon cycle, locking atmospheric CO₂ into marine carbonates and providing a flux of alkalinity to the oceans. Carbonate weathering, on the other hand, has no net effect on CO₂

Chapter 6

drawdown on million-year timescales, but over the coming decades to centuries may accelerate, providing both a transient CO₂ sink and a source of alkalinity (Beaulieu *et al.* 2012).

Forests, together with their symbiotic mycorrhizal fungi are major drivers of silicate mineral weathering in forest soils (Landeweert *et al.* 2001; Quirk *et al.* 2012). However, despite the abundance of carbonate rocks on the land surface globally (Dürr *et al.* 2005; Amoiette-Suchet *et al.* 2003), there is limited knowledge about their rates of weathering as influenced by the temperate and boreal forest ecosystems that overlie them.

Chapter 1 reviewed current knowledge of key mechanisms of biological mineral weathering in general, and this thesis describes the involvement of trees and their mycorrhizal partners in soil formation; carbonate mineral weathering and phosphorus biogeochemical cycling to address knowledge gaps identified by this review. This chapter consolidates findings of previous chapters, first summarising principle conclusions.

6.2 Principle conclusions

1. Mycorrhizal functional type (arbuscular mycorrhiza, AM, and ectomycorrhiza, EM) plays a dominant role in determining soil physico-chemical characteristics. This challenges the long-standing assertion that tree functional group is the main influence on pedogenesis and that the greatest differences in soil chemistry are found between evergreen needle-leaf and deciduous broadleaf species.
2. Carbonate rock weathering in forest soils is accelerated by a wide range of mature trees and their mycorrhizal fungi.
3. Kinetic constants derived in abiotic laboratory setups cannot be used to accurately predict carbonate weathering rates within ecosystems. Accurate grain surface area measurements help reconcile theoretical and field-observed dissolution rates for dolomite-, but not for calcite-containing rock grains, which weather up to 4 orders of magnitude slower than expected.
4. Carbonate weathering rate enhancement is most marked in soils beneath tree taxa hosting ectomycorrhizal (EM) associations, an effect that is linked to rhizosphere acidification by this fungal group.

5. Fungal hyphae are able to biosense phosphorus in both carbonate and silicate substrates, preferentially colonising rock grains where P-concentrations are highest.
6. Carbonates accumulate phosphorus throughout weathering and may act as an effectively-renewable P-source.

6.3 Mycorrhizas as drivers of soil physico-chemical differences

Forests provide both a renewable fuel source and a cost-effective tool to remove CO₂ from the atmosphere. However, since the 1980s there has been a decline in tree planting in the UK, which is now gradually reducing the size of this CO₂ sink (Read *et al.* 2009). In the near future, the forested land area in the UK is planned to increase, both tree replanting recently felled plantations, and land conversion to new forests (Independent Panel on Forestry 2012). It is well established that tree species identity affects pedogenesis and resulting soil properties, and this has been a focus of literature for decades (Ovington 1953; Miles 1985, 1986; Binkley and Valentine 1991; Binkley 1994; Augusto *et al.* 2015). The variety of geochemical changes observed in relation to different tree species doubtless impact on long-term forestry ventures, and understanding these is vital for managing the environmental impacts of this industry.

Over the years, many, seemingly conflicting, soil responses to tree species have been documented (Binkley 1994). Much research has been confounded by selection of sites with a plot history that favours certain tree species and data from few long-term, replicated experiments are available to rigorously investigate this issue (Binkley and Valentine 1991). There are many engrained beliefs about forest soils, the most prevalent of these being the influence of tree functional group and litter input. For example, gymnosperms acidify soils compared to angiosperms, as stated in classic studies such as Ovington (1953):

“The influence of the individual tree species is dependent upon the initial site conditions and the silvicultural management of the plots, but the general trend, although exceptions do occur, is for conifers to intensify the increased acidity of the upper soil to a greater extent than the hardwood species.”

Despite evidence either opposing or suggesting a more complex view (France 1989; Binkley and Giardina 1998), this dogma persists (Augusto *et al.* 2015), and contrasting experimental outcomes may be dismissed as the result of site specific differences, a one off. Even when the number of these anomalies accumulates, the

Chapter 6

initial idea is too deep-rooted in popular belief to change. Far from wishing to criticise the work of Ovington, which is used extensively in Chapter 2, early studies such as this do not employ statistical analyses to rigorously test hypotheses, despite their elegant experimental design. Our re-analysis of his 1951 dataset shows no significant impact of tree-functional group on soil pH.

There is a need to update forest soil research to embrace the rigorous standards employed by other disciplines, and reconsider the evidence-base for many of our long-held beliefs (Binkley and Menyailo 2005). Chapter 2 revisits the Bedgebury forest plots first studied by Ovington, and presents a time-course of soil property evolution 22, 45 and 85 years after tree planting in 1929. By combining historical data (Ovington 1953, 1956, 1958; Howard and Howard 1984a,b), from 3 angiosperm and 6 gymnosperm monospecies plots, with a recent resampling in 2014, we have shown mycorrhizal type, and not tree functional group is instrumental in determining soil properties.

In the largest common-garden forest experiment to date, including both 9 Ovington plots and the 14 species used in weathering experiments, soil pH was lowest where trees hosted EM fungi. This challenges the long-standing assertion that tree-functional group and litter input is the main influence determining soil physico-chemical characteristics and highlights the dominant role played by mycorrhizas upon biogeochemical processes (Leake *et al.* 2004).

Tree species identity, and their regulation of soil properties, has important consequences for mineral weathering. Trees mediate rhizosphere microbial communities, including mycorrhizal fungi (Talbot *et al.* 2008), which in turn affect soil acidity by both LMWOA exudation and soil organic matter (SOM) decomposition.

6.3.1 Limitations of common garden experiments

Use of a common-garden experiment, such as that at Bedgebury provides the best tool for removing site-specific bias when investigating the soil forming functions of individual tree species. There are, of course, important limitations to this kind of experiment (Binkley and Menyailo 2005). In the context of our study, the most important is that within their natural ranges, the tree species planted would be unlikely to be found on the same Brown Earth soil type as that at Bedgebury pinetum (Figure 2.7A). To what extent tree impacts on potentially unrepresentative soil types mirror those within their native setting is unknown. Other limitations include the establishment of sites on former agricultural land with a history of fertilisation, and the short time span of my research project.

Binkley and Menyailo (2005) note that there is too little information on the effects of tree species to understand the time course of their influence on soil characteristics. Some species alter soils more rapidly than others; however, if established for a long period, the eventual end-points might converge. This is demonstrated in Chapter 2, where although there is evidence of continually evolving soil properties, such as the mounting soil extractable P concentration, there are no overall impacts of either tree or mycorrhizal functional group, beside that on pH. The re-analysis of soils within the forest plots at Bedgebury makes this the longest record of species-specific influences on temperate forest soils in a common garden experiment.

6.4 Reconciling field and laboratory carbonate weathering rates

This study presents a unique comparison of carbonate and silicate weathering regulation by major tree-mycorrhizal functional groups. Evidence from a year-long field experiment at Bedgebury pinetum confirms weathering rate enhancement of calcite- and dolomite-containing carbonates by a wide range of mature trees and their mycorrhizas.

Carbonate weathering rates in the field are still far slower than predicted using laboratory-derived rate constants (White and Brantley 2003). Laboratory experiments have demonstrated kinetic constants to differ between rocks, depending on exact mineralogy, structure, and permeability (Palandri and Kharaka 2004; Kirstein *et al.* 2016), and it is questionable to what degree results of these studies are applicable to the field situation. The ease of performing small-scale laboratory experiments to test weathering hypotheses is, of course, very useful. However, to ensure their relevance to ecosystem-scale weathering, future work must address two contributing issues to reconcile their weathering rates:

Firstly laboratory experiments vastly overestimate dissolution rates by potentially over 4 orders of magnitude for calcite and 1-2 orders of magnitude for silicates (White and Brantley 2003). I have reduced this discrepancy to within 2 orders of magnitude for both calcite and dolomite dissolution by normalising weathering rate to BET surface area and using kinetic constants from a recent study of low temperature carbonate dissolution more applicable to field conditions (5, 12.5 and 25°C; Kirstein *et al.* 2016). However, there is still scope for developing abiotic studies with more realistic conditions, for instance by using more complex substrates; reducing mineral-water contact time; and performing experiments close to equilibrium. Measurement of solution electrical conductivity, combined with modern data logging equipment would enable us to track changes in weathering rates in a substrate such as sterile soil during

Chapter 6

fluctuations in external conditions. For instance, weathering rock grains could be subjected to diurnal temperature variations, repeated cycles of wetting and drying, or changing drainage regimens.

Secondly, field studies underestimate carbonate weathering rates due to an overestimation of rock grain surface area. Weathering surfaces in soils are occluded by adsorption of organic matter and accumulation of secondary mineral precipitates. Accurate surface area measurement helps normalise dissolution rates and narrow the gap between theoretical and field, yet there is currently no accurate approach to estimating reactive mineral surface areas in complex substrates like soils (Brantley and Melliott 2000). There is a lack of understanding about how much mineral surface is available for dissolution reactions, further confounded by the observation that some types of surface are more reactive than others (Luttge *et al.* 2003; Arvidson *et al.* 2003).

6.5 Evolving plant-mycorrhiza associations affect carbonate weathering

The findings presented here highlight the potential of mycorrhizosphere processes to accelerate disintegration and dissolution of carbonate rock grains. In particular, I have shown that rhizosphere acidification by tree taxa hosting EM fungal associations promote the most rapid dissolution of acid-susceptible carbonate minerals. This parallels results of previous field studies which observed the most rapid silicate weathering in forest plots hosting EM partners (Quirk *et al.* 2012).

Mycorrhizal fungi acidify the soil via several mechanisms including respiratory CO₂ release; carbonic anhydrase catalysis of carbonic acid formation; and the production of LMWOA exudates; the latter of which is not a known strategy of AM fungi (Landeweert *et al.* 2001; Thorley *et al.* 2015).

Mycorrhizal weathering provides host plants with exclusive access to growth-limiting mineral nutrients, such as phosphorus from apatite (Leake *et al.* 2008). This was observed at Bedgebury, where phosphorus acquisition was a key driver of silicate weathering and prompted significant hyphal colonisation (Quirk *et al.* 2012). Fungal hyphae also colonised carbonate rock grains, and the extent of colonisation was positively related to phosphorus concentration. Hyphal colonisation of a P-containing mineral source implies that P contained within carbonates can be transported through the mycorrhizal network to provide some nutritional benefit to host trees (Leake *et al.* 2008).

However, while P-reserves of silicate rock grains were depleted, overall, carbonates exhibited a net increase in phosphorus content, the origins of which are not fully resolved in this study. It is likely that this P is inorganic in nature, because alkaline microenvironments, such as those surrounding dissolving carbonate grains, promote precipitation of P-complexes with base cations. Two possible sources of additional P were investigated, and suggest that P is neither contained within residual organic matter, nor does it simply adsorb from the soil solution. There may be a case for phosphorus originating both passively (P_P) from the surrounding environment and by active import by micro-organisms (P_A); and accumulation occurs when combined active and passive P-inputs exceed losses (P_{loss}) from leaching and active mycorrhizal weathering and export.

There is, however, to my knowledge no literature precedent for the novel finding of P-accumulation by carbonates. This leads me to propose a new model of P-biogeochemical cycling in calcareous soils:

$$\Delta P = (P_P + P_A) - P_{loss} \quad (13)$$

An important next step is to test this model, and assess which processes dominate phosphorus accumulation. Isotope tracer experiments using artificial carbonate substrates doped with ^{33}P would enable visualisation of P-transport and quantification of P accumulation. This would also allow verification of P-uptake by plants and mycorrhizas following carbonate weathering, and establish a functional link between hyphal colonisation and plant P-nutrition.

If mycorrhizal hyphae can mobilise P from carbonate rock grains, as they can from silicates (Leake *et al.* 2008), then carbonate weathering in soil may be important, not only for release of P contained within mineral, but for its ability to act as an effectively renewable P-source, filtering and concentrating P from the surrounding environment.

6.6 Closing Remarks

Field experiments reported in this thesis have demonstrated carbonate weathering enhancement in temperate forest soils, especially by trees hosting EM fungal symbionts. Given the potential of carbonate weathering as a short-term CO₂ sink over decades to centuries, the creation of new woodlands and rejuvenation of existing plantations, present a major opportunity for the UK to adapt forests to benefit future climate change management. Strategic tree planting on calcareous soils might provide a two-fold benefit of CO₂ sequestration, both through carbon uptake during photosynthesis and storage in biomass and by enhancing carbonate mineral dissolution. There is still much uncertainty in how carbonate weathering will respond to future climate change, and to what extent it provides a CO₂ sink. These areas might form a priority for future research. Planting of taxa hosting EM fungal associations may be especially beneficial due to their strengths in enhancing both carbonate and silicate weathering, providing both a belowground carbon sink, and a source of base cations and alkalinity to combat ocean acidification.

Appendix

Table A. 1. Preparation of calibration curve for Murphy-Riley Phosphorus determination. Volumes in brackets apply where samples are highly acidic, such as those from aqua regia digests. For these samples it was necessary to add 0.5 ml of NaOH solution after 15 minutes to enable colour development. Sample blank may be an extraction or digest blank, depending on sample preparation technique. This must be used to ensure colour development in both samples and calibration curves is equivalent.

P (ug P/cuvette)	10ppm P-stock (µl)	Sample blank (ml)	Ascorbic acid (µl)	UHP H2O	Colour developer (ml)	3.44M NaOH – after 15 mins (ml)	Total volume (ml)
0	0	1	100	1.9	0.5	(0.5)	3.5 (4)
0.25	25	1	100	1.875	0.5	(0.5)	3.5 (4)
0.5	50	1	100	1.85	0.5	(0.5)	3.5 (4)
0.75	75	1	100	1.825	0.5	(0.5)	3.5 (4)
1	100	1	100	1.8	0.5	(0.5)	3.5 (4)
2	200	1	100	1.7	0.5	(0.5)	3.5 (4)
2.5	250	1	100	1.65	0.5	(0.5)	3.5 (4)
3	300	1	100	1.6	0.5	(0.5)	3.5 (4)
4	400	1	100	1.5	0.5	(0.5)	3.5 (4)
5	500	1	100	1.4	0.5	(0.5)	3.5 (4)

Table A. 2. Height and diameter at breast height (Mean \pm SEM) of tree species studied at Bedgebury Pinetum. For all species N = 5, except Ginkgo where fewer specimens were available and N = 4. Where trees had been coppiced and were growing multiple trunks, these were treated as a single trunk with cross sectional area (CSA) equivalent to the sum of CSAs for each individual trunk.

Species	Height (m)	Trunk diameter (m)
Ginkgo biloba	13.9 \pm 2	1.2 \pm 0.2
Metasequoia glyptostroboides	18.9 \pm 1.1	1.2 \pm 0.1
Sequoia sempervirens	33.4 \pm 0.7	3.8 \pm 0.1
Araucaria araucana	13.4 \pm 0.7	1.1 \pm 0.1
Ilex aquifolium	12.4 \pm 0.6	1.6 \pm 0.1
Acer pseudoplatanus	12.6 \pm 0.5	0.8 \pm 0.1
Liriodendron tulipifera	15.1 \pm 1.7	1.4 \pm 0.1
Pinus sylvestris	24.5 \pm 1.4	1.6 \pm 0.1
Larix decidua	26.7 \pm 1	1.6 \pm 0.3
Abies alba	25.2 \pm 1.1	1.8 \pm 0.1
Nothofagus dombeyi	24.9 \pm 1.5	1.6 \pm 0.1
Quercus petraea	20.8 \pm 0.5	1.3 \pm 0.1
Eucalyptus coccifera	26.3 \pm 1.4	1.1 \pm 0.04

Table A. 3. Concentrations of major and trace elements in silicate and carbonate rock grains used in weathering field study at Bedgebury pinetum (determined using XRF, GAU-Radioanalytical Laboratories, National Oceanography Centre, Southampton).

		Silicate	Chalk	Dolomite	Marble	Oolite
Major element concentration (wt%)	SiO ₂	75.60	1.61	0.83	0.65	2.59
	TiO ₂	0.38	0.01	0.02	0.01	0.03
	Al ₂ O ₃	10.91	0.16	0.17	0.04	0.39
	Fe ₂ O ₃	2.38	0.12	0.29	0.07	0.38
	MnO	0.04	0.03	0.06	<0.01	0.01
	MgO	0.63	0.42	20.61	0.72	0.44
	CaO	1.56	53.56	29.97	54.07	52.60
	K ₂ O	3.44	0.02	0.05	0.02	0.08
	Na ₂ O	2.45	<0.02	<0.02	<0.02	<0.02
	P ₂ O ₅	0.056	0.046	0.006	0.004	0.015
	Sum	97.44	55.98	52.00	55.58	56.53
	Trace element concentration (ppm)	Ba	882	<10	29	12
Ce		37	<6	<6	<6	<6
Co		<8	<8	<8	25	9
Cr		12	<4	7	<4	19
Cu		46	<2	58	11	15
Ni		29	<2	<2	3	6
Pb		<2	<2	5	<2	<2
Sr		203	545	60	152	446
V		51	12	12	17	15
Zn		4	<2	31	<2	<2
Zr		228	<2	<2	<2	<2

Table A. 4. Additional BET values, the BET constant, and correlation coefficients for unweathered silicate rock grain samples not included in Section 4.3.3.1. Samples are identified by burial duration (~ 7 or 14 months); tree species and tree number in brackets. AA = *Araucaria araucana*; AN = *Abies nordmanniana*; EC = *Eucalyptus coccoifera*; PS = *Pinus sylvestris*; QP = *Quercus petraea*; SS = *Sequoia sempervirens*.

Months	Sample	Analysis date	Degassed mass (g)	BET ± equipment error (m ² /g)	C	Correlation coefficient
0	Silicate 2	03/06/2015	2.0267	0.1950 ± 0.0024	51.32	0.99939
0	Silicate 3	19/06/2015	4.8330	0.1551 ± 0.0005	53.94	0.99996
14	AA (3)	02/10/2015	1.9583	0.4302 ± 0.0034	57.18	0.99975
14	AN (2)	02/10/2015	1.9670	0.2752 ± 0.0021	44.24	0.99977
14	AN (4)	03/06/2015	1.9687	0.2679 ± 0.0042	181.66	0.99902
14	EC (5)	01/10/2015	1.9882	0.2764 ± 0.0021	59.01	0.99978
14	PS (2)	02/10/2015	1.9796	0.2837 ± 0.0043	125.75	0.99912
14	QP (1)	02/10/2015	1.9945	0.2587 ± 0.0043	93.86	0.99891
14	QP (5)	02/10/2015	1.4718	0.3621 ± 0.0039	98.35	0.99954
14	SS (2)	02/10/2015	1.9846	0.4353 ± 0.0033	107.09	0.99977

Method A. 1 Preparation of colour developer solution for spectrophotometric P determination

To 250 ml 2.5M H₂SO₄ (34.75ml conc. H₂SO₄ made up to 250 ml with UHP dH₂O) was added 74 ml of ammonium molybdate solution (4 g (NH₄)₆Mo₇O₂₄/100 ml UHP dH₂O m/v) and 25 ml of antimony potassium tartarate solution (1.454 g K₂Sb₂(C₄H₂O₆)₂ /500 ml UHP dH₂O m/v), before diluting to a final volume of 500 ml.

Method A. 2 Trypan blue lactophenol stain for dead fungal hyphae

Trypan blue stains dead cells as it adheres to the cell membrane. Live cells are not stained by this method as the stain is not absorbed by their functioning membranes. This stain is prepared by dissolving Trypan Blue [0.4g, C₃₄H₂₄N₆O₁₄S₄Na₄] and phenol (50 g) in a mixture of lactic acid (50 ml), glycerol (100 ml) and UHP dH₂O (50 ml).

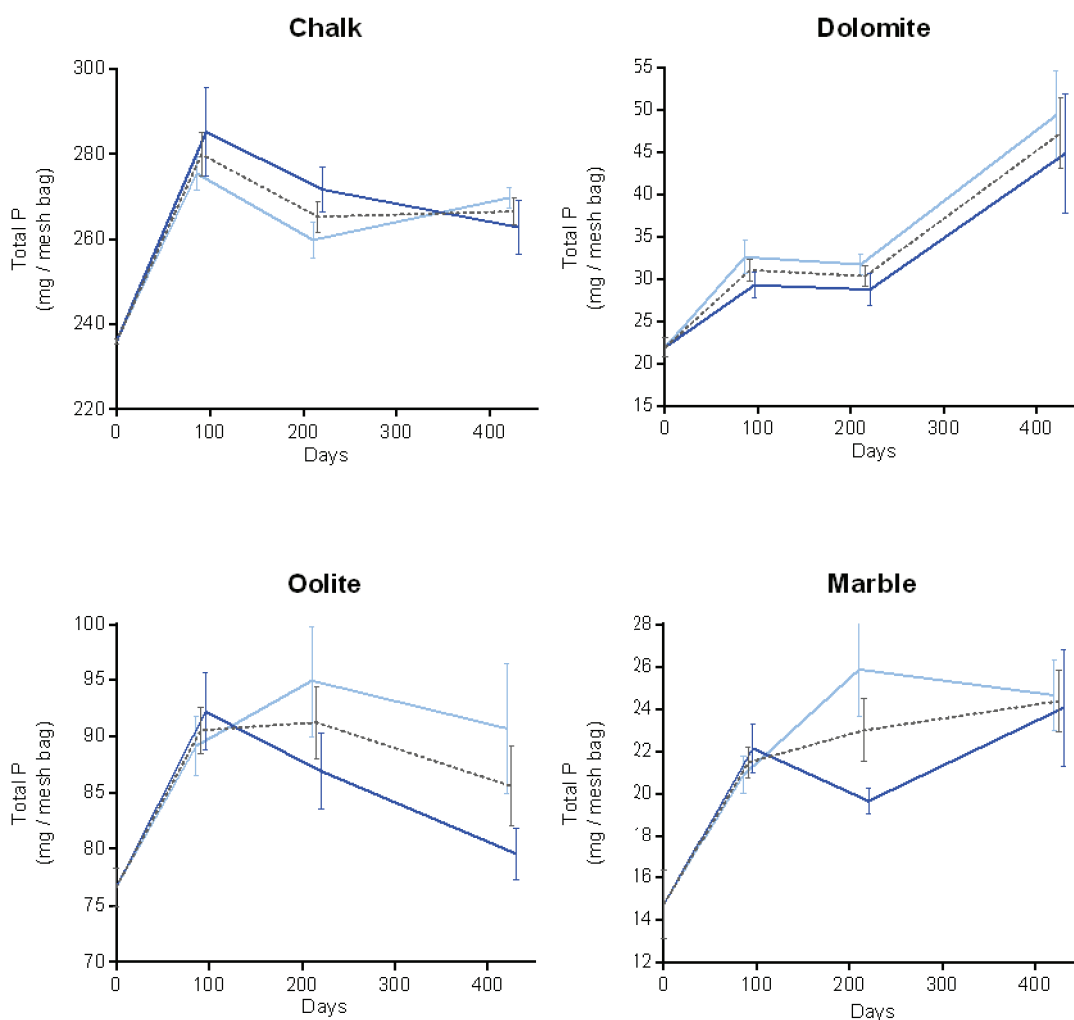


Figure A. 1. Total phosphorus content (Mean \pm SEM), adjusted for weathered sample mass, of chalk, dolomite, oolite and marble rock grain samples (original mass 2.5 g) over a time course of 0, 3, 7 and 14 months weathering in the field, split by mycorrhizal type (AM, light blue lines, N = 7; EM, dark blue lines, N = 6; overall average, grey dashed lines, N = 13 tree species).

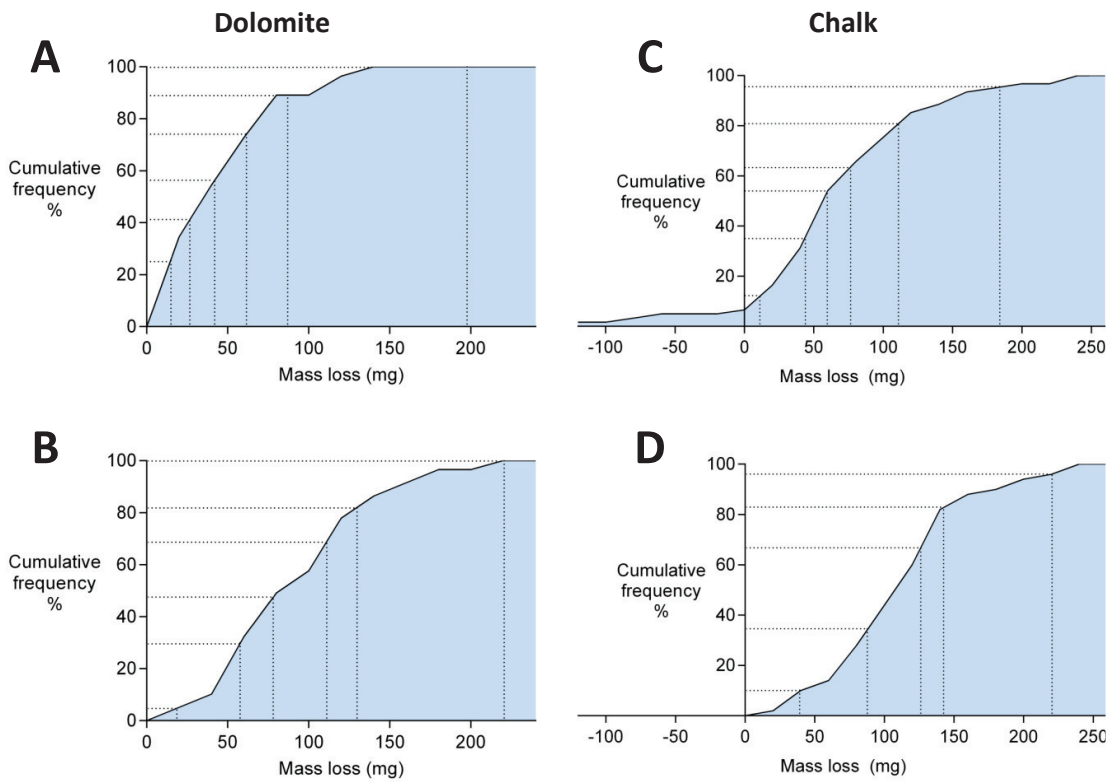


Figure A. 2. Cumulative frequency distribution of **A)** 7 and **B)** 14-month dolomite (left panel); and **C)** 7 and **D)** 14-month chalk (right panel) samples after outlier removal (ROUT method, $Q = 1\%$; cumulative frequency bin size = 20). Samples for BET analysis were selected so that they were approximately evenly spaced throughout the cumulative frequency distribution. Slightly uneven spacing for chalk samples is due to having already used some samples for other analysis techniques so there was insufficient remaining for BET analysis. Approximately 2 g of sample is required for reliable BET surface area determination with this type of rock grain sample.

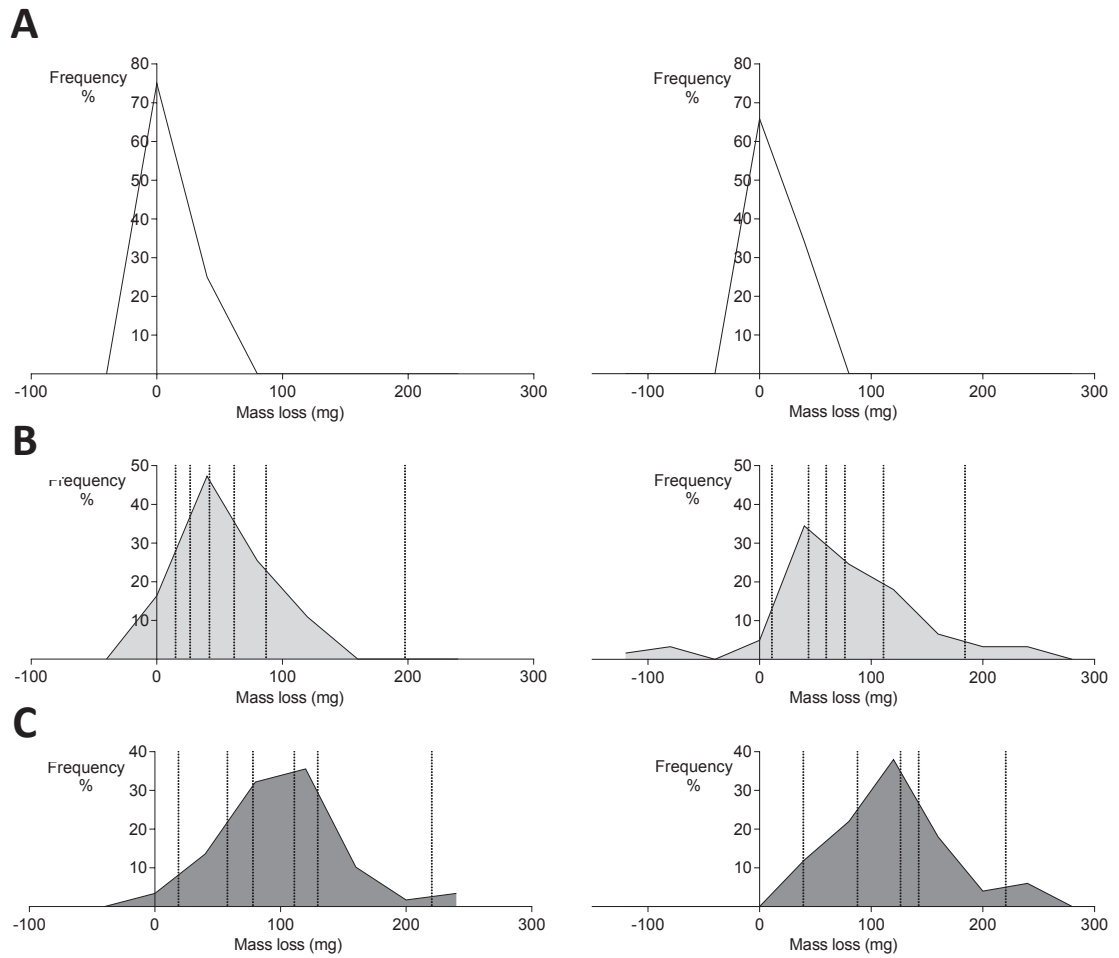


Figure A. 3. Histogram of weathering mass loss data for dolomite (left panel) and chalk (right panel) after **A)** 4, **B)** 7 and **C)** 14 months burial at Bedgebury Pinetum. Vertical dotted lines denote masses of samples selected for BET analysis. Note the minimal overlap of mass loss data for 7 and 14 month samplings toward the right hand tail of the distribution.

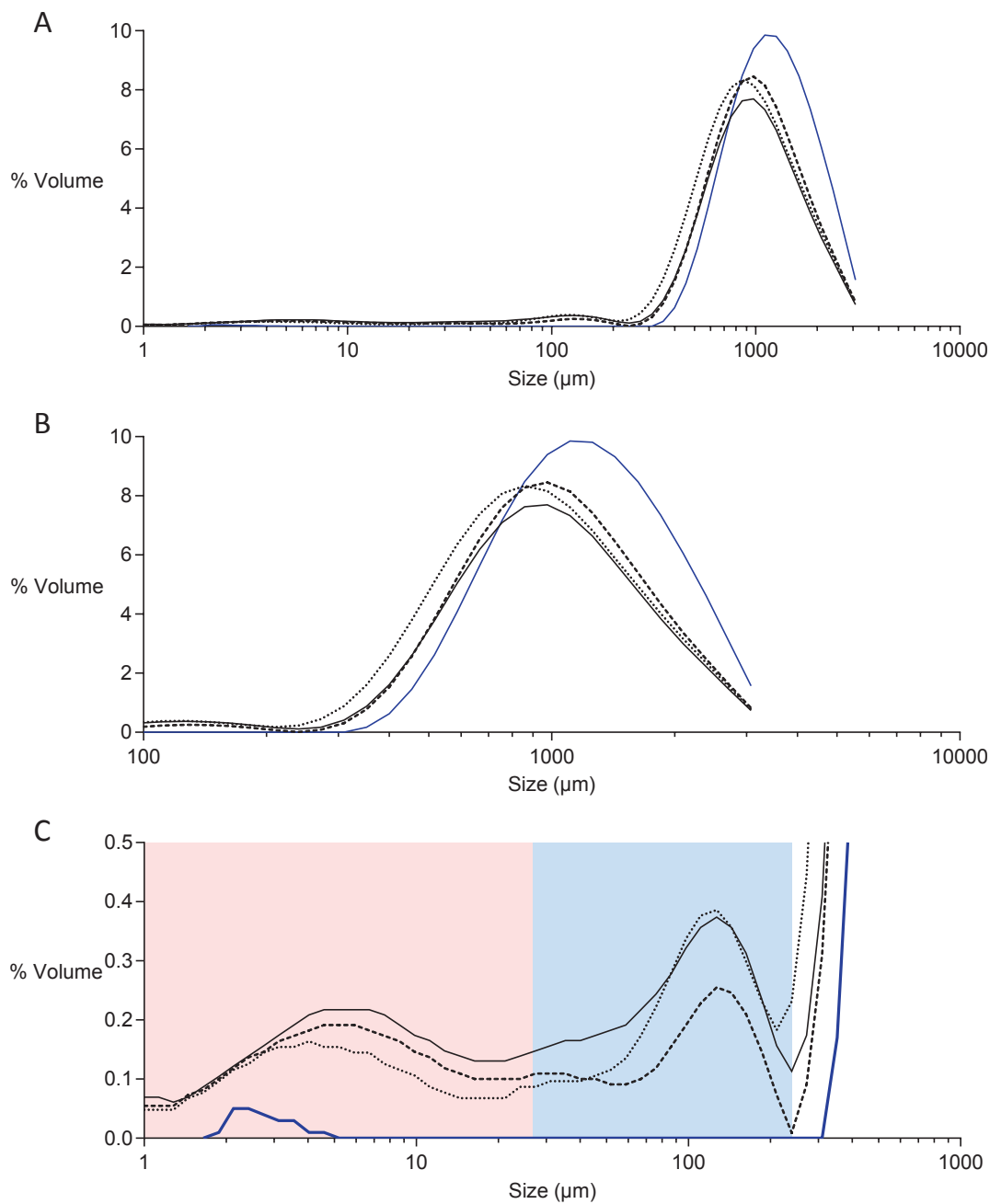


Figure A. 4. Mass-normalised particle size distribution of 1 unweathered (blue line) and 3 chalk samples after 14 months weathering, PS = *P. sylvestris* (black continuous line), EC = *E. coccifera* (long dashes) and ND = *N. dombeyii* (dotted line) measured by wet dispersion. **A)** Overall view of particle size distribution. Expanded sections of **B)** only particles >100 μm diameter and **C)** particles <1000 μm diameter (note the difference in scale). Pink shading represents the range defined for small particles, 0-25 μm and blue shading that for medium particles, 25-240 μm . Above 240 μm particles are classed as large. Each trace is an average of 5 measurements of 10 s duration.

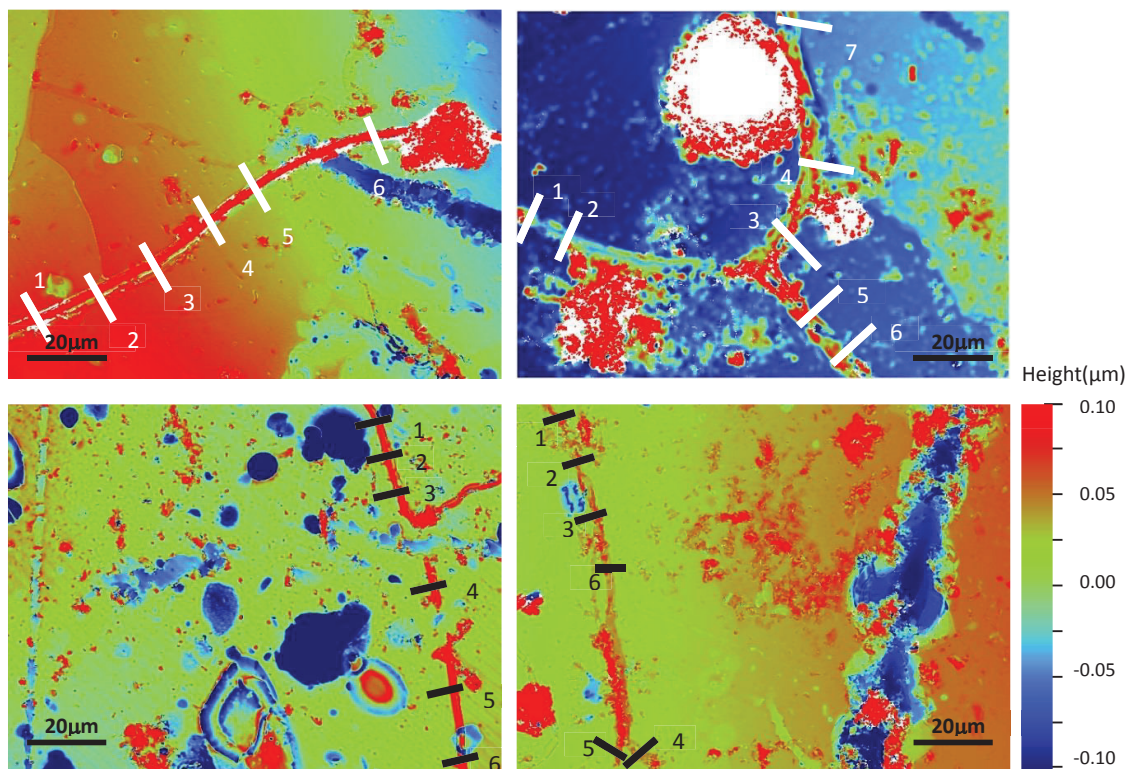


Figure A. 5. Measuring hyphal material width and cross sectional area using Vision software. Putative hyphal material is identified as being raised above the mineral surface and example transects for measurement are shown. Analysis was repeated for channel features which were defined as having lower topography than the surrounding mineral surface and curved or branching morphology.

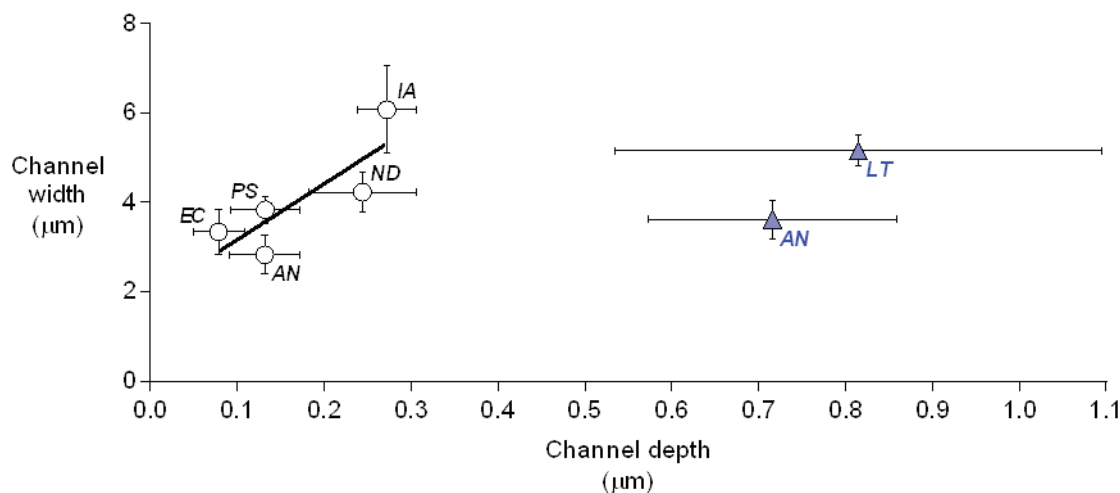


Figure A. 6. Cross plot of measured channel width and depth on muscovite (Mean \pm SEM) from this study showing data points removed from subsequent analyses (AN and LT; blue). These surface features were unusually deep for putative hyphal channels and may have been misidentified channels, or formed by hyphal occupying a previously-formed crack. EC = *E. coccifera*; AN = *A. nordmaniana*; PS = *P. sylvestris*; ND = *N. dombeyii*; IA = *I. aquifolium* and LT = *L. tulipifera* (N = 5 measurements of 2 muscovite chips for each AN, IA, PS, LT and EC and 5 measurements from 3 muscovite chips for ND).

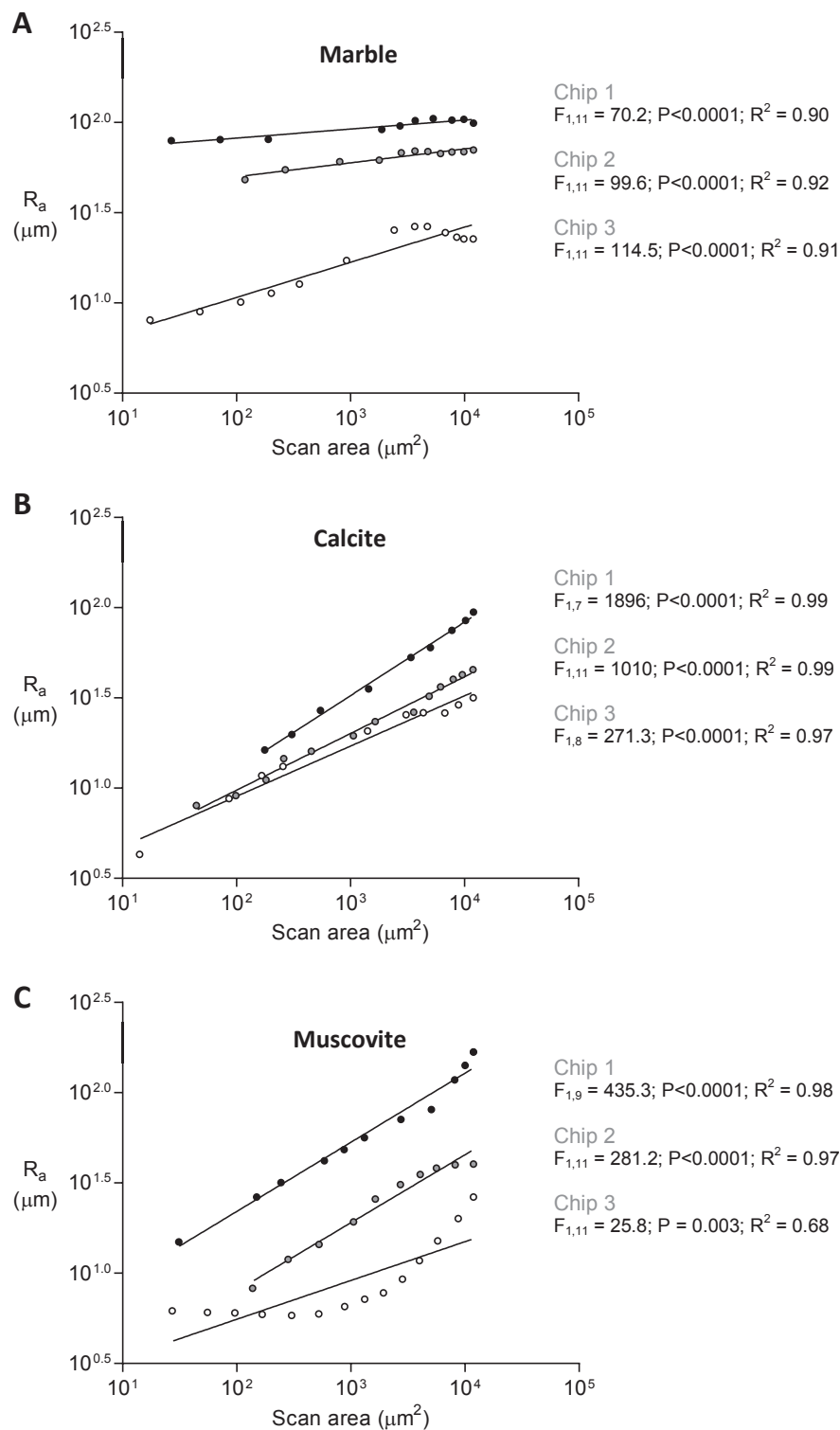


Figure A. 7. Log-log graphs corresponding to Figure 4, showing dependence of average roughness (R_a) on scan area. Three mineral chips were subsampled for each of **A**) marble **B**) calcite and **C**) muscovite. Results of linear regressions for each chip are displayed.

References

- Ainsworth, E. A. and Long, S. P. (2004) 'What have we learned from 15 years of free-air CO₂ enrichment (FACE)? A meta-analytic review of the responses of photosynthesis, canopy properties and plant production to rising CO₂', *New Phytologist*, 165(2), 351-372.
- Ainsworth, E. A. and Rogers, A. (2007) 'The response of photosynthesis and stomatal conductance to rising CO₂: mechanisms and environmental interactions', *Plant, Cell & Environment*, 30(3), 258-270.
- Allen, A. S., Andrews, J. A., Finzi, A. C., Matamala, R., Richter, D. D. and Schlesinger, W. H. (2000) 'Effects of free-air CO₂ enrichment (FACE) on belowground processes in a *Pinus taeda* forest', *Ecological Applications*, 10(2), 437-448.
- Amiotte Suchet, P., Probst, J.-L. and Ludwig, W. (2003) 'Worldwide distribution of continental rock lithology: Implications for the atmospheric/soil CO₂ uptake by continental weathering and alkalinity river transport to the oceans', *Global Biogeochem. Cycles*, 17(2), 1038-1051.
- Anderson, M. (1987) 'The effects of forest plantations on some lowland soils. 1. A Second sampling of nutrient stocks', *Forestry*, 60(1), 69-85.
- Andrews, J. A. and Schlesinger, W. H. (2001) 'Soil CO₂ dynamics, acidification, and chemical weathering in a temperate forest with experimental CO₂ enrichment', *Global Biogeochemical Cycles*, 15(1), 149-162.
- Arocena, J. M., Glowa, K. R. and Massicotte, H. B. (2001) 'Calcium-rich hypha encrustations on *Piloderma*', *Mycorrhiza*, 10(5), 209-215.
- Arvidson, R. S., Ertan, I. E., Amonette, J. E. and Luttge, A. (2003) 'Variation in calcite dissolution rates: A fundamental problem?', *Geochimica et Cosmochimica Acta*, 67(9), 1623-1634.
- Arvieu, J. C., Leprince, F. and Plassard, C. (2003) 'Release of oxalate and protons by ectomycorrhizal fungi in response to P-deficiency and calcium carbonate in nutrient solution', *Annals of Forest Science*, 60(8), 815-821.
- Augusto, L., De Schrijver, A., Vesterdal, L., Smolander, A., Prescott, C. and Ranger, J. (2015) 'Influences of evergreen gymnosperm and deciduous angiosperm tree species on the functioning of temperate and boreal forests', *Biological Reviews*, 90(2), 444-466.
- Augusto, L., Turpault, M.-P. and Ranger, J. (2000) 'Impact of forest tree species on feldspar weathering rates', *Geoderma*, 96(3), 215-237.
- Baker, H. and Clapman, A. R. (1939) 'Seasonal Variations in the Acidity of Some Woodland Soils', *Journal of Ecology*, 27(1), 114-125.
- Balogh-Brunstad, Z., Keller, C. K., Dickinson, J. T., Stevens, F., Li, C. Y. and Bormann, B. T. (2008) 'Biotite weathering and nutrient uptake by ectomycorrhizal fungus, *Suillus tomentosus*, in liquid-culture experiments', *Geochimica et Cosmochimica Acta*, 72(11), 2601-2618.
- Beaulieu, E., Godderis, Y., Donnadieu, Y., Labat, D. and Roelandt, C. (2012) 'High sensitivity of the continental-weathering carbon dioxide sink to future climate change', *Nature Climate Change*, 2(5), 346-349.
- Beaulieu, E., Godderis, Y., Labat, D., Roelandt, C., Oliva, P. and Guerrero, B. (2010) 'Impact of atmospheric CO₂ levels on continental silicate weathering', *Geochemistry Geophysics Geosystems*, 11, 1-18.
- Beerling, D. J. and Royer, D. L. (2011) 'Convergent Cenozoic CO₂ history', *Nature Geoscience*, 4(7), 418-420.
- Berner, R. A. (1992) 'Weathering, plants and the long-term carbon cycle', *Geochimica et Cosmochimica Acta*, 56(8), 3225-3231.

- Berner, R. A. (1997) 'The rise of plants and their effect on weathering and atmospheric CO₂', *Science*, 276(5312), 544.
- Berner, R. A. (2003) 'The long-term carbon cycle, fossil fuels and atmospheric composition', *Nature*, 426(6964), 323-326.
- Berner, R. A., Lasaga, A. C. and Garrels, R. M. (1983) 'The carbonate-silicate geochemical cycle and its effect on atmospheric carbon dioxide over the past 100 million years', *American Journal of Science*, 283(7), 641-683.
- Betts, R. A., Jones, C. D., Knight, J. R., Keeling, R. F. and Kennedy, J. J. (2016) 'El Nino and a record CO₂ rise', *Nature Climate Change*, advance online publication.
- Binkley, D. (1994) *The influence of tree species on forest soils: Processes and patterns*, translated by 994.
- Binkley, D. and Giardina, C. (1998) 'Why do tree species affect soils? The Warp and Woof of tree-soil interactions', *Biogeochemistry*, 42(1-2), 89-106.
- Binkley, D. and Menyailo, O. (2005) 'Gaining insights on the effects of tree species on soils' in *Tree species effects on soils: Implications for global change*, Springer, 1-16.
- Binkley, D. and Valentine, D. (1991) 'Fifty-year biogeochemical effects of green ash, white pine, and Norway spruce in a replicated experiment', *Forest Ecology and Management*, 40(1), 13-25.
- Bligh, E. G. and Dyer, W. J. (1959) 'A rapid method of total lipid extraction and purification', *Canadian journal of biochemistry and physiology*, 37(8), 911-917.
- Blum, J. D., Klaue, A., Nezat, C. A., Driscoll, C. T., Johnson, C. E., Siccama, T. G., (...) and Likens, G. E. (2002) 'Mycorrhizal weathering of apatite as an important calcium source in base-poor forest ecosystems', *Nature*, 417(6890), 729-731.
- Boggs, S. (2009) *Petrology of Sedimentary Rocks*, Cambridge University Press.
- Bonfante, P. and Genre, A. (2010) 'Mechanisms underlying beneficial plant–fungus interactions in mycorrhizal symbiosis', *Nature Communications*, 1, 48.
- Bonneville, S., Morgan, D. J., Schmalenberger, A., Bray, A., Brown, A., Banwart, S. A. and Benning, L. G. (2011) 'Tree-mycorrhiza symbiosis accelerate mineral weathering: Evidences from nanometer-scale elemental fluxes at the hypha-mineral interface', *Geochimica et Cosmochimica Acta*, 75(22), 6988-7005.
- Bonneville, S., Smits, M. M., Brown, A., Harrington, J., Leake, J. R., Brydson, R. and Benning, L. G. (2009) 'Plant-driven fungal weathering: Early stages of mineral alteration at the nanometer scale', *Geology*, 37(7), 615-618.
- Boström, B., Andersen, J. M., Fleischer, S. and Jansson, M. (1988) 'Exchange of phosphorus across the sediment-water interface' in Persson, G. and Jansson, M., eds., *Phosphorus in Freshwater Ecosystems: Proceedings of a Symposium held in Uppsala, Sweden, 25–28 September 1985*, Dordrecht: Springer Netherlands, 229-244.
- Brady, P. V. and Carroll, S. A. (1994) 'Direct effects of CO₂ and temperature on silicate weathering: possible implications for climate control', *Geochimica et Cosmochimica Acta*, 58(7), 1853-1856.
- Brantley, S. (2003) 'Reaction kinetics of primary rock-forming minerals under ambient conditions', *Treatise on geochemistry*, 5, 73-117.
- Brantley, S. L., Kubicki, J. D. and White, A. F. (2008) *Kinetics of water-rock interaction*, Springer.
- Brantley, S. L., Magonigal, J. P., Scatena, F. N., Balogh-Brunstad, Z., Barnes, R. T., Bruns, M. A., (...) and Yoo, K. (2011) 'Twelve testable hypotheses on the geobiology of weathering', *Geobiology*, 9(2), 140-165.
- Brantley, S. L. and Mellott, N. P. (2000) 'Surface area and porosity of primary silicate minerals', *American Mineralogist*, 85(11-12), 1767-1783.
- Brook, G. A., Folkoff, M. E. and Box, E. O. (1983) 'A world model of soil carbon dioxide', *Earth Surface Processes and Landforms*, 8(1), 79-88.
- Brown, P. J., Bradley, R. S. and Keimig, F. T. (2010) 'Changes in extreme climate indices for the northeastern United States, 1870–2005', *Journal of Climate*, 23(24), 6555-6572.

- Brown, S. J., Caesar, J. and Ferro, C. A. T. (2008) 'Global changes in extreme daily temperature since 1950', *Journal of Geophysical Research: Atmospheres*, 113(D5).
- Brunauer, S., Emmett, P. H. and Teller, E. (1938) 'Adsorption of gases in multimolecular layers', *Journal of the American chemical society*, 60(2), 309-319.
- Buss, H. L., Lüttge, A. and Brantley, S. L. (2007) 'Etch pit formation on iron silicate surfaces during siderophore-promoted dissolution', *Chemical Geology*, 240(3), 326-342.
- Cai, W.-J., Hu, X., Huang, W.-J., Murrell, M. C., Lehrter, J. C., Lohrenz, S. E., Chou, W.-C., Zhai, W., Hollibaugh, J. T., Wang, Y., Zhao, P., Guo, X., Gundersen, K., Dai, M. and Gong, G.-C. (2011) 'Acidification of subsurface coastal waters enhanced by eutrophication', *Nature Geoscience*, 4(11), 766-770.
- Casarin, V., Plassard, C., Hinsinger, P. and Arvieu, J. C. (2004) 'Quantification of ectomycorrhizal fungal effects on the bioavailability and mobilization of soil P in the rhizosphere of *Pinus pinaster*', *New phytologist*, 163(1), 177-185.
- Casarin, V., Plassard, C., Souche, G. and Arvieu, J.-C. (2003) 'Quantification of oxalate ions and protons released by ectomycorrhizal fungi in rhizosphere soil', *Agronomie-Sciences des Productions Vegetales et de l'Environnement*, 23(5-6), 461-470.
- Challinor, D. (1968) 'Alteration of surface soil characteristics by four tree species', *Ecology*, 49(2), 286-290.
- Chen, C., Condron, L. and Xu, Z. (2008) 'Impacts of grassland afforestation with coniferous trees on soil phosphorus dynamics and associated microbial processes: A review', *Forest Ecology and Management*, 255(3), 396-409.
- Chen, I. C., Hill, J. K., Ohlemüller, R., Roy, D. B. and Thomas, C. D. (2011) 'Rapid range shifts of species associated with high levels of climate warming', *Science*, 333(6045), 1024-1026.
- Chou, L., Garrels, R. M. and Wollast, R. (1989) 'Comparative study of the kinetics and mechanisms of dissolution of carbonate minerals', *Chemical Geology*, 78(3-4), 269-282.
- Cochran, M. F. and Berner, R. A. (1996) 'Promotion of chemical weathering by higher plants: field observations on Hawaiian basalts', *Chemical Geology*, 132(1), 71-77.
- Cockell, C. S. and Herrera, A. (2008) 'Why are some microorganisms boring?', *Trends in Microbiology*, 16(3), 101-106.
- Condron, L., Cornforth, I., Davis, M. and Newman, R. (1996) 'Influence of conifers on the forms of phosphorus in selected New Zealand grassland soils', *Biology and fertility of soils*, 21, 37-42.
- Cubillas, P., Köhler, S., Prieto, M., Chairat, C. and Oelkers, E. H. (2005) 'Experimental determination of the dissolution rates of calcite, aragonite, and bivalves', *Chemical Geology*, 216, 59-77.
- Dannoura, M., Maillard, P., Fresneau, C., Plain, C., Berveiller, D., Gerant, D., Chipeaux, C., Bosc, A., Ngao, J. and Damesin, C. (2011) 'In-situ assessment of the velocity of carbon transfer by tracing ¹³C in trunk CO₂ efflux after pulse labelling: variations among tree species and seasons', *New Phytologist*, 190(1), 181-192.
- Davis, M. B. and Shaw, R. G. (2001) 'Range shifts and adaptive responses to quaternary climate change', *Science*, 292(5517), 673-679.
- DeLucia, E. H., Hamilton, J. G., Naidu, S. L., Thomas, R. B., Andrews, J. A., Finzi, A. C. and Schlesinger, W. H. (1999) 'Net primary production of a forest ecosystem with experimental CO₂ enrichment', *Science*, 284(5417), 1177-1179.
- Derbyshire, E. and Mellors, T. W. (1988) 'Geological and geotechnical characteristics of some loess and loessic soils from China and Britain: a comparison', *Engineering geology*, 25(2), 135-175.
- Diaz, R. J. and Rosenberg, R. (2008) 'Spreading dead zones and consequences for marine ecosystems', *Science*, 321(5891), 926-929.
- Dijkstra, F. (2003) 'Calcium mineralization in the forest floor and surface soil beneath different tree species in the northeastern US', *Forest Ecology and Management*, 175(1), 185-194.
- Dürr, H. H., Meybeck, M. and Dürr, S. H. (2005) 'Lithologic composition of the Earth's continental surfaces derived from a new digital map emphasizing riverine material transfer', *Global Biogeochemical Cycles*, 19(4), GB4S10.

- Eldhuset, T. D., Swensen, B., Wickstrøm, T. and Wollebæk, G. (2007) 'Organic acids in root exudates from *Picea abies* seedlings influenced by mycorrhiza and aluminum', *Journal of Plant Nutrition and Soil Science*, 170(5), 645-648.
- Elleuche, S. and Pöggeler, S. (2009) 'Evolution of carbonic anhydrases in fungi', *Current Genetics*, 55(2), 211-222.
- Epron, D., Ngao, J., Dannoura, M., Bakker, M., Zeller, B., Bazot, S., Bosc, A., Plain, C., Lata, J. and Priault, P. (2011) 'Seasonal variations of belowground carbon transfer assessed by in situ $^{13}\text{CO}_2$ pulse labelling of trees', *Biogeosciences*, 8(5), 1153-1168.
- Finlay, R., Wallander, H., Smits, M., Holmstrom, S., Van Hees, P., Lian, B. and Rosling, A. (2009) 'The role of fungi in biogenic weathering in boreal forest soils', *Fungal Biology Reviews*, 23(4, Sp. Iss. SI), 101-106.
- Forestry Comission. (1951) *Guide to the National Pinetum and Forest Plots at Bedgebury*, His Majesty's Stationary Office.
- Forestry Comission. (1961) *Bedgebury Pinetum and Forest Plots*, Her Majesty's Stationary Office.
- Forestry Comission. (1972) *Bedgebury Pinetum and Forest Plots*, Her Majesty's Stationary Office.
- France, E. A., Binkley, D. and Valentine, D. (1989) 'Soil chemistry changes after 27 years under four tree species in southern Ontario', *Canadian Journal of Forest Research*, 19(12), 1648-1650.
- Friese, C. F. and Allen, M. F. (1991) 'The spread of VA mycorrhizal fungal hyphae in the soil: Inoculum types and external hyphal architecture', *Mycologia*, 83(4), 409-418.
- Gadd, G. M. (1999) 'Fungal production of citric and oxalic acid: importance in metal speciation, physiology and biogeochemical processes', *Advances in microbial physiology*, 41, 47-92.
- Gaillardet, J., Dupré, B., Louvat, P. and Allègre, C. (1999) 'Global silicate weathering and CO_2 consumption rates deduced from the chemistry of large rivers', *Chemical Geology*, 159, 3-30.
- Gaillardet, J., Viers, J. and Dupré, B. (2003) 'Trace Elements in River Waters' in Turekian, K., ed. *Treatise on Geochemistry*, Oxford: Pergamon, 225-272.
- Garcia, M., Ovasapyan, T., Greas, M. and Treseder, K. (2008) 'Mycorrhizal dynamics under elevated CO_2 and nitrogen fertilization in a warm temperate forest', *Plant and Soil*, 303(1-2), 301-310.
- Gazzè, S., Saccone, L., Ragnarsdottir, K., Smits, M., Duran, A., Leake, J., Banwart, S. and McMaster, T. (2012) 'Nanoscale channels on ectomycorrhizal-colonized chlorite: Evidence for plant-driven fungal dissolution', *Journal of Geophysical Research-Biogeosciences*, 117, G00N09.
- Gazzè, S., Saccone, L., Smits, M., Duran, A., Leake, J., Banwart, S., Ragnarsdottir, K. and McMaster, T. (2013) 'Nanoscale observations of Extracellular Polymeric Substances deposition on phyllosilicates by an ectomycorrhizal fungus', *Geomicrobiology Journal*, 30(8), 721-730.
- Ghasemi, A. R. (2015) 'Changes and trends in maximum, minimum and mean temperature series in Iran', *Atmospheric Science Letters*, 16(3), 366-372.
- Giardina, C. P., Huffman, S., Binkley, D. and Caldwell, B. A. (1995) 'Alders increase soil phosphorus availability in a Douglas-fir plantation', *Canadian journal of forest research*, 25(10), 1652-1657.
- Gislason, S. R., Oelkers, E. H., Eiriksdottir, E. S., Kardjilov, M. I., Gisladottir, G., Sigfusson, B. and Oskarsson, N. (2009) 'Direct evidence of the feedback between climate and weathering', *Earth and Planetary Science Letters*, 277(1-2), 213-222.
- Godderis, Y., Brantley, S. L., Francois, L. M., Schott, J., Pollard, D., Deque, M. and Dury, M. (2013) 'Rates of consumption of atmospheric CO_2 through the weathering of loess during the next 100 yr of climate change', *Biogeosciences*, 10(1), 135-148.
- Goll, D. S., Moosdorf, N., Hartmann, J. and Brovkin, V. (2014) 'Climate-driven changes in chemical weathering and associated phosphorus release since 1850: Implications for the land carbon balance', *Geophysical Research Letters*, 41(10), 3553-3558.
- Gutjahr, A., Dabringhaus, H. and Lacmann, R. (1996) 'Studies of the growth and dissolution kinetics of the CaCO_3 polymorphs calcite and aragonite I. Growth and dissolution rates in water', *Journal of crystal growth*, 158(3), 296-309.

- Hagerberg, D., Thelin, G. and Wallander, H. (2003) 'The production of ectomycorrhizal mycelium in forests: relation between forest nutrient status and local mineral sources', *Plant and Soil*, 252(2), 279-290.
- Hallbäck, L. and Tamm, C. O. (1986) 'Changes in soil acidity from 1927 to 1982–1984 in a forest area of south-west Sweden', *Scandinavian Journal of Forest Research*, 1(1-4), 219-232.
- Halman, J. M., Schaberg, P. G., Hawley, G. J. and Eagar, C. (2008) 'Calcium addition at the Hubbard Brook Experimental Forest increases sugar storage, antioxidant activity and cold tolerance in native red spruce (*Picea rubens*)', *Tree Physiology*, 28(6), 855-862.
- Hansen, J., Kharecha, P., Sato, M., Masson-Delmotte, V., Ackerman, F., Beerling, D. J., Hearty, P. J., Hoegh-Guldberg, O., Hsu, S.-L. and Parmesan, C. (2013) 'Assessing “dangerous climate change”: required reduction of carbon emissions to protect young people, future generations and nature', *PloS one*, 8(12), e81648.
- Hartmann, J., Jansen, N., Duerr, H., Kempe, S. and Koehler, P. (2009) 'Global CO₂-consumption by chemical weathering: What is the contribution of highly active weathering regions?', *Global and Planetary Change*, 69(4), 185-194.
- Hartmann, J., Moosdorf, N., Lauerwald, R., Hinderer, M. and West, A. J. (2014) 'Global chemical weathering and associated P-release - The role of lithology, temperature and soil properties', *Chemical Geology*, 363, 145-163.
- Hartmann, J., West, A. J., Renforth, P., Koehler, P., De La Rocha, C. L., Wolf-Gladrow, D. A., Duerr, H. H. and Scheffran, J. (2013) 'Enhanced chemical weathering as a geoengineering strategy to reduce atmospheric carbon dioxide, supply nutrients, and mitigate ocean acidification', *Reviews of Geophysics*, 51(2), 113-149.
- Haselwandter, K. (2008) 'Structure and function of siderophores produced by mycorrhizal fungi', *Mineralogical Magazine*, 72(1), 61-64.
- Hobbie, S. E., Ogdahl, M., Chorover, J., Chadwick, O. A., Oleksyn, J., Zytowski, R. and Reich, P. B. (2007) 'Tree species effects on soil organic matter dynamics: The role of soil cation composition', *Ecosystems*, 10(6), 999-1018.
- Hobbie, S. E., Oleksyn, J., Eissenstat, D. M. and Reich, P. B. (2010) 'Fine root decomposition rates do not mirror those of leaf litter among temperate tree species', *Oecologia*, 162(2), 505-513.
- Hoffland, E., Giesler, R., Jongmans, A. G. and Breemen, N. (2003) 'Feldspar tunneling by fungi along natural productivity gradients', *Ecosystems*, 6(8), 739-746.
- Hoffland, E., Giesler, R., Jongmans, T. and van Breemen, N. (2002) 'Increasing feldspar tunneling by fungi across a north Sweden podzol chronosequence', *Ecosystems*, 5(1), 11-22.
- Hoppert, M., Flies, C., Pohl, W., Gänzl, B. and Schneider, J. (2004) 'Colonization strategies of lithobiontic microorganisms on carbonate rocks', *Environmental Geology*, 46(3-4), 421-428.
- Howard, P. and Howard, D. (1984b) 'Effects of trees on soil properties, a resampling of JD Ovington's *Pinus nigra* var *maritima* plots at Bedgebury, Abbotswood, and West Tofts'.
- Howard, P., Howard, D. and Lowe, L. (1998) 'Effects of tree species and soil physico-chemical conditions on the nature of soil organic matter', *Soil Biology and Biochemistry*, 30(3), 285-297.
- Howard, P. J. A. and Howard, D. (1984a) 'Effects of trees on soil properties, a resampling of JD Ovington's plots at Bedgebury'.
- Howard, R. J., Ferrari, M. A., Roach, D. H. and Money, N. P. (1991) 'Penetration of hard substrates by a fungus employing enormous turgor pressures', *Proceedings of the National Academy of Sciences*, 88(24), 11281-11284.
- Högberg, M. N., Briones, M. J., Keel, S. G., Metcalfe, D. B., Campbell, C., Midwood, A. J., Thornton, B., Hurry, V., Linder, S. and Näsholm, T. (2010) 'Quantification of effects of season and nitrogen supply on tree below-ground carbon transfer to ectomycorrhizal fungi and other soil organisms in a boreal pine forest', *New Phytologist*, 187(2), 485-493.
- Independent-Panel-on-Forestry (2012) *Independent Panel on Forestry: Final report*, Defra.
- IPCC (2013) 'Climate Change 2013: The physical science basis - Summary for policymakers'.

- IPCC (2014) 'Climate Change 2014: Impacts, adaptation, and vulnerability - IPCC WGII AR5 Summary for policymakers',
- Jackson, R. B., Canadell, J. G., Le Quere, C., Andrew, R. M., Korsbakken, J. I., Peters, G. P. and Nakicenovic, N. (2016) 'Reaching peak emissions', *Nature Climate Change*, 6(1), 7-10.
- Jeffery, E. (2008) 'The marl pits of West Sussex',
- Jones, D. L. and Darrah, P. R. (1994) 'Role of root derived organic acids in the mobilization of nutrients from the rhizosphere', *Plant and soil*, 166(2), 247-257.
- Jongmans, A. G., van Breemen, N., Lundstrom, U., van Hees, P. A. W., Finlay, R. D., Srinivasan, M., Unestam, T., Giesler, R., Melkerud, P. A. and Olsson, M. (1997) 'Rock-eating fungi', *Nature*, 389(6652), 682-683.
- Kalliokoski, T., Nygren, P. and Sievanen, R. (2008) 'Coarse root architecture of three boreal tree species growing in mixed stands', *Silva Fennica*, 42(2), 189.
- Kernan, M., Battarbee, R., Curtis, C., Monteith, D. and E, S. (2010) *UK acid waters monitoring network: 20 year interpretive report*, Environmental Change Research Centre University College London
- Kirstein, J., Hellevang, H., Haile, B. G., Gleixner, G. and Gaupp, R. (2016) 'Experimental determination of natural carbonate rock dissolution rates with a focus on temperature dependency', *Geomorphology*, 261, 30-40.
- Koele, N., Dickie, I., Blum, J., Gleason, J. and de Graaf, L. (2014) 'Ecological significance of mineral weathering in ectomycorrhizal and arbuscular mycorrhizal ecosystems from a field-based comparison', *Soil Biology and Biochemistry*, 69, 63-70.
- Kolo, K., Keppens, E., Preat, A. and Claeys, P. (2007) 'Experimental observations on fungal diagenesis of carbonate substrates', *Journal of Geophysical Research-Biogeosciences*, 112(G1), G01007.
- Konhauser, K. O. (2009) *Introduction to Geomicrobiology*, Wiley.
- Koyuncu, I., Brant, J., Lüttge, A. and Wiesner, M. R. (2006) 'A comparison of vertical scanning interferometry (VSI) and atomic force microscopy (AFM) for characterizing membrane surface topography', *Journal of Membrane Science*, 278(1), 410-417.
- Kuzyakov, Y. and Gavrichkova, O. (2010) 'Review: Time lag between photosynthesis and carbon dioxide efflux from soil: a review of mechanisms and controls', *Global Change Biology*, 16(12), 3386-3406.
- Landeweert, R., Hoffland, E., Finlay, R. D., Kuyper, T. W. and van Breemen, N. (2001) 'Linking plants to rocks: ectomycorrhizal fungi mobilize nutrients from minerals', *Trends in Ecology & Evolution*, 16(5), 248-254.
- Landi, A., Mermut, A. R. and Anderson, D. W. (2003) 'Origin and rate of pedogenic carbonate accumulation in Saskatchewan soils, Canada', *Geoderma*, 117(1-2), 143-156.
- Lapeyrie, F., Chilvers, G. A. and Bhem, C. A. (1987) 'Oxalic acid synthesis by the mycorrhizal fungus *Paxillus involutus*', *New Phytologist*, 106(1), 139-146.
- Leake, J., Johnson, D., Donnelly, D., Muckle, G., Boddy, L. and Read, D. (2004) 'Networks of power and influence: the role of mycorrhizal mycelium in controlling plant communities and agroecosystem functioning', *Canadian Journal of Botany*, 82(8), 1016-1045.
- Leake, J. R., Duran, A. L., Hardy, K. E., Johnson, I., Beerling, D. J., Banwart, S. A. and Smits, M. M. (2008) 'Biological weathering in soil: the role of symbiotic root-associated fungi biosensing minerals and directing photosynthate-energy into grain-scale mineral weathering', *Mineralogical Magazine*, 72(1), 85-89.
- Leake, J. R., Ostle, N. J., Rangel-Castro, J. I. and Johnson, D. (2006) 'Carbon fluxes from plants through soil organisms determined by field ¹³CO₂ pulse-labelling in an upland grassland', *Applied Soil Ecology*, 33(2), 152-175.
- Lee, M. R., Brown, D. J., Smith, C. L., Hodson, M. E., MacKenzie, M. and Hellmann, R. (2007) 'Characterization of mineral surfaces using FIB and TEM: a case study of naturally weathered alkali feldspars', *American Mineralogist*, 92(8-9), 1383-1394.

- Li, W., Yu, L.-J., He, Q.-F., Wu, Y., Yuan, D.-X. and Cao, J.-H. (2005b) 'Effects of microbes and their carbonic anhydrase on Ca^{2+} and Mg^{2+} migration in column-built leached soil-limestone karst systems', *Applied Soil Ecology*, 29(3), 274-281.
- Li, W., Yu, L. J., Yuan, D. X., Wu, Y. and Zeng, X. D. (2005a) 'A study of the activity and ecological significance of carbonic anhydrase from soil and its microbes from different karst ecosystems of Southwest China', *Plant and Soil*, 272(1-2), 133-141.
- Li, W., Zhou, P.-P., Jia, L.-P., Yu, L.-J., Li, X. and Zhu, M. (2009) 'Limestone dissolution induced by fungal mycelia, acidic materials, and carbonic anhydrase from fungi', *Mycopathologia*, 167(1), 37-46.
- Li, Y. H. (1982) 'A brief discussion on the mean oceanic residence time of elements', *Geochimica et Cosmochimica Acta*, 46(12), 2671-2675.
- Lian, B., Yuan, D. and Liu, Z. (2011) 'Effect of microbes on karstification in karst ecosystems', *Chinese Science Bulletin*, 56(35), 3743-3747.
- Liu, W., Zhang, Y., Jiang, S., Deng, Y., Christie, P., Murray, P. J., Li, X. and Zhang, J. (2016) 'Arbuscular mycorrhizal fungi in soil and roots respond differently to phosphorus inputs in an intensively managed calcareous agricultural soil', *Scientific Reports*, 6, 24902.
- Liu, Z. H. (2001) 'Role of carbonic anhydrase as an activator in carbonate rock dissolution and its implication for atmospheric CO_2 sink', *Acta Geologica Sinica-English Edition*, 75(3), 275-278.
- Liu, Z. H. (2011) 'Is pedogenic carbonate an important atmospheric CO_2 sink?', *Chinese Science Bulletin*, 56(35), 3794-3796.
- Liu, Z. H., Yuan, D. X. and Dreybrodt, W. (2005a) 'Comparative study of dissolution rate-determining mechanisms of limestone and dolomite', *Environmental Geology*, 49(2), 274-279.
- Luttge, A., Winkler, U. and Lasaga, A. (2003) 'Interferometric study of dolomite dissolution: A new conceptual model for mineral dissolution', *Geochimica et Cosmochimica Acta*, 67(6), 1099-1116.
- Manning, D. A. C. and Renforth, P. (2013) 'Passive sequestration of atmospheric CO_2 through coupled plant-mineral reactions in urban soils', *Environmental Science & Technology*, 47(1), 135-141.
- Marschner, H. (1995) *Mineral Nutrition of Higher Plants*, Elsevier Science.
- Masterton, W. and Hurley, C. (2005) *Chemistry: Principles and Reactions, Updated Edition*, Cengage Learning.
- Mendoza, R., Escudero, V. and García, I. (2005) 'Plant growth, nutrient acquisition and mycorrhizal symbioses of a waterlogging tolerant legume (*Lotus glaber* Mill.) in a saline-sodic soil', *Plant and Soil*, 275(1), 305-315.
- Met Office. (2013) 'Summer 2013 weather summary'
- Met Office. (2014) 'Autumn 2013 weather summary'
- Met Office. (2015) 'Winter 2013/14 weather summary'
- Met Office. (2016) 'Regional values - Annual 2014'
- Miles, J. (1985) 'The pedogenic effects of different species and vegetation types and the implications of succession', *Journal of Soil Science*, 36(4), 571-584.
- Miles, J. (1986) 'What are the effects of trees on soils?' in Jenkins, D., ed. *Trees and wildlife in the Scottish uplands.*, NERC/ITE, 55-62.
- Moberg, A. and Jones, P. D. (2005) 'Trends in indices for extremes in daily temperature and precipitation in central and western Europe, 1901-99', *International Journal of Climatology*, 25(9), 1149-1171.
- Montanarella, L. (2010) *Soil pH in Europe*, European Soil Data Centre: European Commission.
- Morse, J. W. and Arvidson, R. S. (2002) 'The dissolution kinetics of major sedimentary carbonate minerals', *Earth-Science Reviews*, 58(1-2), 51-84.
- Mueller, K. E., Hobbie, S. E., Chorover, J., Reich, P. B., Eisenhauer, N., Castellano, M. J., Chadwick, O. A., Dobies, T., Hale, C. M., Jagodziński, A. M., Kałucka, I., Kieliszewska-Rokicka, B., Modrzyński, J., Rozen, A., Skorpupski, M., Sobczyk, Ł., Stasińska, M., Trocha, L. K., Weiner, J., Wierzbicka, A. and Oleksyn, J. (2015) 'Effects of litter traits, soil biota, and soil chemistry on soil carbon stocks at a common garden with 14 tree species', *Biogeochemistry*, 123(3), 313-327.

- Navarre-Sitchler, A. and Brantley, S. (2007) 'Basalt weathering across scales', *Earth and Planetary Science Letters*, 261(1-2), 321-334.
- Nihlgård, B. (1971) 'Pedological influence of spruce planted on former beech forest soils in Scania, south Sweden', *Oikos*, 22(3), 302-314.
- NOAA (2015) '2015 Gulf of Mexico dead zone 'above average'', [online], available: [accessed
- NOAA/ESRL (2016) 'Atmospheric CO₂ at Mauna Loa Observatory',
- Nowotny, I., Dahne, J., Klingelhofer, D. and Rothe, G. M. (1998a) 'Effect of artificial soil acidification and liming on growth and nutrient status of mycorrhizal roots of Norway spruce (*Picea abies* L. Karst.)', *Plant and Soil*, 199(1), 29-40.
- Nowotny, I., Schwanz, J. and Rothe, G. M. (1998b) 'Influence of soil acidification and liming on selected enzymes of the carbohydrate metabolism and the contents of two major organic acids of mycorrhizal roots of Norway spruce (*Picea abies* L. Karst.)', *Plant and Soil*, 199(1), 41-51.
- Oh, N. H., Hofmockel, M., Lavine, M. L. & Richter, D. D. 2007. Did elevated atmospheric CO₂ alter soil mineral weathering? An analysis of 5-year soil water chemistry data at Duke FACE study. *Global Change Biology*, 13, 2626-2641.
- Olsson, P. A. (1999) 'Signature fatty acids provide tools for determination of the distribution and interactions of mycorrhizal fungi in soil', *Fems Microbiology Ecology*, 29(4), 303-310.
- Olsson, P. A., Larsson, L., Bago, B., Wallander, H. and Van Aarle, I. M. (2003) 'Ergosterol and fatty acids for biomass estimation of mycorrhizal fungi', *New Phytologist*, 159(1), 7-10.
- Oren, R., Ellsworth, D. S., Johnsen, K. H., Phillips, N., Ewers, B. E., Maier, C., Schafer, K. V. R., McCarthy, H., Hendrey, G. and McNulty, S. G. (2001) 'Soil fertility limits carbon sequestration by forest ecosystems in a CO₂-enriched atmosphere'.
- Ovington, J. D. (1953) 'Studies of the development of woodland conditions under different trees: 1. Soils pH', *Journal of Ecology*, 41(1), 13-34.
- Ovington, J. D. (1956) 'The composition of tree leaves', *Forestry*, 29(1), 22-28.
- Ovington, J. D. (1958a) 'Studies of the development of woodland conditions under different trees: VI. Soil sodium, potassium and phosphorus', *Journal of Ecology*, 46(1), 127-142.
- Ovington, J. D. (1958b) 'Studies of the development of woodland conditions under different trees: VII. Soil Calcium and Magnesium', *Journal of Ecology*, 46(2), 391-405.
- Palandri, J. and Kharaka, Y. (2004) 'A compilation of rate parameters of water-mineral interaction kinetics for application to geochemical modelling', *Open file report 2004-1068*.
- Pallasser, R., Minasny, B. and McBratney, A. B. (2013) 'Soil carbon determination by thermogravimetrics', *PeerJ*, 1, e6.
- Perrin, A.-S., Probst, A. and Probst, J.-L. (2008) 'Impact of nitrogenous fertilizers on carbonate dissolution in small agricultural catchments: Implications for weathering CO₂ uptake at regional and global scales', *Geochimica et Cosmochimica Acta*, 72(13), 3105-3123.
- Phillips, R. P. and Fahey, T. J. (2006) 'Tree species and mycorrhizal associations influence the magnitude of rhizosphere effects', *Ecology*, 87(5), 1302-1313.
- Ponge, J. F., Patzel, N., Delhaye, L., Devigne, E., Levieux, C., Beros, P. and Wittebroodt, R. (1999) 'Interactions between earthworms, litter and trees in an old-growth beech forest', *Biology and Fertility of Soils*, 29(4), 360-370.
- Quirk, J., Beerling, D. J., Banwart, S. A., Kakonyi, G., Romero-Gonzalez, M. E. and Leake, J. R. (2012) 'Evolution of trees and mycorrhizal fungi intensifies silicate mineral weathering', *Biology Letters*, 8(6), 1006-1011.
- Quirk, J., Leake, J. R., Banwart, S. A., Taylor, L. L. and Beerling, D. J. (2014) 'Weathering by tree-root-associating fungi diminishes under simulated Cenozoic atmospheric CO₂ decline', *Biogeosciences*, 11(2), 321-331.
- Raulund-Rasmussen, K., Borggaard, O. K., Hansen, H. C. B. and Olsson, M. (1998) 'Effect of natural organic soil solutes on weathering rates of soil minerals', *European Journal of Soil Science*, 49(3), 397-406.

- Raymond, P. A. and Cole, J. J. (2003) 'Increase in the export of alkalinity from North America's largest river', *Science*, 301(5629), 88-91.
- Raymond, P. A., Oh, N. H., Turner, R. E. and Broussard, W. (2008) 'Anthropogenically enhanced fluxes of water and carbon from the Mississippi River', *Nature*, 451(7177), 449-452.
- Read, D. J. (1991) 'Mycorrhizas in ecosystems', *Experientia*, 47(4), 376-391.
- Read, D. J., Freer-Smith, P. H., Morison, J. I. L., Hanley, N., West, C. C. and Snowdon, P. (2009) Combating climate change: a role for UK forests. An assessment of the potential of the UK's trees and woodlands to mitigate and adapt to climate change, The Stationery Office Limited.
- Read, D. J., Leake, J. R. and Perez-Moreno, J. (2004) 'Mycorrhizal fungi as drivers of ecosystem processes in heathland and boreal forest biomes', *Canadian Journal of Botany-Revue Canadienne De Botanique*, 82(8), 1243-1263.
- Reich, P. B., Oleksyn, J., Modrzynski, J., Mrozinski, P., Hobbie, S. E., Eissenstat, D. M., Chorover, J., Chadwick, O. A., Hale, C. M. and Tjoelker, M. G. (2005) 'Linking litter calcium, earthworms and soil properties: a common garden test with 14 tree species', *Ecology Letters*, 8(8), 811-818.
- Renforth, P., Manning, D. A. C. and Lopez-Capel, E. (2009) 'Carbonate precipitation in artificial soils as a sink for atmospheric carbon dioxide', *Applied Geochemistry*, 24(9), 1757-1764.
- Renforth, P., Washbourne, C. L., Taylder, J. and Manning, D. A. C. (2011) 'Silicate production and availability for mineral carbonation', *Environmental Science & Technology*, 45(6), 2035-2041.
- Renshaw, J. C., Robson, G. D., Trinci, A. P. J., Wiebe, M. G., Livens, F. R., Collison, D. and Taylor, R. J. (2002) 'Fungal siderophores: structures, functions and applications', *Mycological Research*, 106(10), 1123-1142.
- Ronov, A. (1968) 'Probable changes in the composition of sea water during the course of geological time', *Sedimentology*, 10(1), 25-43.
- Rosenstock, N. P. (2009) 'Can ectomycorrhizal weathering activity respond to host nutrient demands?', *Fungal Biology Reviews*, 23(4), 107-114.
- Rosling, A. (2003) *Responses of ectomycorrhizal fungi to mineral substrates*, unpublished thesis Swedish University of Agricultural Sciences.
- Rosling, A., Lindahl, B. D. and Finlay, R. D. (2004a) 'Carbon allocation to ectomycorrhizal roots and mycelium colonising different mineral substrates', *New Phytologist*, 162(3), 795-802.
- Rosling, A., Lindahl, B. D., Taylor, A. F. S. and Finlay, R. D. (2004b) 'Mycelial growth and substrate acidification of ectomycorrhizal fungi in response to different minerals', *Fems Microbiology Ecology*, 47(1), 31-37.
- Rouhier, H. and Read, D. J. (1998) 'Plant and fungal responses to elevated atmospheric carbon dioxide in mycorrhizal seedlings of *Pinus sylvestris*', *Environmental and Experimental Botany*, 40, 237-246.
- Ruddiman, W. (2001) *Earth's Climate*, W.H. Freeman and Company, New York.
- Saccone, L., Gazze, S. A., Duran, A. L., Leake, J. R., Banwart, S. A., Ragnarsdottir, K. V., Smits, M. M. and McMaster, T. J. (2012) 'High resolution characterization of ectomycorrhizal fungal-mineral interactions in axenic microcosm experiments', *Biogeochemistry*, 111(1-3), 411-425.
- Sandnes, A., Eldhuset, T. D. and Wollebaek, G. (2005) 'Organic acids in root exudates and soil solution of Norway spruce and silver birch', *Soil Biology & Biochemistry*, 37(2), 259-269.
- Scarrow, J. H., Curran, J. M. and Kerr, A. C. (2000) 'Major Element Records of Variable Plume Involvement in the North Atlantic Province Tertiary Flood Basalts', *Journal of Petrology*, 41(7), 1155-1176.
- Schaberg, P. G. and Hawley, G. J. (2010) 'Disruption of calcium nutrition at Hubbard Brook experimental forest (New Hampshire) alters the health and productivity of red spruce and sugar maple trees and provides lessons pertinent to other sites and regions'.
- Schmalenberger, A., Duran, A. L., Romero-Gonzales, M. E., Leake, J. R. and Banwart, S. A. (2010) 'Oxalic acid release in ectomycorrhiza mineral weathering', *Geochimica et Cosmochimica Acta*, 74(12), A923.
- Schmidt, G., Ruedy, R., Persin, A., Sato, M. and Lo, K. (2016) 'NASA GISS Surface temperature (GISTEMP) analysis',

- Schneider, C. A., Rasband, W. S. and Eliceiri, K. W. (2012) 'NIH Image to ImageJ: 25 years of image analysis', *Nat Meth*, 9(7), 671-675.
- Smith, S. E. and Read, D. J. (2008) *Mycorrhizal Symbiosis, 3rd Edition*.
- Smith, S. E. and Smith, F. A. (2012) 'Fresh perspectives on the roles of arbuscular mycorrhizal fungi in plant nutrition and growth', *Mycologia*, 104(1), 1-13.
- Smits, M. (2006) *Fungi in biogeochemical cycles: Mineral tunnelling by fungi*, Cambridge University Press.
- Smits, M. M., Bonneville, S., Benning, L. G., Banwart, S. A. and Leake, J. R. (2012) 'Plant-driven weathering of apatite - the role of an ectomycorrhizal fungus', *Geobiology*, 10(5), 445-456.
- Smits, M. M., Hoffland, E., Jongmans, A. G. and van Breemen, N. (2005) 'Contribution of mineral tunneling to total feldspar weathering', *Geoderma*, 125, 59-69.
- Soinne, H. (2009) 'Extraction methods in soil phosphorus characterisation: Limitations and applications'.
- Staddon, P. L., Ramsey, C. B., Ostle, N., Ineson, P. and Fitter, A. H. (2003) 'Rapid turnover of hyphae of mycorrhizal fungi determined by AMS microanalysis of ¹⁴C', *Science*, 300(5622), 1138-1140.
- Stevens, P. A., Norris, D. A., Williams, T. G., Hughes, S., Durrant, D. W. H., Anderson, M. A., Weatherley, N. S., Hornung, M. and Woods, C. (1995) 'Nutrient losses after clearfelling in Beddgelert Forest: a comparison of the effects of conventional and whole-tree harvest on soil water chemistry', *Forestry*, 68(2), 115-131.
- Stewart, M. K. and McDonnell, J. J. (1991) 'Modeling base flow soil water residence times from deuterium concentrations', *Water Resources Research*, 27(10), 2681-2693.
- Subke, J.-A., Vallack, H., Magnusson, T., Keel, S., Metcalfe, D., Högberg, P. and Ineson, P. (2009) 'Short-term dynamics of abiotic and biotic soil: Effluxes after in-situ; pulse labelling of a boreal pine forest', *The New Phytologist*, 183(2), 349-357.
- Sverdrup, H. (2009) 'Chemical weathering of soil minerals and the role of biological processes', *Fungal Biology Reviews*, 23(4), 94-100.
- Szanişzlo, P. J., Powell, P. E., Reid, C. P. P. and Cline, G. R. (1981) 'Production of hydroxamate siderophore iron chelators by ectomycorrhizal fungi', *Mycologia*, 73(6), 1158-1174.
- Tans, P. and Keeling, R. (2013) 'Mauna Loa CO₂ monthly mean data', *NOAA/ESRL, Scripps Institution of Oceanography*.
- Taylor, A. F. S., Martin, F. and Read, D. J. (2000) 'Fungal diversity in ectomycorrhizal communities of Norway spruce (*Picea abies* (L.) Karst) and beech (*Fagus sylvatica* L.) along north-south transects in Europe' in Schulze, E.-D., ed. *Carbon and Nitrogen Cycling in European Forest Ecosystems*, Berlin, Heidelberg: Springer Berlin Heidelberg, 343-365.
- Taylor, L. L., Leake, J. R., Quirk, J., Hardy, K., Banwart, S. A. and Beerling, D. J. (2009) 'Biological weathering and the long-term carbon cycle: integrating mycorrhizal evolution and function into the current paradigm', *Geobiology*, 7(2), 171-191.
- Taylor, L. L., Quirk, J., Thorley, R. M. S., Kharecha, P. A., Hansen, J., Ridgwell, A., Lomas, M. R., Banwart, S. A. and Beerling, D. J. (2016) 'Enhanced weathering strategies for stabilizing climate and averting ocean acidification', *Nature Climate Change*, 6(4), 402-406.
- Thorley, R., Taylor, L. L., Banwart, S. A., Leake, J. R. and Beerling, D. J. (2015) 'The role of forest trees and their mycorrhizal fungi in carbonate rock weathering and its significance for global carbon cycling', *Plant, cell & environment*, 38(9), 1947-1961.
- Tisserant, E., Kohler, A., Dozolme-Seddas, P., Balestrini, R., Benabdellah, K., Colard, A. and Martin, F. (2012) 'The transcriptome of the arbuscular mycorrhizal fungus *Glomus intraradices* (DAOM 197198) reveals functional tradeoffs in an obligate symbiont', *New Phytologist*, 193(3), 755-769.
- Toljander, J. F., Lindahl, B. D., Paul, L. R., Elfstrand, M. and Finlay, R. D. (2007) 'Influence of arbuscular mycorrhizal mycelial exudates on soil bacterial growth and community structure', *Fems Microbiology Ecology*, 61(2), 295-304.
- Turner, B. L., Cade-Menun, B. J., Condon, L. M. and Newman, S. (2005) 'Extraction of soil organic phosphorus', *Talanta*, 66(2), 294-306.

- van Breemen, N., Finlay, R., Lundström, U., Jongmans, A. G., Giesler, R. and Olsson, M. (2000) 'Mycorrhizal weathering: A true case of mineral plant nutrition?', *Biogeochemistry*, 49(1), 53-67.
- van Hees, P. A. W., Godbold, D. L., Jentschke, G. and Jones, D. L. (2003) 'Impact of ectomycorrhizas on the concentration and biodegradation of simple organic acids in a forest soil', *European Journal of Soil Science*, 54(4), 697-706.
- van Hees, P. A. W., Jones, D. L. and Godbold, D. L. (2002) 'Biodegradation of low molecular weight organic acids in coniferous forest podzolic soils', *Soil Biology & Biochemistry*, 34(9), 1261-1272.
- van Scholl, L., Hoffland, E. and van Breemen, N. (2006a) 'Organic anion exudation by ectomycorrhizal fungi and *Pinus sylvestris* in response to nutrient deficiencies', *New Phytologist*, 170(1), 153-163.
- van Scholl, L., Smits, M. M. and Hoffland, E. (2006b) 'Ectomycorrhizal weathering of the soil minerals muscovite and hornblende', *New Phytologist*, 171(4), 805-814.
- Verrecchia, E., Braissant, O. and Cailleau, G. (2006) 'The oxalate-carbonate pathway in soil carbon storage: the role of fungi and oxalotrophic bacteria', *Fungi in biogeochemical cycles*, 289-310.
- Verrecchia, E. P. and Dumont, J. L. (1996) 'A biogeochemical model for chalk alteration by fungi in semiarid environments', *Biogeochemistry*, 35(3), 447-470.
- Walker, T. W. and Syers, J. K. (1976) 'The fate of phosphorus during pedogenesis', *Geoderma*, 15, 1-19.
- Wallander, H. (2000) 'Uptake of P from apatite by *Pinus sylvestris* seedlings colonised by different ectomycorrhizal fungi', *Plant and Soil*, 218(1-2), 249-256.
- Wallander, H. and Hagerberg, D. (2004) 'Do ectomycorrhizal fungi have a significant role in weathering of minerals in forest soil?', *Symbiosis*, 37(1-3), 249-257.
- Wallander, H. and Thelin, G. (2008) 'The stimulating effect of apatite on ectomycorrhizal growth diminishes after PK fertilization', *Soil Biology & Biochemistry*, 40(10), 2517-2522.
- Wang, B. and Qiu, Y. L. (2006) 'Phylogenetic distribution and evolution of mycorrhizas in land plants', *Mycorrhiza*, 16(5), 299-363.
- Wang, Q. and Li, Y. (2010) 'Phosphorus adsorption and desorption behavior on sediments of different origins', *Journal of Soils and Sediments*, 10(6), 1159-1173.
- Ward, M. B., Kapitulčinová, D., Brown, A. P., Heard, P. J., Cherns, D., Cockell, C. S., Hallam, K. R. and Ragnarsdóttir, K. V. (2013) 'Investigating the role of microbes in mineral weathering: Nanometre-scale characterisation of the cell-mineral interface using FIB and TEM', *Micron*, 47, 10-17.
- West, T. O. and McBride, A. C. (2005) 'The contribution of agricultural lime to carbon dioxide emissions in the United States: dissolution, transport, and net emissions', *Agriculture Ecosystems & Environment*, 108(2), 145-154.
- White, A. (2003) 'Natural weathering rates of silicate minerals', *Treatise on geochemistry*, 5, 133-168.
- White, A. F., Blum, A. E., Schulz, M. S., Bullen, T. D., Harden, J. W. and Peterson, M. L. (1996) 'Chemical weathering rates of a soil chronosequence on granitic alluvium: I. Quantification of mineralogical and surface area changes and calculation of primary silicate reaction rates', *Geochimica et Cosmochimica Acta*, 60(14), 2533-2550.
- White, A. F. and Brantley, S. L. (1995) 'Chemical weathering rates of silicate minerals: an overview', *Chemical Weathering Rates of Silicate Minerals*, 31, 1-22.
- White, A. F. and Brantley, S. L. (2003) 'The effect of time on the weathering of silicate minerals: why do weathering rates differ in the laboratory and field?', *Chemical Geology*, 202(3-4), 479-506.
- Williams, P. and Fong, Y. T. (2010) *World map of carbonate rock outcrops v3.0*, sheet School of Environment, University of Auckland,
- Williamson, P. (2016) 'Emissions reduction: Scrutinize CO₂ removal methods', *Nature*, 530(7589), 153.
- Woodward, F. I. and Lomas, M. R. (2004) 'Vegetation dynamics – simulating responses to climatic change', *Biological Reviews*, 79(3), 643-670.
- Yeager, A. F. (1935) 'Root systems of certain trees and shrubs grown on prairie soils', *Journal of Agricultural Research*, 51(12), 1085-1092.
- Zeebe, R. E. (2012) 'History of seawater carbonate chemistry, atmospheric CO₂, and ocean acidification', *Annual Review of Earth and Planetary Sciences, Vol 40*, 40, 141-165.